The diffraction of atoms by light

Duncan H. J. O'Dell

H.H. Wills Physics Laboratory,
University of Bristol.

A thesis submitted in partial fulfilment
of the requirements for admission to
the degree of Doctor of Philosophy
of the University of Bristol.

December 21, 1998

Abstract

The diffraction of a coherent, stationary, beam of atoms from a standing wave of light is considered. Particular attention is paid to long interaction times for which the motion of the atoms inside the light field must be taken into account. This is the regime of dynamical diffraction, and is treated within the framework of a set of differential difference equations due to Raman and Nath. The popular Raman-Nath approximation, in which the kinetic energy imparted to the atoms by the light wave is ignored, is no longer valid and the full equations must be solved.

When the interaction between the atoms and the light is very weak then few beams are produced. To describe spontaneous emission from the atom one can invoke a complex potential as a model for dissipation. If the atom beam is obliquely incident one finds anomalously high transmission close to the Bragg angles which is the physical manifestation of degeneracies in non-Hermitian matrices.

The classical limit is approached when the atom-light interaction is strong, producing many beams. The classical dynamics (geometrical rays) reveal that the farfield intensity pattern is dominated by caustics. These proliferate with increasing interaction distance. Two methods are presented for analytically treating the semiclassical limit of the wave mechanics. The first begins with W.K.B. solutions to the continuised Raman-Nath equations. Mapping onto parabolic cylinder functions removes the spurious divergences of the W.K.B. solutions, giving eigenvectors which are uniformly valid for all scattering angles and may be summed to give the wavefunction. The second method transforms the original W.K.B. eigensum, using the Poisson summation formula, giving a new sum, each term of which has classical significance. This method shows that wave theory decorates the classical caustics with an Airy function intensity profile, as predicted by catastrophe theory.

TO MY PARENTS

Declaration of originality

The work presented here was carried out at the University of Bristol between October 1994 and November 1998. It has not been submitted previously for a degree at this or any other university. Care has been taken to correctly attribute the work of others. A number of the other results, especially the earlier ones, were achieved to a greater of lesser degree under the guidance of my supervisor Michael Berry.

Acknowledgements

I have greatly enjoyed my time in Bristol. My existence here has been greatly facilitated by a grant from the university. From the academic point of view, I owe everything to the creative and brilliant mind of Professor Sir Michael Berry: whether directly from illuminating discussion, or implicitly from his many writings, his ideas pervade this thesis. The many fine meals cooked by Michael and Monica Berry also deserve a mention. I am likewise indebted to the deep thoughts of John Hannay with whom I have had many invaluable discussions, and who made several crucial suggestions.

Aspects of this work benefited greatly from visits to the groups of Professor A. Zeilinger and Professor W. Schleich. Their hospitality and time was greatly appreciated. During a visit to the latter group, I was very fortunate to meet Professor V. Yakovlev whose enthusiasm for the continuised Raman-Nath approach provided the stimulus for the work contained in the last three chapters.

Many others, including my peers, superiors, and visitors to Bristol, have contributed to my understanding of physics. In particular, I thank Jon Wallington for proof reading this thesis. Any mistakes that remain are of course entirely his fault.

On the purely social side, I also salute the valiant attempts of my friends here in Bristol and elsewhere, as well of the university Cross Country running club, in trying to prevent me from ever doing any work. Please forgive me.

Finally I thank my parents for their unfailing support, and doing all the things that parents quite selflessly do.

"This I'll Defend"

Motto of clan MacFarlane of loch Lomond, to which I trace tenuous ancestry.

"We hold these truths to be self evident . . . "

The American declaration of Independence. An important reference.

Contents

List of Figures

List of Tables

Introduction

This thesis concerns various aspects of the diffraction of atoms by gratings made of light. The subject deserves attention not least because it is the reverse of the more usual situation. Whilst the first experimental demonstrations were conducted only fifteen years ago, the subject has rapidly evolved into an established field now referred to as 'atom optics'. Early investigations relied on exactly this novelty of the optics analogy: all the scalar wave properties of light can in principle be reproduced with atoms; there are now experimentally realisable atom lenses, beam splitters, interferometers and so on.

The idea that the *external* states of particles might be manipulated coherently[1] by electromagnetic radiation began with Kapitza and Dirac [43] in 1933. They speculated that an electron beam could be Bragg reflected from a standing light wave (formed from two progressive waves) by stimulated Compton scattering. Light sources in their day, such as mercury lamps, were so weak that they predicted only a fraction of the order of 10^{-14} of the electrons in the incident beam would be scattered. Kapitza and Dirac conceded that "the experiment could scarcely be made with ordinary continuous sources of light", and indeed it took the invention of the laser, and the use of atoms rather than electrons (atoms have a *resonant* interaction with light due to their internal states, as realised by Kazantsev and Surdutovich [44] in 1975) to finally put Kapitza and Dirac's idea into practice. Nevertheless, the basis of Kapitza and Dirac's scattering mechanism, whereby a photon is absorbed by an electron from one of the progressive waves but is then emitted into the other, counter propagating, wave, because of the stimulating action of this second wave mode, holds true also for atoms. Thus, in honour of their original contribution, atomic diffraction from standing light waves is often referred to as 'Kapitza-Dirac scattering'.

However, demonstrations of de Broglie's hypothesis (1923-1924) are not new: direct confirmations came with experiments such as those by Davisson and Germer who succeeded in diffracting electrons as early as 1927. Nor are atoms the first non-fundamental particles to be diffracted. Neu-

[1] 'Coherent' is taken here to imply that all the relevant interactions are included in the Hamiltonian, and that interference between the states of the particle is fully taken into account.

trons are known to 'contain' other more fundamental particles and yet diffract as a single entity with a single centre of mass wavefunction (though of course there may be finer structure to be seen at very high energies).

So once the initial excitement surrounding the diffraction of a new type of quantum particle had subsided, there was a necessity for the subject to deliver new physics, not just reproduce that of other fields. Being the most massive objects to have been diffracted so far[2], combined with the strength of the atom-light interaction, atoms provide an ideal method for coherently accessing the small wavelength, or semiclassical regime. Semiclassical systems serve as a bridge between the bizarre quantum and the more familiar classical worlds. Matching the two theories requires the characterisation of emergent features, such as caustics, whose seeds are contained in the wave theory, but which only become fully developed in the classical limit. However, this limit is not a simple one, and necessitates the use of some semiclassical 'techniques' which will be introduced and used as needed.

The focus will not be entirely upon the small wavelength behaviour: the versatility of the atom-light interaction allows a brief excursion into a model for a dissipative potential. Counter-intuitive features can be identified which are the physical manifestation of degeneracies in non-Hermitian matrices.

Whilst the study is strongly physically motivated, the investigations described in this thesis are almost entirely concerned with solutions of Mathieu's equation [1]

$$\frac{d^2y}{dv^2} + (a - 2q\cos 2v)y = 0. \tag{1}$$

and so stand independently of atom optics. Indeed, once the governing Hamiltonian has been found, only time independent solutions of Schrödinger's equation will be considered. Then one is solving a Helmholtz equation so there is not really any quantum mechanics in this thesis. Having accepted that particles behave as waves, there is nothing further contained here that would surprise a 19^{th} century physicist (Schrödinger himself believed that real quantum mechanics begins with entanglement).

Chapter 1 gives a brief overview of atom optics from the experimental perspective, showing how this research fits into the rest of the field. Chapter 2 explains the nature of the atom-light interaction and hence how Mathieu's equation arises. The treatment of the classical mechanics is given in Chapter 3 which is then used for comparison with the quantum behaviour described in the rest of the thesis: in particular Chapter 4 introduces the Raman-Nath equation, a differential difference equation, which is the principal tool used in developing the wave mechanics associated with dynamical diffraction. The stationary Raman-Nath equation is nothing but a recursion rela-

[2]The diffraction of a Bose-Einstein condensate is eagerly awaited.

tion for the Fourier coefficients of the Mathieu equation. Chapter 5 takes a step back and seeks to justify the use of several greatly simplifying approximations, such as taking the atomic beam as being infinitely wide.

The majority of this thesis requires that spontaneous emission from the atom be suppressed, but Chapter 6 positively requires it to give a complex potential (q in Mathieu's equation, (1), becomes a complex number) which is a model for dissipation. The final three chapters all examine the semiclassical limit of the Raman-Nath equation. Chapter 7 shows that in this limit the Raman-Nath equation can be 'continuised', giving solutions analogous to the W.K.B. approximations to ordinary differential equations. Stationary solutions to the continuised Raman-Nath equation are then further developed in Chapter 8. These 'uniform' solutions remain valid even at the turning-points where the W.K.B. solutions diverge. Finally, in Chapter 9, the sum of W.K.B. eigenvectors, which together make up the wavefunction, is transformed using the Poisson summation formula, giving terms which each have a classical interpretation.

Before confusion arises, it is worth pointing out that the term 'semiclassical' has two different meanings in the two branches of physics which overlap in this thesis. The atomic physics community commonly uses 'semiclassical' to describe an approximation whereby the atoms are treated as quantum systems, but the radiation to which they are coupled is treated as classical. This approximation is indeed used in Chapter 2. Semiclassical analysis, on the other hand, is a collection of methods and approximations appropriate when the de Broglie wavelength of a particle is very small in comparison to the spatial variation of the potential in which it moves. It is then often convenient to use Planck's constant, $\hbar$, as a parameter of quantum theory rather than a constant of nature. In this work the context should always make the usage clear.

Chapter 1

Atomic diffraction in practice

1.1 Motivation

The studies which will be described in this thesis were originally conceived in the light of a set of pioneering experiments conducted from the mid 1980' s onwards. These investigations really marked the birth of a new field; atom optics. Although theoretical papers pointing out the possibilities had appeared over ten years earlier, the technical difficulties associated with the manipulation of atoms by light slowed experimental progress. Spurred by the success of the first experiments however, the area exploded into life, and has frequently been in the healthy position of being experimentally driven. It is fitting, therefore, to begin by presenting the basic experimental set-up used, this serves to fix ideas and will provide the platform from which all developments will be made.

1.2 An Experimental set-up

The experimental scheme depicted in Figure 1.1 is taken from Moskowitz *et al.* [58]. Sodium atoms emerge from a heated reservoir with a thermal distribution of velocities. An atom beam with a velocity distribution is analogous to a light beam containing many colours. To control the longitudinal ($\mathbf{z}$) velocity, the sodium atoms were combined with an inert gas which expands supersonically through a nozzle. As a result of the effusion, the sodium beam attains a velocity of around 1000 m/s, with a measured velocity dispersion $\frac{\Delta v}{v} = 11\%$ at FWHM.

Passage through a pumping laser beam (not shown) transfers the atoms into an internal electronic state suitable for the interaction with the standing wave laser field. Transverse ($\mathbf{x}$) velocity selection is then achieved via a number of collimating slits. Thus, it is a roughly 'monochromatic' beam of sodium atoms that passes through the waist of the standing wave laser field formed by

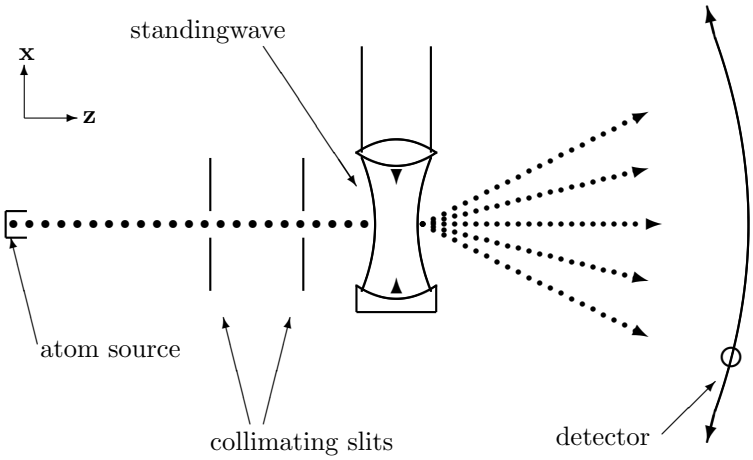

Figure 1.1: A typical experimental set-up used in the investigation of atomic diffraction.

the reflection of the primary laser beam back onto itself by a mirror.

Finally there is a scanning detector in the farfield which measures the angular intensity distribution of the diffracted atoms. To accomplish sufficient collimation and then angular resolution[1], there may be longitudinal distances of several metres between the various components of the apparatus.

Following the initial demonstrations of atomic diffraction [57, 58, 39] there have been many modifications to this basic theme, including:

- Angled incidence: Figure 1.1 demonstrates an atomic beam perpendicularly incident upon the standing wave. However, one may just as easily tilt the atomic beam so the atoms have a non-vanishing initial transverse velocity [65, 50, 51, 53, 52, 34]. Features analogous to those found in x-ray diffraction in crystals, such as Bragg resonances and anomalous transmission (to be described in detail in Chapter 6) can be seen.

- Atomic interferometers: the behaviour of the atoms in the standing wave can result in complicated interference (diffraction)—as shall be shown in subsequent chapters. It is possible however, by employing one or more standing wave lasers after the first, to spatially separate

[1]The deflection angles involved are very small. The transverse velocity conferred to a sodium atom by the absorption of a single photon is approximately 2.6 cm/s. When the ratio of this transverse velocity is taken with the longitudinal velocity of some 1000 m/s, it becomes clear that to detect a single photon momentum transfer the detector must be capable of a resolution of some 26 μradians.

by *macroscopic* distances, and then recombine, two specific diffracted beams which emerge from each 'light grating'. The simplest of interference patterns, a sinusoid, can then observed [72, 33] between the two different classical paths along which the atoms could travel. Due to the very small atomic de Broglie wavelength, such interferometers are extremely sensitive to local differences in the environment between the two 'arms'.

- Time dependent potentials: the standing wave can be modulated by moving the mirror back and forth in the transverse direction. This induces a periodic (in time) displacement of the standing wave. The Hamiltonian describing such a system is formally identical to that of the kicked rotor—a famous example of classically chaotic motion. One of the features often inherited by waves whose corresponding classical behaviour is chaotic, is *dynamical localisation*. This is indeed what is observed experimentally [56].

- Cold atoms: firing atoms at the interaction region in a supersonic beam is relatively simple and has the benefit of high atom fluxes. A far more elegant method though, is to first cool the atoms, in a magneto optical trap for instance [46], or maybe, in the future, emit them from a coherent source—the so-called 'atom-laser'—and then drop them under gravity through the laser fields. In this way, the velocity of the atoms can be precisely controlled—eliminating the velocity dispersion. Another advantage of this method is the attainment of long interaction times, as slowly moving atoms spend longer in the laser beam.

More complete summaries, containing further variations, may be found in the review article by Adams, Sigel and Mlynek [2], and in the two books by Balykin and Letokhov [6], and Kazantsev, Surdutovich and Yakovlev [45].

1.3 The system parameters

Using the basic layout described above it is now possible to identify the key parameters of the system. Prior to this though, it should be mentioned that a fair proportion of the finer features of real laboratory atomic diffraction, described below, will subsequently be ignored. The specific reasons will be given in each case. As a general philosophy though, the models which will be used have been stripped of as many 'distractions' as possible in order isolate the basic characteristics which this thesis seeks to emphasise. The cost of this is absolute numerical accuracy. The fundamental form of the behaviour will obviously be correct however, and Chapter 5 will try to address these approximations more thoroughly.

1.3.1 Properties of the atomic beam

A few words are necessary concerning the meaning of the words 'atomic beam'. A complete description would consider each atom as an individual wave packet. The farfield pattern would then be time dependent (or an average over this time dependence); waxing and waning as the leading edge, then main body, and finally the tail of the wavepacket, reached the detector. For the purposes of this work, such details are an unnecessary complication and the essential behaviour will be captured by treating the incident beam as a continuous plane wave. Although a beam consists of many atoms, the interference pattern is considered to arise only from the interference of *each atom* with *itself*. The individual atoms are quantum mechanical particles and so the detector collapses each atomic 'matter wave' into a particular direction (diffracted beam) with a probability given by the modulus squared of the amplitude to be travelling in that direction. Each atom acts independently: a beam consisting of many identical atoms plays the rôle of an ensemble of identical experiments and thus the complete interference pattern is eventually mapped out.

Choice of atom

Choosing a suitable species is a matter of the utmost importance and requires a fantastic knowledge of the detailed electronic structures of the candidates. Most groups have their own favourites, based on the perceived suitability of a particular transition. The early experiments [57, 58, 39] generally used sodium, since careful use of the $3S_{\frac{1}{2}} \longrightarrow 3P_{\frac{3}{2}}$ transition results in a good approximation to a two-level system. More recent investigations have favoured metastable neon [33, 34] and rubidium [46], whilst the realisation of a *complex* interaction between atom and laser (modelling dissipation—as will be discussed at length) requires an effective three level scheme such as that found in argon [62].

Approximate masses[2]: *Na* 23 *amu; Rb* 85.5 *amu; Ar* 40 *amu.*

Spontaneous emission

As shall be discussed in Chapter 2, one way of understanding the diffractive action of the standing wave on the atoms, is by the absorption and stimulated emission of photons from the two counter-propagating laser beams. The atoms can also de-excite, however, by spontaneous emission. An atom exhibiting spontaneous emission moves in an effectively random fashion which may be regarded as diffusive—a quite different pattern of behaviour from diffraction. Given a long enough interaction time with the electromagnetic field, it is inevitable that the atom will eventually emit spontaneously. A number of theoretical [78, 27, 77, 75] approaches have evolved to cope with

[2] 1 atomic mass unit = 1.66054×10^{-27} kg

the diffusive motion. They mainly assume the validity of the deterministic approach until some threshold time, after which the system is treated statistically by using a Fokker-Planck equation to simulate the spread of the momentum distribution. An experiment has also been carried out to examine the transition from diffraction to diffusion [36].

The rate at which an atom spontaneously decays is the natural decay rate of the excited state, Γ—the phenomenological decay constant introduced by Einstein for an *excited* atom sitting in a vacuum—multiplied by the probability for the atom to be in that excited state. By detuning the laser frequency from resonance with the atom, the probability of the atom to be in the excited state is reduced (Chapter 2) and thus the deterministic region can extended.
Spontaneous decay rate for the stated transition in Na: $\approx 2\pi \cdot 10\,MHz$.

Atomic wavelength

The very essence of wave-particle duality is the de Broglie wavelength of the atom which depends on its mass and velocity:

$$\lambda_{\text{de Broglie}} = \frac{h}{mv}$$

Typical value for Na in a supersonic beam: $\lambda_{\text{de Broglie}} \approx 0.17\,\text{Å}$.

Coherence

That the atoms have identical physical attributes, such as velocity, is important for producing sharp diffraction patterns. Slight differences in the velocity of each atom cause the set of diffracted beams belonging to each atom to lie in slightly different directions, and hence the final diffraction pattern is blurred out. Deviations from the ideal are reflected in the coherence of the beam. A plane wave is completely coherent. Coherence of the beam then, is synonymous with velocity dispersion.
Typical dispersion for supersonic beam: $\frac{\Delta v}{v} \approx 11\%$.

Width of the beam

As already alluded to, the laser standing wave acts as a grating. An essential property of the standing wave is its periodicity, and this together with the atomic de Broglie wavelength, is all that is required to determine the angular separation of the maxima and minima of the diffracted beams, in accordance with the familiar Fraunhofer diffraction theory. The transverse width of the atomic beam dictates the number of elemental 'unit cells' of the standing wave which are illuminated. An infinitely wide illumination of a grating causes the diffracted beams to become

infinitely narrow (in angle). A narrow illumination on the other hand, causes the emergence of intermediate structure; subsidiary maxima and minima, so the beam width is an important factor.

The collimation slits are used to control the width of the atomic jet plume. It is a subtle question as to how the slit gap determines the width of the atomic beam. Clearly the atom beam cannot be wider than the gap (it being assumed that the gap is too wide to induce any significant diffraction itself). However, just because a bunch of randomly arriving particles are confined to pass through a gap, does not imply that the individual transverse width of the wave packet associated with each atom is equal to the gap; it might be much less.

Taking the typical slit width to be 10^{-5} m and the longitudinal separation of the two slits as 0.9m [53], one can determine the maximum uncertainty in the momentum for the transmission of classical particles to be:

$$\Delta p \approx 2 \cdot 10^3 \cdot 23 \cdot 1.66 \times 10^{-27} \cdot \frac{10^{-5}}{0.9} = 8.5 \times 10^{-28} \text{ kg m/s}.$$

Using $\Delta x \Delta p \geq \hbar/2$ gives a minimum atomic wave packet width of $\Delta x = 6.2 \times 10^{-8}$ m. The atomic beam width must therefore lie between this and the value of the slit width itself. Section 1.3.2 gives the dimensions of the elemental cell of the laser standing wave, and shows that the atomic beam width covers between 1/5 and 33 of the elemental cells. The full range of diffraction behaviours described above is therefore possible. Remaining faithful to the principle of absolute simplicity wherever possible, the remainder of this work, with the exception of Chapter 5, will take the atomic beam as being infinitely wide. Chapter 5 will consider the effects of more physically realistic beams.
Typical range for beam width: 6.2×10^{-8}—10^{-5} *m.*

1.3.2 Properties of the standing wave laser field

Wavelength

The requirement that the laser light has a frequency resonant or quasi-resonant with the chosen atomic transition obviously provides a general constraint. So the size of each elemental cell of the standing wave,

$$d_{\text{sw}} = \lambda_{\text{laser}}/2$$

(λ_{laser} is the wavelength of the two individual counter propagating beams that form the standing wave) is approximately set once the transition has been specified. The frequency difference between the laser and the selected transition is known as the detuning, Δ. The strength of atom-field interaction depends upon Δ, and as mentioned above, it can be used to control the spontaneous emission rate of the atoms.
Typical values of Δ*: 0–2*π *GHz.*

Typical wavelength: $\lambda_{\text{laser}} = 0.589\,\mu m$.
Note that the detuning is very small compared to the frequency of the light: $\Delta/\omega_{\text{laser}} \approx 10^{-6}$.

Width of the standing wave laser field

As indicated in Figure 1.1, the laser beam can be focussed down from its initial width, and in this way the interaction time of the atoms with the laser can be reduced. The smallest laser waist to have been used is $25\,\mu$m [58]. Conversely, the beam could also be telescopically expanded, giving widths of up to 5cm [84], but no experiment has yet been performed with such a wide interaction zone. When the beam is focussed right down, the light wave fronts have considerable curvature. From the photon viewpoint, since the position of the photons is relatively well known, their momentum is more uncertain. Either way, the momentum transferred is no longer solely in the transverse direction and the diffracted beams will have some angular spread.

The longitudinal profile of the laser beam is often taken to be a Gaussian. When the beam is expanded, the natural shape is likely to be a central flat plateau with smooth wings at either end, see Figure 1.2. By physically masking the beam, one could in principle produce any (diffraction

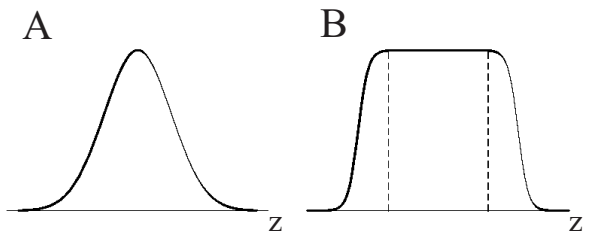

Figure 1.2: A comparison of possible laser beam longitudinal profiles: A) Gaussian, B) Flat with smooth wings.

limited) function of **z** one wanted; a linear ramp, a saw-tooth pattern etc.. Obtaining analytical solutions with a smooth profile rapidly becomes difficult however. Once again, to keep things simple, the transverse profile will henceforth be taken to be flat: the atoms will start already in the laser at one end, and propagate for a fixed distance under the influence of the field. This ignores the effect of the wings. Since the principal interest of this thesis is in long interaction times (a long central plateau) this seems a sensible thing to do—it is assumed that the motion of the atoms is not altered during the relatively short passage through the wings. Indeed, as shall be shown in the next chapter, the potential seen by an atom whilst in the laser is very small ($\approx 10^{-29}$ J) compared

to the longitudinal kinetic energy of a supersonic atom ($\approx 10^{-20}$ J)—the infinitesimal climb up into the potential has a vanishingly small effect on the longitudinal motion, which will be taken as a constant, and provided the wings are short, can only have a small effect on the transverse motion. Chapter 5 contains a numerical examination of this.

One has to be a little careful though, as the effect on the *internal* states, which actually determine the potential, is not so simple. A very sudden entry into the potential (short wings), is like a hammer blow, fully exciting the atomic transition. A slower, more adiabatic, entry into the potential allows the internal states of the atom to settle to a steady state before the potential has changed by much, and the transition need be only slightly excited. Although interesting, such effects will not be examined further, and it will be assumed that the switch-on of the potential is slow enough to ensure adiabatic entry, but quick enough so as to have negligible effect on the transverse motion.

Typical values of standing wave width: 25μm–15mm [34].

Power of the laser

As shall be shown in Chapter 2, the magnitude of the atom-laser interaction depends on the electric field strength. The stronger the electric field, the more diffracted orders are produced. If the beam is expanded, then the laser power must be increased to compensate for the increased area over which the energy is spread.

Typical laser power: 0.5mW–100mW

1.4 Unexplored parameter ranges

Following the success of the early experiments, the shrewd manipulation of the parameters outlined above has led to the observation of many distinct aspects of diffraction. In conjunction, theoretical models have been derived whose numerical solutions accurately describe and sometimes predict these developments; a few analytic solutions are also known. Experience with another physical system, the diffraction of light by ultrasound, shows, however, that there exists a rich set of phenomena associated with a long *coherent* interaction time [16, 61], an area which remains to be explored in atom optics. 'Coherent' refers to the absence of spontaneous emission. This is the regime of *dynamical diffraction*, where the motion of the atoms inside the laser potential must be properly accounted for—in particular this is something that none of the established analytical solutions consider[3]. The incorporation of long, coherent, propagation times into atom optics is

[3]Except for the rather special case of a very weak interaction *and* incidence at a Bragg angle: the so called "two beam approximation" is then valid, and this is correct for arbitrary interaction times. This will be discussed and

the main purpose of this thesis. The results have a wider applicability though since they hold for any semiclassical (in the small de Broglie wavelength sense) system obeying Mathieu's equation (Equation 1). What makes atom optics so special is the versatility of the interaction between the atom and the field, and the relative ease by which the various system parameters can be varied: by simply changing the laser power, the transverse component of the de Broglie wavelength can be taken from roughly equal to the standing wave cell (a very quantum situation) to being many times less, and so begin to probe the classical limit; by changing the focussing of the laser beam, different interaction times can be selected; by positively encouraging spontaneous emission, rather than suppressing it, the interaction can be interpreted as being dissipative with a complex representation, and so on. This is why atom optics is so unique.

used in Chapter 6.

Chapter 2

Light forces

2.1 Motivation

To calculate the motion of an atom subjected to an electromagnetic field clearly requires an understanding of the forces involved. An atom, of course, is not a fundamental particle. This at once means that the potential seen by the atom is not so straight forward and will require some explanation, and this chapter attempts that. Conversely, a more complicated interaction results in richer behaviour. Sufficiently rich, in fact, that the understanding of 'light forces', and their application to laser cooling, lead to the awarding of the 1997 Nobel prize to S. Chu, C. Cohen-Tannoudji, and W. D. Phillips. The full, glorious, details required to understand how atoms can be cooled to a few microKelvin will not be required here however[1], so the treatment will be at a more elementary level.

2.2 The basic mechanism

By way of introduction, it is useful to approach diffraction from a purely descriptive viewpoint in terms of photons. Although the semiclassical approach will be used for the calculation of the actual potential, particles (photons) exchanging momentum with particles (atoms) is perhaps more intuitive. In fact, even in the midst of the semiclassical derivations, the term 'photon' will be used (somewhat loosely) if it serves to clarify the discussion. Also, throughout this discussion, the atom and the electromagnetic field will be treated as separate, but interacting, systems. Although seemingly natural, this separation is perhaps arbitrary and it is worth pointing out that they

[1] For instance, polarisation gradients in the laser field were crucial to explain how such low temperatures were attained, but the effects due to the polarisation of the standing wave used here will be neglected.

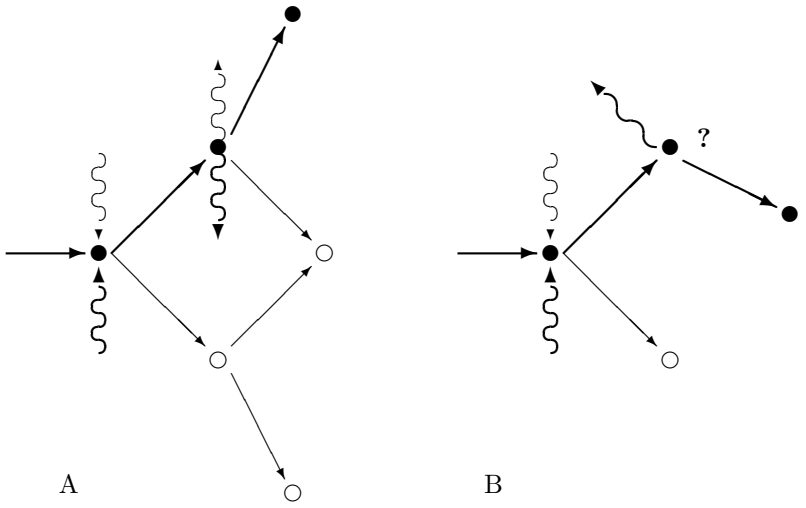

Figure 2.1: How the microscopic processes deflect the atoms: A) absorption and stimulated emission moves the atoms about on a quantised ladder, each rung separated by $2\hbar\mathbf{K}$; B) absorption and spontaneous emission places the atom at a random position between the rungs.

may be considered as a single system (with overall eigenstates therefore) under the 'dressed-atom' picture of Cohen-Tannoudji [27].

A laser then, is a remarkable device which shall be considered here as capable of macroscopically populating just one mode of the electromagnetic field with photons. The experimental set-up shown in Figure 1.1 depicts the laser beam being reflected back on itself, so the mirror populates the complementary, counter propagating mode. The infinite number of other, empty, modes make up the vacuum. A simple two-level atom moving across the standing wave is a quantum system coupled to every one of the modes. If the atom is initially in the ground state then it may 'absorb' a photon from one of the modes. The very high photon population of the laser filled modes makes it much more probable that the atom will obtain a photon from one of these (and this is the only energy conserving option), and in so doing, also taking up that photon's momentum. Thus the absorption process results in the atom receiving a $1\hbar\mathbf{K}$ kick in one of the two transverse directions, where $\mathbf{K}$ is the wave-vector of the laser field. Now it is the turn of the excited atomic eigenstate to feel the coupling to the external field. An interaction with either of the two filled modes gives rise to stimulated emission, whereas a union with any of the vacuum modes delivers a spontaneously emitted photon. As illustrated in Figure 2.1, the stimulated emission ejects the photon back into one of the two laser modes—if it's the mode from which the photon originated, then the momentum

conveyed to the atom cancels the initial absorption recoil; if it's the other, counter-mode, then the net effect of the absorption-stimulated emission cycle is a $2\hbar\mathbf{K}$ momentum transfer in one of the two transverse directions. The whole process may now repeat and thus populate higher diffraction orders, each of which is separated by $2\hbar\mathbf{K}$. By contrast, if the atom emits 'spontaneously' into one of the vacuum modes, which are homogeneously directed, then the atom receives momentum in an effectively random direction, and so moves out of the diffracted beam structure. The cycle of absorption followed by spontaneous emission is, of course, put to good use in the most basic form of laser cooling. An atom heading directly into a resonant laser beam continually accepts photons from the oncoming beam, reducing its velocity in that direction, but emits in a random direction. After many absorptions and emissions the overall effect is that the atom is cooled since the average momentum transfer from all the spontaneously emitted photons is zero[2], and so it is as though there is a force acting only against the atom.

2.3 The Hamiltonian

The following arguments follow those presented in the books by Allen and Eberley [4], Loudon [48], but especially the excellent text co-authored by Cohen-Tannoudji, Dupont-Roc and Grynberg [25].

Consider a two energy-eigenstate atom, with ground state $|a\rangle$, and an excited state $|b\rangle$, separated by $\hbar\omega_0$

$$H_{internal}\,|a\rangle = 0\,|a\rangle \tag{2.1}$$

$$H_{internal}\,|b\rangle = \hbar\omega_0\,|b\rangle \tag{2.2}$$

The total atomic Hamiltonian is the sum of contributions from the internal states, and, crucially for the purposes of including atomic centre of mass motion, the external states

$$H_A = \underbrace{\frac{\mathbf{P}^2}{2m}}_{\text{external}} + \underbrace{\hbar\omega_0\,|b\rangle\,\langle b|}_{\text{internal}} = \frac{\mathbf{P}^2}{2m} + \begin{pmatrix} \hbar\omega_0 & 0 \\ 0 & 0 \end{pmatrix}. \tag{2.3}$$

It can be assumed that the external electromagnetic field is not strong enough to significantly alter the internal states themselves, but merely cause transitions between them. Alternatively, one could just include such 'radiative shifts' in the atomic eigenfrequency ω_0.

The incident radiation field due to the laser may be considered as classical, but all the other, initially empty, modes, which collectively make up the vacuum, are quantum in nature—they are

[2]For each polarisation the probability to emit in *opposite* directions is equal, even though the angular dependence of the emission is not uniform; it might follow the radiating Hertzian dipole's pattern for instance. When the three polarisations are considered together then the emission is spherically symmetric.

dominated by quantum fluctuations. If the atom interacts with both of these fields, then within the electric dipole approximation the total Hamiltonian is

$$H = H_A + H_R - \underbrace{\mathbf{d}\cdot(\mathbf{E}_c + \mathbf{E}_q)}_{\text{dipole interaction}} \tag{2.4}$$

where $\mathbf{E}_c$ is the classical electric field due to the laser and $\mathbf{E}_q$ is due to the quantum modes, both evaluated at the centre of the atom[3]. The classical field due to the laser has a frequency ω_L , so let

$$\mathbf{E}_c = \mathbf{E}_c(\mathbf{r},t) = \mathcal{E}_0(\mathbf{r})\cos\omega_L t. \tag{2.5}$$

H_R is the Hamiltonian of the quantum radiation field, and $\mathbf{d}$ is the electric dipole moment operator belonging to the atom. It has a matrix representation written in the atomic internal eigenbasis as

$$\mathbf{d} = \begin{pmatrix} 0 & d_{b\,a} \\ d_{ab} & 0 \end{pmatrix} \tag{2.6}$$

which, in accordance with the form of an interaction Hamiltonian, is purely off-diagonal[4]—that is to say it induces transitions between the two atomic states. For simplicity let it be assumed that the elements of Equation (2.6) are real so that

$$\mathbf{d}_{ab} = \langle a|\mathbf{d}|b\rangle = \mathbf{d}_{b\,a} = \langle b|\mathbf{d}|a\rangle\,. \tag{2.7}$$

Notice that the Hamiltonian (2.4) does not take into account changes in the classical field due to the interaction with the atom—these being negligible.

2.4 The atomic wavefunction

The total atomic wavefunction is constructed from all the different possible states in which the atom can exist. When considering just the internal degrees of freedom, a general atomic state may be written as a linear combination of the two energy eigenstates

$$|\Psi(t)\rangle = C_a(t)\,|a\rangle + C_b(t)\,|b\rangle\,\mathrm{e}^{-\mathrm{i}\omega_0 t} \tag{2.8}$$

[3]Atomic electron radii are typified by the Bohr radius $a_0 = 4\pi\epsilon_0\hbar^2/m_{elec}e^2 \approx 5\times10^{-11}\,\mathrm{m}$, which is much smaller than the spatial variation of the $\mathbf{E}_c$ given by $\lambda_{\mathrm{laser}} = 0.589\,\mu\mathrm{m}$.

[4]The off-diagonality arises because the dipole moment has odd parity: $\mathbf{d} = e\mathbf{r}$ and so when $\mathbf{r}\to-\mathbf{r}$, then $\mathbf{d}\to-\mathbf{d}$. This means that when the matrix elements are found with respect to the atomic basis, the integrands of the diagonal elements are odd functions of position and thus the integrals vanish: $\mathbf{d}_{bb} = \int \mathbf{b}^*(\mathbf{r})\,\mathbf{d}(\mathbf{r})\,\mathbf{b}(\mathbf{r})\,d\mathbf{r} = \mathbf{d}_{aa} = 0\,.$

where the coordinate representations of the ket vectors in Equation 2.8 are

$$\langle \mathbf{r}|\Psi(t)\rangle = \mathbf{\Psi}(\mathbf{r},t) \tag{2.9}$$

$$\langle \mathbf{r}|a\rangle = \mathbf{a}(\mathbf{r}) \begin{pmatrix} 0 \\ 1 \end{pmatrix} \tag{2.10}$$

$$\langle \mathbf{r}|b\rangle = \mathbf{b}(\mathbf{r}) \begin{pmatrix} 1 \\ 0 \end{pmatrix}. \tag{2.11}$$

By way of illustration, one might take $\mathbf{a}(\mathbf{r})$ and $\mathbf{b}(\mathbf{r})$ as the (n,l,m_l) hydrogenic states $\psi_{100}(r,\theta,\phi)$ and $\psi_{211}(r,\theta,\phi)$ for instance. The atom at *rest* is thus described by

$$\mathbf{\Psi}(\mathbf{r},t) = \begin{pmatrix} C_a(t)\,\mathbf{a}(\mathbf{r}) \\ C_b(t)\,\mathbf{b}(\mathbf{r})\mathrm{e}^{-\mathrm{i}\omega_0 t} \end{pmatrix}. \tag{2.12}$$

Embracing the external degrees of freedom, the wave function is written

$$|\Psi(t)\rangle = \sum_{n=-\infty}^{\infty} C_{a,n}(t)\,|a,n\rangle + \sum_{n=-\infty}^{\infty} C_{b,n}(t)\,|b,n\rangle\,\mathrm{e}^{-\mathrm{i}\omega_0 t} \tag{2.13}$$

where n labels the external states with the discrete transverse momentum $n\hbar\mathbf{K}$. Transforming the internal co-ordinates into the atomic centre of mass frame and treating them as independent[5], the wave function in the (external[6]) coordinate representation may now be expressed in a plane wave basis

$$|\Psi(x,t)\rangle = \sum_{n=-\infty}^{\infty} C_{a,n}(t)\,|a\rangle\,\mathrm{e}^{\mathrm{i}nKx} + \sum_{n=-\infty}^{\infty} C_{b,n}(t)\,|b\rangle\,\mathrm{e}^{-\mathrm{i}\omega_0 t}\mathrm{e}^{\mathrm{i}nKx}. \tag{2.14}$$

2.5 Adiabatic following

A considerable simplification of the problem of an atom moving in a spatially inhomogeneous radiation field emerges upon the realisation that there are two distinct time scales involved. For a 'slowly' moving atom (referring to Figure 1.1, the relevant motion is in the transverse direction—for which the atom is initially stationary—so the 'slow' condition is fulfilled) the internal degrees of freedom evolve much more rapidly than the external ones. The time scale for the internal evolution is determined by the Rabi frequency[7], Ω, defined in Equation (2.24) below. The two-level atom is a driven oscillator with damping (Γ), and Ω is the angular frequency of oscillation between the internal states. Typical experiments have $\Omega/2\pi \geq 30$MHz [37]. So the internal states develop

[5] In other words, expressing the ket vector as a product state: $|a,n\rangle = |a\rangle\,|n\rangle$.

[6] Eqn (2.14) is in a convenient form, but it can be unravelled further to include the explicit dependence on the internal co-ordinates in the atomic centre of mass frame, ϱ say, by taking $\langle\varrho|\Psi(x,t)\rangle$. This gives $\mathbf{\Psi}(x,\varrho,t) = \sum C_{a,n}(t)\mathbf{a}(\varrho)\mathrm{e}^{\mathrm{i}nKx} + \sum C_{b,n}(t)\mathbf{b}(\varrho)\mathrm{e}^{-\mathrm{i}\omega_0 t}\mathrm{e}^{\mathrm{i}nKx}$.

[7] Or by Γ if $\Gamma > \Omega$.

over times $T_{int} = 1/\Omega$ seconds. During one internal cycle, the transverse position of the atom has changed by

$$\Delta\mathbf{x} = v_x\, T_{int} = n\frac{2\hbar\mathbf{K}}{m}T_{int} \leq n\, 2\times 10^{-9}\mathrm{m} \tag{2.15}$$

where n records the number of absorption-stimulated emission cycles accumulated, and upon exit from the laser beam indexes the diffracted beams. Clearly, $\Delta\mathbf{x}$ is much smaller than the optical wavelength λ_{laser}, so the external field that the atom feels barely alters over many internal transitions. This discrepancy allows the internal states to continually acclimatise to the new external environment—the atom is always in a steady state since it can react to changes in the field so quickly. Since the internal states adiabatically follow the external states, one may treat the two independently: the external force on the atom, despite being dictated by the internal dynamics, now becomes just a function of position.

As a result of the adiabatic shadowing of the external states by the internal ones, one may solve for the internal dynamics regarding the external field strength as a parameter. If the external field were weak, then one could try and solve for the coefficients $C_a(t)$ and $C_b(t)$ of Equation (2.8) using time-dependent perturbation theory. The situation one is interested in here however, is where many diffraction orders are produced: the field is strong enough to drive the atom through very many absorption and emission cycles. Perturbation theory is then inappropriate. A non-perturbative approach which also incorporates a relatively simple description of spontaneous emission is through the optical Bloch equations.

2.6 The optical Bloch equations

2.6.1 Evolution equation for the atomic density matrix

In what follows it will be more convenient[8] to represent the state of the atom in terms of bilinear products of the coefficients $C_a(t)$ and $C_b(t)$, rather than by the bare coefficients themselves. This leads to the definition of the atomic density matrix σ as

$$\sigma = \begin{pmatrix} \sigma_{bb} & \sigma_{ba} \\ \sigma_{ab} & \sigma_{aa} \end{pmatrix} \equiv \begin{pmatrix} C_b^* C_b & C_b^* C_a \\ C_a^* C_b & C_a^* C_a \end{pmatrix}. \tag{2.16}$$

[8]In fact particles forming a subsystem of a larger system are best described by a density operator. Even if the global system is in a pure state described by a state vector (obeying a Schrödinger equation), the particle subsystem is generally to be found in a statistical mixture of states. The density operator describing this mixture is obtained by taking a partial trace over the global density operator to remove the variables not involved in the subsystem. It might be possible to write a Schrödinger equation for the subsystem, but one would typically have to invoke a complex potential which expresses the fact that certain quantities (such as the total energy of the subsystem for instance) are not conserved. This is exactly the situation found in Chapter 6.

Note that the diagonal elements σ_{bb} and σ_{aa}, are the *populations* of the upper and lower levels respectively so that

$$\sigma_{bb} + \sigma_{aa} = 1. \tag{2.17}$$

The off-diagonal elements are often referred to as the *coherences* between the states $|a\rangle$ and $|b\rangle$ and are related by

$$\sigma_{ba} = \sigma_{ab}^{*}. \tag{2.18}$$

If there is no coupling to the quantum modes, $\mathbf{E}_q$, then the time evolution of σ is given by the Schrödinger equation

$$\mathrm{i}\hbar\dot{\sigma} = \left[H_A - \mathbf{d}\cdot\mathcal{E}_0\cos\omega_L t, \sigma\right]. \tag{2.19}$$

Extending Equation (2.19) to properly include the effect of the vacuum modes would require quantum field theory. However the appearance of the atomic populations in Equation (2.19) tempts one into adopting Einstein's procedure [30] of accounting for spontaneous emission by introducing a phenomenological decay constant, Γ. The atomic spinor is formally identical to a spin-half system, and it was in the context of the problem of a spin subjected to an oscillatory magnetic field that Rabi [66] solved equations analogous to Equation (2.19). It was Bloch [18] however, who, when considering nuclear spins, extended Rabi's solutions by including the phenomenological damping terms into the dipole oscillations. The various terms in the density matrix time evolution equation become

$$\dot{\sigma}_{bb} = \mathrm{i}\Omega\cos\omega_L t\,(\sigma_{ba} - \sigma_{ab}) - \Gamma\sigma_{bb} \tag{2.20}$$

$$\dot{\sigma}_{aa} = -\mathrm{i}\Omega\cos\omega_L t\,(\sigma_{ba} - \sigma_{ab}) + \Gamma\sigma_{bb} \tag{2.21}$$

$$\dot{\sigma}_{ab} = \mathrm{i}\omega_0\sigma_{ab} - \mathrm{i}\Omega\cos\omega_L t\,(\sigma_{bb} - \sigma_{aa}) - \frac{\Gamma\sigma_{ab}}{2} \tag{2.22}$$

$$\dot{\sigma}_{ba} = -\mathrm{i}\omega_0\sigma_{ba} + \mathrm{i}\Omega\cos\omega_L t\,(\sigma_{bb} - \sigma_{aa}) - \frac{\Gamma\sigma_{ba}}{2} \tag{2.23}$$

with

$$\Omega \equiv -\frac{\mathbf{d}_{ab}\cdot\mathcal{E}_0(\mathbf{r})}{\hbar} \tag{2.24}$$

which is the Rabi frequency that characterises the strength of the coupling between the incident wave and the atom.

The damping terms replace a more sophisticated treatment of the $-\mathbf{d}\cdot\mathbf{E}_q$ coupling; by simply adding them in it is as if the two couplings are uncorrelated. This is known as the 'approximation of independent rates of variation'. The inclusion of the damping terms for the populations is obvious, but the half rates found in the coherences is less so. For the purposes of uncorrelated relaxation of the excited atomic state into all the vacuum modes m, it is sufficient to assume

$$\Gamma_{ba} = \Gamma_{ab} = \frac{1}{2}\left(\sum_{m\neq a}\Gamma_{a\to m} + \sum_{m\neq b}\Gamma_{b\to m}\right) = \frac{\Gamma_{bb}}{2} \tag{2.25}$$

since $\Gamma_{a\to m} = 0$. More details can be found in [25].

2.6.2 The rotating wave approximation

Using Equation (2.7), the dipole operator may be expressed in terms of raising and lowering operators

$$\mathbf{d} = \mathbf{d}_{ab}(\overbrace{|b\rangle\langle a|}^{\text{raising}} + \underbrace{|a\rangle\langle b|}_{\text{lowering}}) \equiv \mathbf{d}_{ab}(\mathcal{R} + \mathcal{L})\,. \tag{2.26}$$

The interaction Hamiltonian can be rewritten in terms of these operators

$$-\mathbf{d}\cdot\mathcal{E}_0\cos\omega_L t = \frac{1}{2}\hbar\Omega\left(\mathcal{R}\mathrm{e}^{-\mathrm{i}\omega_L t} + \mathcal{L}\mathrm{e}^{\mathrm{i}\omega_L t} + \mathcal{L}\mathrm{e}^{-\mathrm{i}\omega_L t} + \mathcal{R}\mathrm{e}^{\mathrm{i}\omega_L t}\right)\,. \tag{2.27}$$

The exponentials, $\mathrm{e}^{-\mathrm{i}\omega_L t}$ and $\mathrm{e}^{\mathrm{i}\omega_L t}$, are associated, respectively, with the absorption and emission of a photon. The first two terms in Equation (2.27) therefore describe processes whereby the atom rises from $|a\rangle$ to $|b\rangle$ by absorbing a photon or falls from $|b\rangle$ to $|a\rangle$ by emitting a photon. Close to resonance, these processes are much more likely than the two remaining 'antiresonant' terms whereby the atom de-excites by absorbing a photon and excites by emitting one. The rotating wave approximation consists of the neglection of the last two terms in Equation (2.27).

2.6.3 The time-independent atomic evolution equation

Carrying through the rotating wave approximation on Equations (2.20–2.23) and making the change of variables

$$\tilde{\sigma}_{ba} = \sigma_{ba}\mathrm{e}^{\mathrm{i}\omega_L t} \tag{2.28}$$

$$\tilde{\sigma}_{ab} = \sigma_{ab}\mathrm{e}^{-\mathrm{i}\omega_L t} \tag{2.29}$$

$$\tilde{\sigma}_{bb} = \sigma_{bb} \tag{2.30}$$

$$\tilde{\sigma}_{aa} = \sigma_{aa} \tag{2.31}$$

removes the explicit time dependence of the evolution equations for the internal atomic density matrix. Thus Equations (2.20–2.23) become

$$\frac{\mathrm{d}}{\mathrm{d}t}\tilde{\sigma}_{bb} = \mathrm{i}\frac{\Omega}{2}(\tilde{\sigma}_{ba} - \tilde{\sigma}_{ab}) - \Gamma\tilde{\sigma}_{bb} \tag{2.32}$$

$$\frac{\mathrm{d}}{\mathrm{d}t}\tilde{\sigma}_{aa} = -\mathrm{i}\frac{\Omega}{2}(\tilde{\sigma}_{ba} - \tilde{\sigma}_{ab}) + \Gamma\tilde{\sigma}_{aa} \tag{2.33}$$

$$\frac{\mathrm{d}}{\mathrm{d}t}\tilde{\sigma}_{ab} = -\mathrm{i}\Delta\tilde{\omega}_{ab} - \mathrm{i}\frac{\Omega}{2}(\tilde{\sigma}_{bb} - \tilde{\sigma}_{aa}) - \frac{\Gamma}{2}\tilde{\sigma}_{ab} \tag{2.34}$$

$$\frac{\mathrm{d}}{\mathrm{d}t}\tilde{\sigma}_{ba} = \mathrm{i}\Delta\tilde{\omega}_{ba} + \mathrm{i}\frac{\Omega}{2}(\tilde{\sigma}_{bb} - \tilde{\sigma}_{aa}) - \frac{\Gamma}{2}\tilde{\sigma}_{ba} \tag{2.35}$$

with

$$\Delta \equiv \omega_L - \omega_0 \tag{2.36}$$

being the detuning of the laser from the atomic transition.

2.6.4 The Bloch vector

The variables

$$u \equiv \frac{1}{2}\left(\tilde{\sigma}_{ab} + \tilde{\sigma}_{ba}\right) \tag{2.37}$$

$$v \equiv \frac{1}{2\mathrm{i}}\left(\tilde{\sigma}_{ab} - \tilde{\sigma}_{ba}\right) \tag{2.38}$$

$$w \equiv \frac{1}{2}\left(\tilde{\sigma}_{bb} - \tilde{\sigma}_{aa}\right) \tag{2.39}$$

are the components of the 'Bloch vector'. Written it terms of the Bloch vector, Equations (2.32–2.35) simplify to just three equations, known as the *optical Bloch equations*

$$\dot{u} = \Delta v - \frac{\Gamma}{2}u \tag{2.40}$$

$$\dot{v} = -\Delta u - \Omega w - \frac{\Gamma}{2}v \tag{2.41}$$

$$\dot{w} = \Omega v - \Gamma w - \frac{\Gamma}{2}. \tag{2.42}$$

Physically, w represents half the difference in the populations of the two levels. The meaning of u and v becomes clear if the expectation value of the dipole $\mathbf{d}$ is calculated

$$\begin{aligned}\langle \mathbf{d} \rangle &= \mathrm{Tr}(\sigma \mathbf{d}) = \mathbf{d}_{ab}(\sigma_{ab} + \sigma_{ba}) \\ &= \mathbf{d}_{ab}\left(\tilde{\sigma}_{ab}\mathrm{e}^{\mathrm{i}\omega_L t} + \tilde{\sigma}_{ba}\mathrm{e}^{-\mathrm{i}\omega_L t}\right) \\ &= 2\mathbf{d}_{ab}\left(u\cos\omega_L t - v\sin\omega_L t\right). \end{aligned} \tag{2.43}$$

Thus u and v are the components of $\langle \mathbf{d} \rangle$ which are, respectively, in phase and in quadrature with the incident driving field.

2.6.5 Geometric interpretation

It is worth briefly mentioning the well known, and highly illuminating, geometric interpretation of the optical Bloch equations. In the absence of spontaneous decay, Equations (2.40–2.42) may be written as a single vector precession equation

$$\frac{\mathrm{d}\mathbf{\Phi}}{\mathrm{d}t} = \mathbf{Y} \times \mathbf{\Phi} \tag{2.44}$$

where the Bloch vector $\mathbf{\Phi}$ is

$$\mathbf{\Phi} \equiv (u, v, w) \tag{2.45}$$

and the torque $\mathbf{Y}$ is

$$\mathbf{Y} \equiv (\Omega, 0, -\Delta). \tag{2.46}$$

Figure 2.2 indicates how $\mathbf{\Phi}$ precesses about the torque vector at a frequency

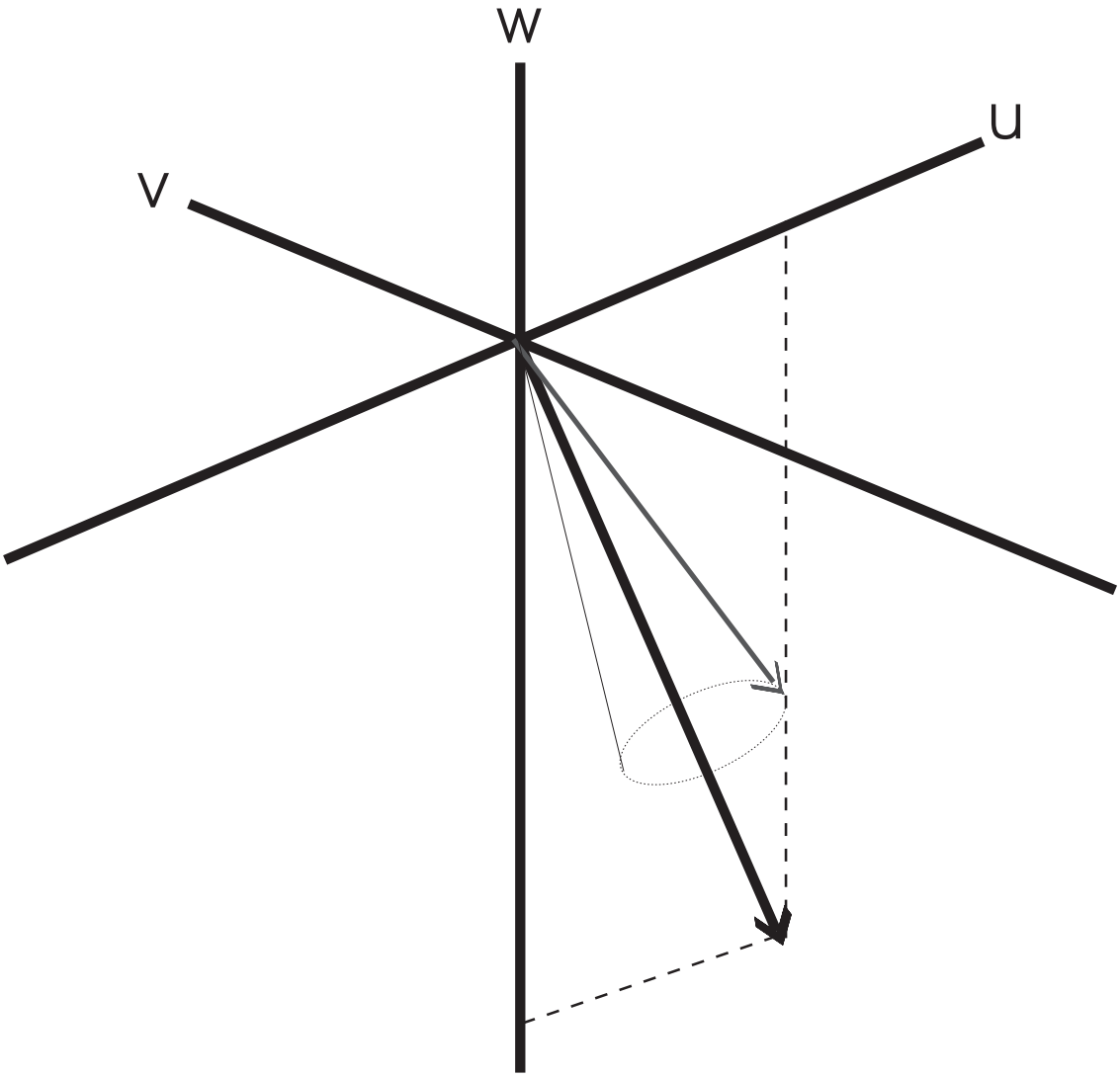

Figure 2.2: The precession of the (loss free) Bloch vector $\mathbf{\Phi}$ about the torque vector $\mathbf{Y}$.

$$|\mathbf{Y}| = \sqrt{\Omega^2 + \Delta^2}\,. \tag{2.47}$$

Examining the geometric picture immediately yields a wealth of information. The precession frequency is the frequency at which the undamped atom oscillates between the the states, Equation (2.47) shows how the detuning, Δ, modifies the exact on-resonance value which is given by

the naked Rabi frequency, Ω. Further, when $\Delta = 0$ the atom completes full oscillations between the ground and excited states ($\mathbf{Y}$ lies along the u axis and one then reads off the maximal values of w which are attained—w being half the population difference, see Equation (2.42)). However, at non-zero values of Δ, full excitation is no longer possible, and in the limit as $|\Delta/\Omega| \to \infty$, the atom remains in the ground state.

Adiabatic following also has a satisfying representation here: the Rabi frequency, Ω, is a function of the field strength (Equation (2.24)), so as an atom moves about in the field, the value of the Rabi frequency changes and hence the torque vector, $\mathbf{Y}$, moves around. The geometric picture indicates that if adiabatic following is to occur, the precession of the Bloch vector must be much faster than the movement of the guiding torque vector—the Bloch vector must really be able to follow the torque vector around—allowing the atom to constantly adjust and remain in a steady state.

Finally, the rotating wave approximation also has an interpretation: if the time dependency of the density matrix elements is restored (Equations (2.28–2.31)), then the result is a more complicated picture in which there are two counter rotating torques—one of which, at resonance, rotates along with the Bloch vector (which rotates itself) and so is able to act efficiently upon it, whilst the other, which rushes past twice each rotation, has a much smaller influence. The rotating wave approximation consists of ignoring the counter-rotating component.

Despite clear strengths in describing the damping-free behaviour of the internal states of the two-level atom, the geometric picture loses appeal when decay is included—in particular the simple precessing vector model no longer holds, and so ultimately it is simpler to solve the optical Bloch equations algebraically when the complete description is required.

2.6.6 Solving the optical Bloch equations

The optical Bloch equations (2.40–2.42) are linear differential equations with constant coefficients, so the solution can be phrased in terms of a superposition of exponentials. The full solution to the 'Bloch matrix' was first given by Torrey [81]. However, because of the adiabatic following property, it will be assumed that the atom has always achieved a steady state which is defined by the fixed values of the detuning and decay constant, and the parametrically included field. The transient response as the atom moves about in the spatially varying field will be ignored. Setting the time

derivatives to zero in the optical Bloch equations (2.40–2.42) leads to the solutions

$$u_{\rm st} = \frac{\Omega}{2}\frac{\Delta}{\Delta^2 + (\Gamma^2/4) + (\Omega^2/2)} \tag{2.48}$$

$$v_{\rm st} = \frac{\Omega}{2}\frac{\Gamma/2}{\Delta^2 + (\Gamma^2/4) + (\Omega^2/2)} \tag{2.49}$$

$$w_{\rm st} + \frac{1}{2} = \sigma_{bb}^{\rm st} = \frac{\Omega^2}{4}\frac{1}{\Delta^2 + (\Gamma^2/4) + (\Omega^2/2)} \tag{2.50}$$

where $w_{\rm st} + \frac{1}{2}$ is the steady state population of the upper level. Note that the in quadrature component of the dipole, $v_{\rm st}$, and the upper state population behave as a Lorentzian absorption curve centred on $\Delta = 0$ when Δ is varied. On the other hand, the in phase component, $u_{\rm st}$, varies as a dispersion curve. This contrasting behaviour is depicted schematically in Figure 2.3.

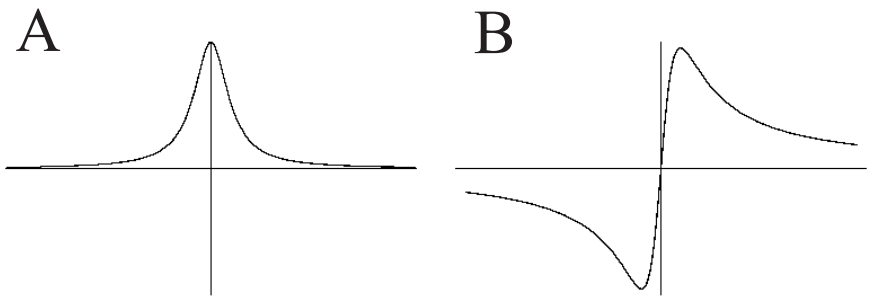

Figure 2.3: Contrasting behaviour as a function of Δ: A) Lorentzian absorption, B) dispersion.

2.7 The external degrees of freedom

2.7.1 An Ehrenfest equation

The assumption of adiabatic following allows the internal dynamics, now expressed as solutions to the optical Bloch equations, to be separated from the external ones. The following method of recombining the two came in a breakthrough paper by Cook [26].

Writing the total Hamiltonian in terms of $\mathbf{P}$ and $\mathbf{R}$, which are the momentum and position of the centre of mass of the atom respectively, gives

$$H = \frac{\mathbf{P}^2}{2m} + H_{\rm internal} + H_R - \mathbf{d}\cdot(\mathbf{E}_c(\mathbf{R},t) + \mathbf{E}_q(\mathbf{R})). \tag{2.51}$$

The Heisenberg equations of motion are the quantum analogues of Hamilton's equations, and when applied to the Hamiltonian (2.51) give

$$\dot{\mathbf{R}} = \frac{\partial H}{\partial \mathbf{P}} = \frac{\mathbf{P}}{m} \tag{2.52}$$

$$\dot{\mathbf{P}} = m\ddot{\mathbf{R}} = -\frac{\partial H}{\partial \mathbf{R}} = \sum_{j=x,y,z} d_j \nabla_{\mathbf{R}} (\mathrm{E}_{cj}(\mathbf{R},t) + \mathrm{E}_{qj}(\mathbf{R})). \tag{2.53}$$

Cook's contribution was to take the expectation value of Equation (2.53) over the atomic wavefunction, giving an Ehrenfest equation

$$m\left\langle \ddot{\mathbf{R}} \right\rangle = \sum_j \left\langle d_j \nabla_{\mathbf{R}} (\mathrm{E}_{cj}(\mathbf{R},t) + \mathrm{E}_{qj}(\mathbf{R})) \right\rangle . \tag{2.54}$$

Taking $\mathbf{r}_G = \langle \mathbf{R} \rangle$ as the centre of the atomic wave packet, the left-hand side of Equation (2.54) becomes $m\mathbf{r}_G$, which is the *force* applied upon the atom. The right-hand side of Equation (2.54) also simplifies.

i) Small electron radius. As mentioned in Section 2.3, electron radii in the atom are characterised by the Bohr radius which is much smaller than the spatial variation of the driving field. It is justifiable then to replace the operator $\mathbf{R}$ with its mean value $\langle \mathbf{R} \rangle = \mathbf{r}_G$. Note that the comparison scale here is the Bohr radius, and not the de Broglie wavelength associated with the atom's external motion.

ii) Averaging out $\mathbf{E}_q$. It seems reasonable (and can be shown rigorously) that the expectation of the gradient of the quantum radiation field at $\mathbf{r}_G$ is zero.

iii) Average dipole. The very short time scale of the internal dynamics in comparison to the external ones, implies that in the expression for the expectation of the dipole, $\langle \mathbf{d} \rangle$, given by Equation (2.43), u and v can be replaced by their steady state values given in Equations (2.48) and (2.49), giving $\langle \mathbf{d}^{\,\mathrm{st}} \rangle$.

Finally then, under these, and all the previous approximations, the Ehrenfest equation (2.54) describing the force of the light upon the atom takes the form

$$m\ddot{\mathbf{r}}_G = \sum_{j=x,y,z} \left\langle d_j^{\mathrm{st}} \right\rangle \nabla \mathrm{E}_{cj}(\mathbf{r}_G, t). \tag{2.55}$$

2.7.2 The dissipative and reactive forces

All that remains in the determination of the light force acting on the atom is the insertion of the classical field

$$\mathbf{E}_c = \mathbf{E}_c(\mathbf{r},t) = \mathcal{P}\mathcal{E}_0(\mathbf{r}) \cos(\omega_L t + \phi(\mathbf{r})) \tag{2.56}$$

into Equation (2.55). $\mathcal{P}$ is the polarisation. Both the amplitude, $\mathcal{E}_0(\mathbf{r})$, and the phase, $\phi(\mathbf{r})$, vary in space to allow for a very general situation. The time origin can however, without loss of generality, always be arbitrarily chosen so that the phase, $\phi(\mathbf{r})$, is zero at the position of the atom $\mathbf{r} = \mathbf{r}_G$[9]:

$$\phi(\mathbf{r}_G) = 0. \tag{2.57}$$

The field (2.56) now coincides with that chosen for the derivation of the optical Bloch equations, Equation (2.5). Taking the gradient of the electric field gives

$$\nabla \mathrm{E}_{cj} = \mathcal{P}_j \left(\cos(\omega_L t)\nabla\mathcal{E}_0 - \sin(\omega_L t)\mathcal{E}_0\nabla\phi\right). \tag{2.58}$$

The steady state, average, dipole is

$$\langle d_j^{\mathrm{st}}\rangle = 2(\mathbf{d}_{ab})_j(u_{\mathrm{st}}\cos\omega_L t - v_{\mathrm{st}}\sin\omega_L t) \tag{2.59}$$

and its product with Equation (2.58) can now be integrated over an optical period (around a femto second) to obtain the mean radiative force upon the atom

$$\mathcal{F} = \sum_j \overline{\langle d_j\rangle \nabla \mathrm{E}_{cj}} = (\mathcal{P}\cdot\mathbf{d}_{ab})(u_{\mathrm{st}}\nabla\mathcal{E}_0 + v_{\mathrm{st}}\mathcal{E}_0\nabla\phi) \tag{2.60}$$

which is composed of two terms; the so called reactive force which depends on the amplitude gradient and the in-phase portion of the dipole,

$$\mathcal{F}_{\mathrm{react}} = (\mathcal{P}\cdot\mathbf{d}_{ab})u_{\mathrm{st}}\nabla\mathcal{E}_0 \tag{2.61}$$

and the dissipative force, proportional to the phase gradient and the quadrature component of the dipole

$$\mathcal{F}_{\mathrm{dissip}} = (\mathcal{P}\cdot\mathbf{d}_{ab})v_{\mathrm{st}}\mathcal{E}_0\nabla\phi. \tag{2.62}$$

2.7.3 Force due to a travelling wave

In the presence of a plane, travelling, wave, which has a phase gradient but no amplitude gradient,

$$\mathbf{E}_c(\mathbf{r},t) = \mathcal{P}\mathcal{E}_0\cos(\omega_L t - \mathbf{K}\cdot\mathbf{r}). \tag{2.63}$$

Only $\mathcal{F}_{\mathrm{dissip}}$ survives and may be written,

$$\mathcal{F}_{\mathrm{dissip}} = \Omega v_{\mathrm{st}}\hbar\mathbf{K} \tag{2.64}$$

[9] A non-zero $\phi(\mathbf{r}_G)$ could always be retained (parametrically) throughout the derivation of the optical Bloch equations, but it would just come along for the ride. As soon as the time integral over an optical period is taken in Equation (2.60) the specific value of the phase becomes irrelevant.

a force which acts in the direction of propagation of the wave. Comparison with Equation (2.50) shows that the dissipative force may also be written

$$\mathcal{F}_{\rm dissip} = \hbar\mathbf{K}\frac{\Gamma}{4}\frac{\Omega^2}{\Delta^2+\Gamma^2/4+\Omega^2/2} = \Gamma\sigma_{bb}^{\rm st}\hbar\mathbf{K} \tag{2.65}$$

and this leads to the following physical insight: the dissipative force is associated with the *absorption* followed by *spontaneous decay* cycle of the atom. The rate at which this cycle proceeds is governed by the probability for the atom to be in the upper state, σ_{bb}, multiplied by the spontaneous decay rate (which is the decay rate for an atom which, it must be remembered, is already in the excited state). The rate of change of the momentum of the atom is therefore this modified decay rate times the single photon momentum transferred upon absorption. An atom moving into the travelling wave will have its forward momentum reduced by scattering light into random directions. The absorption of energy from the laser modes (and consequent loss into the vacuum) with the familiar Lorentzian dependence on detuning from resonance, leads to the the label 'dissipative' force.

2.7.4 Force due to a standing wave

The superposition of two travelling waves results in a standing wave

$$\mathbf{E}_c(\mathbf{r},t) = \mathcal{P}\mathcal{E}_0\cos Kx\cos\omega_L t. \tag{2.66}$$

This time the phase is constant but the amplitude varies in space. Superficially then, it appears that $\mathcal{F}_{\rm dissip}$ is eliminated, and this is occasionally stated. One has to be careful though. It is true that the average force $\mathcal{F}_{\rm dissip}$ defined above does vanish, but this does *not* imply that there is no force due to spontaneous emission in a standing wave. This situation is an artefact of the symmetry of the two counter-propagating waves: being equally likely to take a photon from either mode leads, after many absorptions, to an atomic momentum distribution equally arranged about zero, but with a width corresponding to a random walk. One must not confuse an atom which really does have zero momentum, and one with a symmetrical distribution about zero[10]. For the purposes of spontaneous emission in the presence of symmetrical modes, such as in a standing wave, the dissipative force must be treated separately for each mode.

The spatially varying amplitude of the standing wave means the reactive force is also present

$$\mathcal{F}_{\rm react} = -\frac{\hbar\Delta}{2}\frac{\nabla\left(\Omega^2/2\right)}{\Delta^2+\Gamma^2/4+\Omega^2/2}. \tag{2.67}$$

[10]It is worth noting that the Ehrenfest equation, being a description of a local average itself, is unable to distinguish between wavepackets which are for instance, symmetrically split say, from those with a monotonic profile. Such splitting must occur, however, on the scale of the Bohr radius and so can be ignored here.

Note that the sign of this force can be reversed by switching from red detuning, $\omega_L < \omega_0$, to blue detuning, $\omega_L > \omega_0$, and vice versa. The dispersive (as opposed to Lorentzian absorption) dependence of this force is because it stems from a redistribution of energy between the laser modes, but with no loss to the vacuum. The atom takes photons from one mode and deposits them in the other by absorption and stimulated emission cycles. Each cycle transfers $2\hbar\mathbf{K}$ of momentum to the atom.

It is crucial for the work in subsequent chapters to observe that by operating with *large enough detunings*, the *dissipative* force in a standing wave can be *neglected* in comparison to the reactive force. If, and it's a big if, atoms can be selected with an internal structure that will still admit a two-level description despite larger and larger detunings (that is, other transitions are not excited), then, the model of long interaction times mediated solely by the *coherent* reactive force advocated by the majority of this thesis, becomes better and better.

2.7.5 The standing wave potential

The coherent nature of the reactive force implies that it might derive from some potential

$$\mathcal{F}_{\text{react}} = -\nabla V \tag{2.68}$$

and indeed Equation (2.67) is readily integrated giving

$$V = \frac{\hbar\Delta}{2} \ln\left(1 + \frac{\Omega^2/2}{\Delta^2 + \Gamma^2/4}\right). \tag{2.69}$$

When the detuning is large in comparison to the Rabi frequency, the logarithm can be expanded to give

$$V = \frac{\hbar\Delta}{2} \frac{\Omega^2/2}{\Delta^2 + \Gamma^2/4} \tag{2.70}$$

where $\Omega(x)$ contains the spatial dependence

$$\Omega(x) = \frac{d_{ab}\mathcal{E}_0 \cos Kx}{\hbar}. \tag{2.71}$$

This remarkable result supplies the external potential which a two-level atom in a detuned standing wave experiences. All the complexities of the internal structure are hidden away within it. With large detunings the atom is barely excited at all by the radiation field and is almost always in the ground state (limiting the possibility of a spontaneous emission)—the above potential is really for a ground state atom. Intuitively speaking, it is as if the potential results from a virtual transition where the atom flashes up to the excited state and back again. Alternatively it may be viewed as an AC Stark shift of the ground state [52] (but then the natural width of the upper state, Γ, does not appear in the formula). Elaborate theories do exist describing the 'bipotential'—one for the

dressed ground state and one for the dressed excited state—which results when there is only a small detuning, and the atom is frequently in the upper state. With a weak field, the Rabi frequency is small and the atom spends a relatively long period of time in either the upper or lower state and so really does move about in either of the two potentials. Transitions between these two potentials only occur at the most intense parts of the standing wave—the antinodes. Such interpotential flips can then be couched in the language of Landau-Zener transitions between the dressed states. This fascinating behaviour forms a significant part of the book by Kazantsev, Surdutovich and Yakovlev [45], but is of limited use if the interaction is long enough that spontaneous emission might occur (likely because of the small detuning) and will not be discussed further here.

Chapter 3

Classical atomic motion

3.1 Motivation

Under the conditions discussed in Chapter 2, the external degrees of freedom of an atom moving in a standing wave laser beam are governed by the potential given by Equation (2.70). This was derived using a quantum mechanical internal structure for the atom, but that in itself sets no restriction on whether the external motion of the atom should be considered as classical or quantum. Indeed, the character of the external motion is determined by the de Broglie wavelength of the atom, and this is in turn set by the strength of the potential. A strong potential can impart a large momentum to the atom producing much more classical behaviour than a weak potential capable of transferring only a small number of momentum quanta. A useful *device* for setting the value of the de Broglie wavelength is to vary the magnitude of $\hbar$. Of course $\hbar$ really has the value found in nature, so modifying $\hbar$ must in practice be achieved by varying parameters in the potential such as the electric field strength[1], in line with the statements above. The smaller $\hbar$ becomes, the smaller the resulting λ_{dB}. As λ_{dB} becomes significantly smaller than the scale of variation of the potential (set by λ_{laser}) one enters the realms of semiclassical mechanics and a rich set of phenomena, *caustics*, begins to emerge. Geometrical optics (classical mechanics) is the limit as $\lambda_{\mathrm{dB}} \to 0$. This limit is not a smooth one however, and the phenomena emergent at the onset of the semiclassical regime come to dominate the behaviour, and in some regions are even singular, demarking the failure of the classical mechanics. By examining the classical mechanics, this chapter cuts straight to the chase and focuses upon the features which in this limit are singular, and form the main preoccupation of this thesis.

[1] Confusion might arise because the potential (Equation (2.70)) itself contains $\hbar$. This is a different $\hbar$, pertaining to the internal dynamics, and its value is fixed at 1.05457×10^{-34}Js.

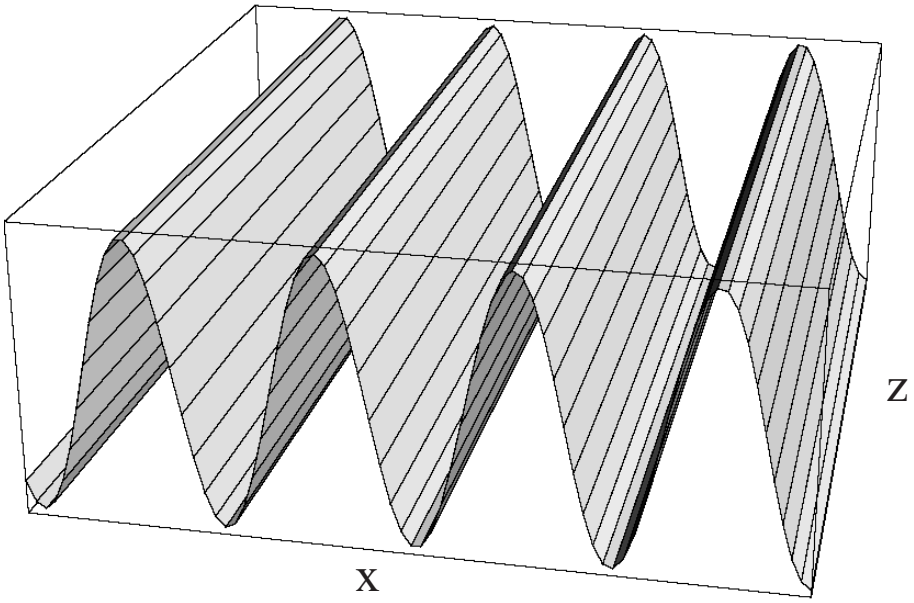

Figure 3.1: The washboard potential.

3.2 The classical Hamiltonian

Writing the potential given by Equation (2.70) out in full

$$V = \frac{d_{ab}^2 \mathcal{E}_0^2}{4\hbar} \frac{\Delta}{\Delta^2 + \Gamma^2/4} \cos^2 Kx \tag{3.1}$$

leads to the definition

$$V_0 \equiv -\frac{d_{ab}^2 \mathcal{E}_0^2}{4\hbar} \frac{\Delta}{\Delta^2 + \Gamma^2/4} \tag{3.2}$$

giving

$$V = -V_0 \cos^2 Kx. \tag{3.3}$$

The minus sign is inserted for convenience so that motion near the origin is in a potential well. The detuning, Δ, can be positive or negative so one is always at liberty to define things in this way. The motion of a particle in a 2-dimensional region having the above potential in the **x**, or transverse, direction, and a constant potential in the **z**, or longitudinal direction, is reminiscent of the motion of a marble on a 'washboard', see Figure 3.1, and obeys the Hamiltonian

$$H = \frac{P_x^2}{2m} + \frac{P_z^2}{2m} - V_0 \cos^2 Kx = E. \tag{3.4}$$

Since the potential does not explicitly contain z, motion in this direction is constant with time and P_z is conserved. As explained in Chapter 1, the large atomic momentum in the longitudinal

direction means the motion in this direction is largely ignorant of the existence of the potential 'slab', and so is almost unaffected by entry to, and exit from, the laser beam. The only influence of the potential upon the longitudinal motion is taken to be the very slight increase in P_z depending upon the transverse entry point, so that the energy is conserved for all the trajectories. If the atom beam is perpendicular to the laser then, initially, $P_x = 0$, so the longitudinal momentum of the atoms is

$$P_z = \sqrt{2m}\sqrt{E + V_0 \cos^2 K x_0} \tag{3.5}$$

where x_0 is the transverse entry point into the potential. The trajectory of the chosen atom is labelled by x_0.

The motion in the washboard potential is really only 1-dimensional—in the transverse direction. The constant longitudinal progress of the atom is super-imposed on top of this. The transverse motion is formally identical to that of an inflexible pendulum, and the Hamiltonian (3.4) is the pendulum Hamiltonian.

3.3 Phase space

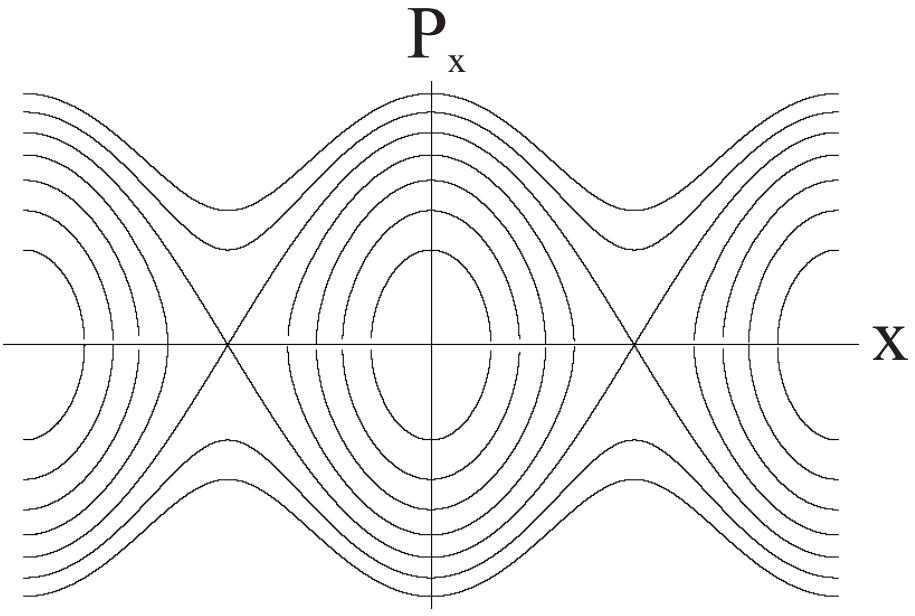

Figure 3.2: The phase space of a pendulum.

Before solving for the motion prescribed by the Hamiltonian (3.4), it is instructive to examine the phase space structure it generates. Figure 3.2 shows some energy contours in the (x,P_x) plane.

There are three contours for which the atom is in libration—trapped in a particular well. The places where the energy contours cut the x-axis are the turning points of the motion in configuration space (x), and the gradient of the energy contour with respect to x becomes infinite. The places where they cut the P_x axis, although well behaved in configuration space, are the turning points in momentum (P_x) space, where the gradient of the energy contour w.r.t. P_x becomes infinite.

The separatrix curve is at the exact border between libration and rotation. The turning points of the separatrix occur at the potential's maxima; the barrier tops. The motion of the particle at the separatrix turning point is infinitely slow. For perpendicular incidence, the separatrix represents the most energetic classical[2] contour possible—it is impossible for the atom to go into rotation. For non-perpendicular incidence, the atoms start with a non-zero transverse momentum and so are able to roll over into the next well, which is rotation (for a pendulum this is the motion which goes right over the top—through the upper, unstable, equilibrium point). Two rotation contours are depicted in Figure 3.2

3.4 Geometrical ray optics

3.4.1 Solution of the trajectory equation

Particles subject to the Hamiltonian (3.4) execute pendulum motion independently in the transverse direction, but this is stretched out along the longitudinal direction. Re-expressing the transverse momentum in Equation (3.4) gives

$$\frac{m}{2}\left(\frac{dx}{dt}\right)^2 + \frac{P_z^2}{2m} - V_0 \cos^2 Kx = E. \tag{3.6}$$

The conservation of P_z means that time and longitudinal distance z are proportional, for $z = tP_z/m$, and so time can be eliminated in favour of z

$$\frac{dx}{dt} = \frac{dx}{dz}\frac{dz}{dt} = \frac{P_z}{m}\frac{dx}{dz} \tag{3.7}$$

so solutions for the trajectories in the (x, z) plane can be sought. For perpendicular incidence, the initial condition at the front edge of the slab (which is defined to be at $z = 0$) is

$$\frac{dx}{dz} = 0. \tag{3.8}$$

Inserting the value of the longitudinal momentum for a transverse entry point, x_0, given by Equation (3.5), together with Equations (3.7) and (3.8) into the Hamiltonian (3.6), gives the trajectory equation

$$\frac{P_z^2}{2m}\left(\frac{dx}{dz}\right)^2 = V_0(\cos^2 Kx - \cos^2 Kx_0) \tag{3.9}$$

[2]Quantum mechanically the above barrier eigenstates are weakly excited even for perpendicular incidence.

and so the problem is reduced to quadrature

$$\int_{x'=x_0}^{x'=x} \frac{dx'}{\sqrt{\cos^2 Kx' - \cos^2 Kx_0}} = \int_{z'=0}^{z'=z} \frac{\sqrt{2mV_0}}{P_z}\, dz' \,. \tag{3.10}$$

The right hand side is integrated immediately, and the l.h.s. is soon converted into a standard form,

$$\begin{aligned}\int_{x'=x_0}^{x'=x} \frac{dx'}{\sqrt{\cos^2 Kx' - \cos^2 Kx_0}} &= \int_{x'=x_0}^{x'=x} \frac{dx'}{\sqrt{\sin^2 Kx_0 - \sin^2 Kx'}} \\ &= \frac{\sqrt{\mu}}{K} \int_{Kx'=Kx_0}^{Kx'=Kx} \frac{d(Kx')}{\sqrt{1-\mu \sin^2 Kx'}}\end{aligned} \tag{3.11}$$

with

$$\mu \equiv \frac{1}{\sin^2 Kx_0}. \tag{3.12}$$

The structure of the integrand matches that of an elliptic integral, but the integration range must first be altered to give the correct limits

$$\int_{Kx_0}^{Kx} (\dots)\, d(Kx') = \int_0^{Kx} (\dots)\, d(Kx') - \int_0^{Kx_0} (\dots)\, d(Kx') \tag{3.13}$$

then

$$\int_{x'=x_0}^{x'=x} \frac{dx'}{\sqrt{\cos^2 Kx' - \cos^2 Kx_0}} = \frac{\sqrt{\mu}}{K} \left[\mathrm{F}(Kx|\mu) - \mathrm{F}(Kx_0|\mu)\right] \tag{3.14}$$

where $\mathrm{F}(\phi|m)$ is the incomplete elliptic integral of the first kind [1], with amplitude ϕ and parameter m. See Appendix A for a summary of the properties of the elliptic integrals.

To ensure that the integrand of Equation (3.11) is explicitly real throughout the integration range, μ must satisfy

$$0 \le \mu \le 1 \tag{3.15}$$

which from the definition (3.12) is clearly not the case. This can be remedied by use of the transformation [1]

$$\mathrm{F}(\phi|m) = \frac{1}{\sqrt{m}} \mathrm{F}(\theta|1/m)\,, \qquad \sin\theta = \sqrt{m}\sin\phi \tag{3.16}$$

which, when applied to the two terms on the r.h.s. of Equation (3.14), gives

$$\frac{\sqrt{\mu}}{K}\mathrm{F}(Kx|\mu) = \frac{1}{K}\mathrm{F}(\arcsin(\sqrt{\mu}\sin Kx)\,|1/\mu) \tag{3.17}$$

$$\begin{aligned}\frac{\sqrt{\mu}}{K}\mathrm{F}(Kx_0|\mu) &= \frac{1}{K}\mathrm{F}(\arcsin(\sqrt{\mu}/\sqrt{\mu})\,|1/\mu) \\ &= \frac{1}{K}\mathrm{K}(1/\mu)\end{aligned} \tag{3.18}$$

where $\mathrm{K}(m) = \mathrm{F}(\pi/2|m)$ is the *complete* elliptic integral of the first kind. In this way the quadrature Equation (3.10) becomes

$$\frac{K\sqrt{2mV_0}}{P_z} z = \mathrm{F}(\arcsin(\sqrt{\mu}\sin Kx)|1/\mu) - \mathrm{K}(1/\mu). \tag{3.19}$$

As it stands, Equation (3.19) is not very useful since one wants to express the transverse position x as a function of longitudinal distance travelled, z, not the other way around as above. This inversion can be accomplished using Jacobian elliptic functions [1], which are defined so that if

$$u \equiv \mathrm{F}(\phi|m) \tag{3.20}$$

then the two elliptic functions $\mathrm{sn}(u|m)$ and $\mathrm{cn}(u|m)$ are

$$\mathrm{sn}(u|m) = \sin\phi \tag{3.21}$$

$$\mathrm{cn}(u|m) = \cos\phi. \tag{3.22}$$

Again, refer to Appendix A for more background information.

Administering these transformations to Equation (3.19), the transverse position as a function of z gives the result (well known of course for a pendulum, and also in the diffraction of light by ultrasound [16]),

$$\sin Kx = \frac{1}{\sqrt{\mu}}\,\mathrm{sn}\left(\frac{K\sqrt{2mV_0}z}{P_z} + \mathrm{K}\left(\frac{1}{\mu}\right)\middle|\,\frac{1}{\mu}\right). \tag{3.23}$$

The instantaneous angle between the trajectory and the z-axis, ϑ, is extremely small in supersonic beam atom optics, usually of the order of 10^{-5} radians, and is determined by the ratio of the two components of the momentum, which is in turn equal to the gradient

$$\vartheta \approx \tan\vartheta = \frac{P_x}{P_z} = \frac{dx}{dz}. \tag{3.24}$$

Since P_z is a constant, transverse momentum and angle are proportional, and the two terms will often be used interchangably. The (transverse) momentum space description of the trajectories is found by substituting the configuration space solution, Equation (3.23), into the original differential trajectory equation, (3.9), and making use of the identity $\mathrm{sn}^2(u|m) + \mathrm{cn}^2(u|m) = 1$,

$$\vartheta \approx \frac{dx}{dz} = \frac{\sqrt{2mV_0}}{P_z\sqrt{\mu}}\,\mathrm{cn}\left(\frac{K\sqrt{2mV_0}z}{P_z} + \mathrm{K}\left(\frac{1}{\mu}\right)\middle|\,\frac{1}{\mu}\right). \tag{3.25}$$

It is convenient to define certain dimensionless quantities which may be referred to as the 'classical transverse position', x_c, and the 'classical longitudinal position', z_c,

$$x_c \equiv Kx \tag{3.26}$$

$$z_c \equiv \frac{\sqrt{2mV_0}Kz}{P_z}. \tag{3.27}$$

Strictly speaking, since P_z is a very weak function of x_0, as given by (3.5), then z_c should also depend very slightly upon x_0. The classical distance, z_c, would then be different for each trajectory. However, the complete domination of P_z over P_x means that one is usually safe in neglecting this fine adjustment. The exception comes when considering the phase along a ray, which involves

exponentiating the momenta, as will be discussed in Section 3.4.3 and in Appendix B. Otherwise z_c will be assumed to be independent of x_0. In terms of the 'classical' scaled distances, the configuration space trajectory equation, (3.23), and the momentum space trajectory equation, (3.25), reduce to

$$\sin x_c = \frac{1}{\sqrt{\mu}}\mathrm{sn}(z_c + \mathrm{K}(1/\mu)\,|\,1/\mu) \tag{3.28}$$

$$\vartheta_c \approx \frac{dx_c}{dz_c} = \frac{1}{\sqrt{\mu}}\mathrm{cn}(z_c + \mathrm{K}(1/\mu)\,|\,1/\mu) \tag{3.29}$$

where the previous small angle approximation is taken to be an equality. Figure 3.3 shows a selection of configuration space geometrical 'rays' for 41 different entry points x_0 equally spaced across one cell of the washboard potential. Figure 3.4 shows the same rays in momentum space. Such pictures have appeared before in the context of the diffraction of light by ulrasound [16, 61, 49] but not in reference to atom optics. The review article [2] does contain an example of a classical atomic momentum distribution in a standing wave, generated by calculating the number of rays which, at a particular depth z, have angles lying between ϑ and $\vartheta + d\vartheta$. When these slices, each of which is for a consecutive value of z, are laid next to one another, the result is a course grained interpretation of Figure 3.4. Similar pictures, in the individual slice format, will also be presented later in this chapter as they are the best way to make a quantitative comparison between the quantum and the classical mechanics.

After comparing the picture of the momentum distribution as a function of z with the quantum version and stating that it "illustrates that many of the features of the light atom interaction can be understood classically", reference [2] goes no further. The reason is that the essence of the classical mechanics lies in the trajectories themselves, a full understanding of which cannot come from the result of their summation, such as in a momentum distribution. In attempting to understand the quantum mechanics however, it *is* indeed *families* of trajectories which are important.

3.4.2 Simple harmonic motion

The simple pendulum corresponds to the small angle solution of the Hamiltonian (3.6). The equivalent situation for atoms follows in exactly the same way: by restricting x_0 to be small. Then the atoms roll around only in the very bottom of the washboard valleys, and the potential they experience is well approximated by

$$V = V_0(x^2 - 1) \tag{3.30}$$

which is of course, apart from the irrelevant constant, $-V_0$, the simple harmonic potential. Oscillations in a harmonic potential are very special since they are all isochronous. The sine curve

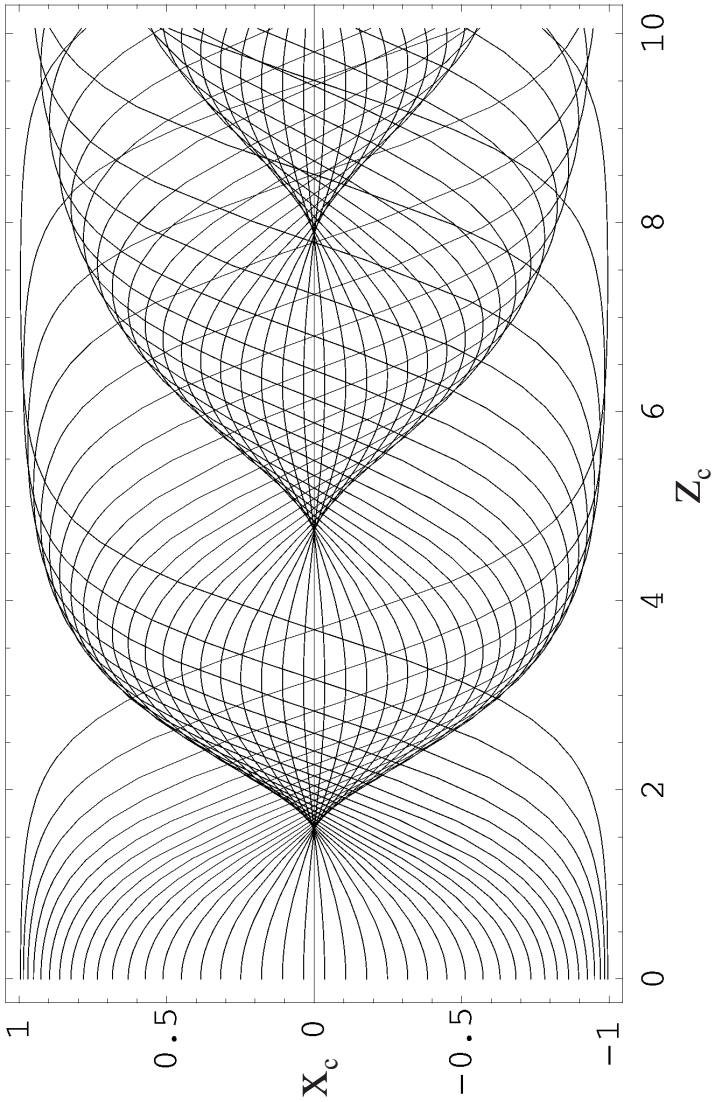

Figure 3.3: Configuration space ray trajectories

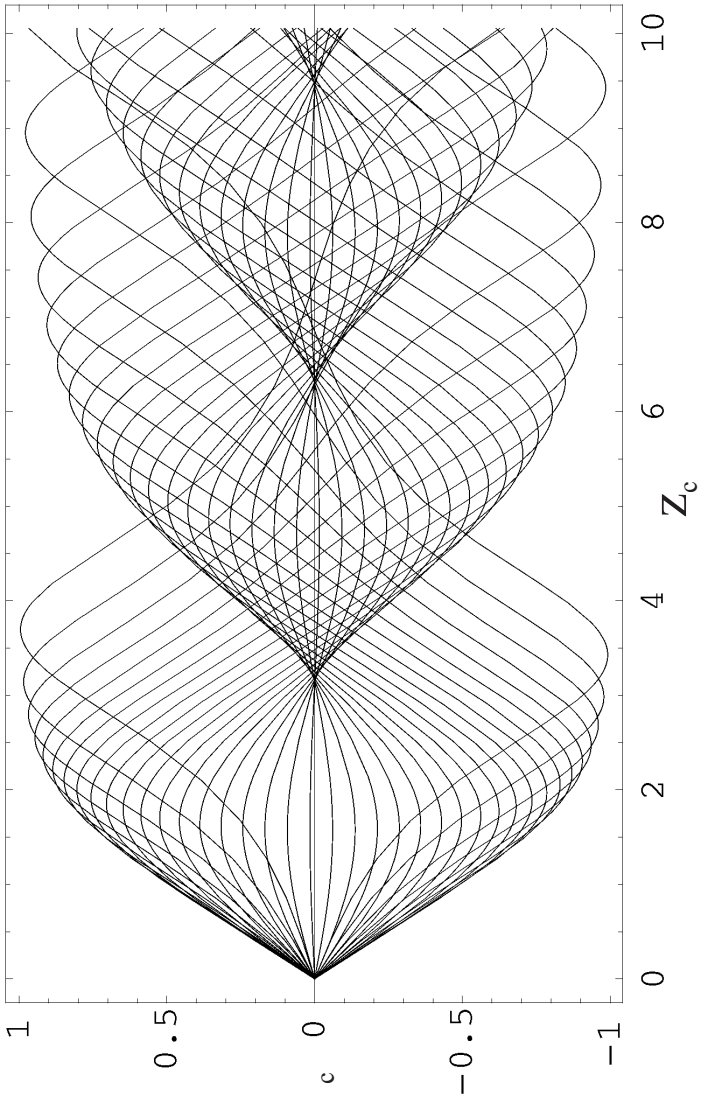

Figure 3.4: Momentum space ray trajectories

solutions

$$x_c = \frac{1}{\sqrt{\mu}} \sin(z_c + \pi/2) \tag{3.31}$$

in the potential (3.30) all have exactly the same period in z ($\propto t$). In particular this means the atom rays are all focussed exactly onto the z axis at the points

$$z_c = (2m+1)\frac{\pi}{2}\,, \qquad m = 0, 1, 2, \ldots \tag{3.32}$$

and indeed the small x_0 trajectories of Figure 3.3 act in this way. This is why lenses are parabolic of course, and if the atoms could be constrained to enter only the parabolic valley floors then the standing wave would act as an atomic lens. Such a device might prove crucial in atom lithography in the semi-conductor industry[3] [54]. The interest here, however, is precisely the smearing of the focus points by the non-harmonic parts of the standing wave. The orbits starting higher up the valley sides miss the foci. The correct description of this apparent anomaly is through catastrophe optics [17].

3.4.3 Caustics and catastrophe theory

Impossible symmetry

Focus points are the most intense parts of an optical field, and as such deserve special attention. It is therefore an important paradigm shift to realise that the familiar focus *point* (or line ...) is highly unlikely—perhaps even impossible for a macroscopic system. This is because they require absolutely perfect symmetry: in the 2-dimensional case, the lens must be perfectly parabolic. Clearly this is rarely the case, and, critically, foci are *unstable* to perturbations in the symmetry—when the parabolic wells become a sinusoid, the foci burst into the cusped structures of Figures 3.3 and 3.4. The focus points have become *caustics*[4]. Like a focus point, caustics are intense, since they are formed from the locus of points where rays touch—a finite amount of energy is concentrated into an infinitely small region—and so both focal points and caustics are singularities of the ray theory. Unlike focus points, caustics have an extended structure and their basic morphology is stable to further perturbation. A focus is best thought of as the limiting form of a caustic as the perturbation in the symmetry is taken to zero. Prior to catastrophe optics, caustics (or 'aberrations' as they are often referred to—a very revealing choice of terminology) were dealt with in a piecemeal fashion—each geometry and the manner in which its symmetry is broken, was treated, by and large, individually. Catastrophe optics systematically categorises the different

[3]The small de Broglie wavelength of atoms manipulated by laser standing waves potentially allows a much finer pattern of tracks to be etched onto computer chips than conventional optical lithography, which is diffraction limited to track spacings of about 100nm.

[4]The word caustic comes from the Greek 'to burn'.

types of caustics which can occur depending on the number of available parameters and variables of the system. The concrete basis for the categorisation is through what is known in catastrophe theory as the generating function, and will be referred to here as S; in optics this is just the optical distance and in mechanics it is the action (in the sense of action-angle variables).

The generating function

Consider a plane wave propagating in two dimensions with a wave vector $\mathbf{K} = (K_x, K_y)$,

$$\psi = \cos(K_x x + K_z z). \tag{3.33}$$

The optical distance, μ, the wave has travelled measures the change in the phase of the wave along its path, and in this case it is the sum $K_x x + K_z z$. In an inhomongeneous medium the wavevector components depend on position, and the optical distance must be found by integrating along the path of propagation. If $d\mathbf{q}$ is an infinitesimal configuration space path element, then

$$\mu = \int \mathbf{K}(\mathbf{q}) \cdot d\mathbf{q}. \tag{3.34}$$

The parallel quantity in mechanical systems is the action, S, which stems from the relation $p = \hbar K$, and so the total action in configuration space is given by a line integral along the classical path (see [76], or Appendix B)

$$S = \hbar\mu = \int_{q_0}^{q} \sum_{j=1}^{n} p_j dq_j \tag{3.35}$$

where q represents the configuration space co-ordinates. The weak x_0 dependence of the longitudinal momentum P_z is introduced through Equation (3.5), and the transverse momentum for an atom entering the potential at position x_0 is, from the energy equation (3.4),

$$P_x = \sqrt{2mV_0}\sqrt{\cos^2 Kx - \cos^2 Kx_0}. \tag{3.36}$$

Substituting the momenta into the expression for the action (3.35) gives

$$S = \int P_z(x_0)\, dz + \sqrt{2mV_0}\sqrt{\cos^2 Kx - \cos^2 Kx_0}\, dx \tag{3.37}$$

where dx and dz are constrained to lie along the path of integration. However, the classical paths—the rays—have already been figured out, as functions of z, directly from the energy equation (3.6). The path integral (3.37) may thus be written as a simple integral in z, with

$$dx = \frac{dx}{dz} dz. \tag{3.38}$$

Noting that P_x may be written as a function of z from

$$\frac{P_x}{P_z} = \frac{dx}{dz} \tag{3.39}$$

where dx/dz is the solved momentum space trajectory (3.25), the configuration space action becomes

$$S = \int_0^z P_z dz' + P_z \left(\frac{dx}{dz'}\right)^2 dz'. \tag{3.40}$$

So substituting in the scaled momentum trajectory solution (3.29), the scaling definitions (3.26), (3.27), and the parameter (3.12), the action becomes

$$\begin{aligned} S =& \frac{P_z^2(x_0)}{K\sqrt{2mV_0}} z_c(x_0) \\ &+ \frac{\sqrt{2mV_0}}{K} \sin^2 x_{0_c} \int_0^{z_c} \mathrm{cn}^2 \left(z_c'(x_0) + \mathrm{K}(\sin^2 x_{0_c}) \middle| \sin^2 x_{0_c} \right) dz_c'. \end{aligned} \tag{3.41}$$

The remaining integral can be written in terms of the known result [1]

$$m \int_0^u \mathrm{cn}^2(t|m) dt = \mathrm{E}(\,\mathrm{arcsin}[\mathrm{sn}(u|m)]\,|\,m) + (m-1)u \tag{3.42}$$

where $\mathrm{E}(\phi|m)$ is an elliptic integral of the second kind (see Appendix A). So now the action becomes

$$\begin{aligned} S(z_c) =& \frac{P_z^2(x_0)}{K\sqrt{2mV_0}} z_c(x_0) \\ &+ \frac{\sqrt{2mV_0}}{K} \left[\mathrm{E}\left(\mathrm{arcsin}\left[\mathrm{sn}(z_c(x_0) + \mathrm{K}(\sin^2 x_{0_c}) \,|\, \sin^2 x_{0_c})\right] \,\middle|\, \sin^2 x_{0_c}\right) \right. \\ &\left. + (\sin^2 x_{0_c} - 1) z_c(x_0) - \mathrm{E}(\sin^2 x_{0_c}) \right]. \end{aligned} \tag{3.43}$$

The action appears to be only a function of z and x_0, and this is indeed true once a value of x_0, which labels the paths, has been chosen, since the transverse position x, as a function of z, is known via the trajectory equation. However, one could also choose a position in configuration space, (x, z) and ask what is the action along the allowed classical paths to that point. From this point of view, x_0 is a variable that labels a classical path compatible with the condition that the path goes to (x, z). In general there may be more than one path—each labelled by its value of x_0. Recognising that the amplitude of the elliptic integral in Equation (3.43), $\mathrm{sn}(z_c + \mathrm{K}(\sin^2 x_{0_c}) \,|\, \sin^2 x_{0_c})$, is actually the configuration space trajectory equation (3.28), and rewriting the second of the z_c terms[5] using the uninverted trajectory equation (3.19), the x dependence of the action can be restored (one is in effect undoing the preordained knowledge of x—that comes from choosing a

[5] As explained in Appendix B, the total action is the sum of the two component actions—one depending only on x, the other only on z.

particular value of x_0—and thus releasing x_0 to be a variable)

$$\begin{aligned} S(x_{0_c}; x_c, z_c) = & \frac{P_z^2(x_0)}{K\sqrt{2mV_0}} z_c(x_0) \\ & + \frac{\sqrt{2mV_0}}{K} \left[\mathrm{E}\left(\arcsin\left[\frac{\sin x_c}{\sin x_{0_c}} \right] \,\middle|\, \sin^2 x_{0_c} \right) \right. \\ & + \cos^2 x_{0_c} \mathrm{F}\left(\arcsin\left[\frac{\sin x_c}{\sin x_{0_c}} \right] \,\middle|\, \sin^2 x_{0_c} \right) \\ & \left. - \mathrm{E}(\sin^2 x_{0_c}) - \cos^2 x_{0_c} \mathrm{K}(\sin^2 x_{0_c}) \right]. \end{aligned} \tag{3.44}$$

Reiterating, in Equation (3.44) it is understood that as soon as the values of x_c and z_c are specified only certain values of x_0 are allowed: these are of course the solved classical trajectories which connect (x_{0_c},0) to (x_c,z_c). The notation $S(x_{0_c}; x_c, z_c)$ reflects this significance: x_{0_c} is a *state variable* and the semicolon separates it from the *control parameters* x_c and z_c. The control parameters set conditions on the rays: suppose, for instance, that the detector were positioned at (x_c,z_c), then one is only interested in the rays which pass through that point. The 'control space', generally spanned by co-ordinates $C = C(c_1, c_2, \ldots)$, but where here there are only $c_1 = x_c$ and $c_2 = z_c$, is the space in which the caustics live. Examining Figures 3.3 and 3.4 one can see that by choosing different values of (x_c,z_c) one can search out the caustics. The state variable x_0 labels the possible rays which match the conditions set by the control parameters. In this case the 'state space', $s = s(s_1, s_2, \ldots)$, has only one dimension, $s_1 = x_{0_c}$, and the control space two, but in general they may have more (or less). The codimension $\mathcal{K}$ is defined to be the dimensionality of the control space minus the dimensionality of the caustic. $\mathcal{K}$ gives the minimum number of control space co-ordinates which must be varied to find the caustic.

3.4.4 The fold and cusp catastrophes

A comprehensive introduction to the Arnol'd-Thom catastrophe theory [5, 80] is beyond the scope of this discussion, but certain remarkable results[6] will be loosely given here. In particular, catastrophe theory makes the following very powerful statement: subject to certain very reasonable conditions, the only structurally stable catastrophes (caustics) which can occur in a 2-D control space are the *fold*, which has $\mathcal{K} = 1$, and the *cusp*, which has $\mathcal{K} = 2$. Thus the two allowed types of caustics are therefore lines (the folds) and points (the cusps) in the control space plane (x,z). Furthermore, the generating function in the vicinity of these caustics maybe written, up to a diffeomorphism, as one of the *normal forms*: polynomials which are linear in the control parameters C, but non-linear in the state variables s. A diffeomorphism is a smooth (differentiable), reversible transformation of the co-ordinates; let $\bar{C}$ and $\bar{s}$ be the transformed variables. The diffeomorphism

[6] Reference should be made to the very readable review of catastrophe optics by M. V. Berry, [17].

relates different actual realisations of catastrophes which are essentially the same—up to a rotation or translation for instance. In general though, the transformation may be any which meets the criteria of a diffeomorphism. In practice, this means finding the transformation which converts the particular generating function one is dealing with into its normal form may be tricky. For the fold one has the cubic normal form

$$S(\bar{s};\bar{C}) = \frac{\bar{s}^3}{3} + \bar{C}\bar{s} \tag{3.45}$$

whereas the cusp has a quartic normal form

$$S(\bar{s};\bar{C}) = \frac{\bar{s}^4}{4} + \bar{C}_2\frac{\bar{s}^2}{2} + \bar{C}_1\bar{s}. \tag{3.46}$$

In reference to Figures 3.3 and 3.4, the folds form the majority of the caustic structure which is along envelopes formed from the points where the rays just overlap. The cusps are the singular points where the lower and upper arms of each fold meet. They are situated where the parabolic focus points would be.

The classical trajectories are those along which the action is stationary w.r.t. infinitesimal variations of the path. This may be interpreted as saying that the classical paths are the result of the constructive interference of quantum waves propagating through the system. As the wavelength is reduced, destructive interference channels all the intensity onto the classical paths. Within this semiclassical view of the world, the significance of the action is that it acts as a phase for the quantum waves. In specifying the normal forms (3.45) and (3.46), the machinary of catastrophe theory has therefore specified the form of the wavefunction near these caustics.

The equivalence of the action (3.44) to the normal forms (3.45) and (3.46) will not be demonstrated here—the algebra produced by the elliptic functions is too complicated. This will wait until after the quantum mechanics has been introduced. The normal forms will then appear quite naturally in Chapter 9. The significance of the normal forms will be discussed further in Section 3.6

3.5 Classical scattering

3.5.1 The angular intensity distribution

Upon emerging from the interaction region into free space, the atoms travel in straight lines towards the farfield where they are detected. Thus the farfield scattering pattern produced after an interaction distance $z_c = D$ is exactly that found at the position $z_c = D$ in Figure 3.4. Considered as a probability distribution, the probability $I\,d\theta$ that a particle is scattered into an angle lying between θ and $\theta + d\theta$ is equal to the probability $G\,dx_{0_c}$ that it arrives at a transverse position lying between x_{0_c} and $x_{0_c} + dx_{0_c}$, where all the x_{0_c} contained in this strip correspond to trajectories

which at $z_c = D$ lie in the specified angular range. One writes

$$I(\theta)\, d\theta = G(x_{0_c})\, dx_{0_c}. \tag{3.47}$$

The goal is to find $I(\theta)$, which gives the relative intensity (probability) as a function of angle. So, rearranging,

$$I(\theta) = G(x_{0_c}) \frac{1}{|\frac{d\theta}{dx_{0_c}}|}. \tag{3.48}$$

Generally though, more than one distinct classical path can have the same transerse momentum at the point D, so the relative intensity becomes the sum over these paths, each labelled by its entry point $x_{0_c}^q$

$$I(\theta) = \sum_q G(x_{0_c}^q) \frac{1}{|\{\frac{d\theta}{dx_{0_c}}\}_q|} \tag{3.49}$$

where $\{d\theta/dx_{0_c}\}_q$ means $d\theta/dx_{0_c}$ evaluated at $x_{0_c}^q$.

3.5.2 Ray tubes

A classical trajectory is an infinitely fine path with no width in x_0. A uniform, infinitely wide atomic beam has $G(x_{0_c})$ equal to a constant determined by the normalisation. Thus there are an infinite number of possible trajectories which are all equally pursued by point particles. In deriving the angular intensity distribution one implicitly introduces the concept of a ray tube—something which has an initial width dx_{0_c} and has associated with it an amplitude $|d\theta/dx_{0_c}|^{-1/2}$. The amplitude quantifies the angular behaviour of the neighbouring rays which make up the tube: if there is only a small angular variation at $z_c = D$, so that the rays lying in the range dx_{0_c} about x_{0_c} are mostly travelling in the same direction, then the amplitude is large and that direction will consequently have large intensity. The square of the amplitude is actually the Jacobian of the mapping between the state space and the control space.

Ray tubes are objects associated with families of rays: a ray tube constitutes the first intuitive step towards a wave description. One can associate with each tube a phase given by the action along the classical path taken by, say, the central ray of the tube. The intensity received at a point is the modulus squared of the interfering ray tube sum

$$\psi(x,z) \approx N \sum_q \frac{1}{\sqrt{\{\frac{d\theta}{dx_{0_c}}\}_q}} \mathrm{e}^{\mathrm{i}\tilde{S}^q(x_{0_c};\vartheta_c,z_c)/\hbar} \tag{3.50}$$

where N is the normalisation, and the amplitude of the q^{th} ray tube is

$$\frac{1}{\sqrt{\{\frac{d\theta}{dx_{0_c}}\}_q}}. \tag{3.51}$$

The phase $\tilde{S}^q(x_{0_c};\vartheta_c,z_c)$ is the momentum space analogue of that given by Equation (3.44). Remarkably then, an approximation to the wavefunction has been found using only classical mechanics and some intuition. A much fuller derivation is given in Appendix B. Unfortunately though, the interfering ray tube sum contains a serious flaw. Caustics have been defined as regions where the individual rays touch—the envelope of a ray family—and are therefore places where a ray tube is focused. All the constituent rays are travelling in the same direction. Referring to Figure 3.4, along an angular caustic the contributing rays have no variation in angle, and each ray represents an infinitesimal change in x_{0_c}. This implies that the amplitude is infinite on the caustics, so the approximation (3.50), and the classical intensity distribution (3.49), break down at exactly the most interesting parts of the scattering pattern.

Note that the modulus of the amplitude has not been taken in the wavefunction expression (3.50). This is because the phase of the amplitude must also be taken into consideration. When a ray takes part in a caustic the inverse of the square of the amplitude, $d\theta/dx_{0_c}$ has a simple zero, and so the phase of the amplitude abruptly changes by π. This is sometimes referred to as 'the phase anomaly at focus' [19]. If this phase is an increase then Equation (3.50) can be written

$$\psi(x,z) \approx N\sum_q \frac{1}{\sqrt{|\{\frac{d\theta}{dx_{0_c}}\}_q|}} \mathrm{e}^{\mathrm{i}\tilde{S}^q(x_{0_c};\vartheta_c,z_c)/\hbar - \mathrm{i}m_q\pi/2} \tag{3.52}$$

where m_q is known as the Maslov index and is a positive integer recording the number of caustics the q^{th} ray has contributed to.

3.5.3 The deflection function

Clearly ϑ_c, as given by Equation (3.29), is responsible for determining the classical scattering behaviour and is sometimes referred to as the deflection function. An examination of the behaviour of this deflection function will lead to a better understanding of the scattering information contained in Figure 3.4. An immediate consequence of Equation (3.29) (or indeed of Equation (3.9)) is that the maximum angle to the z-axis that a ray can achieve is

$$\vartheta_{c_{max}} = 1. \tag{3.53}$$

Physically this corresponds to the maximum transverse momentum that an atom can gain by rolling from the top of a barrier to the valley floor. Figure 3.5 depicts the behaviour of the deflection function at various different depths through the interaction region. Each picture shows the deflection angle achieved by atoms which, at $z_c = 0$, had initial transverse position x_{0_c}. The maxima and minima of these graphs are places where the derivative of the deflection w.r.t. x_{0_c} vanishes and so show which x_{0_c} contribute to caustics at that depth. Each graph is separated from

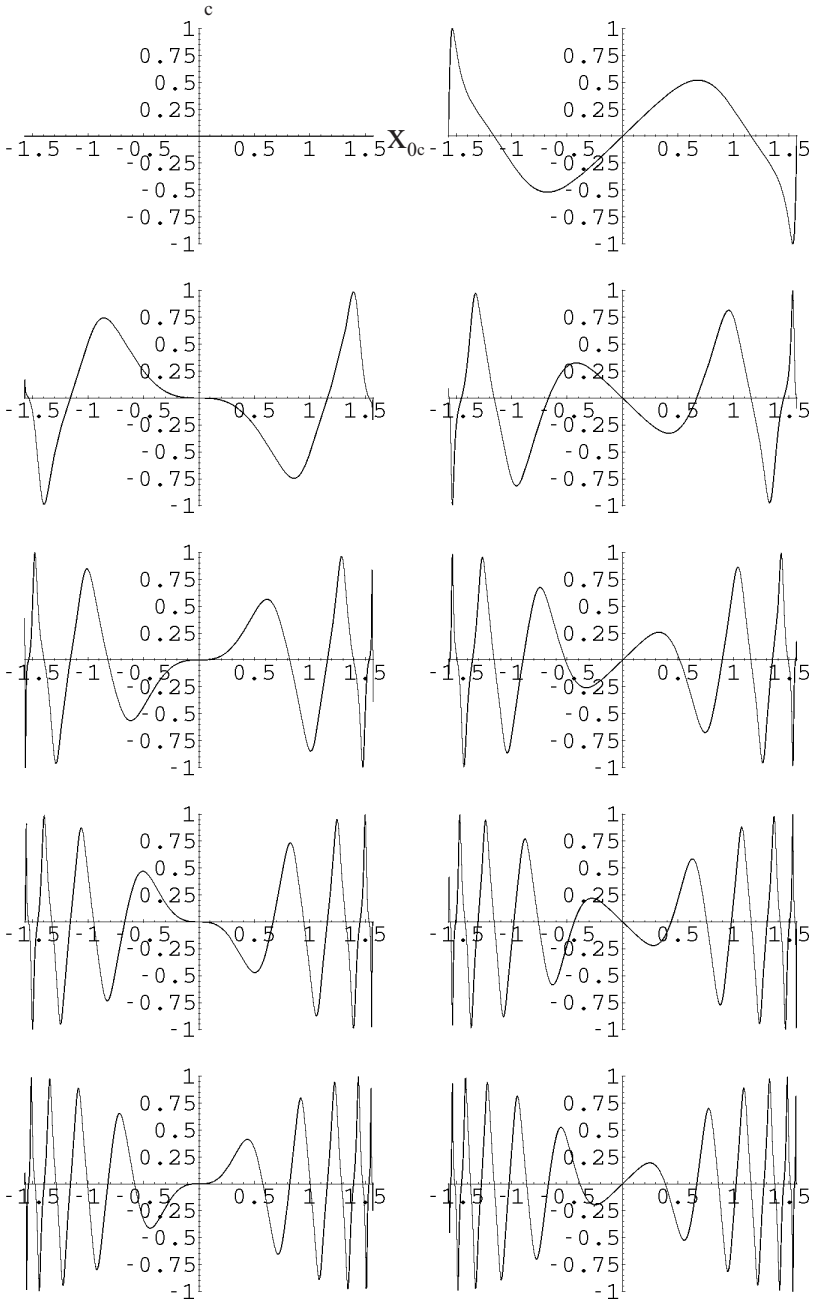

Figure 3.5: A series of plots of the deflection function $\vartheta_c(x_{0_c}, z_c)$ as a function of the *initial* transverse position x_{0_c}, for selected values of z_c. The top left plot has $z_c = 0$, then z_c increases in steps of $3\pi/2$ to the bottom right picture which has $z_c = 27\pi/2$. The maxima and minima represent caustics.

the next by a longitudinal depth, z_c, of $3\pi/2$. By taking the small angle limit of the deflection function equation (3.29) (which corresponds to the parabolic well) the momentum-space-caustic cusp tips, which lie along the z-axis, are found to be located at

$$z_c = 0,\ \pi,\ 2\pi,\ 3\pi, \ldots \tag{3.54}$$

So the deflection graphs alternately lie on, and halfway between, depths at which new caustics are born. This is reflected in the flatness of alternate graphs close to $x_{0_c} = 0$ which gives rise to the very intense cusp tips. As one moves beyond the cusp tips, the caustics flow outwards as folds and build up at the edges. As the folds move outwards their maxima and minima grow shaper—a narrower range of x_{0_c} contribute to them and so they grow weaker. The second derivative of ϑ_c with respect to x_{0_c}, evaluated at the caustic, gives a rough estimate of this behaviour.

3.5.4 A crude calculation of the intensity distribution

To calculate the intensity at a particular point in either configuration or momentum space, whether using the classical or the interfering ray tube expressions, requires a knowledge of which trajectories pass through that point. This is not a simple task as one must invert the deflection function (if it is indeed the angular distribution in which one is interested) to find x_{0_c} as a function of ϑ_c and z_c. Referring to Equation (3.29), and noting that $\mu = 1/\sin^2 x_{0_c}$, it is evident that x_{0_c} appears at three different positions in the expression so inversion is difficult. Methods for finding these trajectories will be discussed in Section 3.5.5. If however, one simply requires a rough estimate for the entire intensity distribution, then a crude but simple method is to take a sample set of trajectories, spaced equally in x_{0_c} say, and propagate them for the required z_c distance. Counting the number that lie in the range $\theta \to \theta + d\theta$ gives an approximation to $I(\theta)$. The accuracy of this method depends both on the number, n, of angular 'bins' of width $d\theta_c = 2/n$, into which the total angular range of 2 (in units of $\vartheta_{c_{max}}$, see Equation (3.53)) is divided, and the number of sample trajectories used. Figures 3.6, 3.7, 3.8 were produced using this prescription, though they show only half the angular range. For perpendicular incidence $I(\theta)$ is symmetrical about $\theta = 0$. Note that, classically, $I(\theta)$ diverges on the caustics. Despite the divergences however, the intensity pattern is still normalisable. Very close to the caustic the intensity goes as $1/\sqrt{\theta}$ and this is integrable[7]. These figures of course have only finite peaks since, numerically, one can only include a finite number of trajectories. The numerical binning procedure also leads to the fine 'jitter' that appears in the intensity profiles—in reality they should be smooth (except at the caustic).

[7]From W.K.B. treatments for instance, to which the current method is closely related, the divergence of the intensity at turning points of the motion, where the momentum P vanishes, goes as $1/P$. Turning point divergences are, however, features associated with a single trajectory, not a family such as with a caustic, so the two are not quite the same. See Appendix B for more discussion.

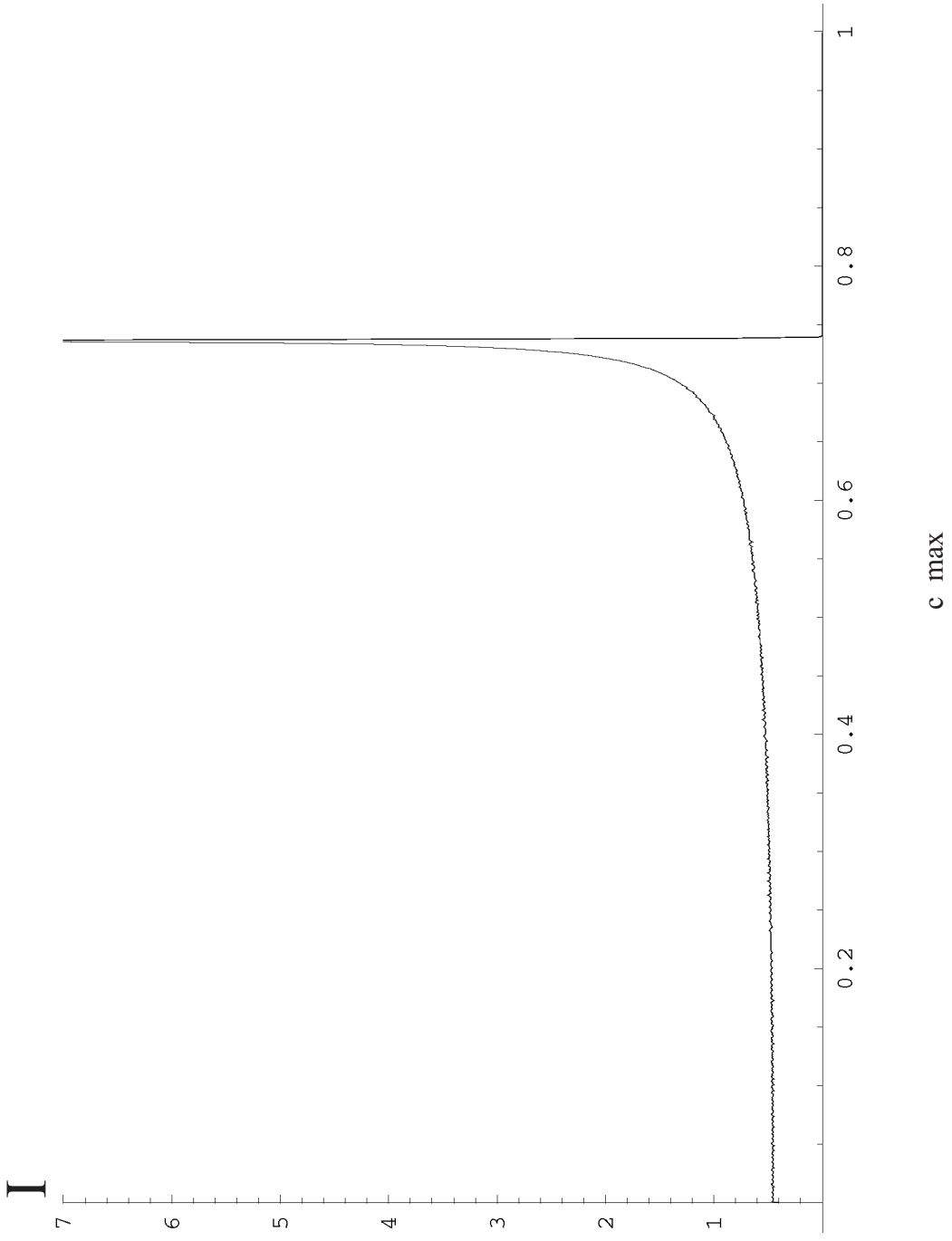

Figure 3.6: The classical angular intensity function calculated at $z_c = \pi/2$ using $20,000$ trajectories and 1001 angular bins.

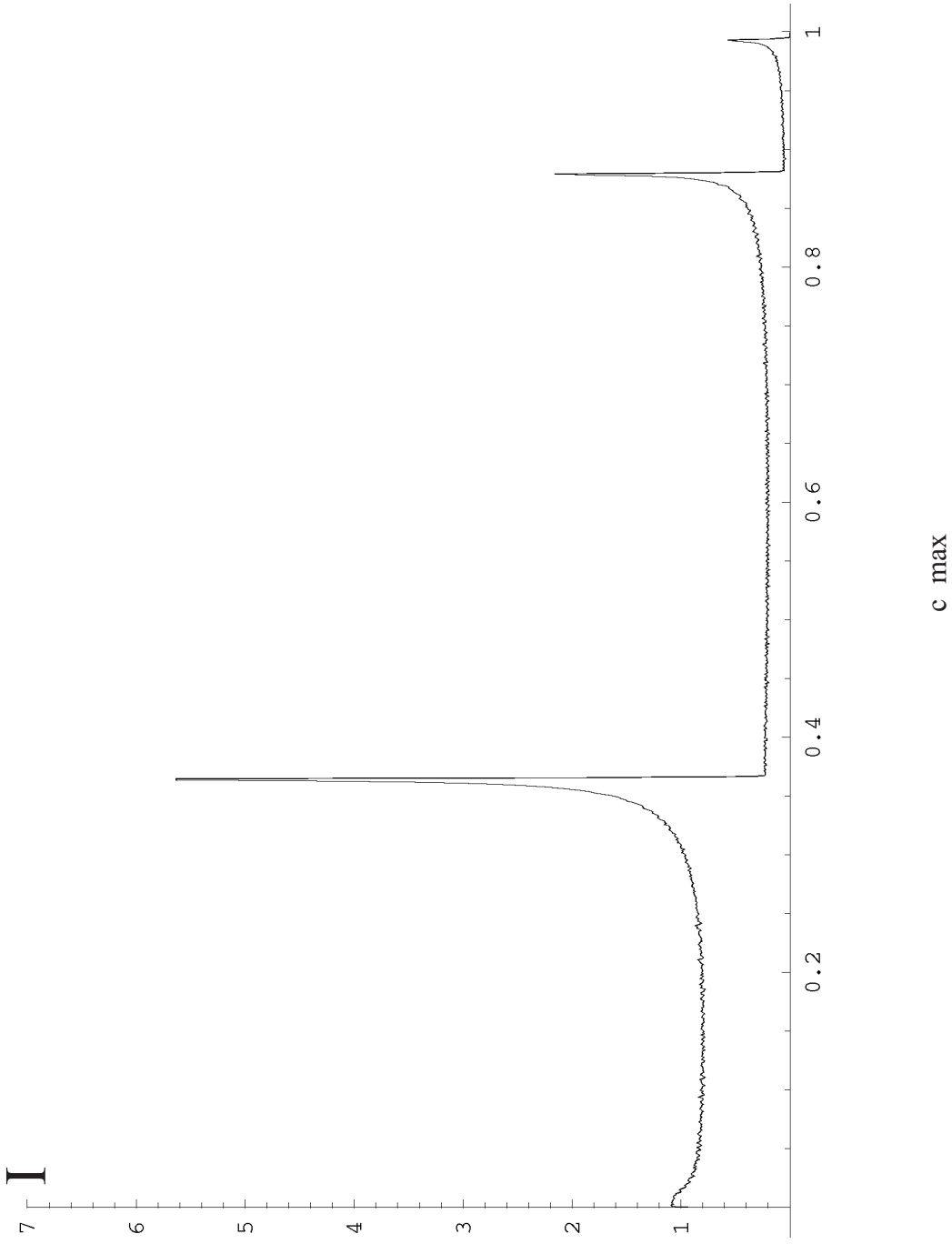

Figure 3.7: The classical angular intensity function calculated at $z_c = 7\pi/2$ using $20,000$ trajectories and 1001 angular bins.

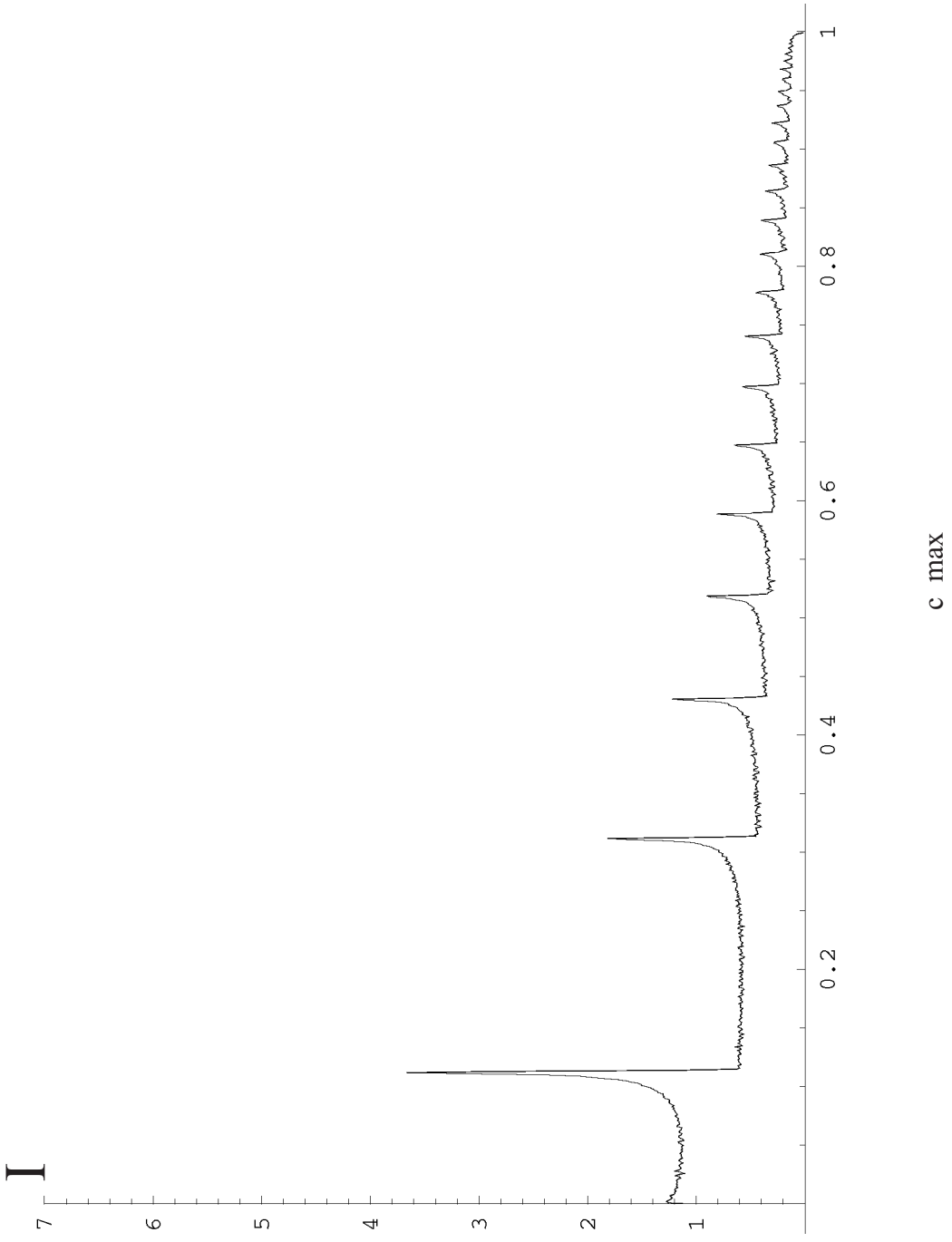

Figure 3.8: The classical angular intensity function calculated at $z_c = 81\pi/2$ using $50,000$ trajectories and 1001 angular bins.

3.5.5 The trajectories to a point

As mentioned in Section 3.5.4 above, the inversion of the trajectory equations (3.28) and (3.29) to find the value(s) of x_{0_c} which satisfy the conditions (x_c, z_c) requires some thought. The classical trajectories are given by Fermat's principle which in this case reads

$$\frac{\partial S}{\partial x_{0_c}} = 0 \tag{3.55}$$

where the action S is expressed as a function of x_{0_c} as in Equation (3.44). However, to avoid complicated algebra, a graphical method will be used instead. The following treatment will be for configuration space trajectories for which $x_c > 0$. For perpendicular incidence the solutions are symmetrical about the z-axis so this will cover all the possibilities. The idea is to consider paths in reverse, propagating from the desired point (x_c, z_c) back to entry face at $z_c = 0$, subject to the condition that at $z_c = 0$, the gradient of the trajectory is zero in accordance with the initial condition for perpendicular incidence. The value of x_c at the entry face is in fact the required value of x_{0_c}. The key to using a reversed trajectory is to realise that, for a generic starting point (x_c, z_c), the trajectory can have a non-zero initial transverse momentum. Thus one must use the trajectory solutions which are generalised to describe oblique incidence, and these are derived in Appendix C. In particular, since the configuration space motion of the atom is bound to the cell of the washboard potential in which it started, the confined trajectory of Equation (C.12) must be used. There are two distinct possibilities which must be considered: situation A where the initial transverse momentum is negative, and situation B for which the initial transverse momentum is positive. Refer to Figure 3.9. The condition that the gradient be zero at z_c is now applied via the momentum space solution, Equation (C.13), giving

$$0 = \sqrt{\mu}\mathrm{cn}\left(z_c + \mathrm{F}\left(\arcsin\left[\frac{\sin x_{0_c}}{\sqrt{\mu}} \right] \middle| \mu \right) \middle| \mu \right) \tag{3.56}$$

where

$$\mu = \sin^2 \tilde{x}_{0_c} + \theta_{0_c}^2. \tag{3.57}$$

The notation $\tilde{x}_{0_c}$ is designed to distinguish the initial transverse position for the reversed trajectory from the actual initial value x_{0_c} which is the desired quantity. As already mentioned above, $\tilde{x}_{0_c} = x_c$.

Now, the incomplete elliptic integral of the first kind which makes up part of the amplitude of the elliptic function in Equation (3.56),

$$\mathrm{F}\left(\arcsin\left[\frac{\sin \tilde{x}_{0_c}}{\sqrt{\sin^2 \tilde{x}_{0_c} + \theta_{0_c}^2}} \right] \middle| \sin^2 \tilde{x}_{0_c} + \theta_{0_c}^2 \right) \tag{3.58}$$

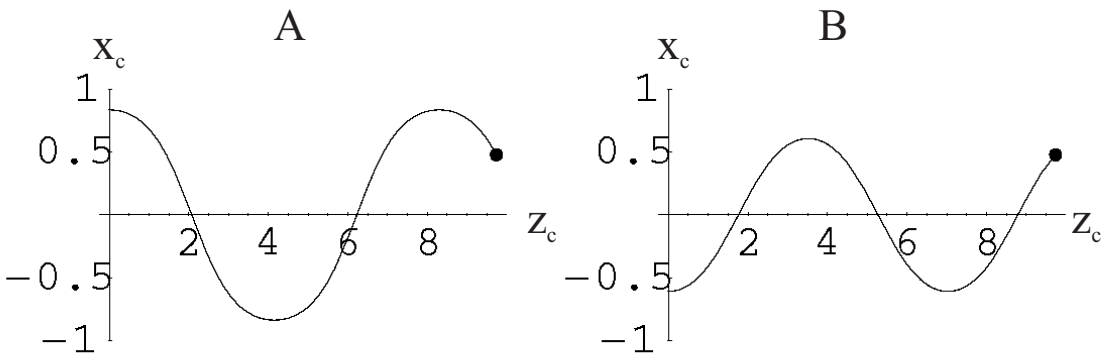

Figure 3.9: Two distinct cases: A) has negative initial transverse momentum, B) has positive initial tranverse momentum.

acts a phase term, capable of advancing the elliptic function somewhere between zero and one quarter of a period (the *complete* elliptic integral of the first kind advances the elliptic function by exactly one quarter—as can be seen when the configuration space and momentum space trajectories, Figures 3.3 and 3.4, are compared to Figure A.1). Thus in Equations (3.56)-(3.58) $\tilde{x}_{0_c}$ is set equal to the value of x_c, and the initial angle, θ_{0_c}, must then be found which produces a trajectory which has zero gradient at $z_c = 0$. Examining Figure 3.10 shows how to apply the momentum condition (3.56) to the two cases. The result is the two equations

$$\text{A:}\quad z_c + \mathbf{F}\left(\arcsin\left[\frac{\sin x_{0_c}}{\sqrt{\mu(\tilde{x}_{0_c},\theta_{0_c})}}\right]\middle|\,\mu(\tilde{x}_{0_c},\theta_{0_c})\right) = (2n+1)\,\mathbf{K}(\mu(\tilde{x}_{0_c},\theta_{0_c})) \tag{3.59}$$

$$\text{B:}\quad z_c - \mathbf{F}\left(\arcsin\left[\frac{\sin \tilde{x}_{0_c}}{\sqrt{\mu(\tilde{x}_{0_c},\theta_{0_c})}}\right]\middle|\,\mu(\tilde{x}_{0_c},\theta_{0_c})\right) = (2n+1)\,\mathbf{K}(\mu(\tilde{x}_{0_c},\theta_{0_c})) \tag{3.60}$$

where n is zero or a positive integer. Since $\tilde{x}_{0_c}$ and z_c are known, the problem of finding the allowed values of θ_{0_c} is now reduced to finding the roots of these equations, w.r.t. θ_{0_c}, for each value of n. This must be done numerically.

The next step is to realise that μ is a constant along the trajectory, whether reversed or not, so the value of x_{0_c} that one was originally seeking comes from

$$\sin^2 x_{0_c} = \sin^2 x_c + \theta_{0_c}^2 \tag{3.61}$$

or explicitly

$$x_{0_c} = \pm \arcsin\left[\sqrt{\sin^2 x_c + \theta_{0_c}^2}\right]. \tag{3.62}$$

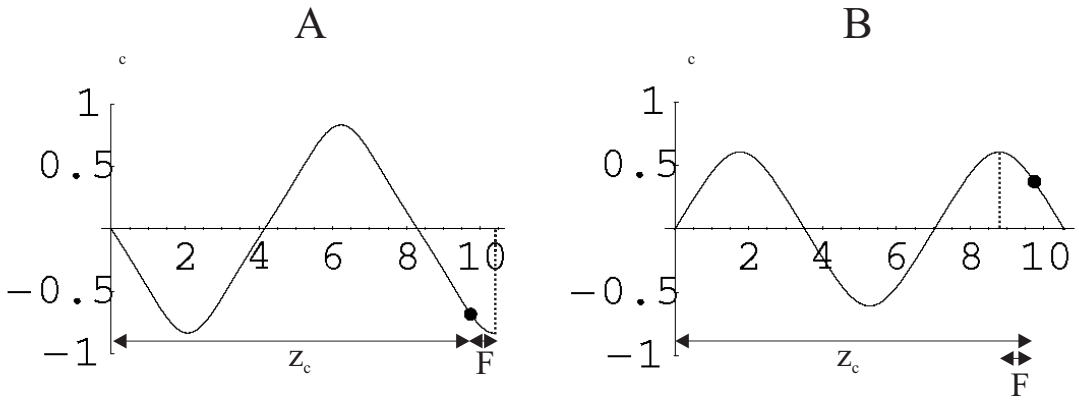

Figure 3.10: Situation A and B in momentum space: A) $z_c + \mathbf{F} = (2n+1)\,\mathbf{K}(\mu)$, B) $z_c - \mathbf{F} = (2n+1)\,\mathbf{K}(\mu)$.

As an example of this method, the configuration point $(0.5, 3.1\pi)$ was chosen. The resulting values of θ_{0_c} and x_{0_c} are listed in Table 3.1. A plot of all the possible classical trajectories is given

Case	n	θ_{0_c}	x_{0_c}
A	0	−0.8775825507	1.5706564685
A	1	−0.8676031850	−1.4384410467
A	2	−0.6856705652	0.9911489172
B	0	0.8775824719	−1.5703988621
B	1	0.8568912153	1.3802016237
B	2	0.1806521096	−0.5378980014
B	2	0.3749815790	−0.6543634172

Table 3.1: The details of the trajectories passing through the configuration point $(0.5, 3.1\pi)$.

in Figure 3.11.

3.5.6 Evaluating the amplitude

Even once the specific trajectories are known, the calculation of the scattering pattern still requires the amplitude given by Equation (3.51). Thus one must be able to differentiate the deflection

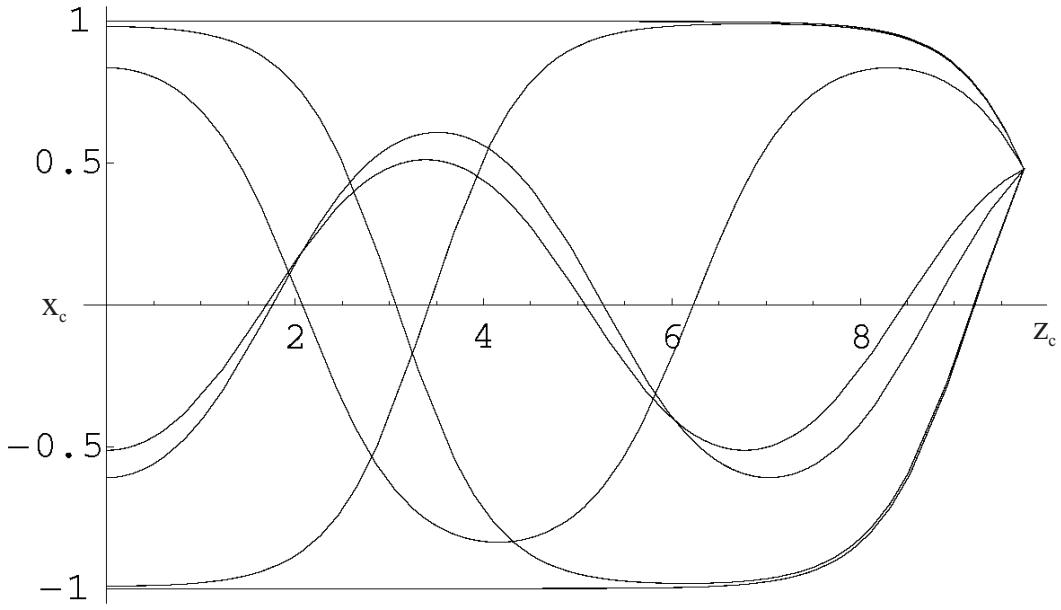

Figure 3.11: The classical trajectories that pass through the configuration point $(0.5, 3.1\pi)$.

function (3.29) by x_{0_c}

$$\begin{aligned}\frac{\partial\vartheta_c}{\partial x_{0_c}} &= \frac{\partial}{\partial x_{0_c}}\sin x_{0_c}\mathrm{cn}\left(z_c+\mathrm{K}(\sin^2 x_{0_c})\middle|\sin^2 x_{0_c}\right) = \frac{\partial}{\partial x_{0_c}}\sin x_{0_c}\mathrm{cn}\left(u(z_c,x_{0_c})\middle|\nu(x_{0_c})\right)\\ &= \cos x_{0_c}\mathrm{cn}\left(u\middle|\nu\right)+\sin x_{0_c}\frac{\partial\mathrm{cn}(u|\nu)}{\partial u}\frac{\partial u}{\partial x_{0_c}}+\sin x_{0_c}\frac{\partial\mathrm{cn}(u|\nu)}{\partial\nu}\frac{d\nu}{dx_{0_c}}.\end{aligned} \tag{3.63}$$

The various required differentiations can be found in Section A.3 of Appendix A, and give, after some cancellation,

$$\begin{aligned}\frac{\partial\vartheta_c}{\partial x_{0_c}} = \cos x_{0_c}\mathrm{cn}(u|\nu)+\mathrm{sn}(u|\nu)\mathrm{dn}(u|\nu)\left(\frac{\mathrm{E}(\mathrm{am}(u|\nu)\,|\nu)-\mathrm{E}(\nu)}{\cos x_{0_c}}-z_c\cos x_{0_c}\right)\\ -\frac{\sin^2 x_{0_c}}{\cos x_{0_c}}\mathrm{sn}^2(u|\nu)\mathrm{cn}(u|\nu).\end{aligned} \tag{3.64}$$

Here, and throughout this section, the x_0 dependence of z_c has been ignored. Equation (3.64) can be further simplified by using the transformation, see P.592 of [1],

$$\mathrm{E}(\mathrm{am}(u|\nu)\,|\nu)-\mathrm{E}(\nu) = \frac{\nu\mathrm{sn}(u|\nu)\mathrm{cn}(u|\nu)}{\mathrm{dn}(u|\nu)}-\mathrm{E}(\mathrm{am}(\mathrm{K}(\nu)-u\,|\nu)\,|\nu) \tag{3.65}$$

and so Equation (3.64) becomes

$$\frac{\partial\vartheta_c}{\partial x_{0_c}} = \cos x_{0_c}\mathrm{cn}(u|\nu)-\mathrm{sn}(u|\nu)\mathrm{dn}(u|\nu)\left(\frac{\mathrm{E}(\mathrm{am}(-z_c|\nu)\,|\nu)}{\cos x_{0_c}}+z_c\cos x_{0_c}\right). \tag{3.66}$$

This, together with the value of x_{0_c} calculated as in Section 3.5.5, can be used in conjunction with Equation (3.51) to find the amplitude associated with a ray tube.

3.5.7 Positions of the caustics

The caustic condition is (see Section 3.5.3)

$$\frac{\partial\vartheta_c}{\partial x_{0_c}} = 0 = \cos x_{0_c}\mathrm{cn}(u|\nu)-\mathrm{sn}(u|\nu)\mathrm{dn}(u|\nu)\left(\frac{\mathrm{E}(\mathrm{am}(-z_c|\nu)\,|\nu)}{\cos x_{0_c}}+z_c\cos x_{0_c}\right) \tag{3.67}$$

which is just the equation which determines the maxima and minima of the plots in Figure 3.5. Finding the set of roots $\{x_{0_c}\}$ of Equation (3.67) for a particular value of z_c, and then inserting these x_{0_c} into the momentum space trajectory equation, gives the angles, θ_c, at which the caustics occur for that value of z_c. As an example, the depth $z_c = 9\pi/2$ was chosen. Figure 3.12 contains plots of the corresponding deflection function and its derivative.

The zeros of the derivative of the deflection function shown in Figure 3.12 together with the predicted positions of the caustics are listed in Table 3.2.

A comparison of the predicted caustic positions with the crude calculation of Section 3.5.4 is shown in Figure 3.13. The correspondence is clearly very good. Also shown, as dots, is a measure of the expected strength of the caustic. The measure is taken to be

$$\left|\left\{\frac{\partial^2\vartheta_c}{\partial x_{0_c}^2}\right\}_{\text{caustic}}\right|^{-1} \tag{3.68}$$

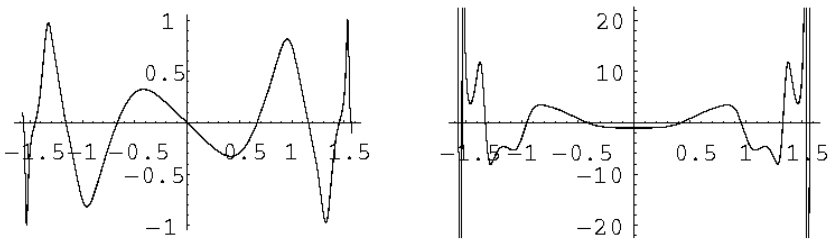

Figure 3.12: A comparison of the deflection function (Equation (3.29))with its derivative w.r.t. x_{0_c} (Equation (3.66)) as functions of x_{0_c}. The value of z_c is $9\pi/2$.

x_{0_c}	$\vartheta_c(x_{0_c}, z_c)$	$\lvert\partial^2\vartheta_c/\partial x_{0_c}^2\rvert^{-1}$
−1.534817	−0.999353	0.000302
−1.325765	0.970047	0.006948
−0.957074	−0.814844	0.042735
−0.416882	0.326394	0.450015
0.416882	−0.326394	0.450015
0.957074	0.814844	0.042735
1.325765	−0.970047	0.006948
1.534817	0.999353	0.000302

Table 3.2: The values of x_{0_c} that give rise to caustics located at ϑ_c at the depth $z_c = 9\pi/2$. The third column gives a measure of the relative caustic strength (the numbers are normalised so their sum equals one).

that is, the second derivative of the deflection function evaluated at the caustic, which, as mentioned in Section 3.5.3, gives an idea of the width of the maxima and minima of the deflection function. In the Figure it is the relative heights of the dots which are important, though for convenience they have been scaled so that the dot corresponding to the inner-most caustic lies at the tip of that caustic. This is not a very fair comparison, since the widths (dots) should be matched with an integral of the intensity under each caustic, not just the peak. In reality the actual value of the intensity at the peaks has no classical meaning since the intensity diverges there. The expression for the second derivative of the deflection function is very long and will not be written down here—the derivatives of the elliptic integrals and functions needed to produce it from the first derivative are given in Appendix A.

3.6 Looking ahead: Quantum scattering and the normal forms

The major drawback of the classical and semiclassical results discussed so far is that they predict the intensity on the caustics to be infinite which is physically unreasonable. This is, however, a fundamentally classical problem which has its origin in the 'point-particle' view of nature.

A more sophisticated approach to finding the wave function, which goes beyond the 'summing over the discrete ray tubes' approach, considers the infinitesimal contribution from every conceivable route from the entry face to the point (x, z) where one wants to know the wavefunction. This is achieved by integrating over all possible paths (whether classical or not) and leads to an integral representation of the wave function. Following Berry [17], one writes

$$\psi(C) = \sqrt{\frac{1}{2\pi \mathrm{i}\hbar}} \int a(s;C) \mathrm{e}^{\mathrm{i}S(s;C)/\hbar}\, ds. \tag{3.69}$$

As before, s and C are the state and control variables and $a(s;C)$ is the 'correct', non-pathological, amplitude. If $a(s;C)$ were known then the problem would be solved.

If $\hbar$ is small then the integral could be approximately evaluated using the method of stationary phase, see Appendix B. This method is accurate as long as the stationary points of the phase are well separated. Physically, the action is stationary for a classical path, so the method of stationary phase picks out just those rays (and their immediate neighbours—a neighbourhood which diminishes as $\hbar$ is reduced) which make the 'classical contribution' to the wavefunction (3.69). The requirement that the stationary points be well separated is violated on a caustic as two or more classical paths converge there, so the method of stationary phase breaks down at the caustics, but then so does the classically derived amplitude too.

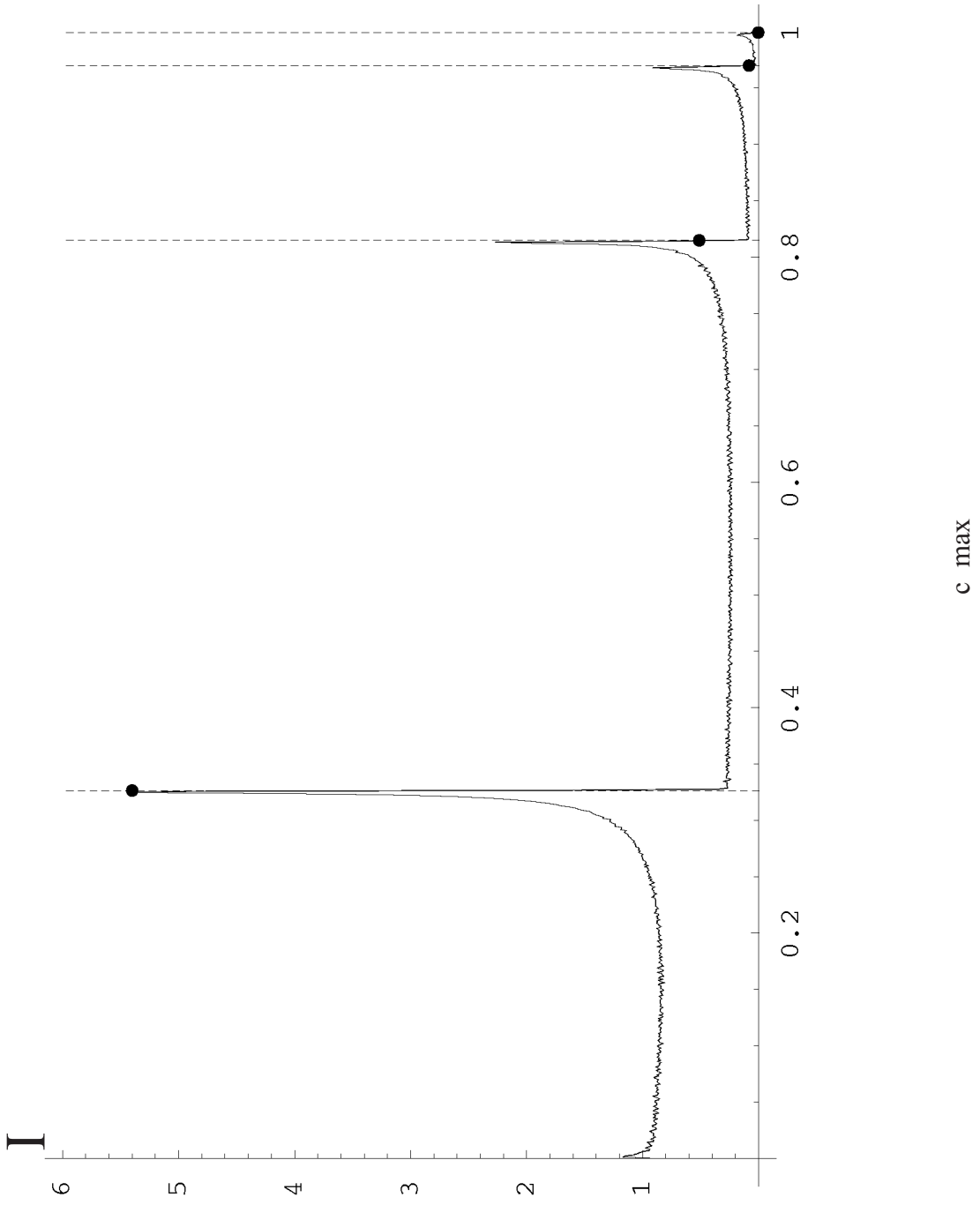

Figure 3.13: The positions of the caustics, for $z_c = 9\pi/2$, as calculated using Equation (3.67) (dashed line) superimposed over a crude calculation of the (half plane) intensity function. The dots give a measure of the relative intensity of each caustic.

Imagining, though, that the well behaved amplitude, $a(s;C)$, of Equation (3.69) is known[8], then for small $\hbar$ one might indeed attempt a form of stationary phase evaluation of Equation (3.69). In the region of a caustic $a(s;C)$ is approximately constant and so may be taken outside the integral. This is because the contributing points, s_q, are close together. Thus the integral becomes

$$\psi(C) = \sqrt{\frac{1}{2\pi \mathrm{i}\hbar}} a(s_q;C) \int \mathrm{e}^{\mathrm{i}S(s;C)/\hbar}\, ds. \tag{3.70}$$

Now the true importance of catastrophe theory becomes clear: near the caustics $S(s;C)$ is given by one of the normal forms, and thus, as alluded to earlier, catastrophe theory predicts the form of the wavefunction at and around these singular points. Only the fold normal form, a cubic, corresponds to a well known integral, that of the Airy function (see Figure 3.14)

$$\mathrm{Ai}(C) = \frac{1}{2\pi} \int_{-\infty}^{\infty} \mathrm{e}^{\mathrm{i}(t^3/3 + Ct)} dt. \tag{3.71}$$

The Airy function evaluation of the integral (3.69) constitutes a more advanced form of the

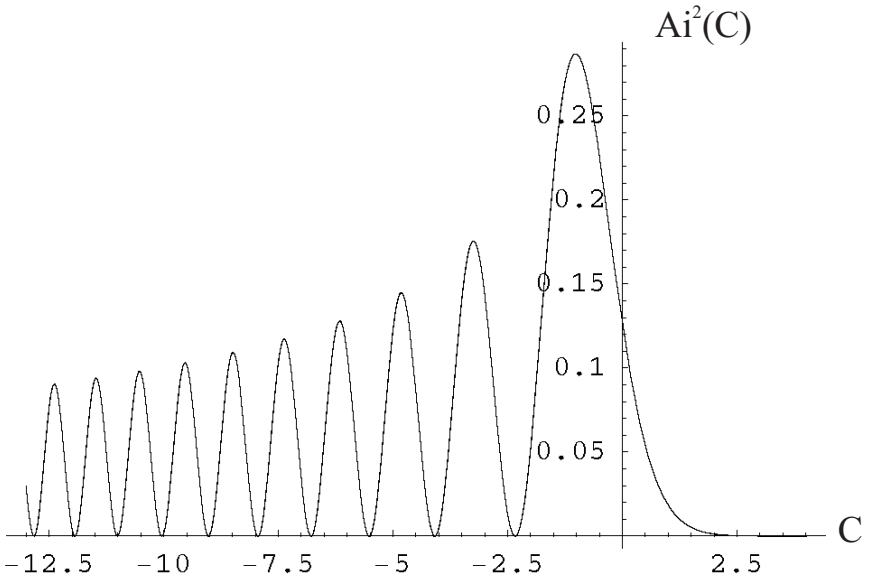

Figure 3.14: The intensity on a (fold) caustic is given by $|\psi|^2 \propto \mathrm{Ai}^2(C)$.

basic quadratic stationary phase method: one which is capable of dealing with two close, or even coalescing stationary points. So, instead of a divergence, the intensity at a caustic is softened by the wave behaviour into a set of intense fringes, the principal of which sits over[9] the actual

[8]For instance one could use Maslov's prescription of moving between momentum and configuration spaces to avoid the caustics in either one.

[9]Note that the peak of the principal fringe does not lie directly at the singularity. Referring to Fig 3.14, the classical divergence is at $C = 0$

(classically) singular point.

Airy obtained his integral in 1838 [3] when studying diffraction near a caustic, so really the Airy function intensity profile is no great revelation. The next integral in the catastrophe theory classification scheme is based on the quartic normal form as mentioned earlier, and describes the cusps. Incredibly, the quartic exponential integral does not appear to have been seriously studied until the work of Pearcy [63] in 1946.

While much has been learned from the classical mechanics, the labour involved in locating paths, correctly assigning Maslov indices, dealing with divergent amplitudes, and so forth, means that the interfering ray sum will not actually be calculated here. A much simpler approach will be introduced in the next chapter through the fully quantum set of equations due to Raman and Nath. Throughout the following quantum treatment though, whenever $\hbar$ becomes small, the underlying classical strucure will begin to emerge. In particular, wherever the classical mechanics predicts a (fold) caustic, one expects to find an Airy function. Finally, in Chapter 9, the classical paths will be 'retrieved' from the quantum formalism by means of a remarkable transformation known as the Poisson summation formula.

Chapter 4

The Raman-Nath equation

4.1 Motivation

Sir Chandrasekhara Venkata Raman (1888–1970) was not only one of the founding fathers of modern science in India, but also a rather colourful character. Of his many brilliant contributions to physics, he is chiefly remembered for his experimental discovery in 1928 of what soon became known as the Raman effect. Subsequent to him being awarded the Nobel prize in 1930, he was made director of the Indian Institute of Science in Bangalore, and with characteristic zeal immediately set about reforming what had become a rather unproductive research institution as well as establishing a physics department[1]. He soon had to resign his directorship in controversy in 1937 but continued on as an active professor until his retirement in 1948, whereupon he took his work across the road (literally) to the specially inaugurated Raman Institute. Despite his pre-eminence as an experimenter, the high point of Raman's research at the Indian Institute of science is considered [82] to be his theoretical contribution to the study of the diffraction of light by ultrasound. As Raman's biographer, Venkataraman [82] (no relation), has put it:

> *Raman loved waves, and this problem had light waves as well as sound waves. What more could he ask for?*

[1] Prior to his arrival, there was only a biochemistry, an electro-technology, and two chemistry departments—the institute had been founded in 1911 on the generosity of the Tata Institute, a charitable organisation named after Jamshedji Nusserwanji Tata, an Indian industrialist and philanthropist, owner of the Tata Iron and Steel Co. The reason for mentioning this is to point out that, during Raman's life time, research in India relied on piecemeal, meagre funds and the patronage of a few benevolent wealthy citizens. Raman had to spend much of his time fighting for financial support, in stark contrast to his contemporaries in Europe, America and the USSR. This only makes his achievements all the more remarkable. All the historical details in this section come from G. Venkataraman's biography of Raman *Journey into Light* [82]

Together with his young collaborator, a twenty-year-old mathematics graduate N. S. Nagendra Nath, they developed, in a series of seven papers published during 1935 [67, 68], 1936 [69, 70, 71, 59] and 1938 [60], a theory, now known as the Raman-Nath theory, which not only accurately accounted for the experimental observations, but did so with great simplicity. The substitution of atoms for light and a laser for ultrasound is formally irrelevant provided one is only considering monochromatic beams (matter waves are self dispersive so wave packets will behave differently). What does change though are the possible magnitudes of the various parameters. Principally, the very small de Broglie wavelength of the atoms facilitates the study of emergent classical features.

4.2 From the Schrödinger equation

Whereas Raman and Nath were considering the ultrasonic diffraction of light, the relevant wave equation to use here is the time independent Schrödinger equation

$$-\frac{\hbar^2}{2m}\left(\frac{\partial^2\Psi}{\partial x^2}+\frac{\partial^2\Psi}{\partial z^2}\right)-V_0\cos^2(Kx)\,\Psi=E\Psi \tag{4.1}$$

where Ψ is taken to be the ground state wavefunction of the stationary atomic beam of energy E, as discussed in Chapter 2. V_0 is given by Equation (3.2). The wavenumber of the two individual counter-propagating members of the standing wave laser beam is K. The total wavenumber of the atomic beam is k. Prior to entering the laser, the wavefunction is taken as being a plane wave

$$\Psi(z)=\mathrm{e}^{\mathrm{i}kz} \tag{4.2}$$

where

$$\frac{\hbar^2k^2}{2m}=E. \tag{4.3}$$

The periodicity of the potential implies a periodic wavefunction (Bloch's theorem), and so an ansatz is made

$$\Psi(x,z)=\mathrm{e}^{\mathrm{i}kz}\sum_{n=-\infty}^{\infty}A_n(z)\mathrm{e}^{2\mathrm{i}nKx}. \tag{4.4}$$

It is assumed that, due to the paraxiality of the system, the behaviour of the wavefunction is dominated by the $\exp(\mathrm{i}kz)$ term. The remaining evolution is then contained in the complex Fourier coefficients, $A_n(z)$, which are assumed to be slowly varying functions of z (which, as before, plays the rôle of time).

In the space beyond the laser the atoms travel freely as plane waves. The coefficients are then constants, maintaining the values they had at the exit face, and the wavefunction, (4.4), can therefore be interpreted as representing a set of diffracted beams travelling at an angle θ to the z-axis where

$$\theta\approx\tan\theta=\frac{2nK}{k}. \tag{4.5}$$

Each A_n is then the amplitude for the beam to be in the n^{th} diffracted order.

To solve the problem one must find the $A_n(z)$. The diffraction pattern measured in the farfield consists of discrete elements, lying at the angles given by Equation (4.5), each having an intensity

$$I_n \equiv |A_n(z = D)|^2 \tag{4.6}$$

where D is the width of the interaction region.

Substituting the trial wavefunction into Schrödinger's equation and writing the cosine in terms of complex exponentials gives

$$\begin{aligned} &- k^2 \mathrm{e}^{\mathrm{i}kz} \sum A_n \mathrm{e}^{2\mathrm{i}nKx} + 2\mathrm{i}k\mathrm{e}^{\mathrm{i}kz} \sum \frac{\partial A_n}{\partial z} \mathrm{e}^{2\mathrm{i}nKx} \\ &+ \mathrm{e}^{\mathrm{i}kz} \sum \frac{\partial^2 A_n}{\partial z^2} \mathrm{e}^{2\mathrm{i}nKx} - \mathrm{e}^{\mathrm{i}kz} \sum 4n^2K^2 A_n \mathrm{e}^{2\mathrm{i}nKx} \\ &+ \frac{2mV_0}{4\hbar^2} \left(\mathrm{e}^{2\mathrm{i}Kx} + 2 + \mathrm{e}^{-2\mathrm{i}Kx}\right) \Psi + k^2 \Psi = 0. \end{aligned} \tag{4.7}$$

Given that the amplitudes are slowly varying with z, the term containing the second rate of change of the amplitude, $\partial^2 A_n/\partial z^2$, will from now on be ignored. This is further justified by noting that its multiplicative constant coefficient is one, as opposed to the large coefficients present in all the other terms. Appendix B cites a typical example where $V_0 \approx 5 \times 10^{-28}$J, $K \approx 10^7\,\text{metres}^{-1}$, $k \approx 10^{11}\text{metres}^{-1}$, and for sodium $m \approx 10^{-26}$kg. This is all associated with the paraxiality of the system.

To pick out the A_n from Equation (4.7), one equates the coefficients of equal exponentials to zero, giving a differential difference equation

$$2\mathrm{i}k\frac{\partial A_n}{\partial z} - 4n^2K^2A_n + \frac{mV_0}{2\hbar^2}\left(A_{n+1} + 2A_n + A_{n-1}\right) = 0. \tag{4.8}$$

Dividing through by $4K^2$ and defining the dimensionless variables

$$\zeta \equiv \frac{2K^2 z}{k} \tag{4.9}$$

$$\Lambda \equiv \frac{mV_0}{4\hbar^2K^2} \tag{4.10}$$

one obtains

$$\mathrm{i}\frac{\partial A_n}{\partial \zeta} - n^2 A_n + \frac{\Lambda}{2}\left(A_{n+1} + 2A_n + A_{n-1}\right) = 0 \tag{4.11}$$

an equation which is central to the rest of this thesis and shall be referred to as the Raman-Nath equation, although in their works they actually used a slightly modified version. A trivial phase transformation of the amplitudes, $A_n \equiv \tilde{A}_n \exp(\mathrm{i}\Lambda\zeta)$, removes the diagonal A_n term with the constant coefficient Λ, leaving

$$\mathrm{i}\frac{\partial \tilde{A}_n}{\partial \zeta} - n^2 \tilde{A}_n + \frac{\Lambda}{2}\left(\tilde{A}_{n+1} + \tilde{A}_{n-1}\right) = 0 \tag{4.12}$$

Effecting the following changes of variables

$$\chi_n \equiv (-\mathrm{i})^n \tilde{A}_n \tag{4.13}$$

$$\eta \equiv -\Lambda\zeta \tag{4.14}$$

$$\rho \equiv \frac{2}{\Lambda} \tag{4.15}$$

gives

$$2\frac{\partial\chi_n}{\partial\eta} - \mathrm{i}\rho n^2\chi_n + \chi_{n+1} - \chi_{n-1} = 0 \tag{4.16}$$

which is the original equation of Raman and Nath.

In either case, each of these differential difference equations represent just one member of an infinite set of linked equations which must be solved for the amplitudes.

4.3 The Raman-Nath approximation

4.3.1 Bessel function recursion relation

The Raman-Nath equation in its original form, that is the second of the two presented above (Equation (4.16)), is immediately amenable to an approximation, first made by Raman and Nath in their original paper [67], and so it is known as *the* Raman-Nath approximation. Ignoring the term containing ρn^2 leaves

$$2\frac{\partial\chi_n}{\partial\eta} + \chi_{n+1} - \chi_{n-1} = 0 \tag{4.17}$$

which is actually a well known recursion relation for Bessel's equation [1]. Thus, within this approximation, the solution for the amplitudes can at once be given as

$$\chi_n(\eta) = J_n(\eta) \tag{4.18}$$

a simple and remarkable result.

Immediately one must ask under what conditions this solution is valid. Firstly it is observed that the origin of the ρn^2 term in the derivation of the full Raman-Nath equation stems from the action of the transverse part of the Laplacian, $\partial^2/\partial x^2$, upon the wavefunction. So ignoring this term corresponds to disregarding the transverse kinetic energy of the atoms, and in turn means that the transverse motion of the atoms is not taken into account. Neglecting the ρn^2 term in this way appears to be a very specific, mathematical simplification, of relevance only to the Raman-Nath equation. In their original paper however, Raman and Nath arrived at this approximation by a more general approach with a much wider applicability which will now be briefly discussed.

4.3.2 Phase gratings

It was Rayleigh [73] who first proposed the concept of phase gratings to describe a medium whose effect upon a traversing wave is to induce a pure phase change without any influence upon the amplitude. An incident wave

$$\Psi(z) = \mathrm{e}^{\mathrm{i}kz} \tag{4.19}$$

passing through a phase grating becomes

$$\Psi(x,z) = \mathrm{e}^{\mathrm{i}\gamma(x,z)}\mathrm{e}^{\mathrm{i}kz} \tag{4.20}$$

where $\gamma(x)$ is a real, periodic, function of x (the periodic condition is required for the medium to qualify as a *grating*, for then it will produce diffracted beams). Raman and Nath were the first to treat an ultrasonic standing wave as a phase grating for light. In a simplification of the 'phase along a ray' treatments of Chapter 3 and Appendix B, they supposed that the rays travelled in straight lines across the medium, undeviated by the presence of the modulated refractive index induced by the ultrasonic wave. Hence the connection with the statements above concerning neglect of transverse motion. The optical distance, $\mu(x,z)$, each ray travels depends on its transverse entry point, x_0, into the medium, for that determines the value of the refractive index along the straight path. From Equation (4.20), γ may be written as the difference between the optical distance due to the grating and the free space evolution of the wave that would have taken place had the grating not been there

$$\gamma = \mu - kz = \mu - \frac{\sqrt{2mE}}{\hbar}z. \tag{4.21}$$

Appendix B demonstrates that, due to the separability of the Hamiltonian (3.4), the optical distance is a conservative function of the configuration co-ordinates, and so depends only on the end points of the trajectory across the interaction region. In particular, since the transverse co-ordinate remains constant, the contribution arising from the transverse momentum is zero. Only the longitudinal term remains so that, using Equation (3.5), one has

$$\mu = \frac{1}{\hbar}\int_0^D P_z\,dz = \frac{\sqrt{2m}}{\hbar}\int_0^D \sqrt{E + V_0\cos^2 Kx}\,dz = \frac{\sqrt{2m}}{\hbar}D\sqrt{E + V_0\cos^2 Kx}. \tag{4.22}$$

Employing the paraxial condition, the square root is expanded to just the first two terms and the $\cos^2 Kx$ term transformed to its double-angle equivalent. Equation (4.21) is then

$$\gamma \approx \frac{\sqrt{2mE}}{\hbar}D\left(1 + \frac{V_0}{4E} + \frac{V_0}{4E}\cos 2Kx\right) - \frac{\sqrt{2mE}}{\hbar}D = \frac{\sqrt{2m}V_0}{4\hbar\sqrt{E}}D\left(1 + \cos 2Kx\right). \tag{4.23}$$

Exploiting the x periodicity of $\gamma(x,z)$ one writes

$$\mathrm{e}^{\mathrm{i}\gamma(x)} = \sum_{n=-\infty}^{\infty} A_n(D)\mathrm{e}^{2\mathrm{i}nKx} \tag{4.24}$$

and then

$$A_n(D) = \frac{K}{\pi} \int_{-\pi/2}^{\pi/2} \mathrm{e}^{\mathrm{i}(\gamma(x,z)-2nKx)} dx. \tag{4.25}$$

Inserting γ from Equation (4.23) gives

$$A_n(D) = \frac{1}{\pi} \mathrm{e}^{\mathrm{i}\frac{\sqrt{2m}V_0}{4\hbar\sqrt{E}}D} \int_{-\pi/2}^{\pi/2} \mathrm{e}^{\mathrm{i}(\frac{\sqrt{2m}V_0}{4\hbar\sqrt{E}}D\cos 2Kx-2nKx)} dKx \tag{4.26}$$

which corresponds to an integral definition of the Bessel function of the first kind [1]. Replacing E in favour of k via Equation (4.3) gives

$$A_n(D) = \mathrm{e}^{\mathrm{i}mV_0D/(2\hbar^2k)}\ \mathrm{i}^n J_n\left(\frac{mV_0}{2\hbar^2k}D\right) \tag{4.27}$$

which, as anticipated, gives the same intensities as Equation (4.18).

The Raman-Nath Bessel function approximation has proved to be a very successful result. Ultrasonic diffraction of light experiments, conducted by Sanders [74] in 1936, provided immediate confirmation of Raman and Nath's predictions (see Berry [16]). Using atoms, the first quantitative experiment was conducted by Gould *et al.* [37] in 1986, giving 'reasonable agreement', whilst recent, very refined experiments, such as those by Rasel *et al.* [72], gave spectacular agreement. However, as mentioned above, the neglect of the transverse motion constitutes a fairly serious approximation. In their fourth paper [70], Raman and Nath themselves pointed out that ρn^2 must be small for the Bessel approximation to hold. This is not an easy condition to satisfy since ρ contains the ratio $\hbar^2/V_0$: a small ρ is consistent with a strong laser field interaction, which, as stressed at the beginning of Chapter 3, can also be understood in terms of a small value of $\hbar$. A small ρ takes one towards the classical regime: many diffracted beams are present. The classical mechanics gives a firm limit on the maximum scattering angle and is stated in Equation (3.53). As one approaches the classical limit by reducing $\hbar$, it can be expected that such a condition is approximately obeyed, and hence the number of diffracted beams can be estimated. Equation (3.53) reads

$$\frac{P_z}{\sqrt{2mV_0}}\,\theta = 1. \tag{4.28}$$

The classical and quantum worlds are linked through the value of θ. Inserting Equation (4.5) and setting $P_z = \hbar k$, the classical mechanics acting through Equation (4.28) predicts

$$N = \frac{2}{\sqrt{\rho}} = \sqrt{2\Lambda} \tag{4.29}$$

where N is the index of largest diffraction order present. Therefore, if one reduces ρ, the number of beams grows in such a way as to thwart any attempt to meet the conditions necessary for the Raman-Nath approximation since the largest orders present will have

$$\rho n^2 = \rho N^2 = 4. \tag{4.30}$$

How then, can the Raman-Nath approximation ever be valid? Firstly it should be noted that Equation (4.29) is only valid in the classical limit; no indication has been given of the number of beams generated in the quantum region where ρ is less than one but not significantly so. Secondly, one can use the understanding that lies behind the phase grating approach, namely that the atoms have no transverse motion during their interaction. Clearly this is really only valid for short interaction times. The larger diffraction orders take some time (distance) to populate—via all the intermediate orders—and so for short interactions the maximum value of n is sufficiently less than that given by Equation (4.29). Going beyond the Raman-Nath approximation, that is, retaining the ρn^2 term is the province of *dynamical diffraction*; a regime in which the motion of the atoms inside the laser induced potential is accounted for.

4.4 Perturbation series

Generally in physics, when one has a very weak interaction, it is natural to seek a perturbative solution consisting of a rapidly converging series. The convergence is assured through an expansion parameter which is a measure of the weakness of the interaction. The first such solution for dynamical diffraction, in the context of the diffraction of light by ultrasound, was given by Brillouin [21, 22] from the scalar Helmholtz wave equation (4.1) in 1921. Subsequently, a simpler derivation has been given by Berry [16]. This section will present other, closely related approaches, based directly on the Raman-Nath equation.

4.4.1 Oblique Incidence

To facilitate use in succeeding sections, the following derivations will encompass oblique incidence. The atom beam may then have an initial transverse wavenumber, a, say. If the total wavenumber is still given by k, then prior to entering the laser beam the wavefunction is

$$\Psi(x,z) = \mathrm{e}^{\mathrm{i}\sqrt{k^2-a^2}\,z}\mathrm{e}^{\mathrm{i}ax} \tag{4.31}$$

and under the influence of the interaction with the standing wave becomes

$$\Psi(x,z) = \mathrm{e}^{\mathrm{i}\sqrt{k^2-a^2}\,z}\sum_{n=-\infty}^{\infty} A_n(z)\mathrm{e}^{\mathrm{i}(2nK+a)x}. \tag{4.32}$$

Substitution into the Schrödinger equation (4.1), and proceeding as in Section 4.2 gives

$$\begin{aligned} -(k^2-a^2)A_n + 2\mathrm{i}\sqrt{k^2-a^2}\,\frac{\partial A_n}{\partial z} - (4n^2K^2 + a^2 + 4naK)A_n \\ + \frac{mV_0}{2\hbar^2}\left(A_{n+1} + 2A_n + A_{n-1}\right) + k^2A_n = 0. \end{aligned} \tag{4.33}$$

Slightly redefining ζ as

$$\zeta \equiv \frac{2K^2 z}{\sqrt{k^2 - a^2}} \tag{4.34}$$

and introducing

$$\alpha \equiv \frac{a}{K} \tag{4.35}$$

leads to the Raman-Nath equation generalised for non-perpendicular[2] incidence

$$\mathrm{i}\frac{\partial A_n}{\partial \zeta} - (n^2 + n\alpha)A_n + \frac{\Lambda}{2}\left(A_{n+1} + 2A_n + A_{n-1}\right) = 0. \tag{4.36}$$

The dimensionless parameter Λ remains the same as given in Equation (4.10). It is convenient to simplify this Raman-Nath equation as before with the phase transformation $A_n \equiv \tilde{A}_n \mathrm{e}^{\mathrm{i}\Lambda\zeta}$ so that one has

$$\mathrm{i}\frac{\partial \tilde{A}_n}{\partial \zeta} - (n^2 + n\alpha)\tilde{A}_n + \frac{\Lambda}{2}\left(\tilde{A}_{n+1} + \tilde{A}_{n-1}\right) = 0. \tag{4.37}$$

It is important to notice that under weak field conditions (when Λ is small), making the Raman-Nath approximation (ignoring the second term) would be totally inappropriate.

4.4.2 The Raman-Nath evolution operator

The full set of Raman-Nath equations are readily amenable to being represented in matrix form. One has

$$\mathrm{i}\frac{\partial \tilde{A}_n}{\partial \zeta} = H_{nm}\tilde{A}_m \tag{4.38}$$

where the H is a square matrix with elements

$$H_{nm} = (n^2 + n\alpha)\delta_{n,m} - \frac{\Lambda}{2}\left(\delta_{n,m-1} + \delta_{n,m+1}\right). \tag{4.39}$$

The matrix equation (4.38) is reminiscent of a time-dependent Schrödinger equation (substitute ζ for time) with time-independent Hamiltonian[3] H, a feature which will be useful in the following sections and chapters. This property whereby the Schrödinger type equation has the 'quantum' scaled distance, ζ, playing the rôle of time is common to paraxial systems in general.

The Schrödinger equation structure of Equation (4.38) suggests an evolution operator type solution

$$\tilde{\mathbf{A}}(\zeta) = \mathrm{e}^{-\mathrm{i}\int_0^\zeta H\, d\zeta'}\tilde{\mathbf{A}}(\zeta = 0) \tag{4.40}$$

for the vector $\tilde{\mathbf{A}}$ whose elements are the $\tilde{A}_n$ amplitudes. The initial condition that the atom beam start in the zeroth order means that one can take

$$\tilde{A}_n(\zeta = 0) = \delta_{n,0}. \tag{4.41}$$

[2] Just to be clear, note that whenever angled incidence is being considered, the notation used will consider the diffracted beam basis as rotating with the angle of incidence. So, for example, the n^{th} beam travels at an angle $\sin\theta = (2nK + a)/k$ to the z-axis.

[3] H is Hermitian.

So one requires

$$\begin{aligned}\int_0^\zeta H\, d\zeta' &= \left[(n^2+n\alpha)\delta_{n,m} - \frac{\Lambda}{2}\left(\delta_{n,m-1}+\delta_{n,m+1}\right)\right]\zeta \\ &\equiv \mathcal{P}(\zeta) - \Lambda\mathcal{Q}(\zeta).\end{aligned} \tag{4.42}$$

So the exponentiated operator of Equation (4.40) now becomes

$$\tilde{A}_n = \mathrm{e}^{-\mathrm{i}(\mathcal{P}_{n,m}-\Lambda\mathcal{Q}_{n,m})}\delta_{m,0}. \tag{4.43}$$

A weak interaction has a small value of Λ, so this will be chosen as the expansion parameter. Expanding the perturbative part of the exponential gives

$$\tilde{A}_n = \mathrm{e}^{-\mathrm{i}\mathcal{P}_{n,m}}\left[\delta_{n,m} + \mathrm{i}\Lambda\mathcal{Q}_{n,m} - \frac{\Lambda^2}{2}\mathcal{Q}^2_{n,m} - \mathrm{i}\frac{\Lambda^3}{3!}\mathcal{Q}^3_{n,m} + \cdots\right]\delta_{m,0}. \tag{4.44}$$

When finding powers of the matrix operators one makes use of relations such as

$$\mathcal{Q}^2_{n,m} = \mathcal{Q}_{n,j}\mathcal{Q}_{j,m}. \tag{4.45}$$

Noting that the $\mathcal{P}$ matrix is diagonal, so that its δ_{nm} operator is redundant when multiplying other Kronecker delta operators, gives

$$\begin{aligned}\tilde{A}_n = \mathrm{e}^{-\mathrm{i}(n^2+n\alpha)\zeta}\Bigg[\,&\delta_{n,m} + \frac{\mathrm{i}\Lambda\zeta}{2}\left(\delta_{n,m-1}+\delta_{n,m+1}\right) - \frac{\Lambda^2\zeta^2}{8}\left(\delta_{n,m-2}+2\delta_{n,m}+\delta_{n,m+2}\right) \\ &-\frac{\mathrm{i}\Lambda^3\zeta^3}{48}\left(\delta_{n,m-3}+3\delta_{n,m-1}+3\delta_{n,m+1}+\delta_{n,m+3}\right)+\cdots\Bigg]\delta_{m,0}\end{aligned} \tag{4.46}$$

Applying the power series to the initial condition $\delta_{m,0}$ yields

$$\tilde{A}_0 = 1 - \frac{\Lambda^2\zeta^2}{4} + \mathcal{O}\left((\Lambda\zeta)^4\right) \tag{4.47}$$

$$\tilde{A}_{\pm1} = \mathrm{e}^{-\mathrm{i}(1\pm\alpha)\zeta}\left[\frac{\mathrm{i}\Lambda\zeta}{2} - \frac{\mathrm{i}\Lambda^3\zeta^3}{16} + \mathcal{O}\left((\Lambda\zeta)^5\right)\right] \tag{4.48}$$

$$\tilde{A}_{\pm2} = \mathrm{e}^{-\mathrm{i}(4\pm2\alpha)\zeta}\left[-\frac{\Lambda^2\zeta^2}{8} + \mathcal{O}\left((\Lambda\zeta)^4\right)\right] \tag{4.49}$$

$$\tilde{A}_{\pm3} = \mathrm{e}^{-\mathrm{i}(9\pm3\alpha)\zeta}\left[-\frac{\mathrm{i}\Lambda^3\zeta^3}{48} + \mathcal{O}\left((\Lambda\zeta)^5\right)\right] \tag{4.50}$$

where the higher diffraction orders require the $\mathcal{Q}^4$ term and above. These solutions serve to illustrate the way the diffracted beams fill out as the interaction region is traversed. Unfortunately they suffer from being doubly perturbative in the sense that, to obtain solutions valid for longer interaction times but with a constant value of the interaction strength Λ, one must find the higher order terms.

4.4.3 The Born perturbation series

Methods that treat the interaction between the quantum wave and the potential as a perturbation on top of the free-space evolution give what is known as a Born series. This section reproduces

the approach due to Berry [16], where the Laplace transform of the Raman-Nath equation is used, but incorporates oblique incidence. Defining

$$S_n(p) \equiv \int_0^\infty \tilde{A}_n(\zeta) \mathrm{e}^{-p\zeta}\, d\zeta \tag{4.51}$$

and noting that

$$\int_0^\infty \frac{\partial \tilde{A}_n}{\partial \zeta} \mathrm{e}^{-p\zeta}\, d\zeta = -\tilde{A}_n(0) + pS_n(p) \tag{4.52}$$

the Laplace transformed Raman-Nath equation is written

$$\mathrm{i}(pS_n(p) - \delta_{n,0}) = (n^2 + n\alpha)S_n - \frac{\Lambda}{2}(S_{n+1} + S_{n-1}) \tag{4.53}$$

or

$$\left[(\mathrm{i}p - n^2 - n\alpha)\delta_{n,m} + \frac{\Lambda}{2}(\delta_{n,m-1} + \delta_{n,m+1})\right] S_m = \mathrm{i}\delta_{n,0} \tag{4.54}$$

where the advantage of the Laplace transformed Raman-Nath equation is that it not only incorporates the initial condition that the beam is in the zeroth state, but also renders the R-N equation into an algebraic difference equation. As before, Equation 4.54 can be written in terms of two operators, one of which is perturbative,

$$\mathcal{U}_{n,m} \equiv (\mathrm{i}p - n^2 - n\alpha)\delta_{n,m} \tag{4.55}$$

$$\mathcal{V}_{n,m} \equiv \frac{\Lambda}{2}(\delta_{n,m-1} + \delta_{n,m+1}) \tag{4.56}$$

and becomes

$$[\mathcal{U} + \mathcal{V}]_{n,m} S_m = \mathrm{i}\delta_{n,0}. \tag{4.57}$$

Operating on both sides with the inverse of $\mathcal{U}$ would give

$$(\delta_{n,m} + [\mathcal{U}^{-1}\mathcal{V}]_{n,m})S_m = \mathrm{i}\mathcal{U}^{-1}\delta_{n,0} \tag{4.58}$$

or

$$S_m = -[\mathcal{U}^{-1}\mathcal{V}]_{m,n} S_n + \mathrm{i}[\mathcal{U}^{-1}]_{m,n}\delta_{n,0}. \tag{4.59}$$

For small Λ, and hence $\mathcal{V}$, the solution S_m may therefore be approximated by

$$S_m = \mathrm{i}[\mathcal{U}^{-1}]_{m,n}\delta_{n,0}. \tag{4.60}$$

This can be considered as a first guess which is then itself substituted into the r.h.s. of Equation (4.59) giving the second guess

$$S_m = -\mathrm{i}[\mathcal{U}^{-1}\mathcal{V}\mathcal{U}^{-1}]_{m,n}\delta_{n,0} + \mathrm{i}[\mathcal{U}^{-1}]_{m,n}\delta_{n,0}. \tag{4.61}$$

Continuing this iterative process generates a series solution to the problem. For the purposes of this and Chapter 6, only one more iteration will be required so that

$$S_m = \mathrm{i}\left[\mathcal{U}^{-1}\mathcal{V}\mathcal{U}^{-1}\mathcal{V}\mathcal{U}^{-1} - \mathcal{U}^{-1}\mathcal{V}\mathcal{U}^{-1} + \mathcal{U}^{-1}\right]_{m,n}\delta_{n,0}. \tag{4.62}$$

Of course, the inverse of the operator U must be known, but from its definition (4.55) this is simply

$$[\mathcal{U}^{-1}]_{m,n} = \frac{1}{\mathrm{i}p - m^2 - m\alpha}\delta_{m,n}. \tag{4.63}$$

The zeroth term (first guess) when applied to the initial condition $\delta_{n,0}$ accordingly gives

$$[\mathcal{U}^{-1}]_{m,n}\delta_{n,0} = \frac{1}{\mathrm{i}p}\delta_{n,0}. \tag{4.64}$$

Multiplying out the operators as before in Section 4.4.2 one has

$$\begin{aligned}\left[\mathcal{U}^{-1}\mathcal{V}\mathcal{U}^{-1}\right]_{m,n} = \frac{\Lambda}{2}\Bigg(&\frac{\delta_{m,n+1}}{[\mathrm{i}p - m^2 - m\alpha]\,[\mathrm{i}p - (m-1)^2 - (m-1)\alpha]} \\ &+ \frac{\delta_{m,n-1}}{[\mathrm{i}p - m^2 - m\alpha]\,[\mathrm{i}p - (m+1)^2 - (m+1)\alpha]}\Bigg)\end{aligned} \tag{4.65}$$

and so

$$\left[\mathcal{U}^{-1}\mathcal{V}\mathcal{U}^{-1}\right]_{m,n}\delta_{n,0} = \frac{\Lambda}{2}\left(\frac{\delta_{m,1}}{[\mathrm{i}p - 1 - \alpha]\,\mathrm{i}p} + \frac{\delta_{m,-1}}{[\mathrm{i}p - 1 + \alpha]\,\mathrm{i}p}\right). \tag{4.66}$$

The second order term is

$$\begin{aligned}&\left[\mathcal{U}^{-1}\mathcal{V}\,\mathcal{U}^{-1}\mathcal{V}\,\mathcal{U}^{-1}\right]_{m,n} = \\ &\frac{\Lambda^2}{4}\Bigg(\frac{\delta_{m,n+2}}{[\mathrm{i}p - m^2 - m\alpha]\,[\mathrm{i}p - (m-1)^2 - (m-1)\alpha]\,[\mathrm{i}p - (m-2)^2 - (m-2)\alpha]} \\ &\quad + \frac{\delta_{m,n-2}}{[\mathrm{i}p - m^2 - m\alpha]\,[\mathrm{i}p - (m+1)^2 - (m+1)\alpha]\,[\mathrm{i}p - (m+2)^2 - (m+2)\alpha]} \\ &\quad + \frac{\delta_{m,n}}{[\mathrm{i}p - m^2 - m\alpha]\,[\mathrm{i}p - (m-1)^2 - (m-1)\alpha]\,[\mathrm{i}p - m^2 - m\alpha]} \\ &\quad + \frac{\delta_{m,n}}{[\mathrm{i}p - m^2 - m\alpha]\,[\mathrm{i}p - (m+1)^2 - (m+1)\alpha]\,[\mathrm{i}p - m^2 - m\alpha]}\Bigg)\end{aligned} \tag{4.67}$$

giving

$$\begin{aligned}\left[\mathcal{U}^{-1}\mathcal{V}\,\mathcal{U}^{-1}\mathcal{V}\mathcal{U}^{-1}\right]_{m,n}\delta_{n,0} = \frac{\Lambda^2}{4}\Bigg(&\frac{\delta_{m,2}}{[\mathrm{i}p - 4 - 2\alpha]\,[\mathrm{i}p - 1 - \alpha]\,\mathrm{i}p} + \frac{\delta_{m,-2}}{[\mathrm{i}p - 4 + 2\alpha]\,[\mathrm{i}p - 1 + \alpha]\,\mathrm{i}p} \\ &+ \frac{\delta_{m,0}}{\mathrm{i}p\,[\mathrm{i}p - 1 + \alpha]\,\mathrm{i}p} + \frac{\delta_{m,0}}{\mathrm{i}p\,[\mathrm{i}p - 1 - \alpha]\,\mathrm{i}p}\Bigg).\end{aligned} \tag{4.68}$$

Taking the inverse Laplace transform of the various terms, one finds, up to second order in Λ, the following amplitudes

$$\begin{aligned}\tilde{A}_0 = 1 - \frac{\mathrm{i}\Lambda^2}{4}\Bigg(&-\frac{\zeta}{(1-\alpha)} - \frac{\zeta}{(1+\alpha)} \\ &+ 2\frac{\mathrm{e}^{-\mathrm{i}(1-\alpha)\zeta/2}}{(1-\alpha)^2}\sin\left[\frac{(1-\alpha)}{2}\zeta\right] + 2\frac{\mathrm{e}^{-\mathrm{i}(1+\alpha)\zeta/2}}{(1+\alpha)^2}\sin\left[\frac{(1+\alpha)}{2}\zeta\right]\Bigg)\end{aligned} \tag{4.69}$$

$$\tilde{A}_{\pm 1} = \mathrm{i}\Lambda\frac{\mathrm{e}^{-\mathrm{i}(1\pm\alpha)\zeta/2}}{(1\pm\alpha)}\sin\left[\frac{1\pm\alpha}{2}\zeta\right] \tag{4.70}$$

$$\tilde{A}_{\pm 2} = -\frac{\Lambda^2}{4}\,\frac{(1\pm\alpha)\mathrm{e}^{-\mathrm{i}(4\pm 2\alpha)\zeta} - (4\pm 2\alpha)\mathrm{e}^{-\mathrm{i}(1\pm\alpha)\zeta} + (3\pm\alpha)}{(1\pm\alpha)(4\pm\alpha)(3\pm\alpha)}. \tag{4.71}$$

It is apparent that for very weak potentials the zeroth beam dominates except for certain special angles of incidence. As one moves away from perpendicular incidence ($\alpha = 0$), the first of these special angles occurs when $\alpha = \pm 1$. These are the first order *Bragg angles* and obey Bragg's law

$$2d_{sw} \sin\theta = \mathsf{m}\lambda_{dB} \tag{4.72}$$

with $\mathsf{m} = \pm 1$. Substituting in $d_{sw} = \lambda_{laser}/2$ (the periodicity of the standing wave), $\lambda_{dB} = 2\pi/k$, and $\sin\theta = a/k$, Bragg's law then reads

$$\alpha = \mathsf{m} \tag{4.73}$$

where m is a positive or negative integer. Bragg angles correspond to specular reflection from the

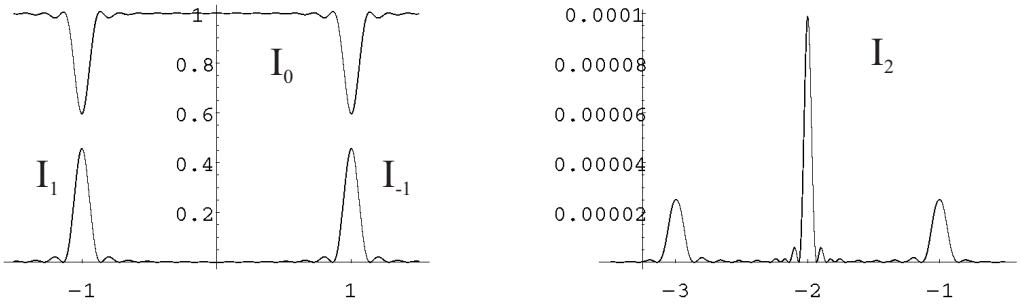

Figure 4.1: The intensities of the zeroth, first, and second order diffracted beams, as given by perturbation theory, as a function of the scaled angle α. The Bragg angles lie at $\alpha = -1, -2, -3, \ldots$. These plots were made with $\Lambda = 0.03$, $\zeta = 45$. Note the different scale on the ordinate of I_2.

parallel 'planes' (running in the z direction) of the periodic 'lattice' of the standing wave. Thus, when $\alpha = -1$, $\sin\theta_{in} = -K/k$ and $\sin\theta_{out} = K/k$, which is the result of a $2\hbar K$ momentum transfer, and so the atoms have been deflected from the zeroth to the first diffracted beam. The second diffraction order is also excited when $\alpha = -1$. This is not Bragg scattering, and is consequently weaker. This process requires a momentum transfer of $4\hbar K$. Figure 4.1 quantitatively shows how, as the angle of incidence is varied, the first diffracted beam flashes out at the expense of the zeroth beam when the angle sweeps through the first Bragg angle. The most right-hand of the three peaks of I_2 shows the diminutive second order excitation which accompanies the vastly dominant Bragg scattering.

The next angle to give a resonance is registered as the largest of the I_2 peaks and this is centered at the second Bragg angle, $\alpha = 2$. The third Bragg angle also appears as a small peak

in the second order (but again this is not Bragg scattering). Figure 4.2 illustrates the favoured scattering processes that occur when $\alpha = -1$ and $\alpha = -2$ as if the atoms were being reflected from 'Bragg planes'. It is clear that as soon as the symmetry associated with perpendicular incidence is broken, then so too is the symmetry of the scattering into the positive and negative diffraction orders. In particular, Bragg diffraction (back-scattering from the 'planes') is greatly preferred over von Laue diffraction (transmission- scattering).

The ζ dependence of the perturbative solutions displays an oscillatory behaviour; intensity 'wanders' (in the original terminology of Raman and Nath) among the orders. Such behaviour with increasing depth is known in the field of electron diffraction as 'pendellösung' (pendulum) oscillation. As ζ becomes larger, the angular dependence of the beams becomes sharper. A range of input angles around the Bragg angle are channelled into an ever narrower output range. Examining $\tilde{A}_1$, when ζ gets very large, the limiting values of the amplitude at the Bragg angle diverges as ζ, so, like the previous perturbation series, there are problems for long interaction times, but in this case only at the Bragg angles. Despite this deficiency, these solutions are certainly useful for illustrative purposes, and, crucially, indicate that for weak potentials, if one restricts attention to incidence close to the first Bragg angle, only two beams really need be considered—the zeroth and first diffracted orders. When dealing with just two beams the problem can be solved exactly, giving the correct coupling between the two waves and no divergences. This is the well known 'two-beam' solution and will be taken up in Chapter 6.

When the atoms have a transverse velocity, one might wonder if there are any Doppler effects which should be taken into account due to the atoms seeing a shifted laser frequency in their frame of reference. Such effects are certainly ignorable for Sodium travelling at 1000m/s at an angle of incidence corresponding to the first Bragg angle. For then

$$v_x = 1000 \times \sin\theta = 1000 \times \frac{K}{k} = 1000 \times \frac{10^7}{3.7 \times 10^{11}} \approx 0.03\text{ms}^{-1} \tag{4.74}$$

and so

$$\frac{v_x}{c} \approx 10^{-10}. \tag{4.75}$$

As long as the detuning from resonance is large (necessary for the validity of all the treatments so far) it seems that even if the atoms acquire substantial transverse velocities the Doppler effect need not be considered. Chapter 6 examines a slightly different scheme in which the laser is assumed to be tuned close to resonance. Providing one remains firmly in the quantum realm of small total transverse momentum transfer inside the laser beam, and small angles of incidence, such as the first Bragg angle, then one is still safe in ignoring Doppler shifts.

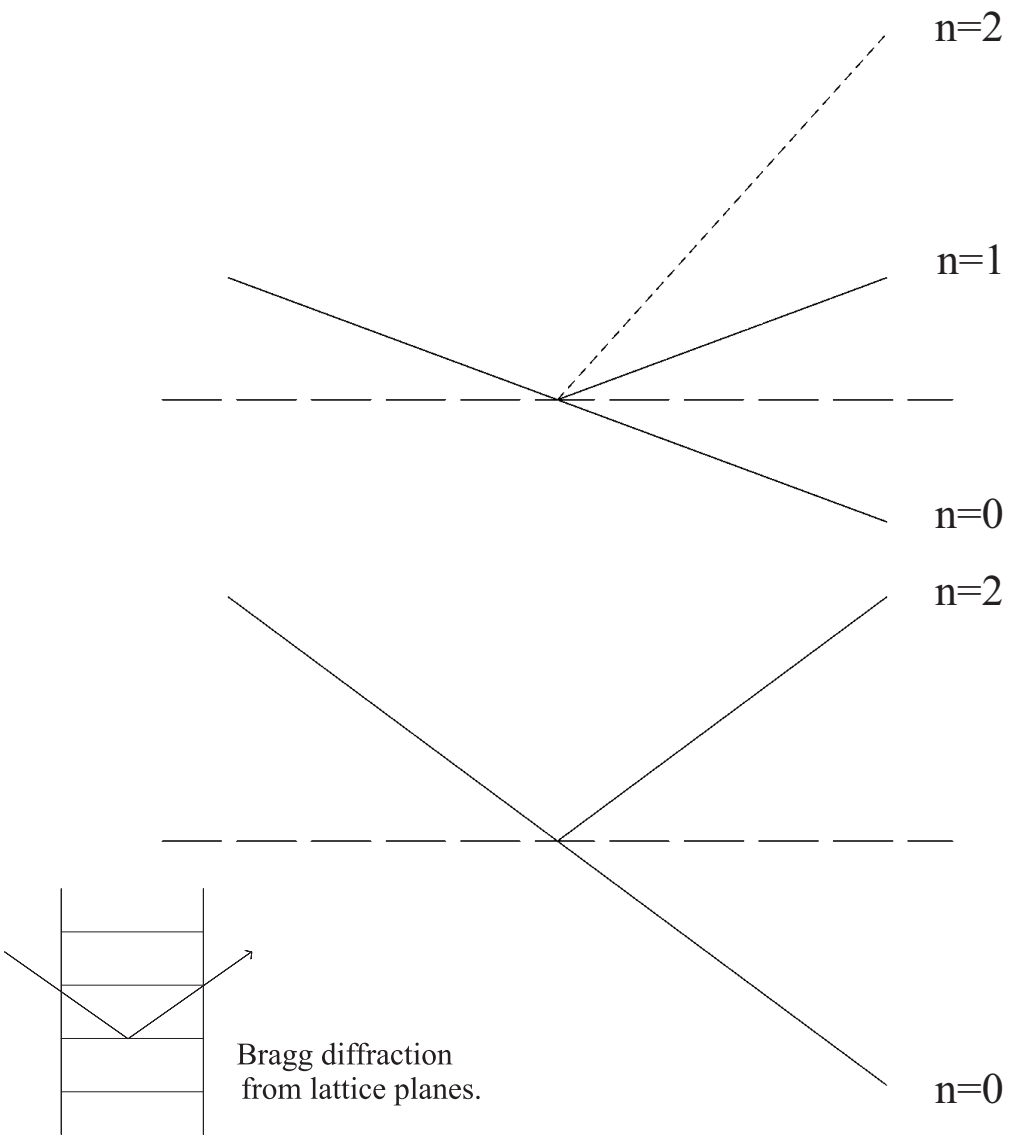

Figure 4.2: Two diagrams showing the resonant diffraction processes which take place when the angle of incidence is set at the first and then the second Bragg angles. The solid lines correspond to processes with an amplitude proportional to Λ or greater (Bragg diffraction), and the short dashed lines represent those occuring with an amplitude of order Λ^2.

4.5 Towards the classical limit

4.5.1 Numerical diagonalisation

The perturbative approach of the last section is useful for weak potentials. Weak potentials represent the very quantum end of the (transverse) energy scale. As the potential increases in strength, Λ becomes a large number and the system moves into the semiclassical regime—wave properties such as interference, remain, but the classical skeleton, which contains the turning point stucture, begins to show through. The set of R-N equations may then be truncated so that they include only a few more amplitudes than the classical maximum (one expects tunnelling into the non-classical region, but this is exponentially small) given by N, see Equation (4.29). Solving the R-N equations now becomes a real challenge. One might try to simultaneously integrate (numerically) the equations from $\zeta = 0$ to the required depth $\zeta = D$. However, when the interest is in long interaction times then it becomes more economical to find the eigenvectors of the Raman-Nath matrix. Defining

$$\tilde{A}_n \equiv B_n \mathrm{e}^{-\mathrm{i}E\zeta} \tag{4.76}$$

the perpendicular incidence R-N equation (4.12) becomes

$$E^j B_n^j = n^2 B_n^j - \frac{\Lambda}{2}\left(B_{n+1}^j + B_{n-1}^j\right) \tag{4.77}$$

where E_j is the eigenvalue belonging to the j^{th} eigenvector whose elements are B_n^j. It is no surprise that this stationary R-N equation is just the recurrence relation between the coefficients of even solutions of the Fourier analysed Mathieu equation [1], since it is from Fourier analysing the Schrödinger equation (4.1), that is also an example of a Mathieu equation, that the R-N equation is obtained. In the theory of the Mathieu equation, the eigenvalues E^j are referred to as the 'characteristic values'. The tridiagonal R-N matrix given by Equation (4.77) is

$$E\begin{pmatrix} B_{-N} \\ \vdots \\ B_{-1} \\ B_0 \\ B_1 \\ \vdots \\ B_N \end{pmatrix} = \begin{pmatrix} -\frac{\Lambda}{2} & N^2 & -\frac{\Lambda}{2} & & & & & & \\ & \ddots & \ddots & \ddots & & & & & \\ & & -\frac{\Lambda}{2} & 1 & -\frac{\Lambda}{2} & & & & \\ & & & -\frac{\Lambda}{2} & 0 & -\frac{\Lambda}{2} & & & \\ & & & & -\frac{\Lambda}{2} & 1 & -\frac{\Lambda}{2} & & \\ & & & & & \ddots & \ddots & \ddots & \\ & & & & & & -\frac{\Lambda}{2} & N^2 & -\frac{\Lambda}{2} \end{pmatrix} \begin{pmatrix} B_{-N} \\ \vdots \\ B_{-1} \\ B_0 \\ B_1 \\ \vdots \\ B_N \end{pmatrix}. \tag{4.78}$$

The eigenvectors describing quantum particles subject to periodic potentials are known as Bloch waves. Being eigenvectors, the Bloch waves propagate undisturbed through the laser beam. The farfield interference pattern generated by the interaction is given by the superposition of these

Bloch waves (each multiplied by its individual phase (4.76)) which matches the initial conditions. Denoting the j^{th} momentum space Bloch wave as $|\chi_j\rangle$, the total wavefunction is written

$$|\Psi\rangle = \sum_{j=0}^{N} c_j \ |\chi_j\rangle \ \mathrm{e}^{-\mathrm{i}E_j D} \tag{4.79}$$

where

$$c_j = \mathrm{e}^{\mathrm{i}E_j D}\langle\chi_j \ |\Psi(\zeta = 0)\rangle = \langle\chi_j \ |\delta_{n,0}\rangle = B_0^j \tag{4.80}$$

is the overlap of the j^{th} Bloch wave with the initial condition that the atoms are all in the zeroth beam. Both $|\chi_j\rangle$ and c_j can be taken as real. The convention will be adopted whereby the Bloch waves are indexed so that the smallest eigenvalue corresponds to $j = 1$. 'Smallest' means the negative eigenvalue with the largest absolute magnitude. In the standard theory of the Mathieu equation [55], the solutions B_n^j corresponding to the characteristic value E^j can be developed using continued fractions (and this approach is also taken by Berry [16]—though there the continued fraction technique is applied to the Laplace transfomed R-N equation (4.54)). Here however, the Bloch waves will be obtained by numerical diagonalisation of the R-N matrix (4.78); Figures 4.3–4.7 were constructed in this way. They all have the same classical mechanics in that they each correspond to the same classical depth of $z_c = 3\pi/2$. In reference to the classical picture, Figure 3.4, the intensity patterns are vertical slices, from the z-axis up, that record the probability distribution for the atom beam between the second and the third cusp, so just two caustics are expected. Figure 4.3 is the most quantum, with relatively few beams being produced, and each successive picture shows the effect of making the system more classical by increasing Λ. The relatively short interaction distance was chosen to keep the pictures simple. In particular, the first, outer, caustic, whose cusp is at $z_c = 0$, is 'clean' in the sense that there are no trajectories contributing to that part of the distribution which are not taking part in the caustic. And, as predicted, the caustic is decorated with a beautiful Airy function. While the second, inner caustic, that was born at $z_c = \pi$ is clearly discernable, the Airy distribution has been disrupted by interference with orbits not taking part in the caustic (see Figure 3.4). In contrast to the carefully orchestrated phases of the caustic trajectories, a non-caustic trajectory effectively has a discordant 'random' phase which wreaks havoc with the ordered oscillations of the Airy function. The caption to each figure also states the number of beams that the classical mechanics predicts using Equation (4.29). The degree to which this prediction is obeyed provides another measure of how classical each picture is.

The final two pictures, Figure 4.8, show the momentum space intensity as function of distance into the laser beam for two different values of Λ. These were created by combining slices at successive distances. If, rather than just illustrating the classical momentum space trajectories,

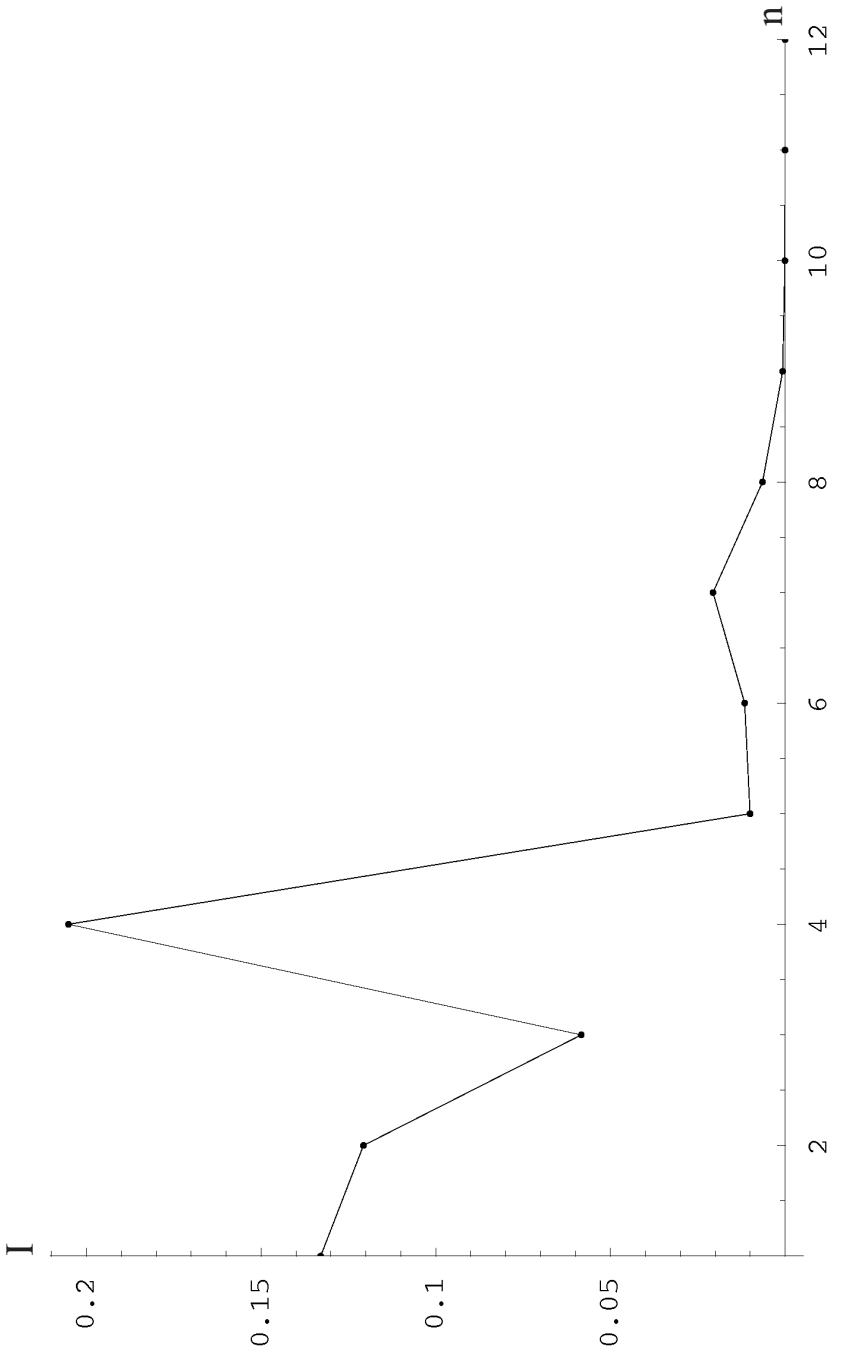

Figure 4.3: The farfield intensity calculated by numerical diagonalisation of the R-N matrix (4.78) for $\Lambda = 25$ and $z_c = 3\pi/2$. Each dot is the actual intensity of the n^{th} order and the continuous line joins them. Predicted number of beams: 7.

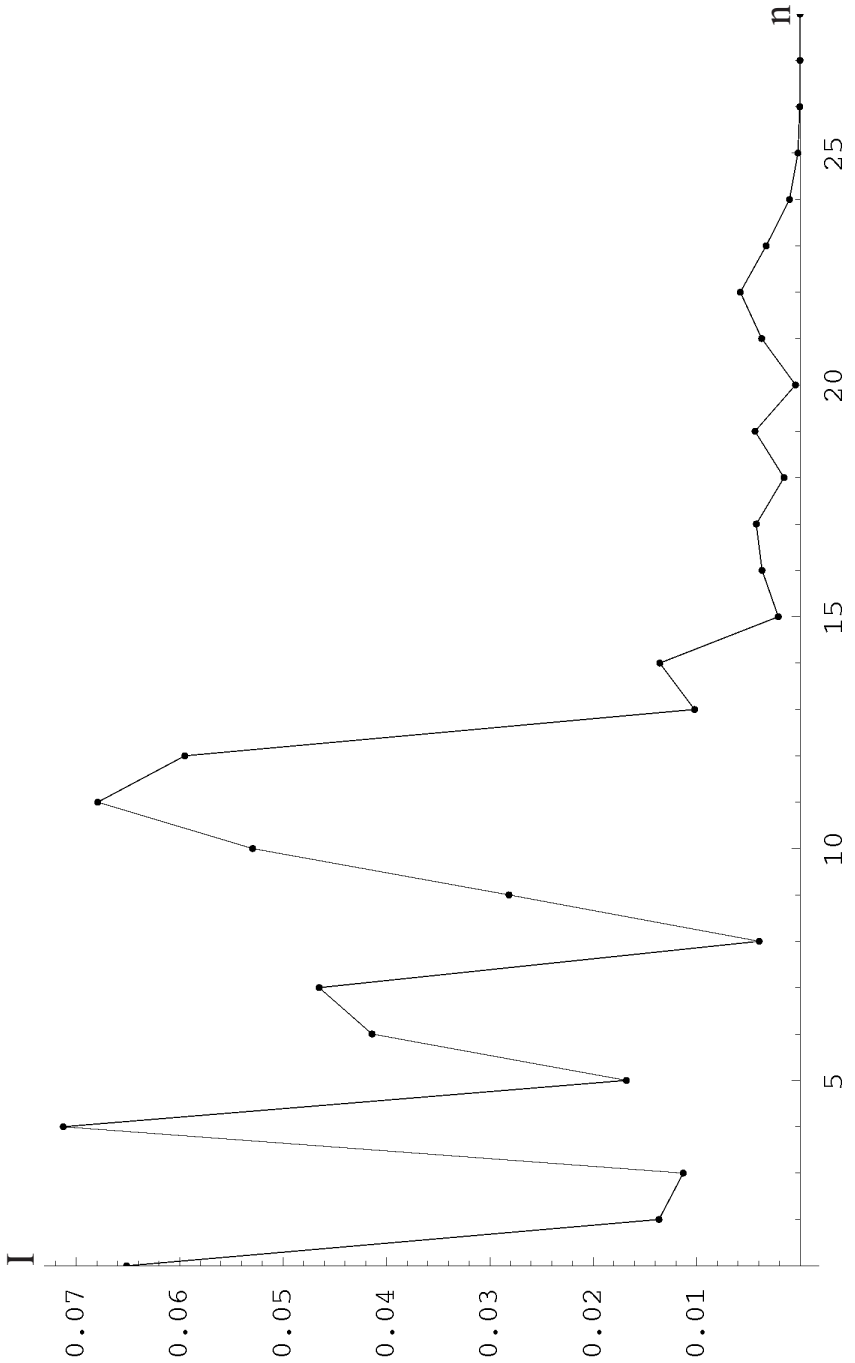

Figure 4.4: The farfield intensity calculated by numerical diagonalisation of the R-N matrix (4.78) for $\Lambda = 250$ and $z_c = 3\pi/2$. Each dot is the actual intensity of the n^{th} order and the continuous line joins them. Predicted number of beams: 22.

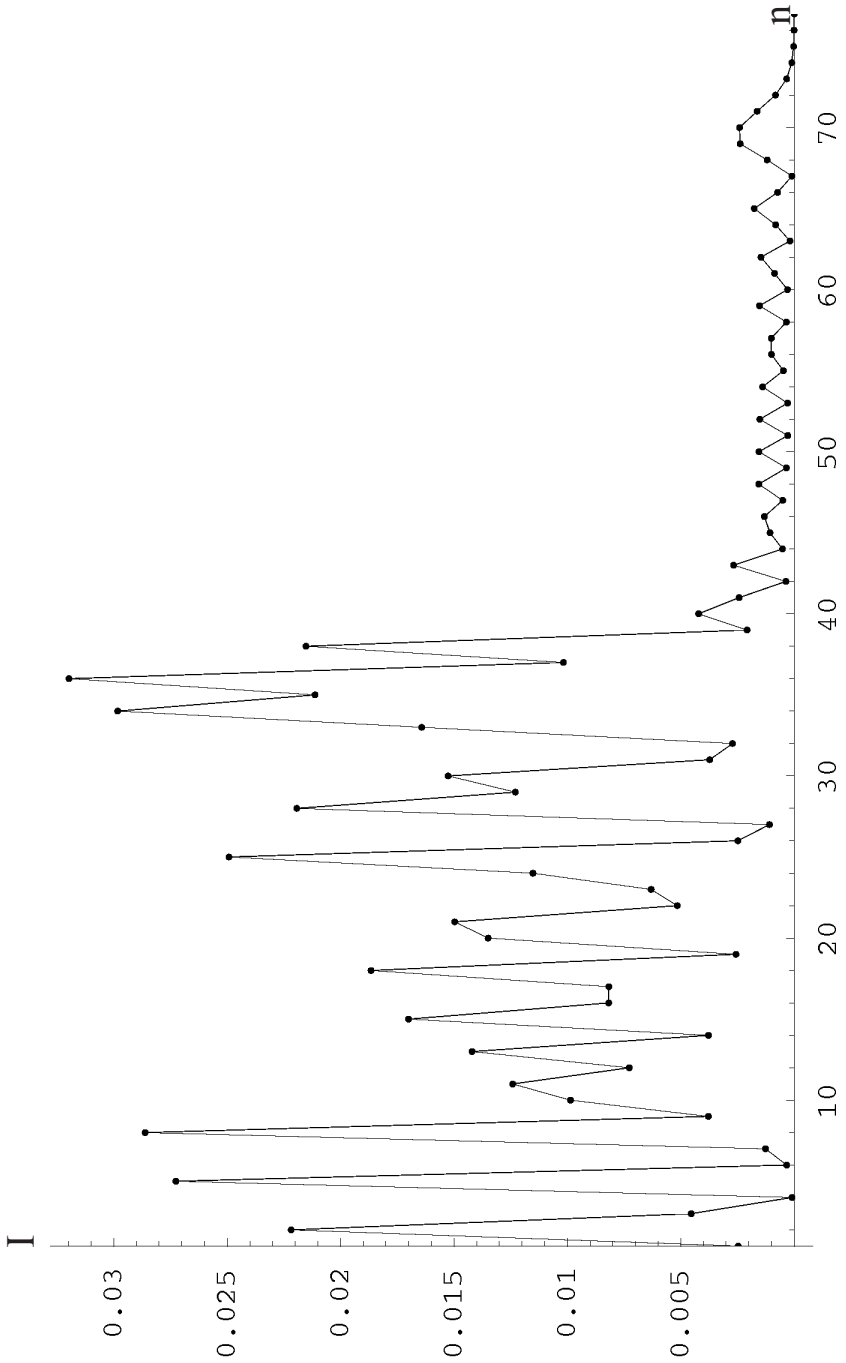

Figure 4.5: The farfield intensity calculated by numerical diagonalisation of the R-N matrix (4.78) for $\Lambda = 2500$ and $z_c = 3\pi/2$. Each dot is the actual intensity of the n^{th} order and the continuous line joins them. Predicted number of beams: 71.

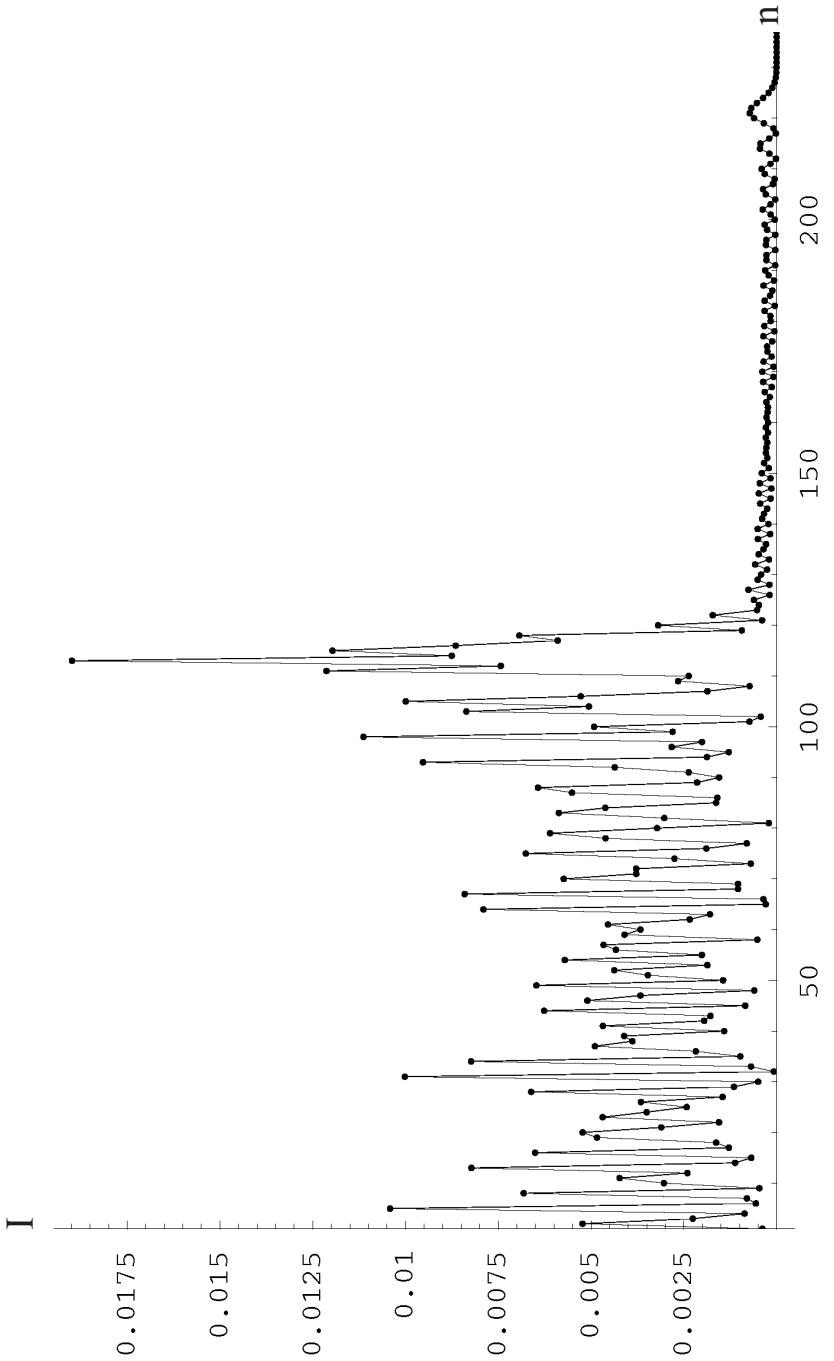

Figure 4.6: The farfield intensity calculated by numerical diagonalisation of the R-N matrix (4.78) for $\Lambda = 25 \times 10^3$ and $z_c = 3\pi/2$. Each dot is the actual intensity of the n^{th} order and the continuous line joins them. Predicted number of beams: 224.

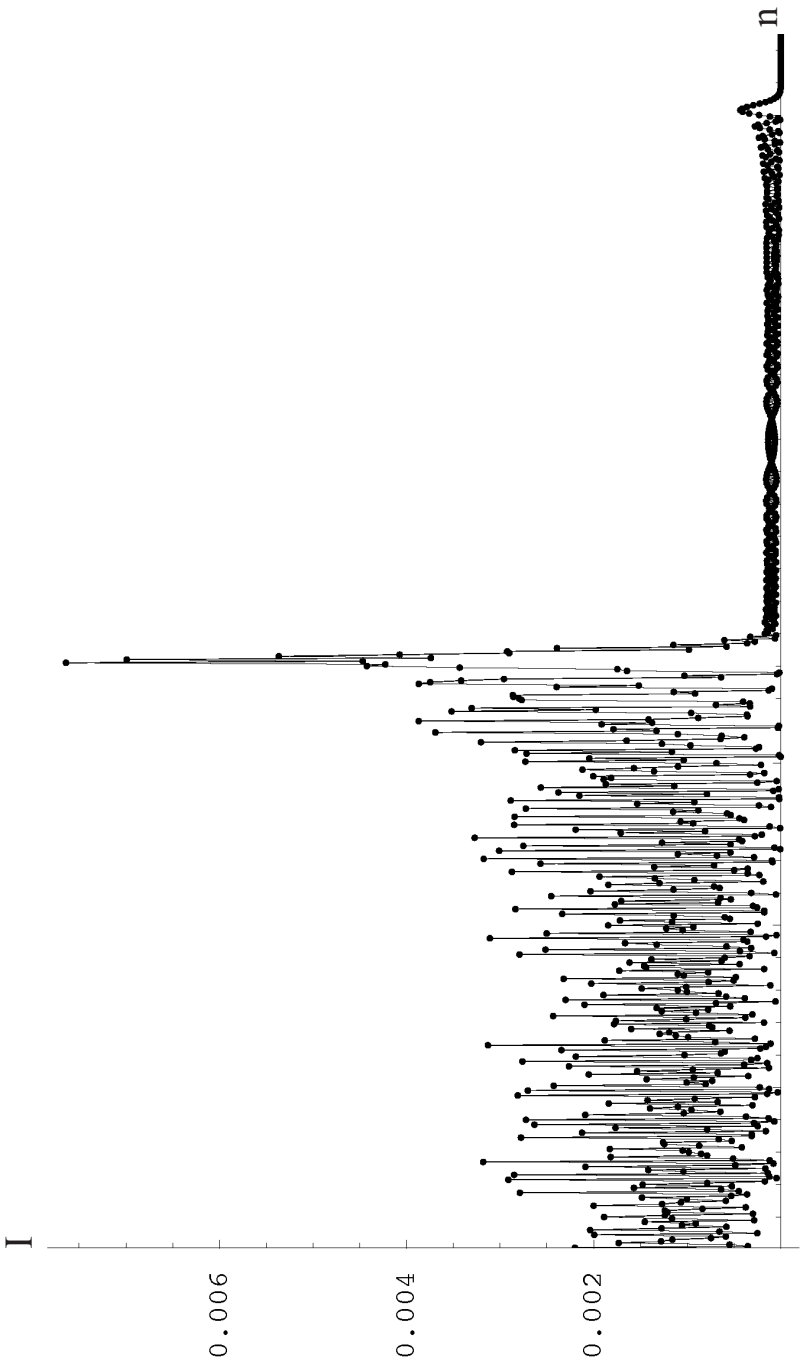

Figure 4.7: The farfield intensity calculated by numerical diagonalisation of the R-N matrix (4.78) for $\Lambda = 25\times10^4$ and $z_c = 3\pi/2$. Each dot is the actual intensity of the n^{th} order and the continuous line joins them. Predicted number of beams: 707.

Figure 3.4 had shown the intensity resulting from their summation, then these pictures would be the quantum equivalent, though only for z_c between 3 and 4.

4.5.2 The range of the eigenvalues

A related prediction to the maximum possible number of diffracted beams, is the range of the eigenvalues satisfying the stationary R-N equation (4.77). The R-N equation is actually an equation for the transverse motion—the constant longitudinal evolution having been separated out by the inclusion of the e^{ikz} term in the wavefunction. Clearly the range of transverse energies that an atom can extract from the washboard potential is 0–V_0 Joules. The energy operator acting on the *bound* transverse eigenvectors would therefore give eigenvalues also lying in this range. Taking advantage of the fact that $P_z = \hbar k$ is a constant of the motion, the energy operator can be expressed as

$$i\hbar\frac{\partial}{\partial t} = i\hbar\frac{dz}{dt}\frac{\partial}{\partial z} = i\frac{\hbar^2 k}{m}\frac{\partial}{\partial z}. \tag{4.81}$$

Therefore, using the definition (4.9) for ζ,

$$i\frac{\partial}{\partial \zeta} = \frac{m}{2\hbar^2 K^2}\cdot i\hbar\frac{\partial}{\partial t} \tag{4.82}$$

and, noting the definition of Λ (4.10), the eigenvalues generated by the $\partial/\partial\zeta$ operator naturally lie between 0 and 2Λ, since $\partial/\partial t$ on an eigenvector pulls down a factor lying between 0 and $iV_0/\hbar$. However, the removal of the constant diagonal term by the phase transformation $A_n = \tilde{A}_n \exp(i\Lambda\zeta)$, means that when the R-N equation is expressed in terms of $\tilde{A}$, and hence B_n, the bound state eigenvalues lie in the range

$$-\Lambda < E^j_{\text{bound}} < \Lambda. \tag{4.83}$$

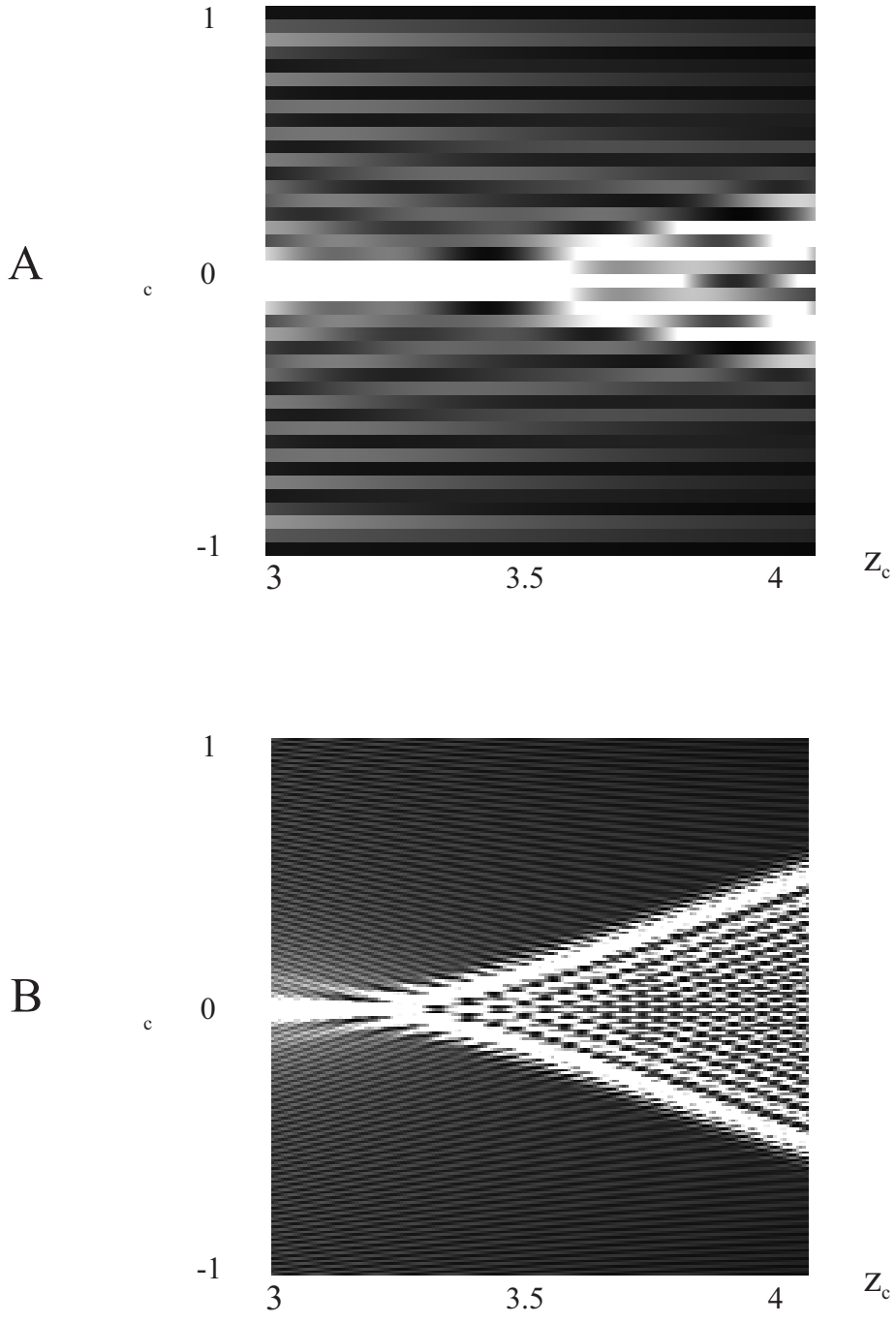

Figure 4.8: An atomic cusp and folds; the momentum space intensity as a function of depth. A) $\Lambda = 25$, B) $\Lambda = 250$. Note that the angle co-ordinate has also been scaled in terms of the classical angle, and the higher intensity areas are lighter in colour.

Chapter 5

A realistic model?

5.1 Motivation

The Raman-Nath equations (4.12) describe the stationary scattering of an infinitely wide wave from a one dimensional potential. This is the simplest possible model for diffraction from a thick grating. Chapter 1 indicated that while a number of investigators have already gone on to probe more complicated situations, the more modest behaviour associated with this most basic situation has received little attention.

However, before too much effort is expended in studying the plain Raman-Nath equations, it is important to check that this is a realistic model. Of the many refinements that might be addressed, it seems reasonable to single out the presence of a longitudinal profile for the potential, and a finite width of atomic beam, as being two features inherent in any experiment which might have significant effects. It is *not* the purpose of this chapter to give a detailed account of the influence of these extra parameters; the treatment will be as brief as possible. The intention is merely to indicate that experiments can be conducted in regimes where either the effects are negligible or at worst only modify the details; the basic form of the structures contained in the solutions of the Raman-Nath equations remain intact.

5.2 Finite atomic beam

The presumption so far has been that the atom beam is a plane wave of infinite transverse extent. If the atom beam is to be limited in $\mathbf{x}$ in some way, then this necessarily introduces some spread into the transverse momentum. The question then becomes, to what extent are the diffracted beams blurred?

5.2.1 A Gaussian beam

A reasonable model for a *coherent*, normalised, incident atomic wavefunction is the Gaussian

$$\Psi_{\text{incident}} = \Psi(x, z = 0) = \frac{1}{\sqrt{L}(2\pi)^{1/4}}\, \mathrm{e}^{-x^2/(4L^2)} \tag{5.1}$$

where L gives a measure of the width of the beam. This can itself be represented as an integral over transverse plane waves, $\exp(\mathrm{i}ax)$, each weighted by the Gaussian factor $\exp(-a^2L^2)$

$$\begin{aligned}\Psi(x,0) = \frac{1}{\sqrt{L}(2\pi)^{1/4}}\mathrm{e}^{-x^2/(4L^2)} &= \frac{1}{\sqrt{L}(2\pi)^{1/4}}\mathrm{e}^{-x^2/(4L^2)}\ \frac{L}{\sqrt{\pi}}\ \int_{-\infty}^{\infty} \mathrm{e}^{-[aL-\mathrm{i}x/(2L)]^2}\ da \\ &= \sqrt{\frac{L}{\pi\sqrt{2\pi}}} \int_{-\infty}^{\infty} \mathrm{e}^{\mathrm{i}ax - a^2L^2}\ da.\end{aligned} \tag{5.2}$$

In order that all the component waves should have the same total wavenumber, k say, (recall also Section 4.4.1) the longitudinal wavenumber is taken as $\sqrt{k^2 - a^2}$. Assuming that the beam is not too narrow, so L is of reasonable size, then the most important contributions to the wavefunction come from waves with small values of the transverse wavenumber a—especially when compared to the magnitude of k. One therefore expands the longitudinal wavenumber as

$$\sqrt{k^2 - a^2} \approx k - \frac{a^2}{2k}. \tag{5.3}$$

Incorporating the z dependence of the initial wavefunction gives

$$\Psi(x, z) = \sqrt{\frac{L}{\pi\sqrt{2\pi}}}\mathrm{e}^{\mathrm{i}kz} \int_{-\infty}^{\infty} \mathrm{e}^{\mathrm{i}ax - a^2L^2}\mathrm{e}^{-\mathrm{i}a^2z/(2k)}\ da. \tag{5.4}$$

Inside the interaction region the wavefunction develops side beams as before

$$\Psi(x, z) = \sqrt{\frac{L}{\pi\sqrt{2\pi}}}\mathrm{e}^{\mathrm{i}kz} \int_{-\infty}^{\infty} \mathrm{e}^{-\mathrm{i}a^2z/(2k) - a^2L^2} \sum_{n=-\infty}^{\infty} A_n(a, z)\mathrm{e}^{\mathrm{i}(a+2nK)x}\ da. \tag{5.5}$$

This is just a weighted integral over partial waves, each of which corresponds to a particular value of the initial transverse wavenumber a

$$\psi(a) = \mathrm{e}^{\mathrm{i}\sqrt{k^2-a^2}z} \sum_{n=-\infty}^{\infty} A_n(a, z)\mathrm{e}^{\mathrm{i}(a+2nK)x} \tag{5.6}$$

and obeys its own independent Raman-Nath equation; the a dependence in the notation for the amplitudes $A_n(a, z)$, is intended to reflect this. The wavefunction (5.5) has a continuous momentum distribution and is no longer periodic in $\mathbf{x}$. The diffraction amplitude which has the transverse momentum s (direction $\theta \approx s/k$) after traversing the potential for distance $z = D$, is given by the

Fourier transform of the wavefunction (5.5)

$$\begin{aligned} B(s,D) &= \frac{1}{2\pi}\int_{-\infty}^{\infty}\Psi(x,D)\mathrm{e}^{-\mathrm{i}sx}\,dx \\ &= \sqrt{\frac{L}{\pi\sqrt{2\pi}}}\mathrm{e}^{\mathrm{i}kD}\int_{-\infty}^{\infty}\mathrm{e}^{-\mathrm{i}a^2D/(2k)-a^2L^2}\sum_{n=-\infty}^{\infty}\delta(a+2nK-s)A_n(a,D)\,da \\ &= \sqrt{\frac{L}{\pi\sqrt{2\pi}}}\mathrm{e}^{\mathrm{i}kD}\sum_{n=-\infty}^{\infty}\mathrm{e}^{-\mathrm{i}(s-2nK)^2D/(2k)}\mathrm{e}^{-(s-2nK)^2L^2}A_n(s-2nK,D) \end{aligned} \tag{5.7}$$

where the Dirac delta function representation

$$\delta(t-t_0) = \frac{1}{2\pi}\int_{-\infty}^{\infty}\mathrm{e}^{\mathrm{i}\alpha(t-t_0)}\,d\alpha \tag{5.8}$$

has been used. The amplitude $B(s,D)$ is made up from a sum of contributions from the different diffraction orders labelled by n; but these contributions are weighted by a Gaussian centred at s. Alternatively, viewed as a function of s, the pattern is a series of Gaussians centred at each of the angles $\theta = s/k = 2nK/k$. Each of the diffracted beams has inherited the Gaussian dependence of the incident beam—this is not surprising since the Fourier transform of a Gaussian is another Gaussian.

A necessary condition for the infinite beam to be a reasonable model for any experiment may now be stated as the requirement that the individual diffracted beams should be clearly visible. That is, the Gaussians, as functions of s, should not overlap to any great extent. From Equation (5.7), this condition is seen to be

$$L \gg \frac{1}{2K}. \tag{5.9}$$

Now, since the width of each well of the sinusoidal potential is $x = \pi/K$, the individual beam visibility requirement translates into ensuring that the initial beam, which is vaguely of width L, must illuminate many wells of the standing wave laser. The numbers given in Section 1.3.1 suggest that the majority of experiments would indeed fulfil this condition. Indeed it would be quite a feat to perform an experiment on a single well.

5.2.2 The rocking curves

The non-overlapping condition greatly simplifies the task of finding the intensity pattern, for then one can approximate the diffraction probabilities by

$$|B(s,D)|^2 \approx \frac{L}{\pi\sqrt{2\pi}}\sum_{n=-\infty}^{\infty}\mathrm{e}^{-2(s-2nK)^2L^2}|A_n(s-2nK,D)|^2 \tag{5.10}$$

so that the intensity of the n^{th} beam is

$$|B_n(s,D)|^2 \approx \frac{L}{\pi\sqrt{2\pi}}\,\mathrm{e}^{-2(s-2nK)^2L^2}|A_n(s-2nK,D)|^2. \tag{5.11}$$

An important consideration is the s dependence of the amplitudes $A_n(s - 2nK, D)$. This can be addressed by examining the *rocking curves* which describe the behaviour of the amplitudes as the angle of incidence is varied (the amplitudes rotate with incidence angle). If there is significant structure in the amplitudes on a scale $|s - 2nK| < 1/L$, i.e. before the Gaussian kills off the A_n, then this behaviour will appear in the farfield pattern and is not accounted for by the infinite beam approximation. If on the other hand the amplitudes are roughly constant over this range then one can take

$$I_n(s - 2nK, D) = |A_n(s - 2nK, D)|^2 \approx |A_n(0, D)|^2 \tag{5.12}$$

in which case the infinite beam approximation is adequate. Three examples of rocking curves for the first ten beams are shown in Figures 5.1–5.3. The rocking curves were generated by numerically solving a new set of Raman-Nath equations for each value of the scaled input angle α (4.35). Had these curves been generated experimentally with a Gaussian beam, then there would of course be a Gaussian envelope on each curve as explained above, but it is not included here. Figures 5.1 and 5.2 have the same value of Λ, but different depths, demonstrating that, as might be expected, the the rocking structure becomes more complicated with increasing depth. To obtain a good approximation to the infinite beam approximation, one would therefore require an ever wider input beam for increasing width of interaction zone, so that the Gaussian over each diffracted amplitude is sufficiently narrow to smooth away any structure.

The same is true when Λ is increased. Figure 5.1 and 5.3 share the same value of the depth, but Λ has been increased to 200 for the latter.

The width of the beam is therefore a factor which can influence the farfield pattern. If an experiment were to be conducted exploring the long interaction time region, it would clearly be advisable to first check the rocking curves so an estimate of the necessary width could be made. The risk of not doing so is a farfield pattern that is too complicated to interpret.

5.3 A smooth potential envelope

In reality the potential does not switch on suddenly at $z = 0$, and switch off at $z = D$, but has some smooth profile which will be denoted $f(z)$, so that the Hamiltonian (3.4) becomes

$$H = \frac{P_x^2}{2m} + \frac{P_z^2}{2m} - V_0 f(z) \cos^2 Kx = E. \tag{5.13}$$

The remarks made in Chapter 1 suggested that the ideal profile for long interaction times would be smooth wings either side of an essentially flat plateau. As far as comparison with the flat potential is concerned; the shorter the wings the better.

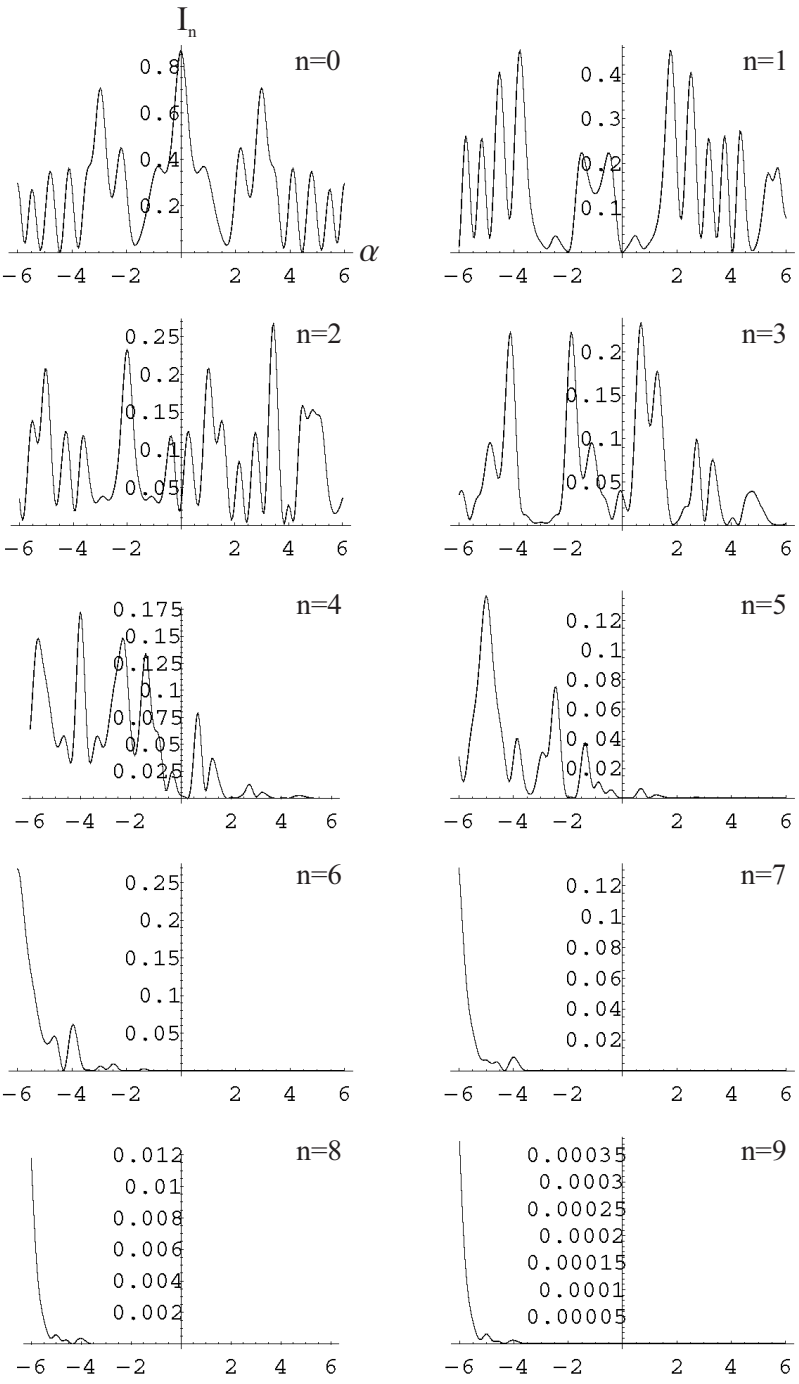

Figure 5.1: The rocking curves of the zeroth and first nine beams for $\Lambda = 10$, $\zeta = 3$.

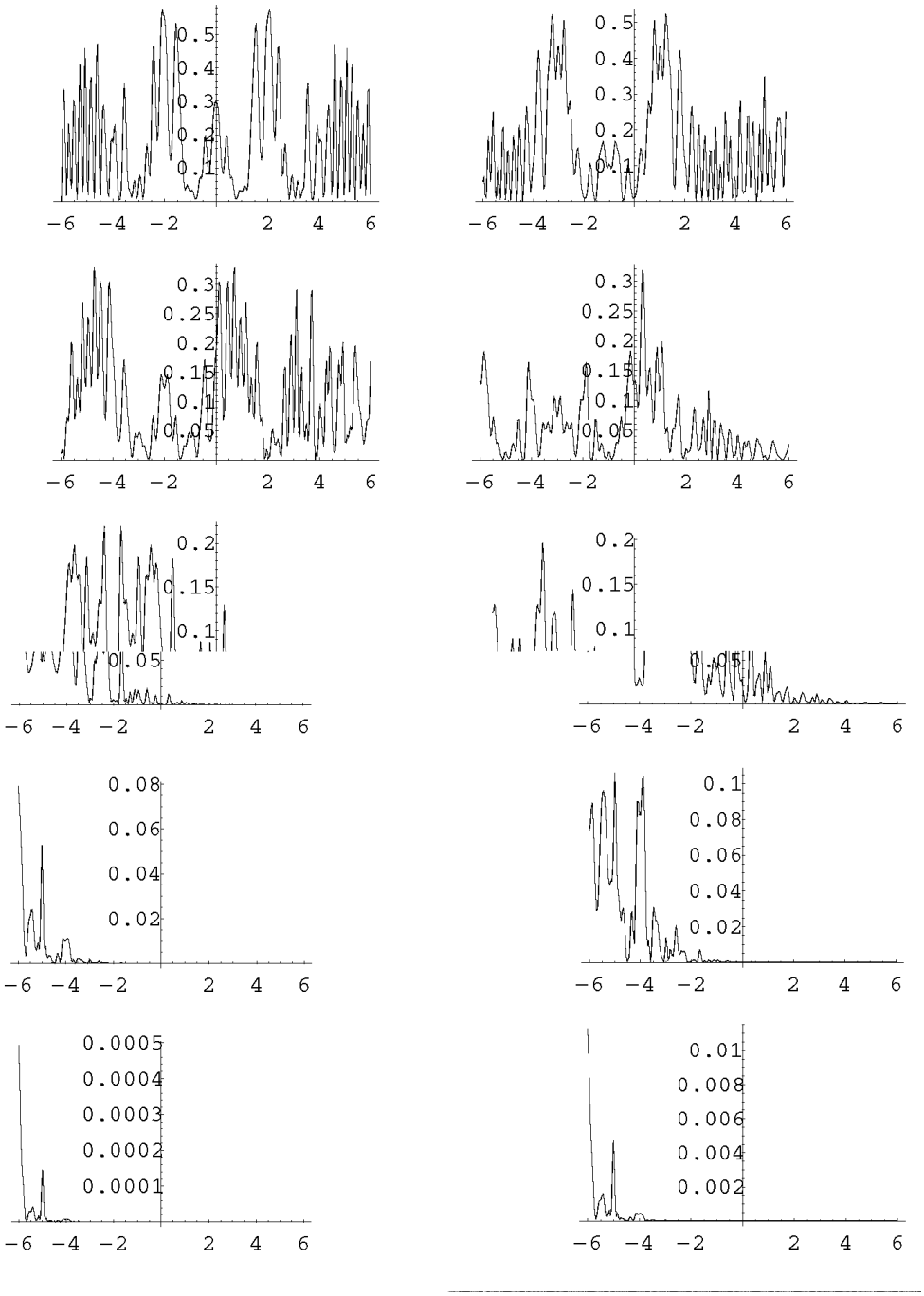

Figure 5.2: The rocking curves of the zeroth and first nine beams for $\Lambda = 10$, $\zeta = 9$.

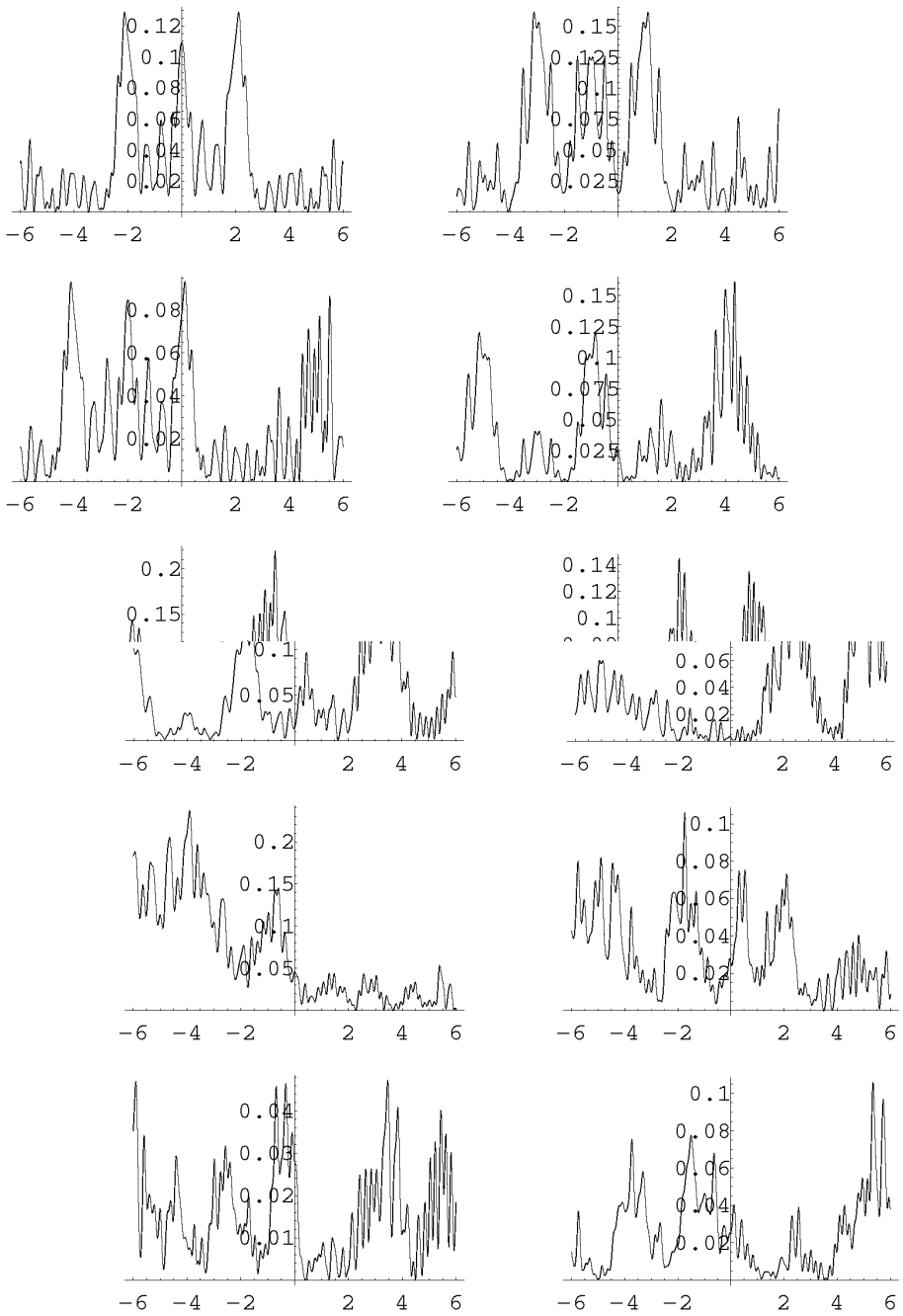

Figure 5.3: The rocking curves of the zeroth and first nine beams for $\Lambda = 200$, $\zeta = 3$.

However, the most standard candidate for $f(z)$ is a Gaussian, this being accepted as the typical intensity profile for a laser beam. The Gaussian is not an ideal envelope, since it contains no central plateau. Despite the presence of a width parameter, this is of little value since the potential is always either switching-on or off; there is no constant section for comparison. A function which comes closer to the ideal is $f(z) = \tanh(z/w)$. For computational purposes propagation would be begun at some finite negative value of z, but which is great enough to approximate to $z = -\infty$, where the initial condition

$$P_x(z = -\infty) = 0 \tag{5.14}$$

is enforced. The value of the single parameter w determines the width of the wings, and propagation may then proceed indefinitely along the nearly flat plateau. Of course, to obtain the correct switching off behaviour, another tanh function must be used back to back with the first. In their book *Mechanical Action of Light on Atoms* [45], Kazantsev, Surdutovich, and Yakovlev show that the two-beam Raman-Nath equation can be solved for a tanh envelope: the Raman-Nath equations, being paraxial, are first order in z. Substituting the equation for one of the beams into the other gives a second order differential equation which is similar to a Schrödinger equation with a tanh potential. This has solutions in terms of hypergeometric functions (see the text on quantum mechanics by Landau and Lifshitz). The two solutions, one due to each tanh, must then be matched in the middle and satisfy the boundary condition (5.14). The solution of Kazantsev *et al.* is one of only a very few analytic solutions for the smooth profile which exist—and being restricted to the two beam case, is of limited use for the general problem.

The need to incorporate smooth wings into the laser profile is considered in an experimental paper by Moskowitz *et al.* [57]. They establish that even supersonic atom beams have adiabatic entry into their laser because the internal evolution, governed by the Rabi frequency, Ω (Equation (2.24)), of the atom is so fast. Their calculation, which was for an intense laser field, went as

$$\Omega \times (\text{field ``turn-on'' time}) \sim 10^9 \text{sec}^{-1} \times 10^{-8} \text{sec} = 10 \tag{5.15}$$

which suggests that atoms can undergo ten internal cycles during entry into the field. From the known longitudinal speed of the atoms, their estimation of the width of the entry wing is only $\sim 10\mu$m. However, for their experiment, the internal evolution was sufficiently rapid that by the time the atom reached the constant region of the potential, it might, at the very most, be in the tenth diffracted beam. Clearly, for a fixed width of wing, this number depends on the Rabi frequency which is in turn a linear function of the field strength. For more intense fields, the wings can be made shorter and still achieve the same adiabatic entry. In the semiclassical limit, for which the wings are of greatest importance[1] the motion of the atom into the tenth diffracted beam during

[1] The weak field case has a small Rabi frequency so the entry may well be non-adiabatic, but the field is considered

entry is of negligible consequence.

Nevertheless, a number of calculations will now be made using the 'worst case scenario' Gaussian envelope (which has nothing but wings) to demonstrate that the basic form of the behaviour familiar from the preceding chapters is still maintained.

5.3.1 Classical motion

The action for an oscillating system, taken over half a period

$$S_x = \int_{x_{min}}^{x_{max}} P_x \, dx \tag{5.16}$$

is known to be accurately conserved despite the change in some parameter of the Hamiltonian, provided that change is slow in comparison with the period. If the longitudinal profile is slowly varying in comparison with the transverse oscillation frequency, then this raises the possibility of using the conservation of action to help find the motion of the atoms. Unfortunately however, this method is not applicable to the current situation for reasons that were first discussed by J. H. Hannay in 1986 [41]. Although motion within a well is likely to obey the conservation of action, there is a blatant exception when considering motion near the separatrix. Then the motion can become infinitely slow and hence violate the requirement that it greatly exceed the rate of change of the parameter. Hannay realised (and derived the generic effects on the action) that any change of a parameter that brought an orbit close to a separatrix (such as the top of a barrier where it effectively gets trapped) was likely to occasion problems. Considering the situation here, the separatrix energy is taken from zero to some value and then back again, and thus it seems that *every* single trajectory is capable of traversing the separatrix at some point during its evolution (which implies escaping into the neighbouring well). Thinking in configuration space, it may so happen that a particular trajectory is not in the correct position at the correct time to experience the change in period, but there is certainly a risk that it may occur.

Under these circumstances, any hope of attacking the problem analytically was abondoned in favour of numerical demonstrations. For numerical convenience, rather than taking an actual Gaussian as the envelope, the Gaussian-like function

$$f(z) = \begin{cases} \mathrm{e}^{-z^2/(w^2-z^2)} & |z| < w \\ 0 & |z| > w \end{cases} \tag{5.17}$$

was used. This has the advantage of definitely (and smoothly) switching on/off at $z = \mp w$ (see Figure 5.4). Figure 5.5 shows the classical trajectories, with envelope (5.17), obtained numerically

weak enough that this should cause little disturbance to the internal equilibrium of the atom which is necessary for the validity of the potential derived in Chapter 2.

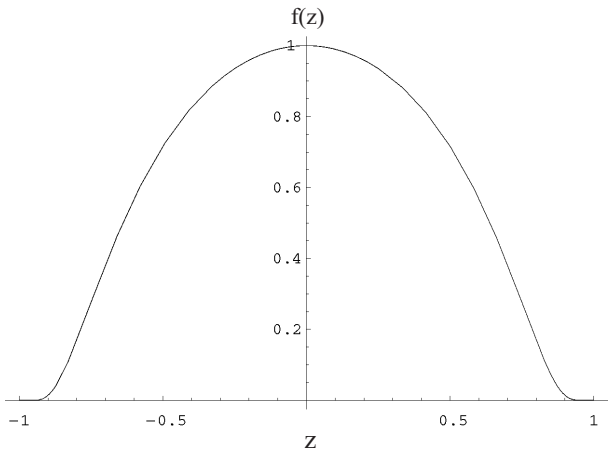

Figure 5.4: The 'Gaussian-like' envelope function $f(z) = \exp(-z^2/(w^2 - z^2))$, plotted for $w = 1$.

from the Hamiltonian (5.13) by integrating Hamilton's equations; all the parameters have been put equal to unity, except the energy, which has been chosen as $E = 0.5$, and the width, which was set at $w = 15$. The motion, whilst different, still produces caustics of a similar nature to before. Note how the configuration space rays have been slightly 'crushed' down into the well. This behaviour is parameter dependent, so, for instance, choosing a greater value of E would give less crushing. Notice also how, as the potential decays away, the trajectories are able to slip into the neighbouring wells. This is the separatrix crossing behaviour. Once again it is emphasised that taking a flat potential envelope with short wings, the behaviour can be made arbitrarily close to the constant longitudinal potential case.

5.3.2 Quantum intensities

Following through the derivation of the Raman-Nath equations for normal incidence, as given in Section 4.2, but now including the z-envelope for the potential as in Equation (5.13), one obtains the modified Raman-Nath equations

$$\mathrm{i}\frac{\partial A_n}{\partial \zeta} = n^2 A_n - f(\zeta)\frac{\Lambda}{2}\left(A_{n+1} + 2A_n + A_{n-1}\right). \tag{5.18}$$

The r.h.s. is no longer ζ-independent, so eigenvectors of the Raman-Nath matrix (see Equation (4.78)) do not exist. Numerical solutions must therefore be found by the simultaneous integration of the (truncated) set of Raman-Nath equations. When the envelope (5.17) is used, the initial

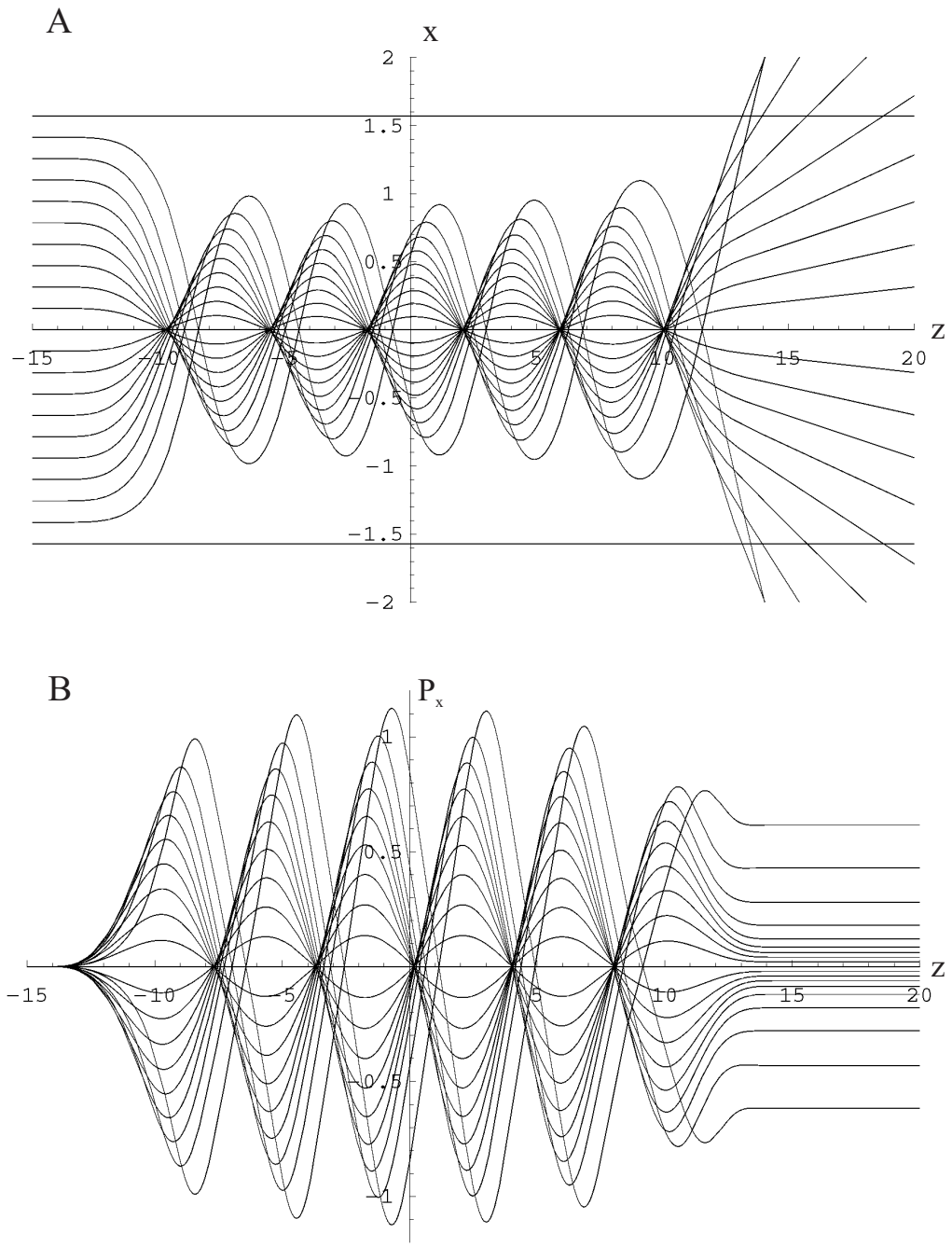

Figure 5.5: The classical motion with the longitudinal envelope (5.17), $E = 0.5$, $w = 15$; A) configuration space, B) (transverse) momentum space.

condition is

$$A_n(\zeta = -w) = \delta_{n,0} \tag{5.19}$$

and the integration must be taken from $-w$ to $+w$. Figure 5.6 gives the intensity patterns resulting from three different values of the width w, for which the Raman-Nath equations (5.18) were integrated using the fourth order Runge-Kutta method. All correspond to the classical energy $E = 0.5$, and the last, Figure 5.6 C), has the same width, $w = 15$, as the classical pictures 5.5. Any specific comparison with the flat potential over the same distance would be poor, but the pictures indicate that the same Airy function behaviour still survives (as is guaranteed by catastrophe theory).

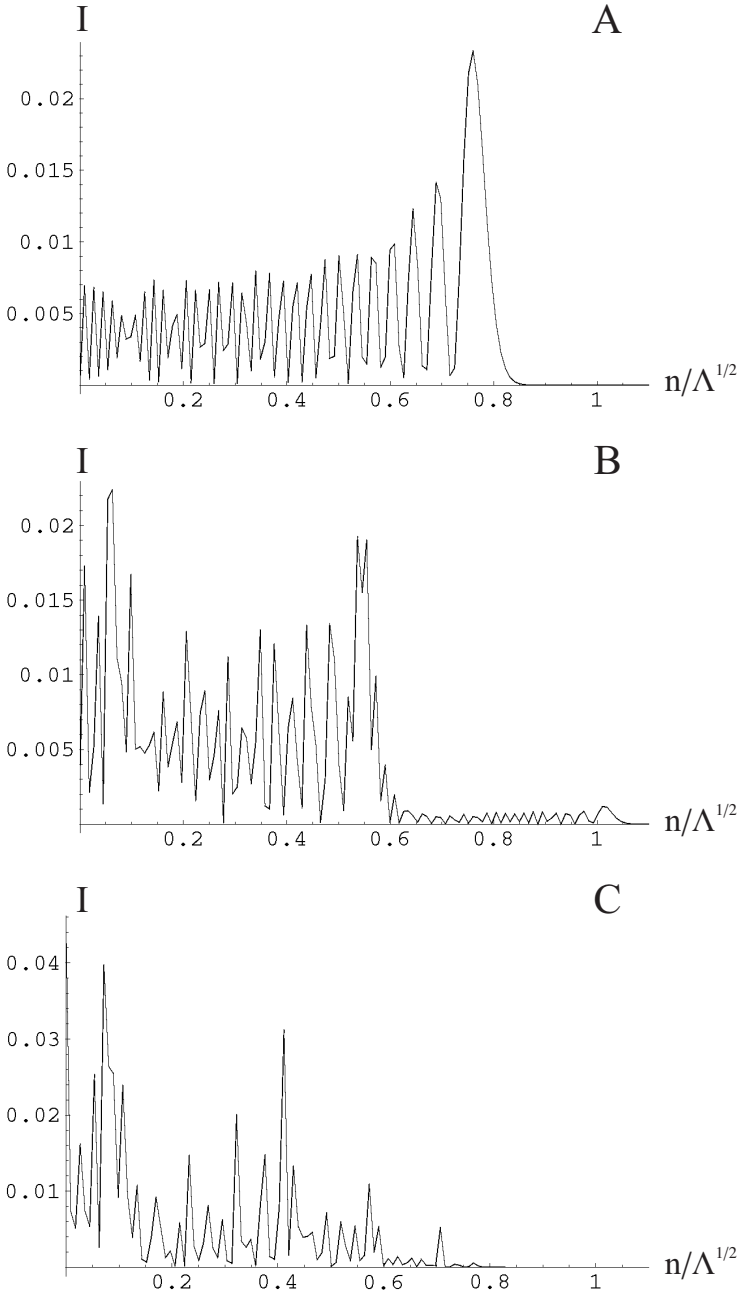

Figure 5.6: Some quantum farfield patterns generated under the longitudinal envelope (5.17), with $\Lambda = 12500$, and corresponding to the classical mechanics given by $E = 0.5$, and the following widths: A) $w = 0.671$ ($\zeta : -0.006 \rightarrow +0.006$), B) $w = 4.472$ ($\zeta : -0.04 \rightarrow 0.04$), C) $w = 15$ ($\zeta : -0.134 \rightarrow 0.134$).

Chapter 6

A complex potential

6.1 Motivation

Atom optics has a number of features which make it an attractive setting for novel investigations into simple quantum mechanical phenomena. The tiny de Broglie wavelength which is attainable because of the strongly resonant atom-light interaction (allowing a large momentum transfer) gives rise to very delicate interference phenomena. The nature of such interference in the classical limit was studied numerically in Chapter 4 and will continue in the following chapters. Here however a partial return is made to the very quantum end of the wavelength scale. In particular, weak field Bragg scattering will be re-examined but this time in the presence of spontaneous emission; such a situation can be modelled using a complex (in the sense of real and imaginary numbers) potential. The equations of weak field Bragg (dynamical) scattering are so simple that the analysis can be made without recourse to numerics, and, because of the influence of the complex potential, lead to an uncomplicated picture of quantum behaviour in a dissipative environment. Unlike the Hermitian case, the Hamiltonian describing the complex potential is capable of degeneracies which will be shown to strongly affect the scattering; effects such as 'anomalous Borrmann transmission' are observed which are the physical manifestation of degeneracies in 2×2 matrices. Unfamiliar behaviour persists into the semiclassical limit and contrasts strongly with caustic dominated farfield patterns which have been observed so far.

6.2 The dissipative potential

The key ingredient for achieving degeneracies in this atom optics system is the presence of a complex potential, the imaginary part of which models dissipation. Such a potential was introduced by D.O.

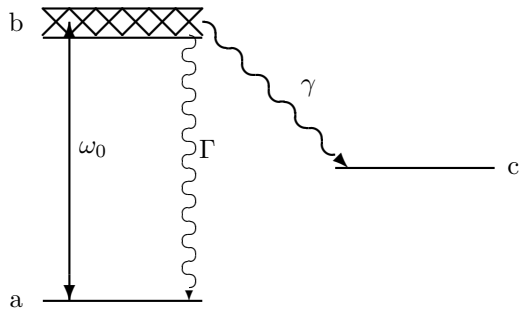

Figure 6.1: The three level atom: a two level atom with decay to a third state c. It is assumed that $\gamma \gg \Gamma$. The incident radiation is tuned to ω_0.

Chudesnikov and V. P. Yakovlev in 1991 [24] (see also Oberthaler *et al.* [62]) and is based on an effective three level internal atomic energy level scheme: two working levels; a ground or metastable state coupled to an excited state by the quasi-resonant laser field—exactly as before—but this time there is a third level to which the excited state rapidly decays (permanently). See Figure 6.1

The absorption-stimulated emission Rabi oscillations between the working levels, which are responsible for the quantised external motion of the atom, compete with fast decay to the third level (decay of the excited state to the ground state is assumed to be much slower and is therefore ignored). A significant difference with the situation considered before now is that the laser is taken to be tuned on resonance, so the upper state is readily excited by the incident photons. However, because of the weak field conditions, and if the dissipative decay is sufficiently rapid, at any moment in time the atom has only a small chance of actually being in the excited state.

Thus the population of the excited level adiabatically clings to that of the ground state and may be eliminated, allowing the equation of motion for the atomic density matrix to be written as a Schrödinger equation for the ground state with a complex potential, (see Equation (E.13))

$$V(x) = \frac{d_{ab}^2 \mathcal{E}_0^2}{4\hbar\left(\Delta + \mathrm{i}\frac{\gamma}{2}\right)} \cos^2 Kx \tag{6.1}$$

where γ is the decay rate from the excited state to the *third* state, but, as before, Δ is the detuning from the working transition (for which d_{ab} is the dipole matrix element). Chudesnikov and Yakovlev derive this expression in their 1991 paper [24]. Appendix E gives a different (but related) derivation.

Complex potentials arise when attention is focussed upon just a sub-system of the whole. Here, because it is just the ground state wavefunction that is being calculated, atoms which have decayed into the third level are ignored. The decay modelled by the imaginary part of the potential represents the loss of atoms from the two-level ground↔excited state subsystem. This is a useful manoeuvre since it allows one to continue to treat the subsystem as evolving coherently in the sense that the random momentum kicks received during spontaneous emission do not need to be considered. Thus the subsystem remains restricted to the quantised diffraction pattern, and the more serious developments requiring a Fokker-Planck approach as mentioned in Chapter 1 are not necessary.

There are many types of effect which an 'environment' can have on a subsystem. That which is considered here is among the most basic since the environment has no effect on the subsystem other than to remove probability. An immediate question is whether such a situation can be accomplished experimentally. Fortunately it can since the detectors used in the farfield are so sensitive that they can be set so as to only be triggered by atoms which are in the ground state and do not register atoms in any of the other states.

6.3 Intensity sum rule for the diffracted beams

When the detuning, Δ, is zero (this is a slightly moot point since the upper state has a finite width, so the detuning can only be zero up to this width) the potential (6.1) becomes purely imaginary

$$V(x) = -\mathrm{i}\frac{d_{ab}^2\mathcal{E}_0^2}{2\hbar\gamma}\cos^2 Kx = -\mathrm{i}\widetilde{V}_0\cos^2 Kx \tag{6.2}$$

and the resulting Raman-Nath equation is (see Equation (4.36))

$$\mathrm{i}\frac{\partial A_n}{\partial\zeta} + \left[\mathrm{i}\Lambda - n(n+\alpha)\right]A_n + \mathrm{i}\frac{\Lambda}{2}\left(A_{n+1} + A_{n-1}\right) = 0 \tag{6.3}$$

where Λ remains the same as in its definition (4.10) except that $\widetilde{V}_0$ is substituted for V_0.

For the real potential the total intensity in all the beams is conserved

$$\sum_{n=-\infty}^{n=\infty} |A_n|^2 = 1. \tag{6.4}$$

One might expect that here, due to the dissipation, the total intensity would decay exponentially with depth ζ. However, things are not that simple. Multiplying Equation (6.3) by A_n^* and then subtracting its complex conjugate multiplied by A_n gives

$$\mathrm{i}\frac{\partial A_n A_n^*}{\partial\zeta} + \mathrm{i}\frac{\Lambda}{2}\left(A_n^*A_{n+1} + A_n^*A_{n-1} + 2A_n^*A_n + A_nA_{n+1}^* + A_nA_{n-1}^*\right) = 0. \tag{6.5}$$

Multiplying by $(-1)^n$ and summing, only the diagonal terms survive

$$\sum_{n=-\infty}^{n=\infty} (-1)^n \left(\frac{\partial A_n A_n^*}{\partial \zeta} + 2\Lambda A_n A_n^* \right) = 0. \tag{6.6}$$

This can be re-written as

$$\frac{\partial}{\partial \zeta} \sum_{n=-\infty}^{n=\infty} (-1)^n A_n A_n^* \mathrm{e}^{2\Lambda\zeta} = 0 \tag{6.7}$$

which implies that the sum is equal to a constant. Using the initial condition

$$A_n(\zeta = 0) = \delta_{n,0} \tag{6.8}$$

one immediately concludes that the exponentially decaying quantity is an alternating sum of the intensities

$$\sum_{n=-\infty}^{n=\infty} (-1)^n \left| A_n(\zeta) \right|^2 = \mathrm{e}^{-2\Lambda\zeta}. \tag{6.9}$$

This condition provides a powerful check on numerical calculations.

6.4 Non-Hermitian degeneracies

Section 4.4 showed that for a very weak potential (small Λ), and incidence close to the first Bragg angle, only the zeroth and first diffracted beam really need be considered; the coupling to the other beams being very small. Unfortunately the Born perturbation solution of Section 4.4.3 diverged at the Bragg angle for large enough ζ. To overcome this defect it will be assumed that in the vicinity of the Bragg angle, beams other than the zeroth and first can in fact be totally ignored, and the scattering problem solved exactly in terms of these two. This is known as 'the two-beam solution'.

To explore angles close to the first Bragg angle ($\alpha = -1$) it is convenient to define

$$\alpha = -1 + \beta \tag{6.10}$$

so that β measures the deviation from Bragg incidence. Including only the A_0 and A_1 amplitudes one has

$$\mathrm{i}\frac{\partial}{\partial \zeta} \begin{pmatrix} A_0 \\ A_1 \end{pmatrix} = \mathcal{M} \begin{pmatrix} A_0 \\ A_1 \end{pmatrix} \tag{6.11}$$

where

$$\mathcal{M} = \begin{pmatrix} -\mathrm{i}\Lambda & -\frac{\mathrm{i}}{2}\Lambda \\ -\frac{\mathrm{i}}{2}\Lambda & \beta - \mathrm{i}\Lambda \end{pmatrix}. \tag{6.12}$$

Clearly $\mathcal{M}$ is non-Hermitian. Its eigenvalues are

$$\lambda_\pm = \frac{\beta}{2} - \mathrm{i}\Lambda \pm \frac{1}{2}\sqrt{\beta^2 - \Lambda^2} \tag{6.13}$$

corresponding to eigenvectors

$$|\chi_\pm\rangle = \begin{pmatrix} -\mathrm{i}\Lambda \\ \\ \beta \pm \sqrt{\beta^2 - \Lambda^2} \end{pmatrix}. \tag{6.14}$$

The combination of eigenvectors which satisfy the initial condition (6.8) give the diffracted amplitudes

$$\begin{pmatrix} A_0 \\ A_1 \end{pmatrix} = B_+ |\chi_+\rangle \, \mathrm{e}^{-\mathrm{i}\lambda_+\zeta} + B_- |\chi_-\rangle \, \mathrm{e}^{-\mathrm{i}\lambda_-\zeta} \tag{6.15}$$

with

$$B_\pm = \mathrm{i}\frac{\sqrt{\beta^2 - \Lambda^2} \mp \beta}{2\Lambda\sqrt{\beta^2 - \Lambda^2}}. \tag{6.16}$$

The presence of a degeneracy for angles such that $\beta = \pm\Lambda$ is emphasised. As the degeneracy is approached, the two eigenvectors (6.14) become parallel; no longer spanning the two-dimensional space in which they live. In response, to maintain the distinct identities of A_0 and A_1, the coefficients $B_\pm$ diverge (but only in such a way that the amplitudes themselves remain finite). This behaviour contrasts with the Hermitian situation for which the eigenvectors remain orthogonal even at the degeneracy and so continue to span the space.

6.4.1 The eigenvalues close to a degeneracy

The coinciding eigenvalues at $\beta = \pm\Lambda$ represent a physical realisation of a degeneracy in a 2×2 matrix. Degeneracies in physics are novel because, generally speaking, Hermitian systems receive much more attention than non-Hermitian ones. Hermitian systems rarely exhibit degeneracies because their degeneracies live in a three dimensional space, generically requiring three parameters to search them out (unless there is some special symmetry of the matrix). This can be seen by considering a general matrix h, say, which is a function of parameter space $\mathbf{R}$

$$h(\mathbf{R}) = \begin{pmatrix} h_{11}(\mathbf{R}) & h_{12}(\mathbf{R}) \\ h_{21}(\mathbf{R}) & h_{22}(\mathbf{R}) \end{pmatrix} \tag{6.17}$$

which has eigenvalues

$$\lambda_\pm(\mathbf{R}) = \frac{h_{11} + h_{22}}{2} \pm \frac{1}{2}\sqrt{(h_{11} - h_{22})^2 + 4h_{12}h_{21}}. \tag{6.18}$$

Degeneracy occurs when

$$\lambda_+ - \lambda_- = 0 = \sqrt{(h_{11}(\mathbf{R}) - h_{22}(\mathbf{R}))^2 + 4h_{12}(\mathbf{R})h_{21}(\mathbf{R})}. \tag{6.19}$$

For the Hermitian case, h_{11} and h_{22} are real, with $h_{12} = h_{21}^*$. The degeneracy condition (6.19) reduces to the sum of two squares

$$(h_{11}(\mathbf{R}) - h_{22}(\mathbf{R}))^2 + |h_{21}(\mathbf{R})|^2 = 0 \tag{6.20}$$

which requires three separate conditions to be fulfilled

$$h_{11}(\mathbf{R}) = h_{22}(\mathbf{R}) \tag{6.21}$$

$$\mathrm{Re}\,[h_{21}(\mathbf{R})] = 0 \tag{6.22}$$

$$\mathrm{Im}\,[h_{21}(\mathbf{R})] = 0 \tag{6.23}$$

and so at least three parameters must be varied to find a degeneracy. For a general non-Hermitian matrix the degeneracies are easier to locate since the condition (6.19) only states that the real and imaginary parts of the entire r.h.s. must be separately equal to zero, implying that only two parameters are needed. And indeed, the degeneracies of the complex Raman-Nath matrix $\mathcal{M}$ are points in the two dimensional (β, Λ) space. In 1937 Edward Teller [79] showed that the eigenvalue

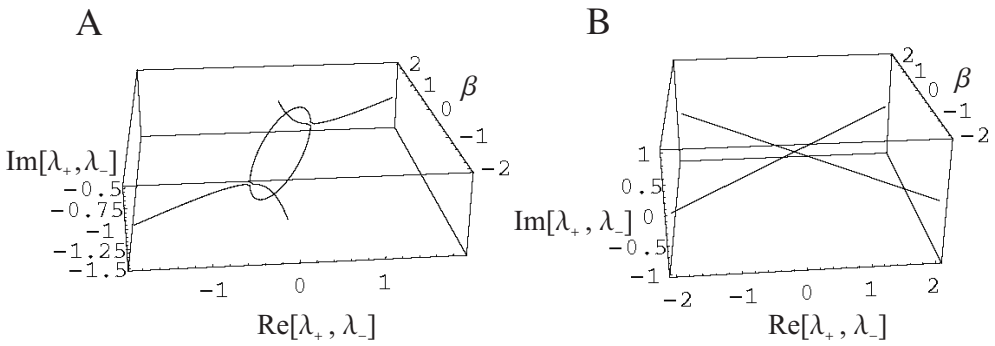

Figure 6.2: The real and imaginary parts of the eigenvalues close to a degeneracy; A) the complex eigenvalues (6.13) as a function of β for $\Lambda = 1$, B) the real eigenvalues due to a Hermitian matrix.

structure local to degeneracies of Hermitian matrices form a double cone (diabolo) centred on the degeneracy. Slices through this diabolo give rise to the familiar 'avoided crossing' behaviour. Figure 6.2 compares the double cone with the quite different response of the non-Hermitian eigenvalue Equation (6.13), which has an imaginary 'bubble' in the region between the degeneracy points.

6.4.2 The eigenvectors close to a degeneracy

The expression (6.15) for the intensities can be simplified by replacing the three variables ζ, β and Λ with two defined as

$$\eta \equiv \frac{1}{2}\zeta\Lambda \tag{6.24}$$

$$\delta \equiv \frac{\beta}{\Lambda} \tag{6.25}$$

so that the degeneracy is at $\delta = \pm 1$. Then

$$I_1 \equiv |A_1|^2 = \mathrm{e}^{-4\eta} \frac{\sin^2\left(\eta\sqrt{\delta^2-1}\right)}{\delta^2-1} \tag{6.26}$$

$$I_0 \equiv |A_0|^2 = \mathrm{e}^{-4\eta} + I_1. \tag{6.27}$$

These formulas satisfy the alternating sum rule (6.9) and they are valid for all η and δ if Λ is small enough.

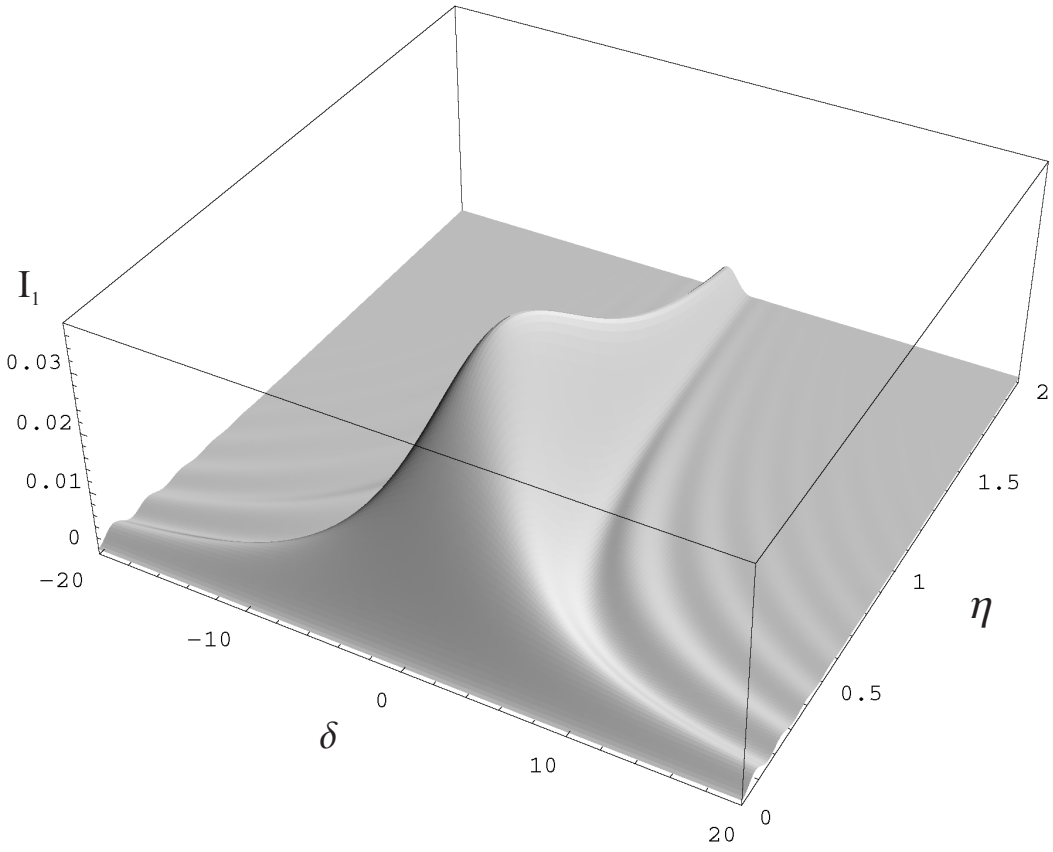

Figure 6.3: Intensity I_1 (Equation (6.26)) of the first Bragg reflected beam for an imaginary potential, as a function of the depth and angular deviation variables η and δ respectively.

Figure 6.3 shows I_1 as a function of depth η and deviation δ from the Bragg angle. The most

notable feature is that the degeneracies at $\delta = \pm 1$ mark the transition from oscillatory (trigonometric) to non-oscillatory (hyperbolic) behaviour of both the thickness dependence (variation with η for fixed δ) and the 'rocking-curves' (variation with δ for fixed η), as demonstrated by the dark fringes (zeros) of the pattern, at

$$\delta_n = \pm\sqrt{1 + \left(\frac{n\pi}{\eta}\right)^2} \qquad (n = 1, 2, \ldots) \tag{6.28}$$

whose asymptote as $\eta \to \infty$ is $\delta_n = 1$. Near the Bragg angle, and for large depths, the decay of the rocking curve is Gaussian, namely

$$I_1 \approx \frac{1}{4}\mathrm{e}^{-2\eta}\mathrm{e}^{-\delta^2\eta} \qquad (\eta \gg 1,\ \delta \ll 1) \tag{6.29}$$

with angular width of the Bragg peak shrinking with thickness as $\Delta\delta \sim 1/\sqrt{\eta}$. From (6.26–6.27) the same decay applies to the total intensity, $I_0 + I_1$, of the transmitted atoms. Alternatively stated, the total transmitted intensity increases anomalously at the Bragg angle, a 'remarkable phenomenon' predicted and observed by Oberthaler *et al.* in 1996 [62], and related to the effect discovered in 1941 by Borrmann [20] for X-rays diffracted by an absorbing crystal. It is interesting to note that the anomalously transmitted beams both have sub-single photon recoil widths for large enough η.

By contrast, the intensities for the 'transparent' (no dissipation—real potential) light grating, with variables still defined by (6.24–6.25), are

$$I_1 = \frac{\sin^2\left(\eta\sqrt{\delta^2+1}\right)}{\delta^2+1} \tag{6.30}$$

$$I_0 = 1 - I_1. \tag{6.31}$$

Now the fringes in the η, δ plane cross the Bragg axis ($\delta = 0$) at $\eta = n\pi$, and the total transmitted intensity is unity irrespective of direction δ.

It is, however, possible to get degeneracies between Bloch waves for transparent gratings. In the many-beam transmission electron microscopy of thin crystals, where the crystal is not a single sinusoid but has many Fourier components, degeneracies can be produced at Bragg angles by varying the voltage (the 'critical voltage effect') [13].

6.4.3 Three beams

Degeneracy can also occur for normal incidence for the imaginary case. If Λ is small enough then all amplitudes are negligible save A_0 and $A_{+1} = A_{-1}$. The Raman-Nath equations for this three beam case are

$$\mathrm{i}\frac{\partial}{\partial\zeta}\begin{pmatrix} A_0 \\ A_1 \end{pmatrix} = \mathcal{N}\begin{pmatrix} A_0 \\ A_1 \end{pmatrix} \tag{6.32}$$

where

$$\mathcal{N} = \begin{pmatrix} -\mathrm{i}\Lambda & -\mathrm{i}\Lambda \\ -\frac{\mathrm{i}}{2}\Lambda & 1-\mathrm{i}\Lambda \end{pmatrix}. \tag{6.33}$$

$\mathcal{N}$ has eigenvalues

$$\lambda_{\pm} = \frac{1}{2} - \mathrm{i}\Lambda \pm \frac{1}{2}\sqrt{1-2\Lambda^2}. \tag{6.34}$$

Now the degeneracy is at $\Lambda = \pm 1/\sqrt{2}$. Solving for the intensities gives

$$I_{\pm 1} \equiv |A_{\pm 1}|^2 = \frac{\Lambda^2}{1-2\Lambda^2}\mathrm{e}^{-2\Lambda\zeta}\sin^2\left(\frac{\zeta}{2}\sqrt{1-2\Lambda^2}\right) \tag{6.35}$$

$$I_0 \equiv |A_0|^2 = \mathrm{e}^{-2\Lambda\zeta} + 2I_1 \tag{6.36}$$

which satisfy the alternating sum rule (6.9). At the degeneracies themselves

$$I_{\pm 1} = \frac{\zeta^2}{8}\mathrm{e}^{-\sqrt{2}\zeta} \tag{6.37}$$

$$I_0 = \left(1+\frac{\zeta^2}{4}\right)\mathrm{e}^{-\sqrt{2}\zeta} \tag{6.38}$$

and as before this marks the transition from oscillatory to hyperbolic behaviour. Figure 6.4 shows that $\Lambda = 1/\sqrt{2}$ is within the three-beam approximation, at least in the region where the intensities are appreciable. For larger ζ, the exact solutions of the Raman-Nath equations (6.3) diverge from the approximations (6.37 and 6.38), because of contributions from the beams with $|n| \geq 2$ (even when these are small, they can vary rapidly as a result of the factor n^2 in (6.3) with $\alpha = 0$, and so can spoil the three beam approximation through their derivatives).

6.5 Nonclassical semiclassical behaviour: many beams

When Λ is large, the laser field acts strongly upon the atom waves. Restricting the discussion to normal incidence ($\alpha = 0$), the aim is to determine the asymptotic distribution of the intensities I_n as the interaction distance ζ increases. It is recalled that for the 'transparent' case the pattern of intensities is dominated by caustics; the envelopes of classical rays, which proliferate with ζ. For an absorbing potential the behaviour is very different; only those rays which avoid the intense parts of the 'washboard' potential survive; namely those that wind around in the very bottom (harmonic) parts of the wells.

6.5.1 Berry's solution

Rather than using rays to calculate the intensities, an approach will be taken which relies on a remarkable insight, due to Michael Berry, who was able to write down the solution by inspection.

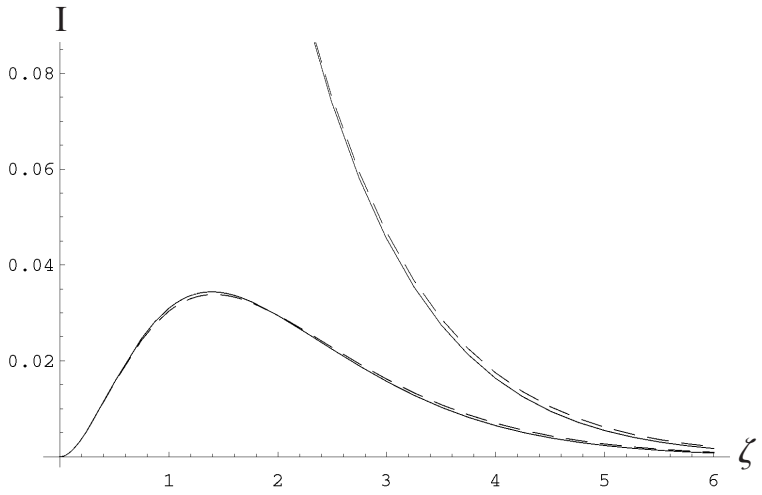

Figure 6.4: The dashed curves are the intensities I_0 (upper curve) and I_1 (lower curve) at normal incidence, in the three beam approximation (6.38 and 6.37) for the potential strength $\Lambda = 1/\sqrt{2}$, for which the governing matrix (6.33) is degenerate. The full curves are the intensities calculated numerically from (6.3) incorporating ± 11 beams for $\alpha = 0$. The next most intense beam, I_2, never exceeds 0.0006.

Firstly, it is convenient to rewrite the Raman-Nath equations (6.3) in different variables B_n defined by

$$A_n(\zeta) \equiv (-1)^n B_n(\zeta). \tag{6.39}$$

Thus, for normal incidence

$$\frac{\partial B_n(\zeta)}{\partial \zeta} = \left[-\mathrm{i}n^2 - \Lambda\right] B_n(\zeta) + \frac{\Lambda}{2}\left[B_{n+1}(\zeta) + B_{n-1}(\zeta)\right]. \tag{6.40}$$

Now the central difference approximation is made

$$B_{n+1}(\zeta) + B_{n-1}(\zeta) - 2B_n(\zeta) \approx \frac{\partial^2}{\partial n^2} B_n(\zeta). \tag{6.41}$$

Such 'continuisation' procedures will be discussed at length in Chapter 7. In particular, it is known (see the second Appendix of [16]), that such a simple replacement is inadequate for the case of the real potential because of the highly oscillatory nature of the wavefunction. Here, however, the higher orders are very heavily damped and so, as will be seen, it works.

One must solve

$$\frac{\partial B_n(\zeta)}{\partial \zeta} = -\mathrm{i}n^2 B_n(\zeta) + \frac{\Lambda}{2}\frac{\partial^2 B_n(\zeta)}{\partial n^2}. \tag{6.42}$$

Berry's solution is

$$B_n(\zeta) \approx \frac{D}{\sqrt{\sinh\left(\zeta\sqrt{2\mathrm{i}\Lambda}\right)}} \exp\left(-n^2\sqrt{\frac{\mathrm{i}}{2\Lambda}}\coth\left(\zeta\sqrt{2\mathrm{i}\Lambda}\right)\right) \tag{6.43}$$

where D is a constant stipulated by the initial conditions. It can be confirmed by direct substitution that (6.43) is in fact an *exact* solution of the *continuised* R-N equation (6.42), and is hopefully therefore a reasonable approximate solution to the discrete problem. However, whilst (6.43) condenses onto the $n = 0$ beam for $\zeta \to \infty$, which seems reasonable, it can never satisfy the initial condition (6.8). Assuming however that (6.43) *is* correct for large ζ, one must somehow still calculate D. This is accomplished by matching (6.43) onto the phase-grating solution (4.18), due to Raman and Nath, for small ζ where, one trusts, both solutions are valid.

6.5.2 Matching to the phase grating solution

When the term containing n^2 in (6.40) is ignored, one arrives at the 'phase-grating solution'

$$B_n(\zeta) \approx \mathrm{e}^{-\Lambda\zeta} I_n(\Lambda\zeta) \tag{6.44}$$

where I_n is the modified Bessel function. This approximation satisfies the alternating sum rule (6.9) exactly since, from [1], $I_n = I_{-n}$, and

$$\mathrm{e}^{-z} = I_0(z) - 2I_1(z) + 2I_2(z) - 2I_3(z) + \cdots. \tag{6.45}$$

Employing the Debye asymptotic approximations [1] giving I_n for $\Lambda\zeta$ and n large, and further approximating these for $\Lambda\zeta \gg n$, one finds

$$\mathrm{e}^{-\Lambda\zeta} I_n(\Lambda\zeta) \approx \frac{\exp\left(-\frac{n^2}{2\Lambda\zeta}\right)}{\sqrt{2\pi\Lambda\zeta}}. \tag{6.46}$$

This matches precisely onto (6.43) for small ζ (taking $\sinh z \sim z$ and $\coth z \sim 1/z$), and identifies D as

$$D = \frac{1}{\sqrt{\pi}} \left(\frac{\mathrm{i}}{2\Lambda}\right)^{1/4}. \tag{6.47}$$

Put together, the diffracted intensities are predicted to be given by the Gaussian distribution

$$I_n \approx a(\zeta,\Lambda) \exp\left(-\frac{n^2}{w^2(\zeta,\Lambda)}\right) \tag{6.48}$$

where the amplitude a, and width w, of the set of diffracted beams are

$$a(\zeta,\Lambda) = \frac{1}{\pi\sqrt{\Lambda\left[\cosh\left(2\zeta\sqrt{\Lambda}\right) - \cos\left(2\zeta\sqrt{\Lambda}\right)\right]}} \tag{6.49}$$

$$w(\zeta,\Lambda) = \Lambda^{1/4} \sqrt{\frac{\cosh\left(2\zeta\sqrt{\Lambda}\right) - \cos\left(2\zeta\sqrt{\Lambda}\right)}{\sinh\left(2\zeta\sqrt{\Lambda}\right) + \sin\left(2\zeta\sqrt{\Lambda}\right)}} \tag{6.50}$$

and this result is expected to be valid for large Λ with ζ not too close to zero.

If $\zeta\sqrt{\Lambda} \gg 1$, then the amplitude decays exponentially and the width saturates

$$a(\zeta,\Lambda) \longrightarrow \frac{1}{\pi}\sqrt{\frac{2}{\Lambda}}\mathrm{e}^{-\zeta\sqrt{\Lambda}} \tag{6.51}$$

$$w(\zeta,\Lambda) \longrightarrow \Lambda^{1/4}. \tag{6.52}$$

Thus the semiclassical width of the momentum distribution is of order $\sim \Lambda^{1/4}$ which is considerably narrower than for the purely real potential, which by Equation (4.29) goes only as $\sim \Lambda^{1/2}$, in other words; many fewer beams are transmitted.

6.5.3 Comparison with numerical calculations

The arguments leading to (6.48), (6.49) and (6.50) are not rigorous, and so it is desirable to test them against numerical solutions of the R-N equations (6.3). Figure 6.5 shows the comparisons; the dots pertain to the numerical calculation, whilst the full curves are based on the various approximations (6.49–6.52) given above. For most of the pictures the chosen value of Λ is quite small, rather than being very semiclassical (large). This is to illustrate the accuracy of the approximations even for parameter regions that are quite 'quantum'.

A The intensities for $\Lambda = 5$, $\zeta = 8$. The dominant decay; $\mathrm{e}^{-\zeta\sqrt{\Lambda}}$, has been removed.

B $\ln[a(\zeta,\Lambda)]$ for $\Lambda = 5$; the numerical values were obtained by taking the logarithm of the intensity of the zeroth beam at various depths.

C The width, $w(\zeta,\Lambda)$, as a function of ζ for $\Lambda = 5$. The value of the width for the numerical calculations was obtained in the following way: assuming that $I_n = a\exp\left(-n^2/w^2\right)$, then taking the logarithm one finds $\ln I_n = \ln a - n^2/w^2$. Thus $w^2(\zeta,\Lambda)$ behaves as the inverse of the gradient for a parabolic curve. Differentiating both sides twice w.r.t. n, and evaluating the result at $n = 0$, say, will then yield twice the gradient. To differentiate the l.h.s. one must use the central difference approximation (6.41). Noting that $I_{+1} = I_{-1}$, one obtains an estimate of the width from $w \approx 1/\sqrt{\ln(I_0/I_1)}$.

D The width, $w(\zeta,\Lambda)$, as a function of Λ for $\zeta = 8$ (not a particularly large value of ζ, again demonstrating unexpected validity, especially considering that this time the *saturated* width (6.52) was used for the full curve). The width of the numerical solution was calculated in the same way as for C.

E The logarithm of amplitude $a(\zeta,\Lambda)$, as a function of Λ for $\zeta = 8$. Again, the *asymptotic* amplitude (6.51) was used for the full curve. As in B, the amplitude was extracted from the numerical expression by using the zeroth beam.

It is clear that the various approximate solutions described above give an accurate description of diffraction by an imaginary 'grating' (periodic potential), especially in the regime of large ζ that is so complicated for transparent gratings. The majority of the contents of this chapter has been published [15].

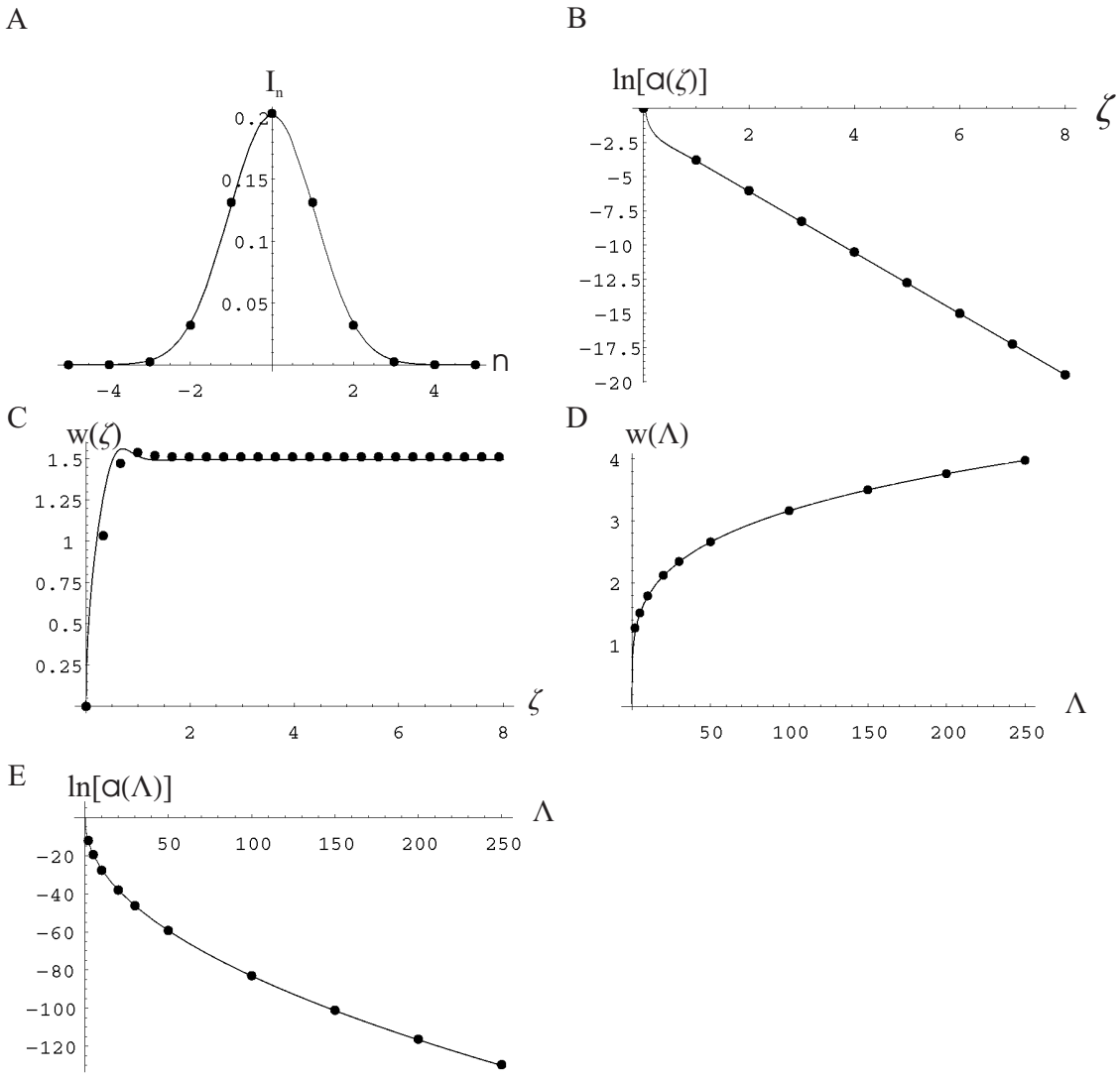

Figure 6.5: The dots are the exact solutions of the R-N equations, the full curves are the calculations based on Berry's solution and its approximations. A), B) and C) were obtained using (6.49–6.50), whilst C) and D) use the further approximations (6.51–6.52).

Chapter 7

Continuising the Raman-Nath equation

7.1 Motivation

As has now been demonstrated, solving the Raman-Nath equation analytically is straight forward enough when there are only two beams to consider. With a deeper potential however, one can induce arbitrarily more beams and the task of finding analytic solutions would seem rather formidable. This is compounded by the Raman-Nath equation being a difference equation. It is true to say that difference equations have been much less studied than their continuous counterparts. Examining the numerically generated farfield intensities of Section 4.5 it is clear that when Λ is large the interference between the Bloch waves becomes very complicated except for the 'clean' outer caustic. However, inspection of any single Bloch wave, such as that shown in Figure 7.1, reveals a smooth envelope—with many individual orders acting in concert to produce each fringe. The rate of change of the amplitudes with order n seems to be relatively slow, and so the question then arises, could perhaps the discrete difference equation (4.77), be approximated by some differential equation which is in some way the continuised version of it? This chapter presents two existing ideas on how to go about this, mainly due originally to Dingle and Morgan [28, 29] and Berry [16], but also discovered independently by Yakovlev [83].

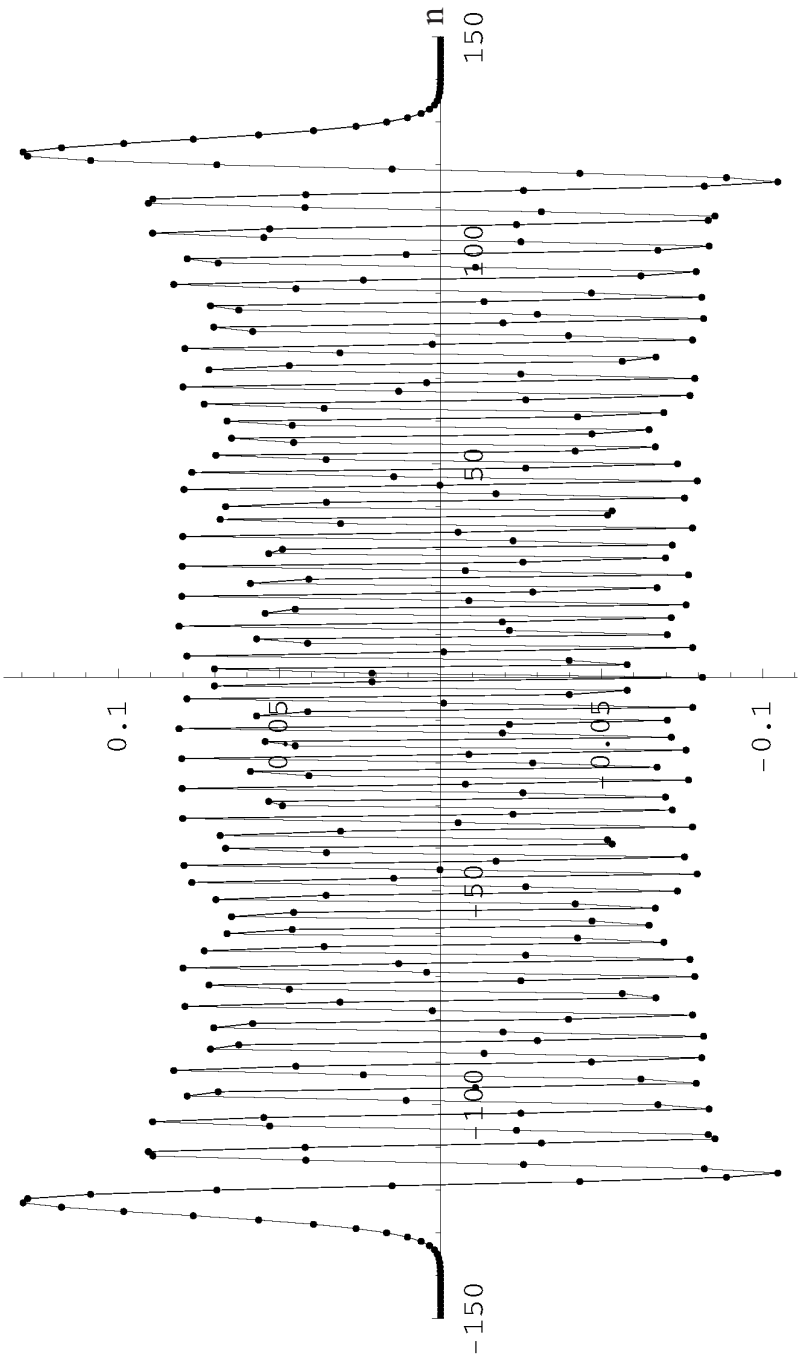

Figure 7.1: Bloch wave (eigenvector) No. 110 (out of 200 bound states) of the R-N matrix (4.78) for $\Lambda = 12500$. The dots are the numerically calculated amplitudes and the continuous line joins them.

7.2 The central difference approximation

If each Bloch wave is assumed to be a continuous function of the continuous variable,

$$y = n\varepsilon \tag{7.1}$$

then the discrete amplitudes are given by the evaluation of this continuous function at the values of y corresponding to integer values of n

$$B_n^j \to \tilde{B}^j(y)\Big|_{y=n\varepsilon}. \tag{7.2}$$

The new variable y is defined in this way since when $n \to n+1$, then $y \to y+\varepsilon$, with ε being some small quantity. That is, the distance between the diffracted orders becomes small, so that

$$B_{n-1}^j \to \tilde{B}^j(y-\varepsilon) \tag{7.3}$$

$$B_{n+1}^j \to \tilde{B}^j(y+\varepsilon) \tag{7.4}$$

and the r.h.s. can be Taylor expanded, transforming the stationary R-N equation (4.77) into

$$\begin{aligned} E\tilde{B}(y) - \frac{y^2}{\varepsilon^2}\tilde{B}(y) + \frac{\Lambda}{2}\Bigg(&\tilde{B}(y) + \frac{d\tilde{B}(y)}{dy}\varepsilon + \frac{1}{2}\frac{d^2\tilde{B}(y)}{dy^2}\varepsilon^2 + \cdots \\ &+ \tilde{B}(y) - \frac{d\tilde{B}(y)}{dy}\varepsilon + \frac{1}{2}\frac{d^2\tilde{B}(y)}{dy^2}\varepsilon^2 + \cdots\Bigg) = 0. \end{aligned} \tag{7.5}$$

Truncating the expansion at the second order terms leaves

$$E\tilde{B}(y) - \frac{y^2}{\varepsilon^2}\tilde{B}(y) + \frac{\Lambda}{2}\left(2\tilde{B}(y) + \frac{d^2\tilde{B}(y)}{dy^2}\varepsilon^2\right) = 0. \tag{7.6}$$

This is really equivalent to making the central difference approximation

$$B_{n+1} + B_{n-1} - 2B_n \approx \frac{\partial^2}{\partial n^2} B_n. \tag{7.7}$$

Letting

$$\varepsilon = \left(\frac{8}{\Lambda}\right)^{1/4} \tag{7.8}$$

$$\psi = \tilde{B}\sqrt{\Lambda} \tag{7.9}$$

one arrives at the equation for the parabolic cylinder function [1] ψ,

$$\frac{d^2\psi}{dy^2} - \left(\frac{y^2}{4} - \frac{E+\Lambda}{\sqrt{2}}\right)\psi = 0. \tag{7.10}$$

At this point one may well question the value of re-writing the Mathieu equation (via the R-N equation) in terms of other special functions. Afterall, the Mathieu functions solve the original problem. Firstly, until very recently, no commercially available computer packages contained

intrinsic Mathieu functions, and so their calculation would have to be by, say, the truncated continued fraction method [1, 16, 55] or diagonalisation[1]. When working in momentum space, as here, either one leaves the problem as a purely numerical exercise, in which case little more can be learnt, or one tries to extract analytic information. The parabolic cylinder equation (7.10) is well studied with many known properties, and here, as asserted above, allegedly describes the behaviour of the momentum space amplitudes, where previously only pure numerics existed. This therefore, if correct, constitutes some sort of an advance[2].

The parabolic cylinder function approach was pursued by Berry [16] in 1965. Unfortunately it was discovered that it gives a very poor match to the true eigenvectors. The reason presumably being that the Taylor series is truncated too early. Only the higher order terms describe the large values of the curvature and its derivatives that are responsible for the rapid oscillations of the eigenvectors as exemplified by Figure 7.1. The approximation worked well for the imaginary potential of Chapter 6 because the wavefunction was a Gaussian; a structure simple enough to be captured successfully by the central difference approximation. Fortunately, in the same work [16], Berry also suggested another approach to continuisation, and it is to this that the next section turns.

7.3 The W.K.B. approach

It has long been appreciated that a slowly varying function, when exponentiated, is capable of describing rapidly oscillating behaviour. This feature lies at the heart of the semiclassical technique known as the W.K.B. method [14]. The first application of such techniques to the R-N equation was by Dingle and Morgan [28, 29], but it has also been developed independently by Yakovlev [83]. The stationary R-N equation (4.77) will first be written in terms of more convenient re-scaled variables. This time, let

$$y = \frac{n}{\sqrt{\Lambda}} \tag{7.11}$$

$$\beta = \frac{E}{\Lambda} \tag{7.12}$$

so that when

$$n \to n+1 \tag{7.13}$$

[1] One computer package, *Mathematica* version 3.0, does now have intrinsic Mathieu functions, but only in configuration space. To find the farfield intensity one must numerically Fourier analyse each Mathieu function.

[2] If this section seems defensive, well it is. It seeks to justify the necessity for this work following a question put by a senior Professor following a talk by the author. The question, quite rightly, ran along the lines "Why bother with all this when the Mathieu functions solve the problem?". The Mathieu functions are indeed well studied functions. They are not however, well enough studied functions.

then

$$y \to y + \frac{1}{\sqrt{\Lambda}} \tag{7.14}$$

and (4.77) becomes

$$(\beta - y^2)B_n + \frac{1}{2}(B_{n+1} + B_{n-1}) = 0. \tag{7.15}$$

Note that, due to the range of magnitudes of the eigenvalues as given by Equation (4.83), the definition of β above implies that for bound states

$$-1 < \beta_{bound} < 1. \tag{7.16}$$

Once again the assumption will be that the amplitudes are really just integer separated points of a continuous function[3]. Keeping things simple, one assumes

$$B_n \to B(y) \tag{7.17}$$

and that

$$B(y) = \mathrm{e}^{\mathrm{i}S(y)} \tag{7.18}$$

where the suggestively named $S(y)$ is analogous to an action. The functions $S(y + (\sqrt{\Lambda})^{-1})$ and $S(y - (\sqrt{\Lambda})^{-1})$ are then Taylor expanded as above, and common terms divided out leaving a differential equation of infinite order

$$\frac{1}{2}\left(\mathrm{e}^{\mathrm{i}(S^i + S^{ii}/2 + S^{iii}/6 + S^{iv}/24 + \cdots)} + \mathrm{e}^{\mathrm{i}(-S^i + S^{ii}/2 - S^{iii}/6 + S^{iv}/24 + \cdots)}\right) = y^2 - \beta \tag{7.19}$$

or

$$\cos\left(S^i + \frac{S^{iii}}{6} + \cdots\right) = (y^2 - \beta)\mathrm{e}^{-\mathrm{i}(S^{ii}/2 + S^{iv}/24 + \cdots)} \tag{7.20}$$

where $S^m = (\sqrt{\Lambda})^{-m}\, \partial^m S/\partial y^m$ are small quantities. Solving for the first derivative one has

$$\frac{1}{\sqrt{\Lambda}}\frac{\partial S}{\partial y} = \arccos\left[(y^2 - \beta)\mathrm{e}^{-\mathrm{i}(S^{ii}/2 + S^{iv}/24 + \cdots)}\right] - \frac{S^{iii}}{6} - \cdots. \tag{7.21}$$

Now

$$\begin{aligned} \mathrm{e}^{-\mathrm{i}(S^{ii}/2 + S^{iv}/24 + \cdots)} &= 1 - \mathrm{i}\left(\frac{S^{ii}}{2} + \frac{S^{iv}}{24} + \cdots\right) - \frac{1}{2}\left(\frac{S^{ii}}{2} + \frac{S^{iv}}{24} + \cdots\right)^2 + \cdots \\ &\equiv 1 + \delta \end{aligned} \tag{7.22}$$

Temporarily writing

$$\kappa = y^2 - \beta \tag{7.23}$$

then Equation (7.21) becomes

$$\frac{1}{\sqrt{\Lambda}}\frac{\partial S}{\partial y} = \arccos\left[\kappa(1 + \delta)\right] - \frac{S^{iii}}{6} - \cdots. \tag{7.24}$$

[3]Dingle and Morgan have also found a discrete form of the W.K.B. formulation for the R-N equation, see [16].

and so the arccos term can itself be Taylor expanded in κ about the point κ

$$\arccos\left[\kappa(1+\delta)\right] = \arccos\left[\kappa\right] - \frac{1}{\sqrt{1-\kappa^2}}\kappa\delta + \frac{1}{2}\,\frac{\kappa}{(1-\kappa^2)^{3/2}}\kappa^2\delta^2 + \cdots \tag{7.25}$$

giving

$$\begin{aligned}\frac{1}{\sqrt{\Lambda}}\frac{\partial S}{\partial y} = \arccos\left[y^2-\beta\right] + \mathrm{i}\frac{y^2-\beta}{\sqrt{1-(y^2-\beta)^2}}\frac{S^{ii}}{2} - \frac{S^{iii}}{6} + \mathrm{i}\frac{y^2-\beta}{\sqrt{1-(y^2-\beta)^2}}\frac{S^{iv}}{24} \\ + \frac{y^2-\beta}{(1-(y^2-\beta)^2)^{3/2}}\frac{(S^{ii})^2}{8} + \cdots .\end{aligned} \tag{7.26}$$

Solving for S^i by iterating to second order in a similar fashion to Section 4.4.3, gives

$$\frac{\partial S}{\partial y} = \sqrt{\Lambda}\ \arccos\left[y^2-\beta\right] - \mathrm{i}\frac{(y^2-\beta)y}{1-(y^2-\beta)^2}. \tag{7.27}$$

Integrating up this equation to find S, it is the second term on the r.h.s. which is the easier of the two integrals to perform since it can be recognised as

$$\frac{(y^2-\beta)y}{1-(y^2-\beta)^2} = \frac{1}{4}\frac{\partial}{\partial y}\ln\left(1-(y^2-\beta)^2\right) \tag{7.28}$$

allowing S to be written as

$$\begin{aligned}S &= \sqrt{\Lambda}\int \arccos\left[y^2-\beta\right]\,dy - \frac{\mathrm{i}}{4}\ln\left(1-(y^2-\beta)^2\right) \\ &\equiv \sqrt{\Lambda}\,S_0(y,\beta) - \frac{\mathrm{i}}{4}\ln\left(1-(y^2-\beta)^2\right).\end{aligned} \tag{7.29}$$

And so the amplitude envelope becomes

$$B(y) = \mathrm{e}^{\mathrm{i}S} = \frac{\mathrm{e}^{\mathrm{i}\sqrt{\Lambda}\int \arccos\left[y^2-\beta\right]\,dy}}{(1-(y^2-\beta)^2)^{1/4}} = \frac{\mathrm{e}^{\mathrm{i}\sqrt{\Lambda}\,S_0(y,\beta)}}{(1-(y^2-\beta)^2)^{1/4}} \tag{7.30}$$

which indeed has the form of a W.K.B. expression. In particular the expression has divergences at the turning-points

$$y = \pm\sqrt{\beta\pm 1}. \tag{7.31}$$

Bearing in mind that bound states have values of $\beta \le 1$ (see Equation (7.16)), then, except for the very rare cases when the eigenvalue happens to be such that $\beta = 1$, *real* turning-points for bound states are located at

$$y_\pm = \pm\sqrt{\beta+1}. \tag{7.32}$$

The remaining integral is more difficult and is therefore reserved for Appendix D. The lower limit of the integration is taken as the positive turning point $y = \sqrt{\beta+1}$ and the result is

$$\begin{aligned}S_0(y_+,y,\beta) &= \int_{\sqrt{\beta+1}}^{y} \arccos\left[y'^2-\beta\right]\,dy' \\ &= y\arccos\left[y^2-\beta\right] - 2\sqrt{1+\beta}\,\mathrm{E}\left(\frac{1}{2}\arccos\left[y^2-\beta\right]\middle|\ \frac{2}{1+\beta}\right).\end{aligned} \tag{7.33}$$

This expression for the phase is valid for $0 \le y \le \sqrt{\beta+1}$. For perpendicular incidence the phase is symmetrical about $y = 0$, and so only this half-range is required. For values of y greater than $\sqrt{1+\beta}$ the phase is purely imaginary, but with care (7.33) still gives the correct answer.

7.3.1 A well in momentum space

Although the remaining calculations in this Chapter and the next will be in momentum space, to keep the analogy with W.K.B. expressions as simple and as familiar as possible, y will be treated as though it were really the independent configuration space co-ordinate, 'q', say. It will be as though momentum space has been temporarily relabelled as a configuration space. Whenever confusion might occur, the actual momentum and configuration spaces will be referred to as (actual) momentum and (actual) configuration space.

Whilst it is useful to think of Equation (7.30) as a W.K.B. type expression, it does have some unusual features, due to its unorthodox derivation from a difference equation, which are unfamiliar from standard W.K.B. solutions. Usually, for the Schrödinger equation

$$\frac{d^2\psi(q)}{dq^2} + \frac{p^2(q)}{\hbar^2}\psi(q) = 0 \tag{7.34}$$

where $p(q)$ is the momentum, one has the approximate solution [14], valid for small $\hbar$ as long as one is not too close to the turning-points ($p(q) = 0$), of

$$\psi^{\pm}_{WKB} \equiv \frac{1}{\sqrt{p(q)}} \exp\left(\pm\frac{\mathrm{i}}{\hbar}\int_0^q p(q')dq'\right) \tag{7.35}$$

where $+/-$ refers to right/left travelling waves.

Here however, referring to Equation (7.30), the momentum function appearing in the amplitude and phase are different. The two momenta,

$$p_1(y,\beta) = \sqrt{1-(y^2-\beta)^2} \tag{7.36}$$

and

$$p_2(y,\beta) = \arccos\left[y^2-\beta\right] \tag{7.37}$$

coincide for $\beta \to -1$, but are quite different when $\beta \to 1$. Examining Figure 7.2 one notes that the momentum appearing in the phase, p_2, is the momentum exhibited by a particle in a simple well. The amplitude momentum, p_1, however, corresponds to a particle in a double well—although except for values of β greater than one, the particle has enough energy to move between the two wells. As far as the W.K.B. method is concerned, it is the turning-point structure that is of paramount importance (see Berry and Mount [14] for a review of the W.K.B. procedure), and so the different local values of the two momenta should present no problems when $\beta < 1$. However, as soon as the turning-point structure of p_1 changes from two to four, at $\beta = 1$, one should expect problems. So, whereas a W.K.B. solution of the (actual) configuration space Mathieu equation problem requires the treatment of an infinite number of wells (due to the $\cos^2 Kx$ potential), the (actual) momentum space W.K.B. solution is considerably easier, especially for the bound states

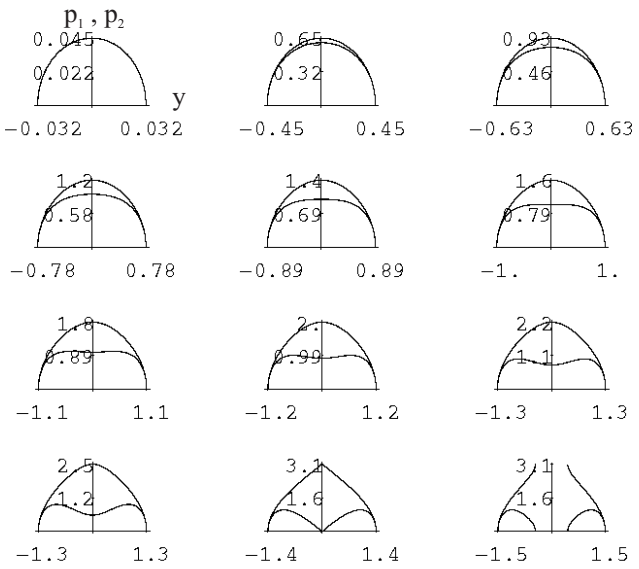

Figure 7.2: A series of plots showing the two momentum functions, p_1 and p_2, as functions of y for different values of β. The top left has $\beta = -0.999$, each successive picture has β increasing by 0.2 until the bottom right which has $\beta = 1.201$. It is the p_1 curve that dips down to zero when $\beta = 1$.

that all reside below $\beta = 1$. The problem of diffraction from a general periodic system (i.e. a crystal) at high energies from the (actual) configuration space point of view was studied by Berry [10] in 1971. Whilst insightful, the work demonstrates that the (actual) configuration space analysis is necessarily quite complicated, and hence this approach has never been whole heartedly adopted by the diffraction physics community.

Comparison with a more general W.K.B. expression

The two differing momenta occuring in (7.30) can be reconciled to some degree by reverting to another W.K.B. solution, whose existence was brought to the attention of the author by J. H. Hannay [40], which is a more general form

$$\psi^{\pm}_{WKB} \propto \frac{1}{\sqrt{\frac{\partial H}{\partial p}}} \exp\left(\pm \frac{\mathrm{i}}{\hbar} \int_0^x p(x')dx'\right) \tag{7.38}$$

of which (7.35) is a special case through the Hamilton equation

$$\frac{p(y)}{m} = \dot{y} = \frac{\partial H}{\partial p}. \tag{7.39}$$

Referring to the phase space shown in Figure 3.2, each curve corresponds to a particular energy (Hamiltonian). In the W.K.B. approximation, the amplitude of the configuration space wavefunction is given by the Jacobian of the mapping from phase space down onto the configuration axis. The 'density' of the energy curves gives a measure of how likely it is for a particle to be in that region of phase space. For each value of the configuration co-ordinate, the rate of change of the p-co-ordinate as one changes the parameter H, i.e. dp/dH, gives this density. And so, in an analogous fashion to the amplitudes used in Chapter 3 and Appendix B, the amplitude is written as in Equation (7.38).

So if the 'true' momentum is taken as the phase momentum p_2, and one is guided by the general W.K.B. expression (7.38) to equate

$$\frac{\partial H}{\partial p_2} = \sqrt{1 - \left(y^2 - \beta\right)^2} = \sqrt{1 - \cos^2 p_2} = \sin p_2 \tag{7.40}$$

then in general

$$H = -\cos p_2 + f(y) = -\left(y^2 - \beta\right) + f(y) \tag{7.41}$$

where $f(y)$ is an unknown function. Since the Hamiltonian is a constant in phase space, the unknown function must be

$$f(y) = y^2 \tag{7.42}$$

so that the Hamiltonian contours are given by

$$H = \beta \tag{7.43}$$

which is consistent with the rest of the structure built up in this chapter.

7.3.2 The Bohr-Sommerfeld condition

For states in a well, single-valuedness of the wavefunction dictates that only certain discrete energies are allowed. These energies are the eigenvalues/characteristic numbers introduced in Section 4.5. In the formalism of this chapter they translate, through definition (7.12), into certain permitted values of β. Semiclassically, these values of β are those that ensure the integral of the W.K.B. phase, Equation (7.33), from one turning-point to the other (that is, the integral across the classically accessible part of the potential well), allow the oscillating part of the W.K.B. wavefunction to match correctly onto (asymptotically) exponentially decaying parts of the wavefunction (that tunnel into the classically forbidden sides of the well).

The action right across the well, given by setting the upper integration limit of Equation (7.33) equal to $-\sqrt{\beta+1}$, is also equal to, for perpendicular incidence, twice the value found by integrating only halfway, to the midpoint of the well at $y = 0$,

$$2S_0(y_+, 0, \beta) = -4\sqrt{1+\beta}\,\mathrm{E}\left(\frac{1}{2}\arccos\left[-\beta\right]\middle|\,\frac{2}{1+\beta}\right). \tag{7.44}$$

The Bohr-Sommerfeld[4] condition then states

$$2\sqrt{\Lambda}\;\left|S_0(y_+, 0, \beta^j)\right| = \left(j+\frac{1}{2}\right)\pi\;, \qquad j = 0, 1, 2, 3\ldots. \tag{7.45}$$

Finding the root of this equation (which must be done numerically) for each value of j gives the β^j eigenvalues. One can also use this expression to find the number of bound states that exist once a value for Λ has been chosen. It is important to note that 'bound' refers to the (actual) configuration space picture for which states can have energies either above or below the 'washboard' potential maximum of V_0. In (actual) momentum space all the states are trapped in a well. The most energetic bound state then, labelled by j_{max}, has the value of β which is closest to one. When Λ is large the eigenvalues lie very close to each other, and in particular,

$$\lim_{\Lambda\to\infty} \beta^{j_{max}} = 1 \tag{7.46}$$

and since

$$\mathrm{E}\left(\frac{\pi}{2}\middle|\,1\right) = 1 \tag{7.47}$$

then

$$\lim_{\Lambda\to\infty} j_{max} = \frac{4\sqrt{\Lambda}\sqrt{2}}{\pi} - \frac{1}{2}. \tag{7.48}$$

[4]Although identical to the Bohr-Sommerfeld rule, this condition on the action across the well is really to be derived by matching the W.K.B. solutions from either turning-point in the middle of the well. One should take care when interpreting this as 'fitting waves in a box', because the W.K.B. solutions are not valid at the turning-point, and so one cannot say, for instance, that the wavefunction at the turning-point is a cosine wave registering a $\pi/4$ phase. Indeed, the Airy function is the correct wavefunction for a first order turning-point.

Although this gives the total number of possible bound states, not all of them are necessarily used in the superposition which gives the complete wavefunction. For perpendicular incidence only the even eigenvectors are excited. Examining the coefficients (4.80) appearing in the superposition, they are given by the value of the corresponding Bloch wave at $y = 0$. This implies that the odd Bloch waves are excluded from the sum as asserted.

7.3.3 Real eigenvectors and normalisation

Since the stationary R-N equation (7.15) is real, it is always possible to find real solutions. This is achieved by constructing a superposition of the two independent solutions: the right and left travelling waves of Equation (7.35). The specific combination of the two solutions which make up the superposition is determined by multiplicative coefficients for each independent solution, and in general these can be functions of y. Semiclassically however, the coefficients may be taken as constants within each classically allowed region, only changing across a turning-point because of Stokes' phenomena. See Berry and Mount [14] for a review. The potential well is a particularly simple case; the boundary conditions are assumed to require exponential decay into both of the classically forbidden sides of the well. This allows the complete determination of the multiplicative superposition coefficients (and hence all the 'Stokes constants') giving the W.K.B. eigenvectors

$$\psi_{WKB} = \frac{\mathcal{N}(\beta)}{\left(1-(y^2-\beta)^2\right)^{1/4}} \cos\left(\sqrt{\Lambda}\, S_0(y_+, y, \beta) + \frac{\pi}{4}\right) \tag{7.49}$$

where S_0 is given by Equation (7.33), and $\mathcal{N}(\beta)$ is a normalisation factor.

The normalisation of the discrete amplitudes B_n follows from the requirement that

$$\sum_{n=-\infty}^{\infty} |B_n|^2 = 1. \tag{7.50}$$

When moving from a summation to the integration in the continuous variable y, care must be taken to include a factor of $\sqrt{\Lambda}$ which comes from the definition (7.11) of y, so that

$$\sum_{n=-\infty}^{\infty} \longrightarrow \int_{n=-\infty}^{\infty} dn \longrightarrow \sqrt{\Lambda} \int_{y=-\infty}^{\infty} dy. \tag{7.51}$$

And so normalising the eigenvectors requires the evaluation of

$$\int_{-\infty}^{\infty} \left|\psi^j_{WKB}(y)\right|^2 \, dy = 1. \tag{7.52}$$

When Λ becomes large, the exponential decay of the wavefunction into the sides of the well becomes very rapid and one can ignore these contributions, so the integral is taken to be just that between the two turning-points of the classical motion. Further, the oscillation of the wavefunction between

the two turning-points is assumed to be very rapid[5] in comparison to the slow variation of the square of the amplitude. The $\cos^2$ term oscillates between zero and $(\sqrt{1-(y^2-\beta)^2})^{-1}$ and so without much loss of accuracy, can be replaced by its average value of half the square of the amplitude. Although the amplitude diverges at the turning-points, as pointed out in Chapter 3, this divergence is still integrable. Local to the turning-point, if one sets

$$y \to \sqrt{1+\beta} - (y_+ - y) \tag{7.53}$$

then

$$\sqrt{1-(y^2-\beta)^2} \longrightarrow \sqrt{4\sqrt{1+\beta}\,(y_+ - y)}. \tag{7.54}$$

So locally the normalisation integral gives

$$\int \frac{d(y_+ - y)}{\sqrt{(y_+ - y)}} = 2\sqrt{y_+ - y} \tag{7.55}$$

and these square-root divergences, it turns out, are narrow enough to have negligible effect. Thus, one takes

$$\frac{\sqrt{\Lambda}}{2}\int_{y_-}^{y_+} \frac{dy}{\sqrt{1-(y^2-\beta)^2}} = \frac{1}{\mathcal{N}^2}. \tag{7.56}$$

The integration is carried out in Appendix F and gives

$$\mathcal{N}^2 = \frac{\sqrt{2}}{\sqrt{\Lambda}\;\mathrm{K}\left(\frac{1+\beta}{2}\right)}. \tag{7.57}$$

Finally then, all the necessary pieces of the W.K.B. approximation to each Bloch wave can be assembled together and an example is shown in Figure 7.3. The resemblance is remarkable. The W.K.B. wavefunction was only calculated at the discrete points corresponding to the diffracted beams, but in the picture these points were joined together by a continuous line to faciliate comparison with the numerical data. The particular Bloch wave shown has $\beta = 0.262$ so it is a little over halfway up the well. As emphasised right from its introduction, the W.K.B. approximation breaks down at the turning-points and this shows up in Figure 7.3. As the actual position of the classical caustic happens here to fall between two discrete points, the divergence doesn't appear as dramatic as it would if a larger value of Λ had been chosen. Finding a solution free from these divergences is the subject of the next chapter.

[5] Amazingly, the normalisation factor derived in this way works well even for the ground state Bloch wave which has the shape of a Gaussian, i.e. is non-oscillatory.

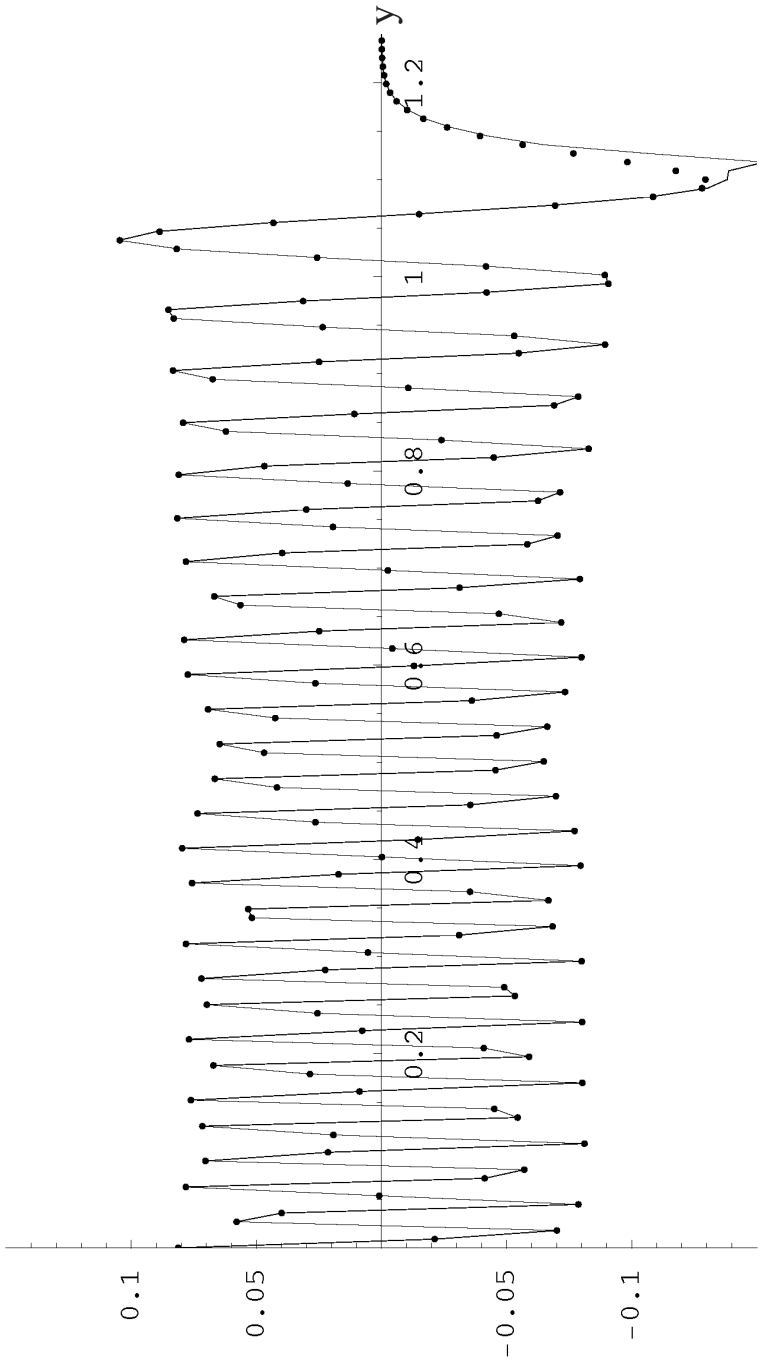

Figure 7.3: A comparison of the numerical (dots) 110^{th} Bloch wave, out of 200 bound states, of the R-N matrix (4.78) for $\Lambda = 12500$, with its W.K.B. approximation (solid line). Since the Bloch wave is symmetrical about $y = 0$, only the positive half is shown.

Chapter 8

The uniform approximation

8.1 Motivation

The W.K.B. approximation, named after G. Wentzel, H. A. Kramers, and L. Brillouin who independently introduced it into quantum mechanics in 1926, actually has its origins in the 19^{th} century, as early as 1817 with Carlini[1] and is thereafter associated with many of the great names of mathematical physics including; J. Liouville (1837), G. Green (1837), G. Stokes (1857,...,1889), Lord Rayleigh (1912) and later, H. Jeffreys (1923,...,1956). Despite its capacity for providing asymptotic solutions to a great variety of differential equations, it has the well known deficiency of diverging at the transition (turning) points. It was not until the middle of this century that a very elegant method, known as the uniform approximation, was developed by Miller and Good (1953) and then Dingle (1956). Although limited in applicability to relatively few situations, when suitable it provides a complete solution—uniformly valid throughout the entire domain without any spurious divergences.

8.2 Comparison with known equations

A very brief introduction will now be given to the uniform approximation. Further details are contained in the review by Berry and Mount [14]. The aim of the method is to obtain an approximate solution of the Helmholtz equation

$$\frac{d^2\psi(q)}{dq^2} + \chi(q)\psi(q) = 0 \tag{8.1}$$

[1]The history of the 'W.K.B.J.' technique is surveyed in Heading's *Introduction to Phase Integral Methods* [42].

in terms of solutions to one of the 'studied' equations, which will be written

$$\frac{d^2\phi(\sigma)}{d\sigma^2} + \Gamma(\sigma)\phi(\sigma) = 0. \tag{8.2}$$

The choice of studied equation is determined by $\Gamma(\sigma)$ (not *the* Gamma function) being in some way similar to $\chi(q)$. This similarity implies that $\phi(\sigma)$ also resembles the wavefunction $\psi(q)$, and "can be changed into it by stretching or contracting it a little and changing the amplitude a little". And so $\psi(q)$ will be expressed in terms of $\phi(\sigma)$

$$\psi(q) = f(q)\phi(\sigma(q)). \tag{8.3}$$

Substitution of this definition into (8.1) and making use of (8.2) leaves

$$\frac{d^2 f}{dq^2} + \chi f\phi - f\left(\frac{d\sigma}{dq}\right)^2 \Gamma\phi + \frac{d\phi}{d\sigma}\left(2\frac{df}{dq}\frac{d\sigma}{dq} + f\frac{d^2\sigma}{dq^2}\right) = 0. \tag{8.4}$$

The amplitude $f(q)$ is as yet unspecified, so it is chosen to simplify (8.4) as much as possible. Putting

$$f = \left(\frac{d\sigma}{dq}\right)^{-\frac{1}{2}} \tag{8.5}$$

renders (8.4) into an equation purely for the 'mapping function' $\sigma(q)$

$$\chi = \left(\frac{d\sigma}{dq}\right)^2 \Gamma - \left(\frac{d\sigma}{dq}\right)^{\frac{1}{2}} \frac{d^2}{dq^2}\left(\frac{d\sigma}{dq}\right)^{-\frac{1}{2}} \tag{8.6}$$

which, when solved, gives σ as a function of q. If a good choice of comparison function $\Gamma(\sigma)$ has been made, then $\sigma(q)$ will be a slowly varying function and the second term on the r.h.s. of (8.4) will be much smaller than the first. Clearly the criterion for this to be the case is

$$\epsilon(q) \equiv \left|\frac{1}{\chi(q)}\left(\frac{d\sigma}{dq}\right)^{\frac{1}{2}} \frac{d^2}{dq^2}\left(\frac{d\sigma}{dq}\right)^{-\frac{1}{2}}\right| \ll 1. \tag{8.7}$$

When this is satisfied, the mapping relation reduces to

$$\frac{d\sigma}{dq} \simeq \left(\frac{\chi(q)}{\Gamma(\sigma)}\right)^{\frac{1}{2}} \tag{8.8}$$

which through definition (8.5) also gives the amplitude f. Thus, by picking two points σ_0 and q_0 which are 'equivalent', one finds $\sigma(q)$ from

$$\int_{\sigma_0}^{\sigma} \sqrt{\pm\Gamma(\sigma)}\, d\sigma = \int_{q_0}^{q} \sqrt{\pm\chi(q)}\, dq \tag{8.9}$$

where the $+$ or the $-$ version can be chosen depending on the situation. The approximate solution to (8.1) is then

$$\psi(q) \simeq \left(\frac{\Gamma(\sigma(q))}{\chi(q)}\right)^{\frac{1}{4}} \phi(\sigma(q)). \tag{8.10}$$

In order for the comparison method to be viable, the mapping from q to σ must be one to one, which requires that $d\sigma/dq$ is never zero or infinite. Examining (8.8) this means that χ and Γ must not diverge—which is assumed to be the case—and more relevantly, their zeros must be made to correspond. The zeros are of course the turning-points, and so, as Berry and Mount emphasise, "in the semiclassical limit all problems are equivalent which have the same *classical turning-point structure*".

The problem of the lone, first order (that is, the potential is locally linear) turning-point leads to the comparison equation

$$\frac{d^2\sigma}{d\sigma^2} - \sigma\phi = 0 \tag{8.11}$$

whose solution is the well behaved Airy function, $\mathrm{Ai}(\sigma)$, and so, close to all first order turning-points, one expects the now ubiquitous Airy profile. If the potential remained as this constant 'ramp' for all q, the Airy function would be a uniform solution, but then, of course, the apparatus described above would not be needed. Typically though, for any smooth potential 'step' featuring a classically allowed region to one side of the turning-point, and by definition a classically forbidden side on the other, the solution is locally an Airy function, which may then be connected to W.K.B. solutions describing the rest of the domain which is free from turning-points. Such a solution is no longer a uniform one, though the Airy function piece is referred to as a 'transitional' approximation, it being only locally uniform. Provided the two turning-points are sufficiently separated, then, when dealing with a potential well, two transitional approximations could be employed to a give a non-diverging approximation to the wavefunction everywhere. Fortunately the well belongs to another solvable class—two first order turning-points[2]—which has a uniform solution.

8.3 The uniform approximation for a well

The unmanipulated stationary Raman-Nath equation (7.15) gives no indication of what function to take for $\chi(y)$. Drawing inspiration from the W.K.B. approximation (7.30) one has a choice of either p_1^2 (7.36), or p_2^2 (7.37). The dual nature of the momentum will become an issue when eigenvectors whose eigenvalues are close to $\beta = 1$ are given special attention. However, it seems natural, in the light of the discussion of Section 7.3.1, to choose the momentum appearing in the phase, p_2.

The simplest comparison equation for a well is

$$\frac{d^2\phi}{d\sigma^2} + \left(t - \sigma^2\right)\phi = 0. \tag{8.12}$$

[2]Which may also coalesce into a single second order turning-point

The parameter t depends on the energy. The 'equivalent points' needed for Equation (8.9) are chosen to be the turning-points. This of course immediately satisfies the requirement that the zeros of Γ and χ correspond. Using (8.9), the integral across the well gives t, for then

$$\int_{y_-}^{y_+} \sqrt{\Lambda} p_2(y,\beta)\, dy \equiv -2\sqrt{\Lambda} S_0(y_+,0,\beta) = \int_{-\sqrt{t}}^{+\sqrt{t}} \sqrt{t-\sigma^2}\, d\sigma = \frac{t\pi}{2} \tag{8.13}$$

where S_0 is given by Equation (7.33). Once t, which is a function of β, is known, the mapping function $\sigma(y)$ can be found from

$$\sqrt{\Lambda} S_0(y_+,y,\beta) = \int_{+\sqrt{t}}^{\sigma(y)} \sqrt{t-\sigma^2}\, d\sigma = \frac{t}{2}\left(\arcsin\left[\frac{\sigma}{\sqrt{t}}\right] + \frac{\sigma}{\sqrt{t}}\sqrt{1-\frac{\sigma^2}{t}} - \frac{\pi}{2}\right). \tag{8.14}$$

Clearly this step must be executed by numerical root finding for each value of y which is required, i.e. those spaced at $1/\sqrt{\Lambda}$ intervals which are the angular positions of the diffracted beams.

The two standard forms of the parabolic cylinder equation are [1]

$$\frac{d^2\Theta}{dg^2} \mp \left(\frac{g^2}{4} \pm a\right)\Theta = 0 \tag{8.15}$$

and the well Equation (8.12) corresponds to taking the upper signs. The most basic independent solutions to the parabolic cylinder equations are an even and an odd power series. However, certain combinations of these two power series lead to another two independent solutions, known as the Whittaker functions, which for large g decay or grow exponentially. Thus it is these Whittaker functions which have the correct properties to match the exponential tunnelling of the physical solution into the sides of the well. The Whittaker solutions to the well equation (8.12) are $D_{(t-1)/2}(\sigma\sqrt{2})$ and $D_{(t-1)/2}(-\sigma\sqrt{2})$. The accepted theory for the potential well uniform approximation would then predict the form of the Bloch wavefunction, correct for all y, to be

$$B(y) = \psi_{\text{uniform}} = \frac{1}{2}\mathcal{N}\, 2^{1/4}\left(\frac{2\mathrm{e}}{t(\beta)}\right)^{t(\beta)/4}\left(\frac{d\sigma(y)}{dy}\right)^{-1/2} D_{(t(\beta)-1)/2}\left(-\sigma(y)\sqrt{2}\right) \tag{8.16}$$

and it is noted that for perpendicular incidence the choice of $+\sigma$ or $-\sigma$ makes no difference (only even eigenvectors are excited). The various terms in this expression will be examined in more detail in subsequent sections.

Inserting the Bohr-Sommerfeld condition (7.45) into the equation for t, (8.13) above, gives the value of t which corresponds to the j^{th} eigenvalue

$$t = 2j + 1. \tag{8.17}$$

When the index of a Whittaker function is an integer, as here, it takes on the more familiar form

$$D_j(\sigma\sqrt{2}) = 2^{-j/2} H_j(\sigma) \mathrm{e}^{-\sigma^2/2} \tag{8.18}$$

where H_j is a Hermite polynomial. However, for the higher[3] Bloch waves, it is best to use, for reasons of speed of computation, the Airy function approximation to the Whittaker functions (see [1]).

8.3.1 Modifying the amplitude

The application of the uniform method to the W.K.B. approximation of the R-N equation requires some adjustment. The existence of two momentum functions means the amplitude term of Equation (8.16),

$$\left(\frac{d\sigma(y)}{dy}\right)^{-1/2} = \left(\frac{t-\sigma^2}{\arccos^2\left[y^2-\beta\right]}\right)^{1/4} \tag{8.19}$$

does not match the W.K.B. behaviour (see Figure 7.2), since in that expression it is p_1 that appears in the amplitude. It is therefore *conjectured* that the standard uniform amplitude term be modified to become

$$\left(\frac{t-\sigma^2}{\arccos^2\left[y^2-\beta\right]}\right)^{1/4} \longrightarrow \left(\frac{t-\sigma^2}{1-\left(y^2-\beta\right)^2}\right)^{1/4}. \tag{8.20}$$

The uniform approximation is formulated so that $\Gamma(\sigma)$ and $\chi(y)$ approach zero together so that the divergence inherent in the W.K.B. solution is tamed. For the conjecture to hold this swapping of the momentum expressions in the amplitude must still lead to the correct behaviour at the turning-points. For $\beta < 1$, both p_1 and p_2 have the same zeros, and crucially for the uniform approximation they go to zero in the same way, namely as the square root of the distance from the zero. Putting $y \longrightarrow \sqrt{1+\beta} - (y_+ - y)$ into p_2 gives

$$\arccos\left[y^2-\beta\right] \longrightarrow \arccos\left[1-2\sqrt{1+\beta}\,(y_+-y)\right] \tag{8.21}$$

but

$$\arccos\left[1-\delta\right] = \sqrt{2\delta}\left(1+\frac{\delta}{12}+\cdots\right) \tag{8.22}$$

and so

$$\arccos\left[1-2\sqrt{1+\beta}\,(y_+-y)\right] \sim \sqrt{4\sqrt{1+\beta}\,(y_+-y)}. \tag{8.23}$$

This is identical to the result for p_1—see Equation (7.53).

L'Hôpital's rule can be used to find the limiting value of the amplitude (8.20) at the turning-point, since

$$\begin{aligned}\lim_{y\to\sqrt{1+\beta}}\left[\frac{t-\sigma^2}{1-\left(y^2-\beta\right)^2}\right] &= \frac{\lim_{y\to\sqrt{1+\beta}}\left[\frac{d}{dy}\left(t-\sigma^2\right)\right]}{\lim_{y\to\sqrt{1+\beta}}\left[\frac{d}{dy}\left(1-\left(y^2-\beta\right)^2\right)\right]} \\ &= \frac{\lim_{y\to\sqrt{1+\beta}}\left[\frac{d\sigma}{dy}\frac{d}{d\sigma}\left(t-\sigma^2\right)\right]}{\lim_{y\to\sqrt{1+\beta}}\left[\frac{d}{dy}\left(1-\left(y^2-\beta\right)^2\right)\right]}.\end{aligned} \tag{8.24}$$

[3] For j greater than 20, say.

By Equation (8.8),

$$\frac{d\sigma}{dy} = \left(\frac{\chi}{\Gamma}\right)^{1/2} = \left(\frac{p_2^2}{\Gamma}\right)^{1/2} \quad \lim_{y\to\sqrt{1+\beta}} \quad \left(\frac{p_1^2}{\Gamma}\right)^{1/2} \tag{8.25}$$

where, as indicated, the last equality holds only when y is close to $\sqrt{1+\beta}$. And thus

$$\begin{aligned}\lim_{y\to\sqrt{1+\beta}}\left[\frac{t-\sigma^2}{1-\left(y^2-\beta\right)^2}\right] &= \lim_{y\to\sqrt{1+\beta}}\left[\frac{\Gamma}{p_1^2}\right] = \lim_{y\to\sqrt{1+\beta}}\left[\frac{\Gamma}{p_2^2}\right] \\ &= \frac{\lim_{y\to\sqrt{1+\beta}}\left[\sqrt{\frac{p_2^2}{\Gamma}}\,(-2\sigma)\right]}{\lim_{y\to\sqrt{1+\beta}}\left[\left(-4y\left(y^2-\beta\right)^2\right)\right]} \\ &= \frac{\lim_{y\to\sqrt{1+\beta}}\left[\sqrt{\frac{p_2^2}{\Gamma}}\right](-2\sqrt{t})}{\left(-4\sqrt{1+\beta}\right)}\end{aligned} \tag{8.26}$$

the last line of which makes use of the fact that by construction, when $y \to \sqrt{1+\beta}$, then $\sigma \to \sqrt{t}$. And so

$$\lim_{y\to\sqrt{1+\beta}}\left[\frac{\Gamma}{p_1^2}\right] = \lim_{y\to\sqrt{1+\beta}}\left[\frac{\Gamma}{p_2^2}\right] = \left(\frac{\sqrt{t}}{2\sqrt{1+\beta}}\right)^{2/3}. \tag{8.27}$$

8.3.2 Matching to the W.K.B. solution

The multiplicative factors of Equation (8.16) in front of the amplitude arise from matching the known asymptotic behaviour of the Whittaker function for large y with that of the W.K.B. solution. When $\sigma \gg t$

$$D_{(t(\beta)-1)/2}\left(\sigma(y)\sqrt{2}\right) \sim \mathrm{e}^{-\sigma^2/2}\left(\sigma\sqrt{2}\right)^{(t-1)/2}. \tag{8.28}$$

The functional form of $\sigma(y)$ for large y is obtained by assuming that when $y \to \infty$, then so also $\sigma(y) \to \infty$, for then

$$\begin{aligned}\frac{t}{2}\left(\arcsin\left[\frac{\sigma}{\sqrt{t}}\right]+\frac{\sigma}{\sqrt{t}}\sqrt{1-\frac{\sigma^2}{t}}-\frac{\pi}{2}\right) &= \frac{t}{2}\left(\frac{\pi}{2}-\mathrm{i}\,\operatorname{arccosh}\left[\frac{\sigma}{\sqrt{t}}\right]+\mathrm{i}\frac{\sigma^2}{t}\sqrt{1-\frac{t}{\sigma^2}}-\frac{\pi}{2}\right) \\ &\overset{\sigma\to\infty}{\longrightarrow} \frac{\mathrm{i}t}{2}\left(-\ln\left[\frac{2\sigma}{\sqrt{t}}\right]+\frac{t}{4\sigma^2}+\cdots \qquad +\frac{\sigma^2}{t}-\frac{1}{2}-\frac{t}{8\sigma^2}+\cdots\right).\end{aligned} \tag{8.29}$$

Which, using (8.14), means

$$-\frac{\sigma^2}{2} \sim \mathrm{i}\sqrt{\Lambda}S_0 + \ln\left[\frac{2\sigma}{\sqrt{t}}\right]^{-t/2} - \frac{t}{4} \tag{8.30}$$

and so, with (8.28) implies

$$D_{(t(\beta)-1)/2}\left(\sigma(y)\sqrt{2}\right) \sim \mathrm{e}^{\mathrm{i}\sqrt{\Lambda}S_0 - t/4}\left(\frac{2\sigma}{\sqrt{t}}\right)^{-t/2} 2^{(t-1)/4}\,\sigma^{(t-1)/2}. \tag{8.31}$$

Now the modified amplitude goes as

$$\left(\frac{t-\sigma^2}{1-\left(y^2-\beta\right)^2}\right)^{1/4} \overset{\sigma\to\infty}{\longrightarrow} \frac{\sqrt{\sigma}}{\left(\left(y^2-\beta\right)^2-1\right)^{1/4}} \tag{8.32}$$

and so

$$\left(\frac{t-\sigma^2}{1-\left(y^2-\beta\right)^2}\right)^{1/4} D_{(t(\beta)-1)/2}\left(\sigma(y)\sqrt{2}\right) \overset{y\to\infty}{\longrightarrow} \frac{\mathrm{e}^{\mathrm{i}\sqrt{\Lambda}S_0}}{\left(\left(y^2-\beta\right)^2-1\right)^{1/4}}\, 2^{-1/4}\left(\frac{t}{2\mathrm{e}}\right)^{t/4}. \tag{8.33}$$

The W.K.B. expression (7.30) (see also (7.49)) on the other hand goes as

$$\psi_{WKB} = \frac{1}{2}\mathcal{N}\frac{\mathrm{e}^{\mathrm{i}\sqrt{\Lambda}\,S_0}}{\left((y^2-\beta)^2-1\right)^{1/4}} \tag{8.34}$$

which means that the factor

$$\frac{1}{2}\mathcal{N}\,2^{1/4}\left(\frac{2\mathrm{e}}{t}\right)^{t/4} \tag{8.35}$$

multiplying the uniform wavefunction ensures the correct asymptotic behaviour.

8.3.3 Comparison with the purely numerical calculation

Some pictures will now be used to compare the uniform method with the results of numerical diagonalisation (which can be taken as the 'exact' result). Figures 8.1–8.5 show a selection of Bloch waves with the uniform calculation shown as a solid line, though as before, only the discrete values of y corresponding to the diffracted beams were used. The dots are the numerical data.

Figures 8.6–8.8 give the total wavefunction, found by summing the Bloch waves, at various depths. Only the bound states were used in both the numerical and uniform calculations.

8.4 The problem of the separatrix

Careful examination of the picture of the 200^{th} eigenstate for $\Lambda = 12500$, reveals the first hint that the uniform approximation used so far has a defect when β begins to approach 1. As apparent from Figure 7.2, two new (real) turning-points appear in the p_1 momentum function when $\beta \geq 1$, as the central dip breaks through the zero line. For relatively small values of Λ the actual divergences due to these turning-points can fall between the diffracted orders and go unnoticed. As Λ increases in magnitude this is no longer the case and the divergences become clearly defined as the classical distribution emerges. As pointed out in the previous chapter, though not discussed, these new turning-points occur at

$$y = \pm\sqrt{\beta-1}. \tag{8.36}$$

8.4.1 Lessons from phase space

Referring back to the phase space picture, Figure 3.2, and as mentioned at the time, the rotation contours have 4 values of P_x where their gradient w.r.t. P_x becomes infinite. Physically, the new probability divergences are due to the atoms sitting on the barrier tops in (actual) configuration

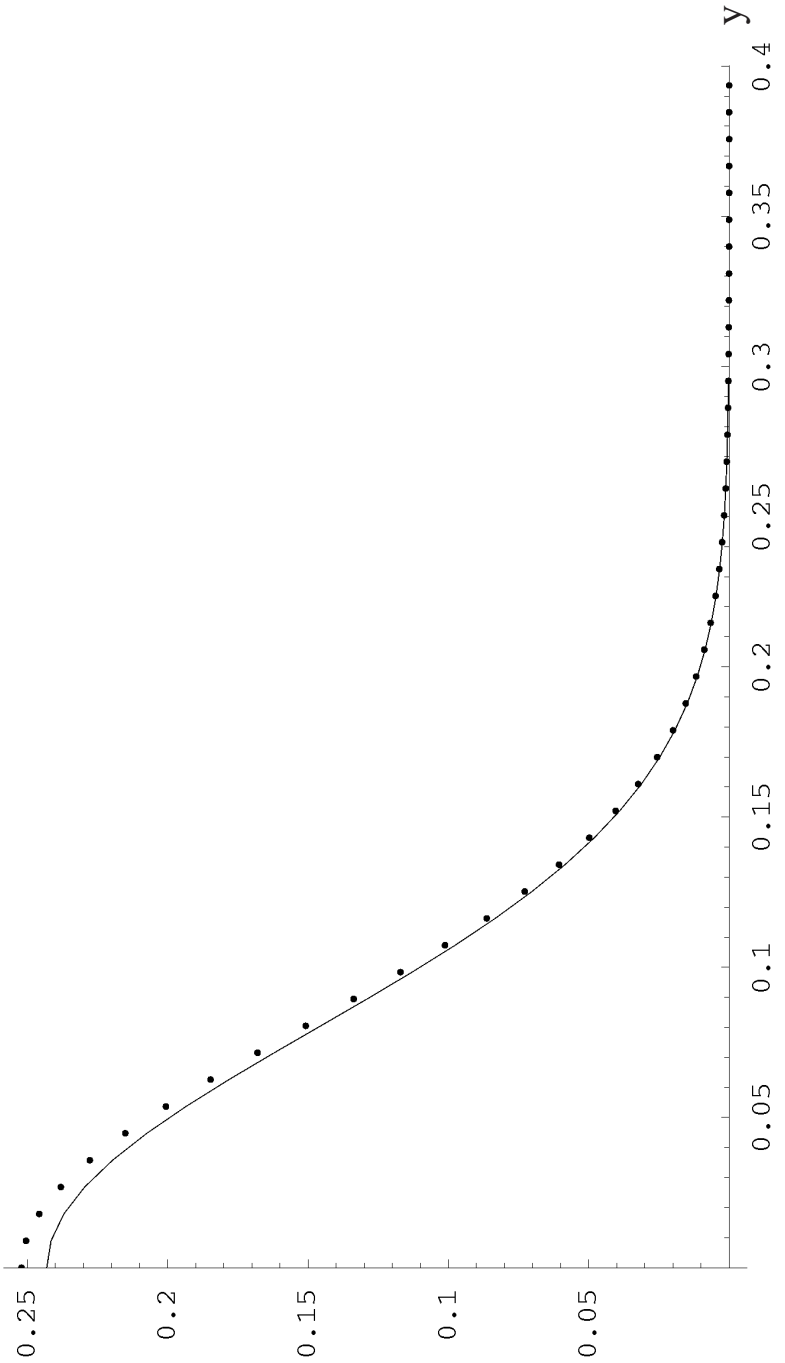

Figure 8.1: A comparison of the numerical (dots) 0^{th} Bloch wave, out of 200 bound states, of the R-N matrix (4.78) for $\Lambda = 12500$, with its uniform approximation (solid line). $\beta = -0.9937$. Since the Bloch wave is symmetrical about $y = 0$, only the positive half is shown.

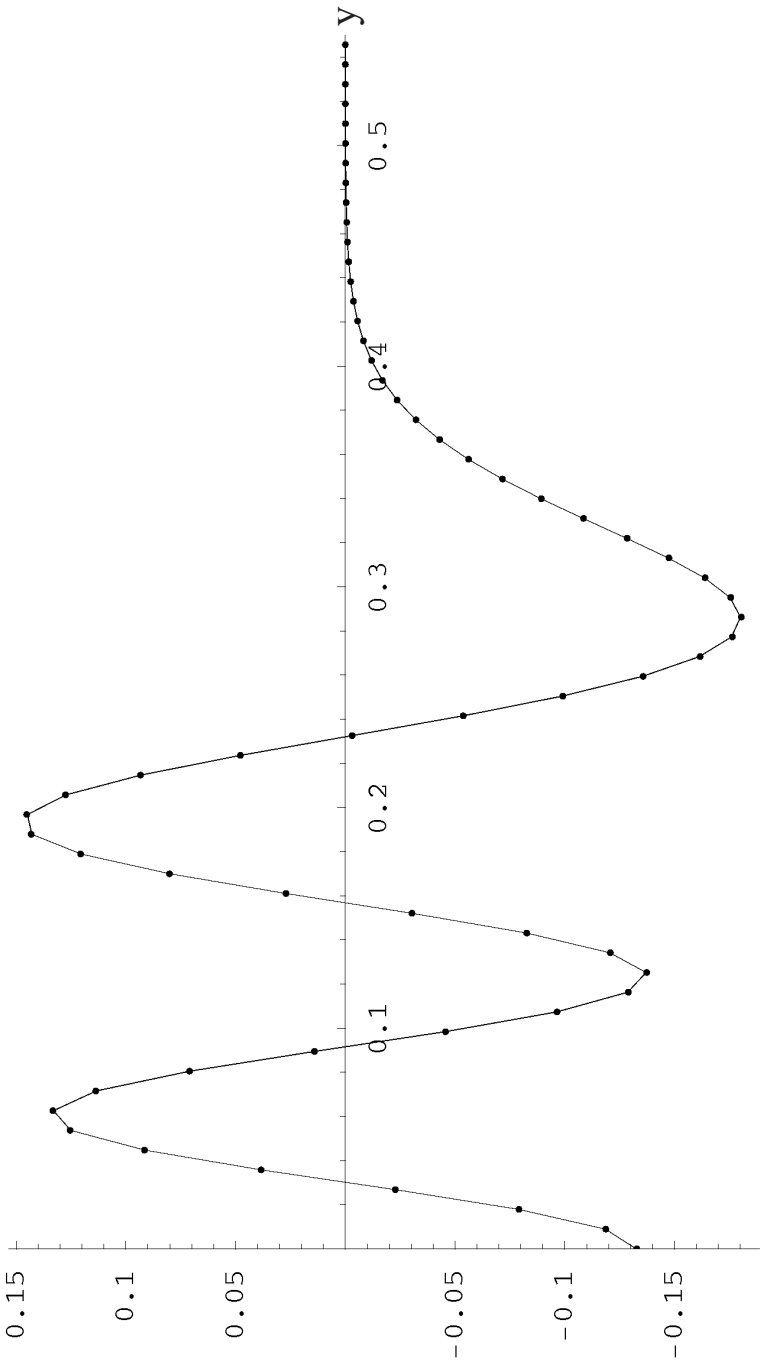

Figure 8.2: A comparison of the numerical (dots) 8^{th} Bloch wave, out of 200 bound states, of the R-N matrix (4.78) for $\Lambda = 12500$, with its uniform approximation (solid line). $\beta = -0.8932$.

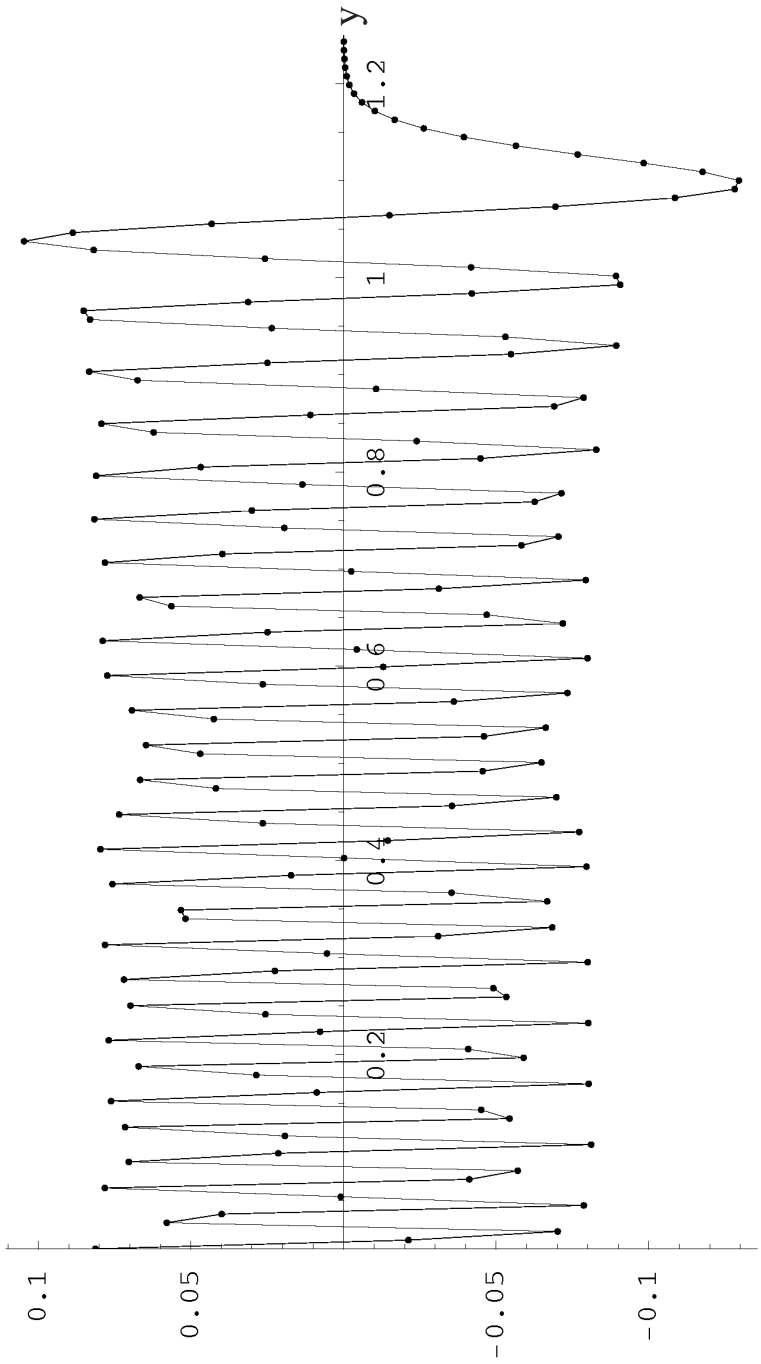

Figure 8.3: A comparison of the numerical (dots) 110^{th} Bloch wave, out of 200 bound states, of the R-N matrix (4.78) for $\Lambda = 12500$, with its uniform approximation (solid line). $\beta = 0.2616$.

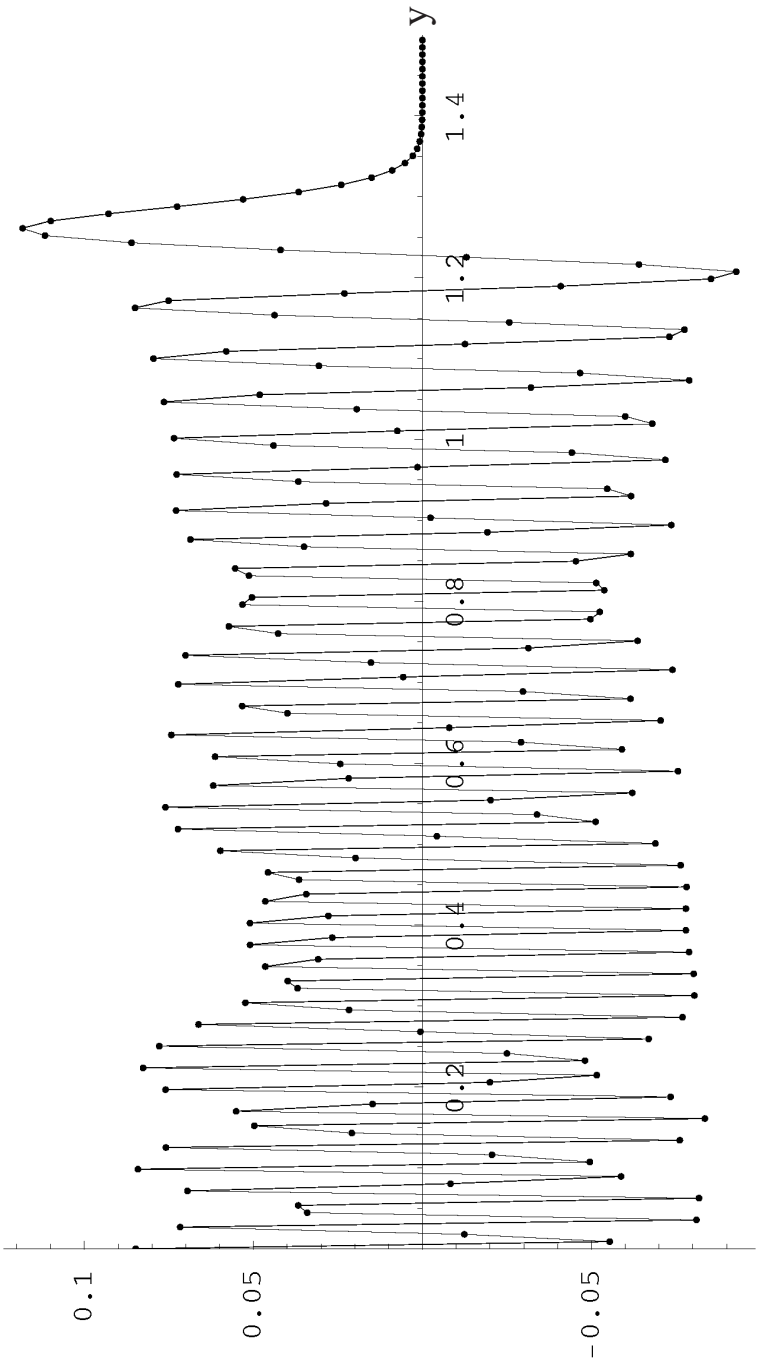

Figure 8.4: A comparison of the numerical (dots) 152^{nd} Bloch wave, out of 200 bound states, of the R-N matrix (4.78) for $\Lambda = 12500$, with its uniform approximation (solid line). $\beta = 0.6532$.

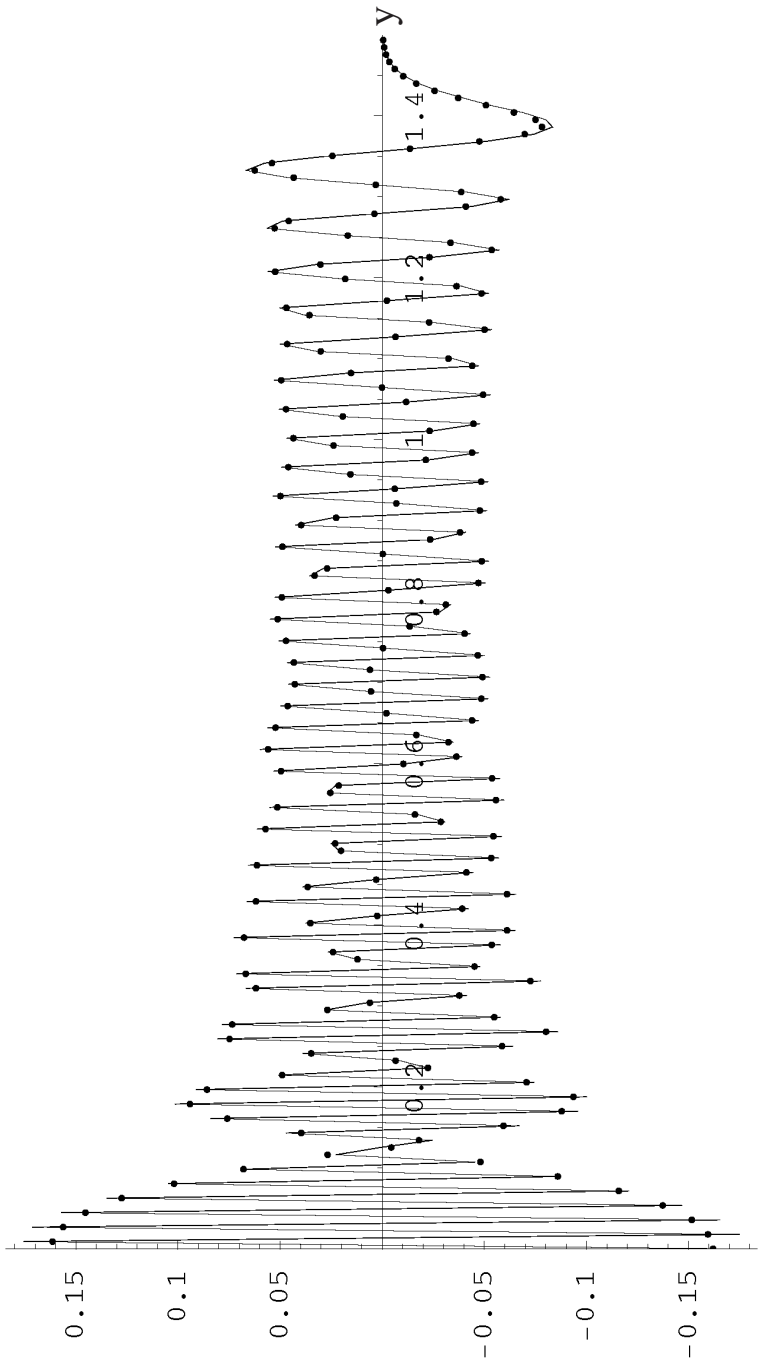

Figure 8.5: A comparison of the numerical (dots) 200^{th} Bloch wave, out of 200 bound states, of the R-N matrix (4.78) for $\Lambda = 12500$, with its uniform approximation (solid line). $\beta = 0.9961$.

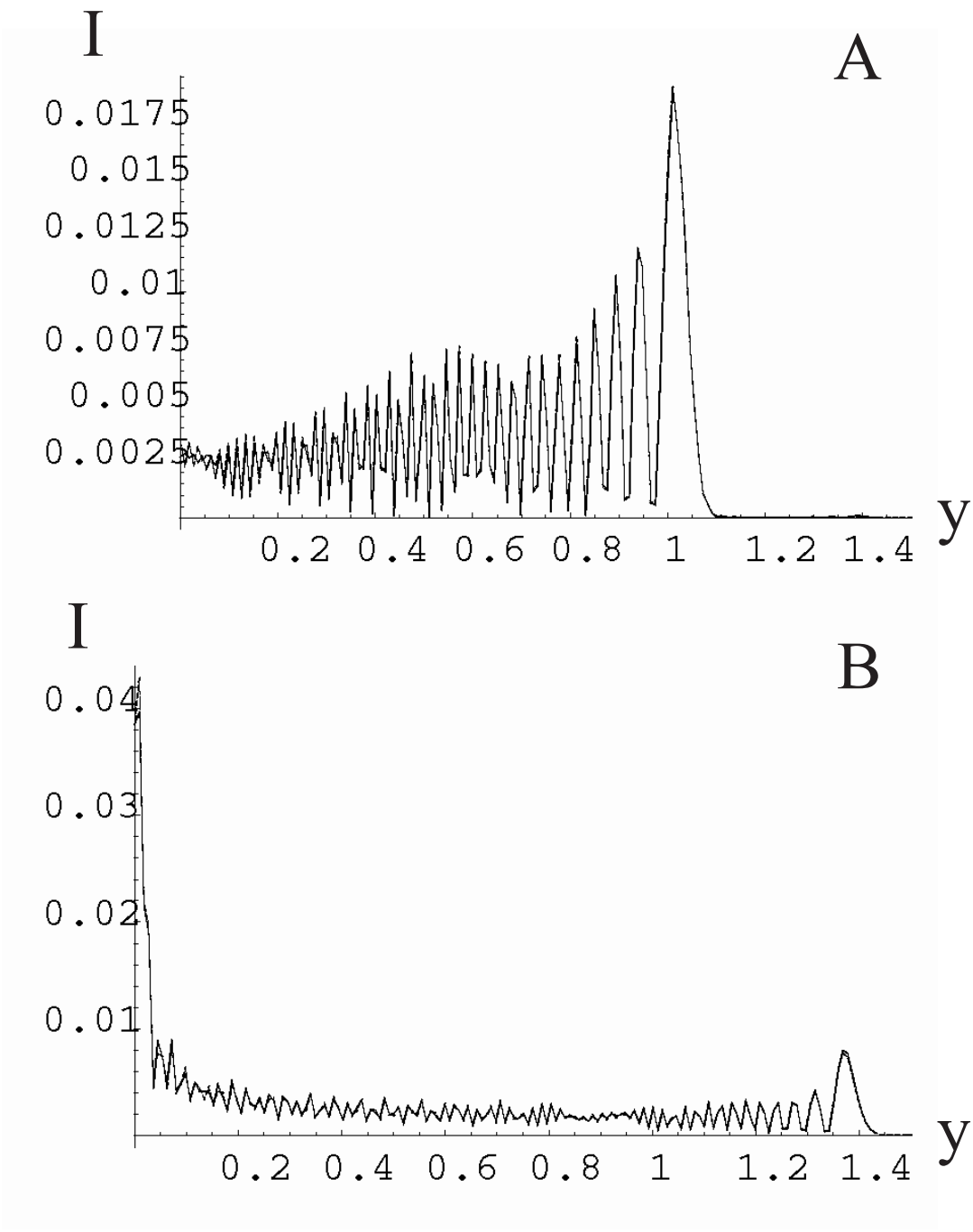

Figure 8.6: A comparison of the farfield wavefunction obtained by numerical diagonalisation (dashed), with the uniform calculation (solid), for $\Lambda = 12500$: A) $\zeta = \pi/2$, B) $\zeta = \pi$.

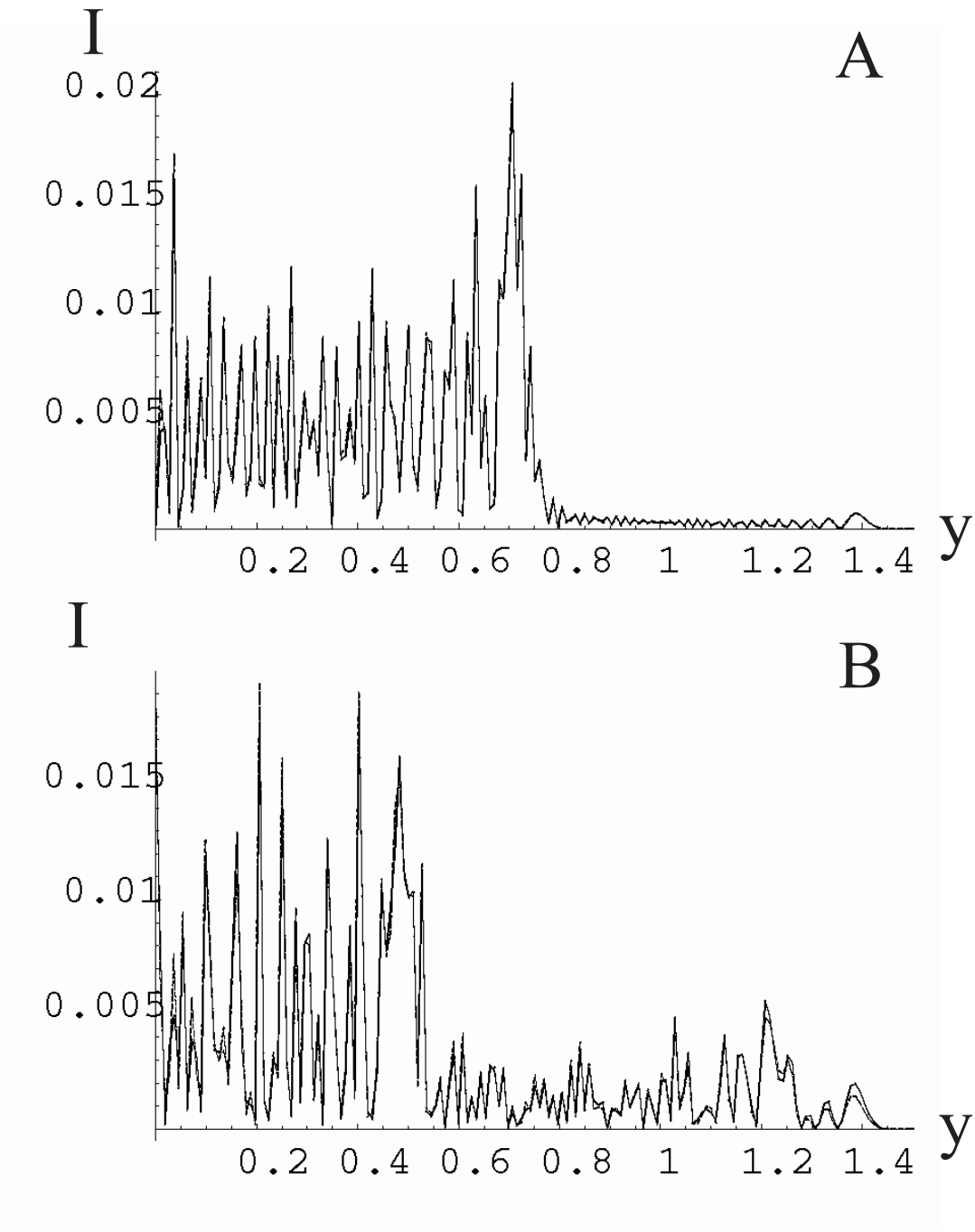

Figure 8.7: A comparison of the farfield wavefunction obtained by numerical diagonalisation (dashed), with the uniform calculation (solid), for $\Lambda = 12500$: A) $\zeta = 3\pi/2$, B) $\zeta = 7\pi/2$.

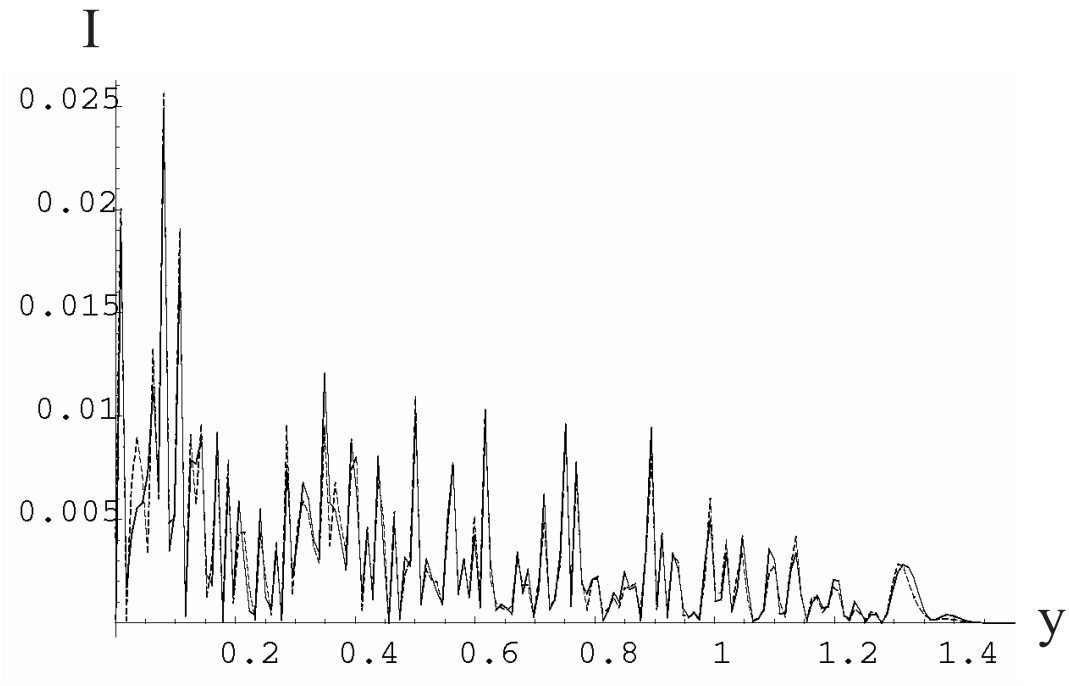

Figure 8.8: A comparison of the farfield wavefunction obtained by numerical diagonalisation (dashed), with the uniform calculation (solid), for $\Lambda = 12500$: $\zeta = 81\pi/2$.

space. These observations can be put on a firmer footing by the following argument, due to Berry. Consider just the transverse Hamiltonian (as pointed out previously, the longitudinal behaviour is constant)

$$H = \frac{P_x^2}{2m} - V_0 \cos^2 x_c = E_x. \tag{8.37}$$

Bound states have $E_x < 0$. The classical phase space distribution for a system with energy E_x is

$$W(x, P_x) = \mathcal{N}\ \delta(E_x - H) \tag{8.38}$$

where $\mathcal{N} = 1/(\int \delta(E_x - H)\ dx_c\ dp)$ is a normalising factor, and the Dirac delta function $\delta(E_x - H)$ specifies a contour in phase space such as those shown in Figure 3.2. The momentum intensity is given by 'projecting' down onto the x_c axis

$$I(P_x) = \int W(x_c, P_x)\ dx_c = \mathcal{N} \int_{-\pi/2}^{\pi/2} \delta\left(E_x - \frac{P_x^2}{2m} + V_0 \cos^2 x_c\right)\ dx_c. \tag{8.39}$$

A property of the delta function is that

$$\delta[g(u)] = \sum_i \frac{1}{|g'(u_i)|} \delta(u - u_i) \tag{8.40}$$

where the u_i are the zeros of $g(u)$, and so

$$\begin{aligned} I(P_x) &= \mathcal{N} \left(|2V_0 \sin x_c \cos x_c|_{\{\cos^2 x_c = P_x^2/(2mV_0) - E_x/V_0\}} \right)^{-1} \\ &= \mathcal{N} \left(|V_0 \sin 2x_c|_{\{\cos^2 x_c = P_x^2/(2mV_0) - E_x/V_0\}} \right)^{-1} \\ &= \mathcal{N} \left(\sqrt{1 - \left(\frac{P_x^2}{mv_0} - \frac{2E_x}{V_0} - 1 \right)^2} \right)^{-1} \\ &= \mathcal{N} \left(\sqrt{\left(\frac{P_x^2}{mV_0} - \frac{2E_x}{V_0} \right) \left(\frac{P_x^2}{mV_0} - \frac{2E_x}{V_0} - 2 \right)} \right)^{-1}. \end{aligned} \tag{8.41}$$

As before, this predicts turning-points at

$$P_{x\ \text{new}} = \pm\sqrt{2mE_x} \tag{8.42}$$

$$P_{x\ \text{old}} = \pm\sqrt{2m}\sqrt{E_x + V_0}. \tag{8.43}$$

The classical intensity expression (8.41) diverges as the square root of the distance from the new turning-points when the energy approaches that of the separatrix. This phase space argument is quite independent of the W.K.B./uniform methods but confirms their validity.

8.4.2 A transformation of the Raman-Nath equation

Of course the current uniform approximation is not set up to handle these new turning-points. Even if there were a uniform approximation for a double well (which there isn't), this would not

be a suitable approach since the phase momentum, p_2, has no idea anything untoward is going on, and still corresponds to a single well. So the usual strategy of a transitional approximation to patch up the wavefunction over the central region of the eigenvectors would be doomed to failure since the phase of the W.K.B. expression registers no such 'barrier-top' behaviour. For a uniform approximation to correctly handle the divergences, the momentum functions in the (modified) 'amplitude' and 'phase' need to be acting in concert. Fortunately there is a transformation which translates the stationary Raman-Nath equation into a form having this property whereby both the momentum functions have turning-points at $y = \sqrt{\beta - 1}$. Defining

$$B_n = (-1)^n C_n \tag{8.44}$$

the stationary R-N equation (7.15) becomes

$$(y^2 - \beta)C_n + \frac{1}{2}(C_{n+1} + C_{n-1}) = 0. \tag{8.45}$$

the difference being a sign change between the parts determining the interaction with neighbouring beams and the part determining the self evolution. Following the arguments of Section 7.3 one obtains an altered equation for the action

$$\frac{\partial S}{\partial y} = \sqrt{\Lambda}\ \arccos\left[\beta - y^2\right] + \mathrm{i}\frac{(\beta - y^2)y}{1 - (\beta - y^2)^2} \tag{8.46}$$

which leads to the W.K.B. formula

$$C(y) = \frac{\mathrm{e}^{\pm \mathrm{i}\sqrt{\Lambda}\ \int \arccos\left[\beta - y^2\right]\, dy}}{\left(1 - (y^2 - \beta)^2\right)^{1/4}} = \frac{\mathrm{e}^{\pm \mathrm{i}\sqrt{\Lambda}\ \bar{S}_0(y,\beta)}}{\left(1 - (y^2 - \beta)^2\right)^{1/4}}. \tag{8.47}$$

The amplitude is the same as before, giving the two sets of turning-points, but the phase momen-

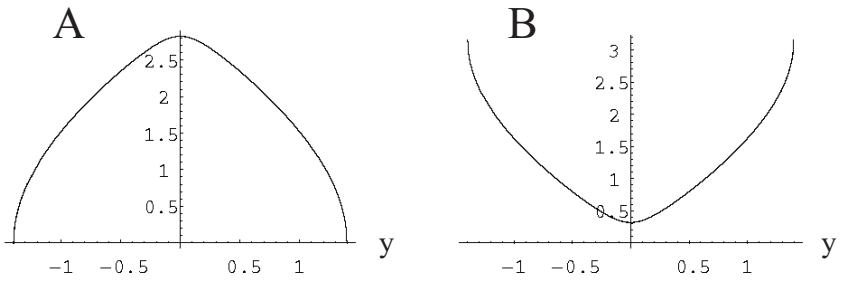

Figure 8.9: A: The original p_2, and B: transformed $\bar{p}_2$, phase momenta for $\beta = 0.95$.

tum

$$\bar{p}_2(y, \beta) = \arccos\left[\beta - y^2\right] \tag{8.48}$$

now has its turning-points at $y = \pm\sqrt{\beta - 1}$ as promised. The cost is the loss of the turning-points at $y = \pm\sqrt{\beta + 1}$. The effect of the transformation seems to be in swapping the rôles of inner and outer turning-points. Figure 8.9 shows that whereas p_2 has the momentum profile for a well, $\bar{p}_2$ has that of barrier which the particle has enough energy to surmount.

8.4.3 The parabolic barrier equation

A transitional approximation can now be legitimately applied to the inner turning-point. The comparison equation for a (smooth) potential barrier is

$$\frac{d^2\phi}{d\sigma^2} + \left(t + \sigma^2\right)\phi = 0. \tag{8.49}$$

Making the change of variables

$$\frac{t}{2} = -a \tag{8.50}$$

$$\sigma = \frac{g}{\sqrt{2}} \tag{8.51}$$

distinguishes the barrier equation as the second (lower signs) of the two forms of the parabolic cylinder equation (8.15). For $t > 0$, the Bloch states are more energetic than the central potential barrier, and classically one has transmission above the barrier. This is referred to as the *underdense* case. The second parabolic cylinder equation has two standard solutions, denoted by $W(a, \pm g)$ which do not have definite parity. A potential barrier, symmetric about $g = 0$, set in the centre of a symmetric well, has bound eigenstates which are either even or odd. The atomic wavefunction is the superposition of all the eigenfunctions, and the coefficents determining this superposition are the values of the eigenfunctions at $y = 0$, see Equation (4.80). Thus only the even eigenfunctions contribute to the total wavefunction. An even solution can be constructed from the standard solutions by writing

$$\psi_{\text{even}} = W(a, +g) + W(a, -g). \tag{8.52}$$

Of the more familiar functions in terms of which the standard solutions can be expressed, the confluent hypergeometric functions, which are rapidly converging power series when a is small (as here) are the most convenient. The same conclusion can also be achieved through the following transformations upon the barrier equation (8.49),

$$t = \mathrm{i}\bar{t} \tag{8.53}$$

$$\sigma = \frac{\bar{\sigma}}{\sqrt{2}}\mathrm{e}^{\mathrm{i}\pi/4} \tag{8.54}$$

and these lead back to the equation

$$\frac{d^2\phi}{d\bar{\sigma}^2} - \left(\frac{\bar{t}}{2} + \frac{\bar{\sigma}^2}{4}\right)\phi = 0 \tag{8.55}$$

which is the same as the first (upper sign) parabolic cylinder equation (8.15) when the following identifications are made

$$g = \bar{\sigma} \tag{8.56}$$

$$a = \frac{\bar{t}}{2}. \tag{8.57}$$

The solutions for the barrier top are not the Whittaker functions since a parabolic barrier does not give an exponentially decaying wavefunction for large g. Instead, for a barrier, the basic even and odd power series solutions, which will be referred to as $\Theta_1(a,g)$ and $\Theta_2(a,g)$ respectively, are the correct choice. The power series solutions are expressed in terms of the confluent hypergeometric functions (in agreement with the comments made above concerning the $W(a,g)$ solutions)

$$\Theta_1(a,g) = \mathrm{e}^{-g^2/4} \; {}_1F_1\left(\frac{a}{2}+\frac{1}{4};\frac{1}{2};\frac{g^2}{2}\right) \tag{8.58}$$

$$\Theta_2(a,g) = g\mathrm{e}^{-g^2/4} \; {}_1F_1\left(\frac{a}{2}+\frac{3}{4};\frac{3}{2};\frac{g^2}{2}\right). \tag{8.59}$$

And so an even eigenfunction requires the even power series

$$\Theta_1\left(\frac{\bar{t}}{2},\bar{\sigma}\right) = \Theta_1\left(-\mathrm{i}\frac{t}{2},\sqrt{2}\sigma\mathrm{e}^{-\mathrm{i}\pi/4}\right). \tag{8.60}$$

8.4.4 The action for an underdense barrier

The underdense barrier does not induce any real turning-points (though of course the proximity of the turning-points to the real axis gives the deviation of the amplitude from the true value) so the natural choice of reference point from which to integrate the phase is $y=\sigma=0$. And so, from an almost identical integration to that presented in Appendix D, one finds

$$\begin{aligned}\bar{S}_0(0,y,\beta) &= \int_0^y \arccos\left[\beta - y'^2\right]\, dy' \\ &= y\arccos\left[\beta-y^2\right] + 2\mathrm{i}\sqrt{1-\beta}\,\mathrm{E}\left(\frac{1}{2}\arccos\left[\beta-y^2\right]\middle|\,\frac{2}{1-\beta}\right) \\ &\quad - \mathrm{E}\left(\frac{1}{2}\arccos\left[\beta\right]\middle|\,\frac{2}{1-\beta}\right).\end{aligned} \tag{8.61}$$

Although it appears that this action contains an imaginary piece this is actually not the case. Properly, the elliptic functions should be transformed so that their parameters lie between zero and one (the parameter used above tends to infinity as β tends to one). When this is done the action $\bar{S}_0$ is explicitly real. However, the transformations produce more complicated expressions so will not be applied here.

To find the value of t, which was previously given by the integral across the well, one must now integrate up the imaginary axis between the points

$$y_{\pm} = \pm\sqrt{\beta - 1} = \pm \mathrm{i}\sqrt{1-\beta}. \tag{8.62}$$

The equivalent points for the underdense barrier comparison equation (8.49) are

$$\sigma = \pm \mathrm{i}\sqrt{t}. \tag{8.63}$$

Letting $y = \mathrm{i}v$ and $\sigma = \mathrm{i}\varsigma$, t is implicitly given by

$$2\mathrm{i}\sqrt{\Lambda}\int_0^{\sqrt{1-\beta}} \arccos\left[\beta + v^2\right]\, dv = 2\mathrm{i}\int_0^{\sqrt{t}} \sqrt{t^2 - \varsigma^2}\, d\varsigma \tag{8.64}$$

which, in a similar to fashion to before, results in the condition

$$4\sqrt{\Lambda}\sqrt{1-\beta}\mathrm{E}\left(\frac{1}{2}\arccos\left[\beta\right]\middle|\, \frac{2}{1-\beta}\right) = \frac{t\pi}{2}. \tag{8.65}$$

The mapping function between σ and y implicitly giving $\sigma(y)$ is

$$\sqrt{\Lambda}\bar{S}_0(0, y, \beta) = \int_0^{\sigma} \sqrt{t + \sigma^2}\, d\sigma = \frac{t}{2}\left(\operatorname{arccosh}\left[\sqrt{1 + \frac{\sigma^2}{t}}\right] + \frac{\sigma}{\sqrt{t}}\sqrt{1 + \frac{\sigma^2}{t}}\right) \tag{8.66}$$

which, together with the value of t, gives the transitional approximation to the wavefunction

$$\begin{aligned} B(y) = (-1)^n C(y) &= (-1)^n \psi_{\text{transitional}} \\ &\propto (-1)^n \left(\frac{t+\sigma^2}{1-(y^2-\beta)^2}\right)^{1/4} \mathrm{e}^{\mathrm{i}\sigma^2/2} \quad {}_1F_1\left(-\mathrm{i}\frac{t}{4} + \frac{1}{4}; \frac{1}{2}; -\mathrm{i}\sigma^2\right). \end{aligned} \tag{8.67}$$

This turns out to be a real function for real t and σ (as it should be), which is valid from $y = 0$ and almost all the way to the outer turning-point, breaking down close to it because it is only set up to deal with the inner turning-point. The constant of proportionality can be obtained by matching the asymptotic behaviour of this function to the W.K.B. solution somewhere between the two transition points.

8.4.5 The asymptotics of the barrier transitional approximation

The confluent hypergeometric function has well known asymptotics. When $|\sigma|$ is large

$$\begin{aligned} &{}_1F_1\left(-\mathrm{i}\frac{t}{4} + \frac{1}{4}; \frac{1}{2}; -\mathrm{i}\sigma^2\right) \\ &\quad = \frac{\Gamma\left(\frac{1}{2}\right)}{\Gamma\left(\frac{1}{4} + \mathrm{i}\frac{t}{4}\right)} \mathrm{e}^{-\mathrm{i}\pi(-\mathrm{i}t+1)/4} \left(-\mathrm{i}\sigma^2\right)^{(\mathrm{i}t-1)/4} \left(1 + \frac{(\mathrm{i}t^2 - 4t - 3\mathrm{i})}{16\sigma^2} + \mathcal{O}\left(\frac{1}{\sigma^4}\right)\right) \\ &\qquad + \frac{\Gamma\left(\frac{1}{2}\right)}{\Gamma\left(\frac{1}{4} - \mathrm{i}\frac{t}{4}\right)} \mathrm{e}^{-\mathrm{i}\sigma^2} \left(-\mathrm{i}\sigma^2\right)^{-(\mathrm{i}t+1)/4} \left(1 + \frac{(-\mathrm{i}t^2 - 4t + 3\mathrm{i})}{16\sigma^2} + \mathcal{O}\left(\frac{1}{\sigma^4}\right)\right) \end{aligned} \tag{8.68}$$

where this time Γ refers to *the* Gamma function. So

$$\begin{aligned}\Theta_1\left(-\mathrm{i}\frac{t}{2},\sqrt{2}\sigma\mathrm{e}^{-\mathrm{i}\pi/4}\right) &= \mathrm{e}^{\mathrm{i}\sigma^2/2}\quad {}_1F_1\left(-\mathrm{i}\frac{t}{4}+\frac{1}{4};\frac{1}{2};-\mathrm{i}\sigma^2\right)\\ &\sim \Gamma\left(\frac{1}{2}\right)\left(-\mathrm{i}\sigma^2\right)^{-1/4}\left(\mathrm{e}^{-\pi(t+\mathrm{i})/4}\mathrm{e}^{\mathrm{i}\sigma^2/2}\frac{\left(-\mathrm{i}\sigma^2\right)^{\mathrm{i}t/4}}{\Gamma\left(\frac{1}{4}+\mathrm{i}\frac{t}{4}\right)}\mathrm{e}^{\ln\left[1+(\mathrm{i}t^2-4t-3\mathrm{i})/(16\sigma^2)\right]}\right.\\ &\qquad\left.+\,\mathrm{e}^{-\mathrm{i}\sigma^2/2}\frac{\left(-\mathrm{i}\sigma^2\right)^{-\mathrm{i}t/4}}{\Gamma\left(\frac{1}{4}-\mathrm{i}\frac{t}{4}\right)}\mathrm{e}^{\ln\left[1-(\mathrm{i}t^2+4t-3\mathrm{i})/(16\sigma^2)\right]}\right)\end{aligned} \tag{8.69}$$

which conveniently reduces to

$$\begin{aligned}&\Theta_1\left(-\mathrm{i}\frac{t}{2},\sqrt{2}\sigma\mathrm{e}^{-\mathrm{i}\pi/4}\right)\\ &\quad\sim 2\frac{\Gamma\left(\frac{1}{2}\right)}{\left|\Gamma\left(\frac{1}{4}+\mathrm{i}\frac{t}{4}\right)\right|}\sigma^{-1/2}\mathrm{e}^{-\pi t/8-t/(4\sigma^2)}\cos\left(\frac{t}{2}\ln\sigma+\frac{\sigma^2}{2}-\mathrm{Arg}\left[\Gamma\left(\frac{1}{4}+\mathrm{i}\frac{t}{4}\right)\right]-\frac{\pi}{8}+\mathcal{O}\left(\frac{1}{\sigma^4}\right)\right).\end{aligned} \tag{8.70}$$

When Λ is large enough σ quickly takes on large values for even modest sizes of y, and so the confluent hypergeometric function attains its asymptotic form in the region between the inner and outer turning-points. It may then be compared to the W.K.B. solution (8.47) for the transformed R-N equation. The left and right travelling W.K.B. waves (8.47) are combined to give a real solution

$$B_{\mathrm{barrier}}(y)=\frac{\mathcal{N}}{\left(1-(y^2-\beta)^2\right)^{1/4}}\cos\left(\sqrt{\Lambda}\bar{S}_0(0,y,\beta)+\mu(\beta)+\sqrt{\Lambda}\pi y\right) \tag{8.71}$$

where the $(-1)^n$ factor has been incorporated into the phase of the cosine as $\sqrt{\Lambda}\pi y$. To enable a direct comparison, the phase of the cosine of Equation (8.70) should also be augmented by the same quantity. The real phase angle $\mu(\beta)$ for this parabolic barrier approximation, which for the simple first order turning-point was equal to $\pi/4$, will this time be determined by consistency with the asymptotic solution (8.70). In order for a comparison to be made, the action $\bar{S}_0(0,y,\beta)$ appearing in the W.K.B. solution must be written in terms of (σ,t), which is accomplished through Equation (8.66). Expanding the r.h.s. of (8.66) for $\sigma\gg t$, one has

$$\frac{t}{2}\left(\mathrm{arccosh}\left[\sqrt{1+\frac{\sigma^2}{t}}\right]+\frac{\sigma}{\sqrt{t}}\sqrt{1+\frac{\sigma^2}{t}}\right)\sim\frac{t}{2}\ln\sigma-\frac{t}{4}\ln t+\frac{t}{2}\ln 2+\frac{\sigma^2}{2}+\frac{t}{4}+\mathcal{O}\left(\frac{t^2}{\sigma^2}\right) \tag{8.72}$$

implying that

$$\mu=\frac{t}{4}\ln t-\frac{t}{2}\ln 2-\frac{t}{4}-\mathrm{Arg}\left[\Gamma\left(\frac{1}{4}+\mathrm{i}\frac{t}{4}\right)\right]-\frac{\pi}{8}. \tag{8.73}$$

Figure 8.10 demonstrates that this expression for μ is correct by comparing the W.K.B. solution (8.71) containing it, with the fully numerical calculation. The value of Λ is reasonably small so the W.K.B. solution diverges only very slightly from the correct value.

The exact solution to the parabolic cylinder equation has thus contributed to the evaluation of the phase of the W.K.B. solution. On the other hand, the W.K.B. solution indicates the necessary

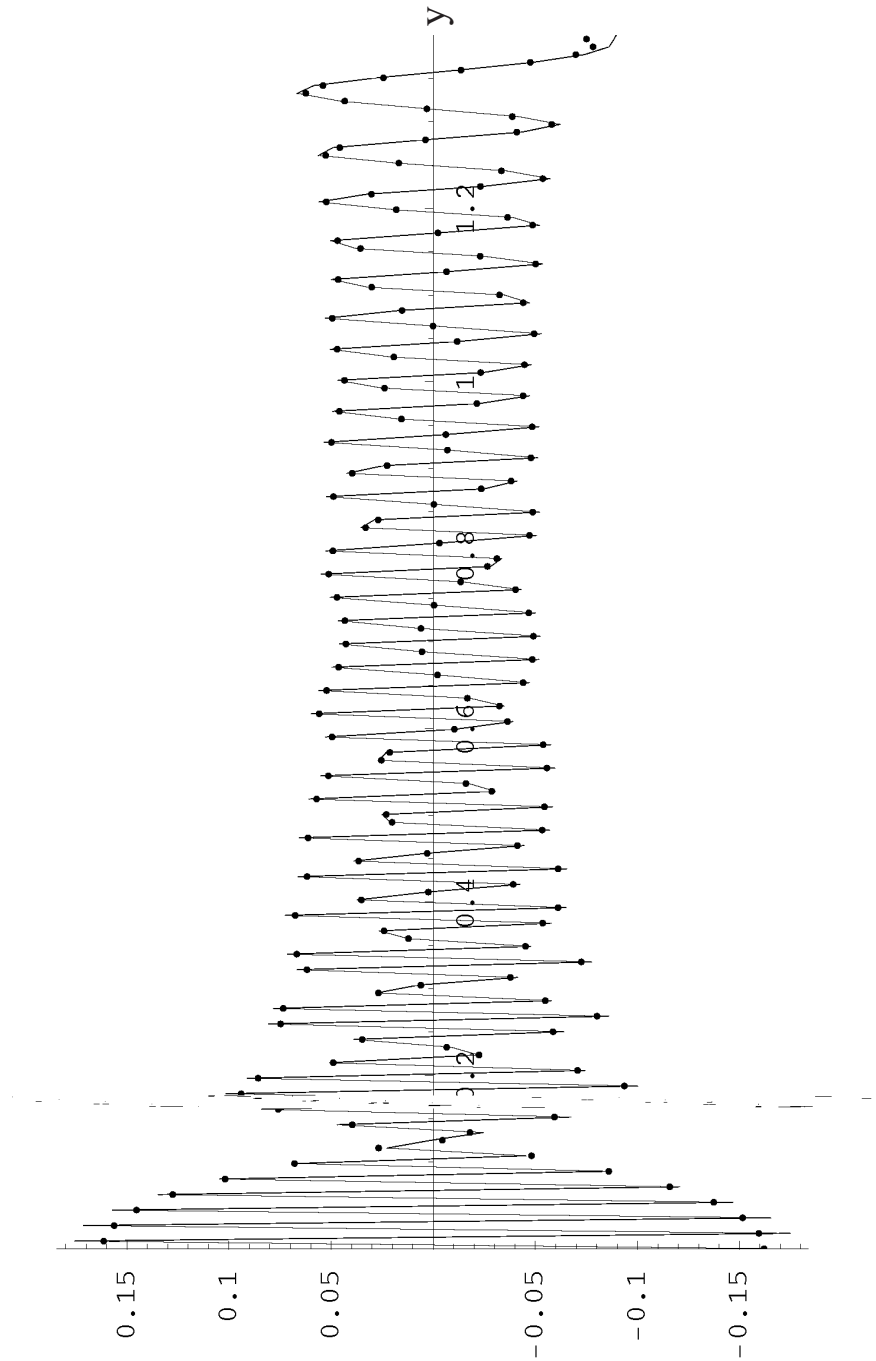

Figure 8.10: The W.K.B. approximation using the underdense parabolic barrier action, see Equation (8.71), and the fully numerical solution. In particular, this tests the derived phase angle μ as given by (8.73). The dots are the numerically calculated points, and the continuous line joins the W.K.B. amplitudes. The value of Λ is 12500 and $\beta = 0.9961$.

modifications needed for the amplitude of the parabolic cylinder equation so that it becomes the correct transitional solution to the particular problem being dealt with. Equating the ampliutdes of Equations (8.70) and (8.71), one finds Equation (8.67) can now be updated to read

$$B_{\text{barrier}}(y) = (-1)^n \mathcal{N} \frac{\left|\Gamma\left(\frac{1}{4}+\mathrm{i}\frac{t}{4}\right)\right| \mathrm{e}^{\pi t/8}}{2\Gamma\left(\frac{1}{2}\right)} \left(\frac{t+\sigma^2}{1-(y^2-\beta)^2}\right)^{1/4} \mathrm{e}^{\mathrm{i}\sigma^2/2} \quad {}_1F_1\left(-\mathrm{i}\frac{t}{4}+\frac{1}{4};\frac{1}{2};-\mathrm{i}\sigma^2\right). \tag{8.74}$$

The parabolic transitional approximation is compared to the fully numerical result in Figure 8.11 A). At first sight the match does not seem too good. The reason is that the normalisation procedure of Section 7.3.3 uses the W.K.B. amplitude factor, which diverges at the turning-points. When there are only the outer-turning-points this method seems to work (see Figures 8.1-8.4) since the divergences are narrow enough to not produce too significant a contribution. However, the appearance of the inner-turning-point divergences close to the separatrix energy now means the normalisation factor is significantly over estimating the magnitude of the wavefunction, and thus reduces the magnitude too much[4] as shown. With relatively little effort one can always resort to numerically normalising the uniformly calculated eigenvectors however, by summing the discrete amplitudes, and when this is carried out the match, shown in Figure 8.11 B), is exceedingly good. This indeed illustrates that it is only the normalising factor which is at fault. Figure 8.11 B) further illustrates that the barrier transitional approximation, Equation (8.74), is correct nearly throughout the entire momentum range—only breaking down close to the *outer* turning-point.

8.4.6 Calculation of the eigenvalues close to the separatrix

There is a slight complication to the calculation of the allowed values of β close to the separatrix which needs to be highlighted. When comparing the values of β obtained by the numerical diagonalisation technique with those obtained via Equation (7.45), it was noticed that as β grew very close to one, the two differed. Apparently the transformation of the phase momentum is more than a device. Somehow the derivation of the basic W.K.B. solution of Chapter 7 has failed to capture the full behaviour of the p_2 function—perhaps it should now afterall contain two turning-points, not one, and so match the structure of the amplitude p_1 term? From the point of view of the eigenvectors this can be overcome by replacing the previous single uniform approximation with two transitional approximations when β approaches one; the parabolic transitional approximation

[4]It is interesting to note that the direct asymptotics for standand solutions $W(a,\pm g)$, as given in *Abramowitz* and *Stegun*, when combined to give ψ_{even} give a *phase* which does not match the confluent hypergeometric asymptotic result (and hence the numerical result), but *does* give an *amplitude* which matches the numerical value to within 1 % for $\Lambda = 12500$. This improved amplitude is achieved by leaving out the Gamma functions and $\exp(\pi t/8)$ terms altogether.

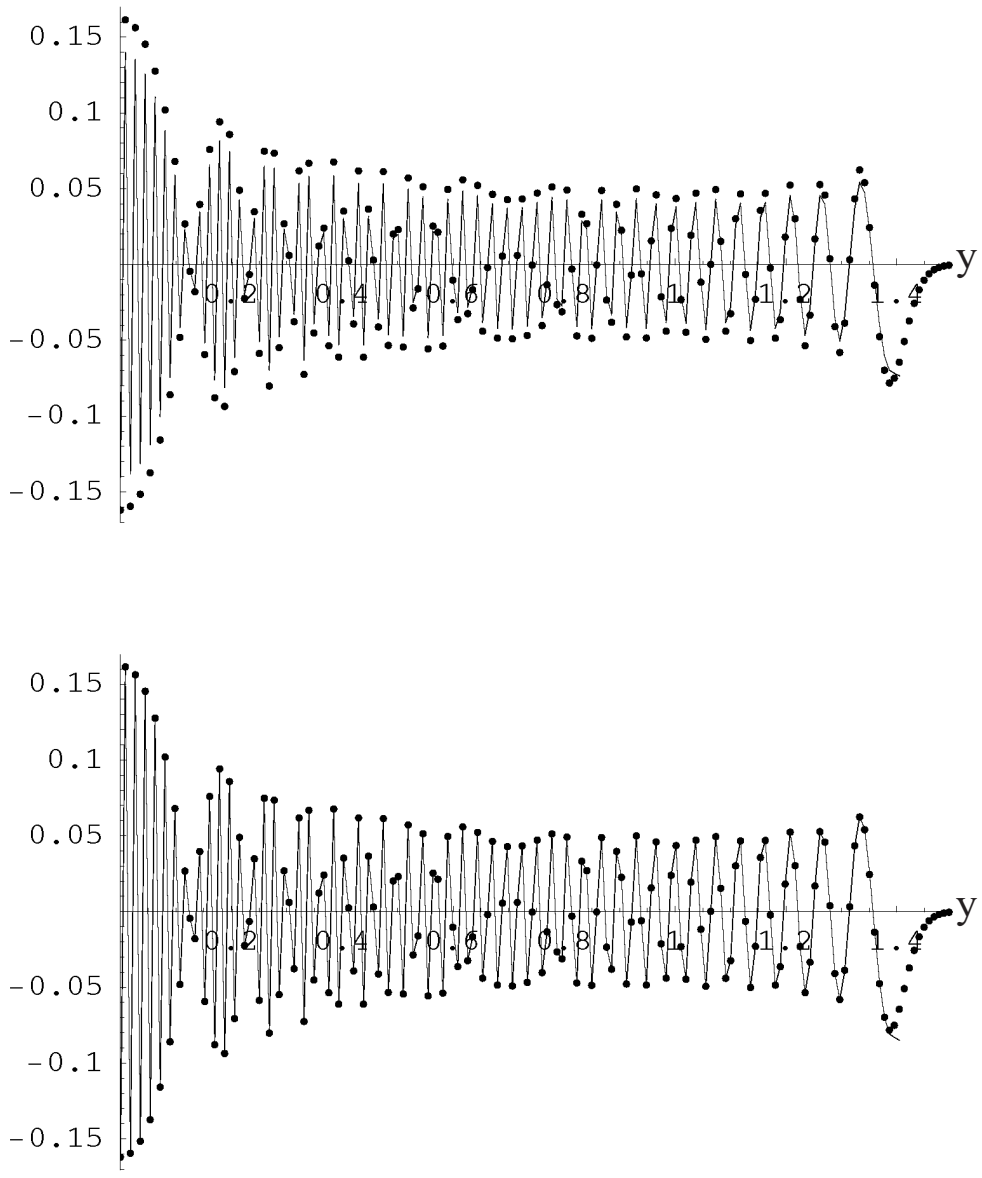

Figure 8.11: The parabolic barrier transitional approximation: A) as given by Equation (8.74); B) the renormalised version. The dots are the fully numerical solution. The value of Λ is 12500 and $\beta = 0.9961$.

to cover the inner turning-point, and an Airy function approximation for the outer turning-point (since this remains a simple first order turning-point). However, to calculate the allowed values of the action which corresponds to the bound states, one needs some expression which is valid throughout the entire region which joins the two turning-points.

The action between two turning-points of different order

The general procedure for finding the action across a classically allowed region which separates two arbitrary types of turning-point does indeed employ two transitional approximations which are each valid at one end of the region, but these must be correctly joined. The quantised values of S, and hence β, are those which correctly match the two somewhere in the region of mutual validity.

The matching is most easily accomplished using the asymptotic forms for the two transitional approximations—which are of course their W.K.B. approximations. In the region between the two turning-points one thus has

$$\begin{aligned} &\frac{1}{\left(1-(y^2-\beta)^2\right)^{1/4}}\cos\left(\sqrt{\Lambda}\bar{S}_0(0,y,\beta)+\mu(\beta)+\sqrt{\Lambda}\pi y\right) \\ &\qquad = \frac{1}{\left(1-(y^2-\beta)^2\right)^{1/4}}\cos\left(\sqrt{\Lambda}S_0(\sqrt{1+\beta},y,\beta)+\frac{\pi}{4}\right) \end{aligned} \tag{8.75}$$

which implies that

$$\sqrt{\Lambda}\bar{S}_0(0,y,\beta)+\mu(\beta)+\sqrt{\Lambda}\pi y = \sqrt{\Lambda}S_0(\sqrt{1+\beta},y,\beta)+\frac{\pi}{4} \tag{8.76}$$

modulo 2π.

A modified Bohr-Sommerfeld rule

The method described above works in conventional situations with W.K.B. expressions developed from (continuous) differential equations. Once again however, the approach has to be modified for the R-N equation—whilst successful for the single well, as soon as the inner turning-points begin to approach the real axis even the matching of the two transitional approximations runs into trouble. The reason is that the continuous descriptions embodied above by Equation (8.75) do not match at all. Only when they are evaluated at the discrete points corresponding to diffracted beams do they match. The transformation (8.44) has produced two different equations whose continuised W.K.B. expressions only respect their common origin at the discrete level. It is then a surprise to find that at the correct (characteristic) values of β the discretely evaluated expressions on either side of Equation (8.75) are in perfect agreement for all y. Both are identical in each

other's supposedly exclusive region of validity. This is rather curious, but the characteristic values of β, which one is able to predict by correctly matching the discrete points of the two W.K.B. expressions, demonstrate that it is correct.

Due to the simultaneous validity for all y, the most sensible point to choose to match the two solutions is $y = 0$. The correct matching condition for even eigenstates becomes one of

$$\cos\left(\mu(\beta)\right) - \cos\left(\sqrt{\Lambda}S_0(y_+, 0, \beta) + \pi/4\right) = 0 \tag{8.77}$$

$$\cos\left(\mu(\beta)\right) - \cos\left(\sqrt{\Lambda}S_0(y_+, 0, \beta) + 5\pi/4\right) = 0 \tag{8.78}$$

the choice depending on whether the terminating Airy function has its peak above or below the y axis. In fact, successive even eigenstates alternate between the two conditions. When using

Λ	j	fully numerical	single well calc.	modified calc.
12500	200	0.996129	0.996824	0.996131
	198	0.987197	0.987337	0.987199
	196	0.976711	0.976759	0.976713
	194	0.965430	0.965461	0.965432
	192	0.953575	0.953599	0.953578
	190	0.941244	0.941264	0.941247
	188	0.928498	0.928515	0.928499
	186	0.915379	0.915394	0.915381
250000	900	0.999954	–	0.999954

Table 8.1: The bound eigenvalues near the separatrix: comparison of numerical result with the standard Bohr-Sommerfeld condition for a well (7.45), and the modified conditions (8.77)–(8.78).

(8.77) and (8.78), it is necessary to express μ, which is in the first instance a function of t, see Equation (8.73), as a function of β through the definition of t (Equation (8.65)). A further subtlety concerning the use of (8.77) and (8.78) is that close to each of the characteristic values there is another zero which does not correspond to an eigenvalue. The correct zeros are those through which the l.h.s. of Equations (8.77) and (8.78) have negative gradients. Table 8.1 compares the values of the top eight bound eigenvalues for $\Lambda = 12500$ as calculated by the different methods which have been outlined so far. Clearly the modified method is superior to the regular Bohr-Sommerfeld scheme when close to the separatrix. This is further emphasised by the last entry on the table which is the last bound eigenvalue for $\Lambda = 250000$. The Bohr-Sommerfeld method predicts only 898 even bound states whereas the modified method accurately finds the value of the 900^{th}.

8.4.7 The Airy transitional approximation

As has already been pointed out, to obtain the complete wavefunction correct for all y one must join the parabolic barrier approximation (8.74) to another transitional approximation which covers the outer, first order, turning-point. It was Airy [3] who in 1838 famously first considered the form of a wavefield near a simple turning-point, but in the context of comparison equations the following formulation stems from Langer in 1937. The comparison equation has already been given in Equation (8.11), and choosing the reference point as $y = y_+ = \sqrt{1+\beta}$, the mapping function $\sigma(y)$ is given by

$$\sqrt{\Lambda} S_0(y_+, y, \beta) = \begin{cases} -\frac{2}{3}\left|\sigma\right|^{3/2} & \text{if } y \leq \sqrt{1+\beta}\ ; \qquad (\sigma < 0) \\ \\ \frac{2}{3}\mathrm{i}\sigma^{3/2} & \text{if } y > \sqrt{1+\beta}\ ; \qquad (\sigma > 0) \end{cases} \tag{8.79}$$

since the expression given for S_0, Equation (7.33), is positive imaginary when $y > y_+$, and negative real when $y < y_+$.

The well known asymptotics of $\mathrm{Ai}(\sigma)$ when $\sigma \gg 0$ are

$$\mathrm{Ai}(\sigma) \sim \frac{1}{2\pi}\, \sigma^{-1/4}\, \mathrm{e}^{-\frac{2}{3}\sigma^{3/2}} \tag{8.80}$$

and so the Langer transitional approximation becomes

$$\psi_{\text{transitional}} = B_{\text{Langer}}(y) = 2\pi\mathcal{N} \left(\frac{\sigma(y)}{1-(y^2-\beta)^2} \right)^{1/4} \mathrm{Ai}\left(\sigma(y)\right). \tag{8.81}$$

8.5 The free eigenstates

As emphasised previously, 'free' is a description which refers to the (actual) configuration space situation of states having transverse energies greater than V_0. In (actual) momentum space there are no free states, the classical bounding of the maximum being set by the initial transverse momentum plus whatever the atoms can extract from the potential—which depends on the (actual) configuration space point, but has a maximum of $\sqrt{2mV_0}$. This is a long-winded way of saying that even for $\beta > 1$, one expects caustics in (actual) momentum space and this is consistent with the structure built up so far. It also demonstrates why the free eigenstates are quantised and not continuous in energy. Somewhat perversely, the states which are free in (actual) configuration space, sit in a double well in (actual) momentum space, and so the central barrier is now *overdense*—meaning that classical transmission is forbidden. For perpendicular incidence, the free 'states' are classically inaccessible, so their contribution to the eigensum of states forming the total wavefunction is exponentially small.

For states with $\beta \gg 1$, the problem is best solved using the W.K.B. technique in (actual) configuration space, since there are no turning-points to contend with. Constraining the discussion to perpendicular incidence means however that only those states with β a little greater than one need be calculated, so the 'close to the separatrix' treatment of the preceeding sections must be generalised to encompass $\beta > 1$. Since the essentials of the uniform method have already been conveyed in the preceeding sections, the following treatment is intended to be more of a 'recipe' than a detailed account.

The overdense barrier equation will be taken as

$$\frac{d^2\phi}{d\sigma^2} + \left(\sigma^2 - t\right)\phi = 0 \tag{8.82}$$

with t a positive quantity. The connection with the parabolic cylinder equation (8.15) is made with the aid of the transformations

$$a = -\mathrm{i}\frac{t}{2} \tag{8.83}$$

$$g = \sqrt{2}\sigma \mathrm{e}^{\mathrm{i}\pi/4}. \tag{8.84}$$

To remove any ambiguity regarding the phase momentum function p_2 for the barrier, it will be written as

$$\bar{p}_2 = \arccos\left[\beta - y^2\right] = \begin{cases} \mathrm{i}\ \mathrm{arccosh}\left[\beta - y^2\right] & \text{if } 0 \le y \le \sqrt{\beta - 1} \\ \\ \pi - \arccos\left[y^2 - \beta\right] & \text{if } \sqrt{\beta - 1} \le y < \sqrt{1 + \beta} \end{cases} \tag{8.85}$$

where the central barrier lies between $\pm\sqrt{\beta - 1}$. The actions generated from these momenta, using $y = \sqrt{\beta - 1}$ as the reference point, are

$$\bar{S}_0^{y<\sqrt{\beta-1}}(\sqrt{\beta-1}, y, \beta) = \mathrm{i}\left(y\ \mathrm{arccosh}\left[\beta - y^2\right] + 2\mathrm{i}\sqrt{\beta - 1}\mathrm{E}\left(\frac{1}{2}\arccos\left[\beta - y^2\right]\middle|\ \frac{2}{1-\beta}\right)\right) \tag{8.86}$$

and

$$\begin{aligned} \bar{S}_0^{y>\sqrt{\beta-1}}(\sqrt{\beta-1}, y, \beta) = \pi y + 2\sqrt{\beta+1}\mathrm{E}\left(\frac{1}{2}\arccos\left[y^2 - \beta\right]\middle|\ \frac{2}{1+\beta}\right) \\ - 2\sqrt{\beta+1}\mathrm{E}\left(\frac{\pi}{2}\middle|\ \frac{2}{1+\beta}\right) - y\ \arccos\left[y^2 - \beta\right]. \end{aligned} \tag{8.87}$$

As before, the comparison equation (8.82) gives rise to the mapping function by setting

$$\bar{S}_0^{y<\sqrt{\beta-1}} = \int_{\sqrt{t}}^{\sigma} \sqrt{\sigma^2 - t}\ d\sigma = \mathrm{i}\frac{t}{2}\left(\arcsin\left[\frac{\sigma}{\sqrt{t}}\right] + \frac{\sigma}{\sqrt{t}}\sqrt{1 - \frac{\sigma^2}{t}} - \frac{\pi}{2}\right) \tag{8.88}$$

and

$$\bar{S}_0^{y>\sqrt{\beta-1}} = \int_{\sqrt{t}}^{\sigma} \sqrt{\sigma^2 - t}\ d\sigma = \frac{t}{2}\left(\frac{\sigma^2}{t}\sqrt{1 - \frac{t}{\sigma^2}} - \mathrm{arccosh}\left[\frac{\sigma}{\sqrt{t}}\right]\right). \tag{8.89}$$

In particular, the 'barrier integral' which fixes the value of t once β is known, can this time be conducted along the real axis, and gives, using (8.86) and (8.88),

$$2\mathrm{i}\sqrt{\Lambda}\sqrt{\beta-1}\mathrm{E}\left(\frac{1}{2}\arccos\left[\beta\right]\middle|\frac{2}{1-\beta}\right)=-\frac{t\pi}{4}. \tag{8.90}$$

The correct solution to the barrier equation is still the even power series

$$\Theta_1(a,g)=\Theta_1\left(-\mathrm{i}\frac{t}{2},\sqrt{2}\sigma\mathrm{e}^{\mathrm{i}\pi/4}\right) \tag{8.91}$$

and so the transitional approximation for the overdense barrier becomes

$$\begin{aligned}B(y)=(-1)^nC(y)&=(-1)^n\psi_{\text{transitional}}\\ &\propto\quad(-1)^n\left(\frac{\sigma^2-t}{1-(y^2-\beta)^2}\right)^{1/4}\mathrm{e}^{-\mathrm{i}\sigma^2/2}\quad{}_1F_1\left(-\mathrm{i}\frac{t}{4}+\frac{1}{4};\frac{1}{2};\mathrm{i}\sigma^2\right).\end{aligned} \tag{8.92}$$

8.5.1 Asymptotic matching to the overdense W.K.B. expression

The transitional wavefunction differs by a few sign changes from the underdense case, and for large σ these produce the modified oscillatory behaviour:

$$\begin{aligned}&\Theta_1\left(-\mathrm{i}\frac{t}{2},\sqrt{2}\sigma\mathrm{e}^{\mathrm{i}\pi/4}\right)\\ &\quad\sim 2\frac{\Gamma\left(\frac{1}{2}\right)}{\left|\Gamma\left(\frac{1}{4}+\mathrm{i}\frac{t}{4}\right)\right|}\sigma^{-1/2}\mathrm{e}^{\pi t/8-t/(4\sigma^2)}\cos\left(\frac{t}{2}\ln\sigma-\frac{\sigma^2}{2}-\mathrm{Arg}\left[\Gamma\left(\frac{1}{4}+\mathrm{i}\frac{t}{4}\right)\right]+\frac{\pi}{8}+\mathcal{O}\left(\frac{1}{\sigma^4}\right)\right).\end{aligned} \tag{8.93}$$

Expanding the r.h.s. of Equation (8.89) for $\sigma\gg t$ gives

$$\frac{t}{2}\left(\frac{\sigma^2}{t}\sqrt{1-\frac{t}{\sigma^2}}-\mathrm{arccosh}\left[\frac{\sigma}{\sqrt{t}}\right]\right)\sim-\frac{t}{2}\ln\sigma+\frac{t}{4}\ln t-\frac{t}{2}\ln 2+\frac{\sigma^2}{2}-\frac{t}{4} \tag{8.94}$$

from which one deduces the unknown phase angle μ, appearing in the W.K.B. approximation for the overdense barrier (see Equation (8.71)), to be

$$\mu=-\frac{t}{4}\ln t+\frac{t}{2}\ln 2+\frac{t}{4}+\mathrm{Arg}\left[\Gamma\left(\frac{1}{4}+\mathrm{i}\frac{t}{4}\right)\right]-\frac{\pi}{8}. \tag{8.95}$$

8.5.2 The overdense eigenvalues

Once again μ can be successfully employed in the accurate determination of the eigenvalues β. Following the empirical observations from the underdense case, the W.K.B. expression emanating from the outer turning-point and that from the inner turning-point are matched at a point y corresponding to one of the beams. This time the choice of $y=0$ is not available since only the phase for the W.K.B. approximation outside the barrier is known. The next most obvious choice is either the inner or outer turning-point since there the phase of the W.K.B. expressions

are simplest, but in general these classically determined points will not fall on a diffracted beam. Selecting a random beam, $y = m/\sqrt{\Lambda}$, with m an integer, giving of value y lying between the two turning-points, will suffice. The condition giving the permitted values of β for even eigenstates then alternates between

$$\begin{aligned}\cos\Bigg(\sqrt{\Lambda}\bar{S}_0^{y>\sqrt{\beta-1}}\left(\sqrt{\beta-1},\frac{m}{\sqrt{\Lambda}},\beta\right)+\mu(\beta)+\sqrt{\Lambda}\pi\frac{m}{\sqrt{\Lambda}}\Bigg)\\ -\cos\left(\sqrt{\Lambda}S_0\left(\sqrt{1+\beta},\frac{m}{\sqrt{\Lambda}},\beta\right)+\frac{\pi}{4}\right)=0\end{aligned} \tag{8.96}$$

and

$$\begin{aligned}\cos\Bigg(\sqrt{\Lambda}\bar{S}_0^{y>\sqrt{\beta-1}}\left(\sqrt{\beta-1},\frac{m}{\sqrt{\Lambda}},\beta\right)+\mu(\beta)+\sqrt{\Lambda}\pi\frac{m}{\sqrt{\Lambda}}\Bigg)\\ -\cos\left(\sqrt{\Lambda}S_0\left(\sqrt{1+\beta},\frac{m}{\sqrt{\Lambda}},\beta\right)+\frac{5\pi}{4}\right)=0.\end{aligned} \tag{8.97}$$

Both of these equations have zeros which do not correspond to the eigenvalues, the correct ones being those for which gradient of the l.h.s.'s is positive (this is the opposite of the underdense case). As before, the accuracy which is achieved proves the method: for $\Lambda = 12500$ the first two free eigenvalues given by numerical diagonalisation are $\beta = 1.003356$ and $\beta = 1.012155$, for which this W.K.B. matching technique gives $\beta = 1.003358$ and $\beta = 1.012156$ respectively.

8.5.3 The overdense eigenvectors

Knowing the value of β, one is then in a position to calculate the transitional approximation to the overdense eigenvector

$$B_{\text{barrier}}(y) = (-1)^n\mathcal{N}\frac{\left|\Gamma\left(\frac{1}{4}+\mathrm{i}\frac{t}{4}\right)\right|\mathrm{e}^{-\pi t/8}}{2\Gamma\left(\frac{1}{2}\right)}\left(\frac{\sigma^2-t}{1-(y^2-\beta)^2}\right)^{1/4}\mathrm{e}^{-\mathrm{i}\sigma^2/2}\quad {}_1F_1\left(-\mathrm{i}\frac{t}{4}+\frac{1}{4};\frac{1}{2};\mathrm{i}\sigma^2\right). \tag{8.98}$$

The Airy function approximation for the outer turning-point remains the same as before. Figure 8.12 shows the first free eigenvector made up of the overdense barrier and Airy function approximations.

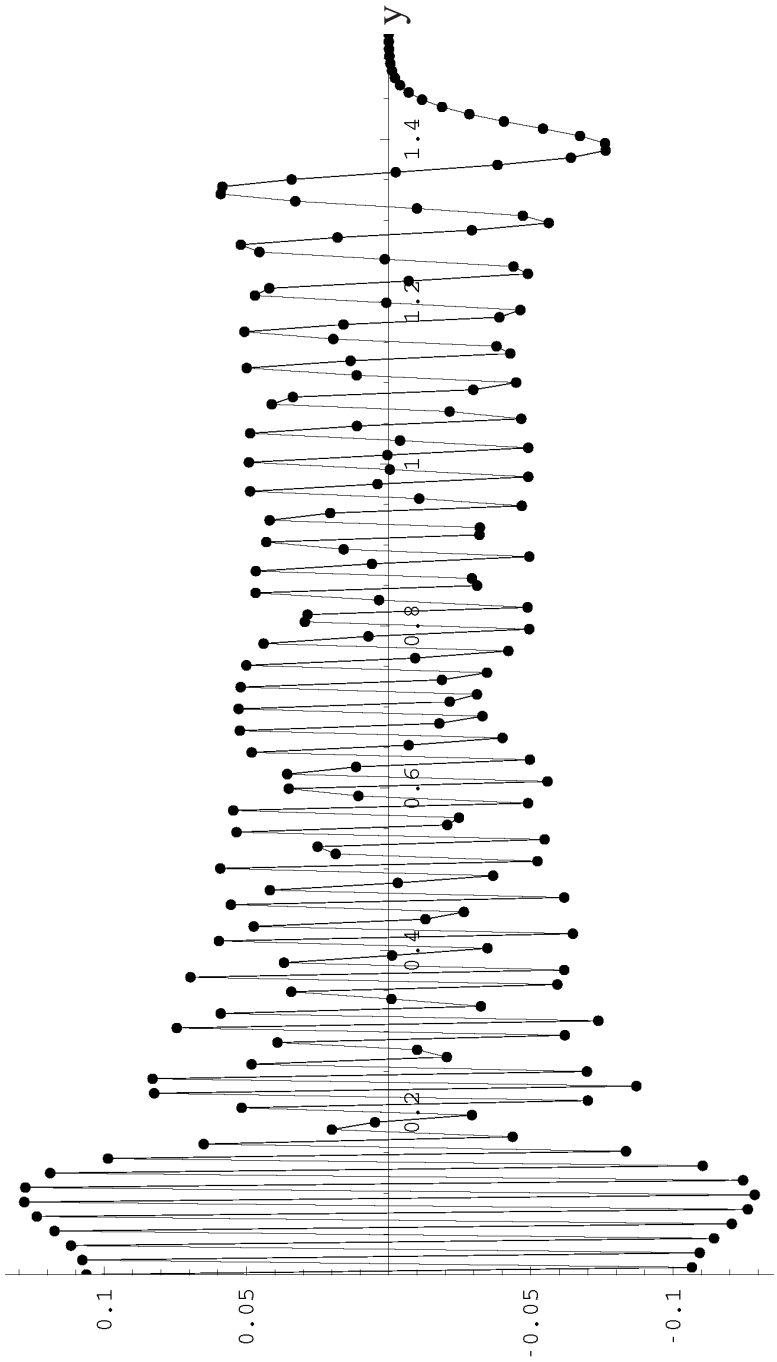

Figure 8.12: The 201$^{\text{st}}$ Bloch wave, which is the first 'free' eigenvector. This requires both the overdense parabolic barrier solution, and an Airy function as transitional approximations. The two are joined at the 83$^{\text{rd}}$ diffracted beam, which is at $y = 0.742$. The dots are the purely numerical calculation.

Chapter 9

Semiclassical scattering: Poisson resummation

9.1 Motivation

Uniformly approximating the eigenvectors and then summing them provides a reasonable method for calculating the total wavefunction at arbitrary depths through the laser grating, and would more than suffice to describe presently conceivable atom optics experiments. However, as the value of $\hbar$ is reduced yet further it is clear that one must sum ever greater numbers of eigenvectors—this number going as $\hbar^{-1}$. In this limit it would seem sensible to return somehow to the 'sum over the classical paths' since this representation gives much more rapid convergence providing the depth is not too great. The mathematical relationship between the two approaches was set forth in a remarkable stroke of insight by Pekeris in his 1950 symposium "*Ray theory vs. normal mode theory in wave propagation problems*" [64] which introduced the Poisson sum formula into this branch of physics. Poisson resummation manipulates the energy eigenvector sum, such that the new sum has terms of classical significance; each term is associated with classical paths which fall into different topological classes. Time and time again Poisson resummation has earned its reputation whether it be in describing electromagnetic waves in a 2-dimensional cavity with perfectly reflecting walls (Pekeris' demonstration problem), the classical feature distinguishing each term being the number of bounces a ray has made off the walls, or the effects on electrons due to an Aharonov-Bohm electromagnetic (gauge) potential, for which the terms index the number of orbits an electron has made around the singular 'source' (Berry 1980 [12]). The advantage of applying the Poisson sum formula rather than the formulae of Chapter 3 is that one doesn't need to know the classical

paths (just the quantum solution!), the Maslov indices are included automatically, and finally it facilitates a method (the uniform approximation for integrals) which eliminates the divergences due to caustics. This chapter concerns the application of these methods to the semiclassical scattering of atoms from a light grating, and once again it is anticipated that Poisson resummation will reinterpret the quantum sum in terms of classical paths.

9.2 The eigensum and the Poisson summation formula

The total wave function is formed from a superposition of the eigenvectors. For a perfectly collimated incident beam the superposition coefficients are the values of the eigenvectors themselves at $y = 0$, and so, using the W.K.B. approximation, Equation (4.79) becomes

$$\Psi = \sum_{j=0}^{\infty} \mathcal{N}^2 \frac{\cos\left(S_0(y_+, y, \beta_j) + \frac{\pi}{4}\right)}{\left(1 - (y^2 - \beta_j)^2\right)^{1/4}} \frac{\cos\left(S_0(y_+, 0, \beta_j) + \frac{\pi}{4}\right)}{\left(1 - \beta_j^2\right)^{1/4}} \, \mathrm{e}^{-\mathrm{i}\sqrt{\Lambda/2}\,\beta_j z_c} \tag{9.1}$$

where the 'quantum distance', ζ, has be re-written in favour of its classical counterpart. The normalisation, $\mathcal{N}$, is still given by (7.57). It is not clear from the outset how the use of the W.K.B. approximations, with their divergences, will affect the final wavefunction. Certainly the relative complexity of the uniform approximations would make their use in the following treatment very much harder if not impossible. For simplicity only the bound states will be included in the sum. This approximation becomes exact in the classical limit as the free states are not excited by the initial beam. As $\hbar \to 0$, the number of bound states will itself tend to infinity.

Intuitively one can imagine that as $\hbar$ becomes smaller, the sum over the discrete index j might be replaced by an integration. As discussed by Berry and Mount [14], it is insufficient to simply replace the sum over j by a single integration over j

$$\sum_{j=0}^{\infty} f(j) \not\longrightarrow \int_0^{\infty} f(j) dj. \tag{9.2}$$

The reason is that the eigenfunction summand is a sensitive function of β, changing considerably as j changes by unity—the eigenvectors alternate between being even and odd in this interval for instance. The correction terms to this simple replacement, as supplied by the Euler-Maclaurin formula which is an asymptotic series of successively higher derivatives of $f(j)$ w.r.t. j, fare little better since the eigenvectors represented by $f(j)$ are oscillatory functions of j—an infinite series of derivatives is required as $j \to \infty$. The correct transformation is the Poisson summation formula

$$\sum_{j=0}^{\infty} f(j) = \sum_{m=-\infty}^{\infty} \int_0^{\infty} f(j) \mathrm{e}^{2\pi \mathrm{i} m j} \, dj \tag{9.3}$$

which is exact. The Maslov index, which must be introduced with great care into the classical paths representation, here appears in a simple and automatic fashion as m.

9.2.1 Replacing the discrete quantum number by a classical variable

Rather than use the quantum 'variable' (number) j, it is convenient to use some classical variable which is more appropriate in the semiclassical limit—whilst j changes furiously, its classical counterpart includes $\hbar$ in such a way that it varies only slightly in comparison. The natural choice is β, which from definition (7.12) is the quantum eigenvalue scaled by $\hbar$. Whilst $0 \leq j \leq \infty$ for bound states in the semiclassical limit, the equivalent range for β is always, $-1 \leq \beta \leq 1$. The relationship between j and β is captured by the original Bohr-Sommerfeld condition of Equation (7.45) which states

$$j = 4\sqrt{\Lambda}\frac{\sqrt{1+\beta}}{\pi}\mathrm{E}\left(\frac{1}{2}\arccos[-\beta]\middle|\frac{2}{1+\beta}\right) - \frac{1}{2}. \tag{9.4}$$

The subtleties associated with the separatrix which were highlighted in the last chapter will be ignored here: Equation (9.4) is assumed to hold for all β. Moving from an integration over j to an integration over β requires the differentiation of (9.4); referring to Equations (A.17) and (A.18) of Appendix A, a straight forward differentiation of the upper limit and integrand of the elliptic integral leaves

$$\frac{dj}{d\beta} = \frac{\sqrt{2}\sqrt{\Lambda}}{\pi}\mathrm{K}\left(\frac{1+\beta}{2}\right). \tag{9.5}$$

When inserted into the Poisson summation formula, the complete elliptic integral contained in this Jacobian cancels with that in the normalisation factor. Thus the Poisson resummed eigensum (9.1), when restricted to the bound states, is written

$$\Psi = \frac{1}{2\pi}\sum_{m=-\infty}^{\infty}\int_{-1}^{1}\frac{\mathrm{e}^{\mathrm{i}\sqrt{\Lambda}\mathcal{A}} + \mathrm{e}^{\mathrm{i}\sqrt{\Lambda}\mathcal{B}} + \mathrm{e}^{\mathrm{i}\sqrt{\Lambda}\mathcal{C}} + \mathrm{e}^{\mathrm{i}\sqrt{\Lambda}\mathcal{D}}}{\left(1-(y^2-\beta)^2\right)^{1/4}\left(1-\beta^2\right)^{1/4}}\,d\beta \tag{9.6}$$

where

$$\begin{aligned}\mathcal{A} &= y\arccos\left[y^2-\beta\right]-2\sqrt{1+\beta}\mathrm{E}\left(\frac{1}{2}\arccos\left[y^2-\beta\right]\middle|\frac{2}{1+\beta}\right)\\ &\quad+2(4m-1)\sqrt{1+\beta}\mathrm{E}\left(\frac{1}{2}\arccos\left[-\beta\right]\middle|\frac{2}{1+\beta}\right)+\frac{\pi}{2\sqrt{\Lambda}}-\frac{\beta z_c}{\sqrt{2}}-\frac{m\pi}{\sqrt{\Lambda}} \qquad (9.7)\\ \mathcal{B} &= y\arccos\left[y^2-\beta\right]-2\sqrt{1+\beta}\mathrm{E}\left(\frac{1}{2}\arccos\left[y^2-\beta\right]\middle|\frac{2}{1+\beta}\right)\\ &\quad+2(4m+1)\sqrt{1+\beta}\mathrm{E}\left(\frac{1}{2}\arccos\left[-\beta\right]\middle|\frac{2}{1+\beta}\right)-\frac{\beta z_c}{\sqrt{2}}-\frac{m\pi}{\sqrt{\Lambda}} \qquad (9.8)\\ \mathcal{C} &= -y\arccos\left[y^2-\beta\right]+2\sqrt{1+\beta}\mathrm{E}\left(\frac{1}{2}\arccos\left[y^2-\beta\right]\middle|\frac{2}{1+\beta}\right)\\ &\quad+2(4m-1)\sqrt{1+\beta}\mathrm{E}\left(\frac{1}{2}\arccos\left[-\beta\right]\middle|\frac{2}{1+\beta}\right)-\frac{\beta z_c}{\sqrt{2}}-\frac{m\pi}{\sqrt{\Lambda}} \qquad (9.9)\\ \mathcal{D} &= -y\arccos\left[y^2-\beta\right]+2\sqrt{1+\beta}\mathrm{E}\left(\frac{1}{2}\arccos\left[y^2-\beta\right]\middle|\frac{2}{1+\beta}\right)\\ &\quad+2(4m+1)\sqrt{1+\beta}\mathrm{E}\left(\frac{1}{2}\arccos\left[-\beta\right]\middle|\frac{2}{1+\beta}\right)-\frac{\pi}{2\sqrt{\Lambda}}-\frac{\beta z_c}{\sqrt{2}}-\frac{m\pi}{\sqrt{\Lambda}}. \qquad (9.10)\end{aligned}$$

9.3 The stationary points

9.3.1 Derivatives of the phase

Clearly one can only contemplate performing the integrals involved in Equation (9.6) using the method of stationary phase—which is of course a suitable technique under semiclassical conditions. To find the points where $\mathcal{A}$, $\mathcal{B}$, $\mathcal{C}$, and $\mathcal{D}$ are stationary, the differentiations of these phases w.r.t. β are required. Appendix G contains a step by step differentiation of $\mathcal{A}$; the other three follow immediately and so

$$\begin{aligned}\frac{d\mathcal{A}}{d\beta} &= -\frac{1}{\sqrt{2}}\mathrm{F}\left(\arcsin\left[\sqrt{\frac{1+\beta-y^2}{1+\beta}}\right]\middle|\frac{1+\beta}{2}\right)+\frac{(4m-1)}{\sqrt{2}}\mathrm{K}\left(\frac{1+\beta}{2}\right)-\frac{z_c}{\sqrt{2}} \qquad (9.11)\\ \frac{d\mathcal{B}}{d\beta} &= -\frac{1}{\sqrt{2}}\mathrm{F}\left(\arcsin\left[\sqrt{\frac{1+\beta-y^2}{1+\beta}}\right]\middle|\frac{1+\beta}{2}\right)+\frac{(4m+1)}{\sqrt{2}}\mathrm{K}\left(\frac{1+\beta}{2}\right)-\frac{z_c}{\sqrt{2}} \qquad (9.12)\\ \frac{d\mathcal{C}}{d\beta} &= \frac{1}{\sqrt{2}}\mathrm{F}\left(\arcsin\left[\sqrt{\frac{1+\beta-y^2}{1+\beta}}\right]\middle|\frac{1+\beta}{2}\right)+\frac{(4m-1)}{\sqrt{2}}\mathrm{K}\left(\frac{1+\beta}{2}\right)-\frac{z_c}{\sqrt{2}} \qquad (9.13)\\ \frac{d\mathcal{D}}{d\beta} &= \frac{1}{\sqrt{2}}\mathrm{F}\left(\arcsin\left[\sqrt{\frac{1+\beta-y^2}{1+\beta}}\right]\middle|\frac{1+\beta}{2}\right)+\frac{(4m+1)}{\sqrt{2}}\mathrm{K}\left(\frac{1+\beta}{2}\right)-\frac{z_c}{\sqrt{2}}. \qquad (9.14)\end{aligned}$$

Setting each of these derivatives equal to zero gives the values of β for which the phases are stationary. Clearly, these roots of the derivatives can only be calculated numerically. Figure 9.1 shows plots of these derivatives for the particular momentum space point ($y = 0.65, z_c = 3\pi/2$).

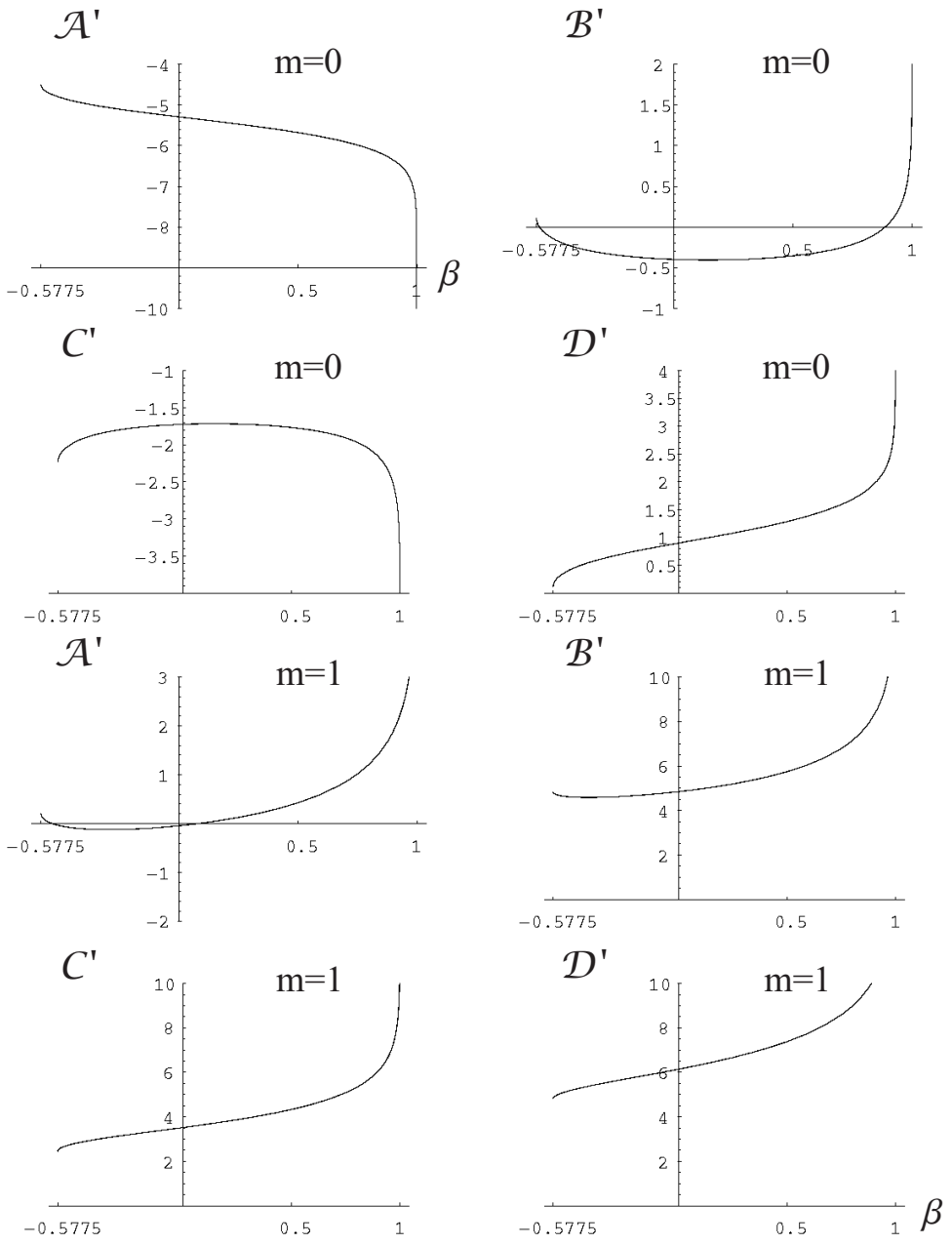

Figure 9.1: The derivatives of the four phases for $m = 0$ and 1, at the momentum space point $(y = 0.65, z_c = 3\pi/2)$.

Only the $m = 0$ and the $m = 1$ terms in the Poisson sum have phases which contain any stationary points at all for this value of (y, z_c), so, semiclassically at least, the other terms can be ignored. Notice that the contributing phases each have two zeros in their derivatives, indicating that they describe the wavefunction in the vicinity of a caustic (see the discussion in Chapter 3 and Appendix B). If one were to reduce the value of z_c slightly, then the zeros would slide down the curve until they coalesced at the point where the minimum actually sat on the zero line. Such a (y, z_c) point would then actually lie on a classical caustic. In general one observes that the evolution of the stationary points with increasing depth (z_c), is given by linearly sliding the graphs of Figure 9.1 downwards. When the stationary point slips off one phase curve it moves onto another. As may be predicted from Figure 9.1, as soon as the left-hand stationary point of $\mathcal{A}(\mathcal{B})$ no longer registers (the right-hand stationary point remains for all z_c) it appears as a lone zero on $\mathcal{C}(\mathcal{D})$ respectively, in such a way that one always has a real wavefunction.

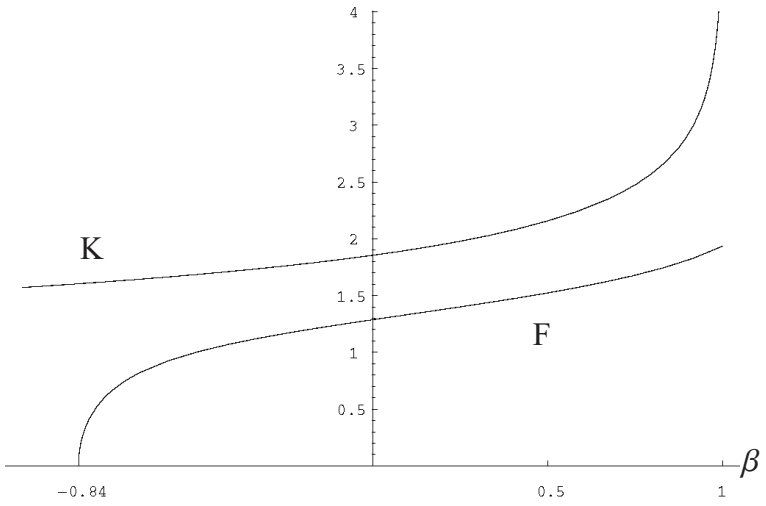

Figure 9.2: The complete, K, and incomplete, F, elliptic integrals plotted as functions of β. The value of y in the incomplete term is 0.4.

To gain more insight into the phase derivatives, the two principle terms are plotted as functions of β in Figure 9.2. Note that both the complete elliptic integral term

$$\mathrm{K}\left(\frac{1+\beta}{2}\right)$$

and the incomplete elliptic integral term,

$$\mathrm{F}\left(\arcsin\left[\sqrt{\frac{1+\beta-y^2}{1+\beta}}\right]\middle|\,\frac{1+\beta}{2}\right)$$

are positive for all the required ranges of β and y. Further, the incomplete term has its largest magnitude, for *all* β, when $y = 0$, for which it is equal to the complete term. As y is increased, the incomplete function is monotonically reduced in size for each value of β. From these facts, and referring to the Equations (9.11)–(9.14), it is deduced that only the $\mathcal{A}$ and $\mathcal{B}$ terms are responsible for the double zeros whilst the remaining two are only capable of single zeros.

9.3.2 Physical interpretation of the Poisson sum

Since the incomplete term achieves its largest value at $y = 0$, as z_c is increased (the graphs are moved downwards) it is the double zero terms which first cross the zero line for each positive value of m, and they do so initially for $y = 0$. As the curve first kisses the zero line, a single stationary point is born and immediately de-coalesces into a double zero. What this process describes is the birth of each cusp point along the z_c axis (see Figure 3.4). It is possible to explicitly calculate the values of z_c at which each new m term develops stationary points. At $y = 0$ the derivatives of the two double point terms are

$$\frac{d\mathcal{A}}{d\beta} = -\frac{1}{\sqrt{2}}\mathrm{K}\left(\frac{1+\beta}{2}\right) + \frac{(4m-1)}{\sqrt{2}}\mathrm{K}\left(\frac{1+\beta}{2}\right) - \frac{z_c}{\sqrt{2}} \tag{9.15}$$

$$\frac{d\mathcal{B}}{d\beta} = -\frac{1}{\sqrt{2}}\mathrm{K}\left(\frac{1+\beta}{2}\right) + \frac{(4m+1)}{\sqrt{2}}\mathrm{K}\left(\frac{1+\beta}{2}\right) - \frac{z_c}{\sqrt{2}} \tag{9.16}$$

and so the zeros first occur when

$$(4m-2)\mathrm{K}\left(\frac{1+\beta}{2}\right) = z_c^{\mathcal{A}} \tag{9.17}$$

$$4m\mathrm{K}\left(\frac{1+\beta}{2}\right) = z_c^{\mathcal{B}}. \tag{9.18}$$

As is evident from Figure 9.2, the complete elliptic function takes on its least value (the point which will cross the zero line first) when $\beta = -1$, for which

$$\mathrm{K}(0) = \frac{\pi}{2}. \tag{9.19}$$

Thus the cusp points occur at

$$z_c^{\mathcal{A}} = (2m-1)\pi \tag{9.20}$$

$$z_c^{\mathcal{B}} = 2m\pi. \tag{9.21}$$

That is, the $\mathcal{A}$ and $\mathcal{B}$ terms take it in turns to produce successive cusps, the combined effect is to produce cusps at $m\pi$, where the Poisson (Maslov) index $m = 0, 1, 2, \ldots$, in agreement with

the classical mechanics. The physical interpretation of the terms of the Poisson sum formula, is therefore that the m^{th} term is required to describe the contribution to the wavefunction from 'classical paths' which have taken part in $(m+1)$ momentum space caustics (the index is offset by 1 because the first caustic begins at the cusp which is at $z_c = 0$). This implies that Poisson resummation of the eigensum, whilst being the only viable method in the extreme semiclassical limit, requires more and more effort for larger and larger values of z_c as one has to include more terms.

9.4 Uniformly evaluating the integrals

The evaluation of the necessary integrals by the method of stationary phase actually constitutes the third stage of what is now recognised as a 'method' (see Berry and Mount [14]) for finding valid semiclassical approximations to the exact quantum eigenseries. The first stage being the change of variables from the quantum number j to the classical quantity β, and the second being the replacement of terms in the summand of the original eigensum by their asymptotic representations for large quantum numbers. Although not explicitly carried out here, one might consider the use of the W.K.B. approximations to the eigenfunctions as being associated with the second stage.

It may come as a surprise to some to learn that the eminent astrophysicist, John A. Wheeler, was responsible, together with Kenneth W. Ford, for two seminal papers which first established this semiclassical 'method' (though it should be mentioned that many authors applied certain individual pieces of the method prior to Ford and Wheeler—see [14]). In these two papers [32, 31] published in 1959, they set out and applied these three stages, though stage three was incomplete as they did not use the Poisson summation formula, relying instead on the intuitive replacement (9.2), which is the zeroth term of the Poisson formula. Apart from unifying the three stages, their crucial contribution was stage three, namely the evalution of their integral by the method of stationary phase.

In 1966 Berry [7] introduced the Poisson summation formula into semiclassical scattering; a couple of authors had already followed up Pekeris's observation of its usefulness in the general short wavelength context, applying it to discontinuous potentials (i.e. an isolated lens or water droplet), but Berry's initial application to 'rainbow scattering' (of which the Airy fringes predicted in this thesis are an example) and then in 1969 [9] to 'glory' scattering (due to the presence of an axial caustic: this requires an extra dimension in the control space) were the first works to use continuous potentials. A further important contribution contained in Berry's two papers [7, 9] (see also [8]) was the use of the *uniform* approximation for *integrals*, which had been a timely invention of Chester, Friedman and Ursell [23] in 1957. This is the analogous procedure for integrals as

the uniform approximation of Chapter 8 was for differential equations. It extends the method of steepest descents so that it remains valid when two saddle points coincide, or are sufficiently close together that the conventional single saddle method fails. Whilst Ford and Wheeler [32, 31] evaluated their stationary phase integrals in terms of transitional approximations, such as the Airy approximation, valid only for restricted angular scattering ranges, the uniform approximation for integrals is valid uniformly throughout the entire domain. The following sections contain descriptions of the method of uniform evaluation of integrals with real stationary points—these are based on unpublished notes by Berry [11].

9.4.1 The isolated stationary point

The integrals of Equation (9.6) fall into two classes: those terms with one stationary point in the phase and those with two. The phases with a single zero can be any of $\mathcal{A}, \mathcal{B}, \mathcal{C}$ or $\mathcal{D}$, depending on the value of the parameters y and z_c. A general term in Equation (9.6) can be written

$$\Psi_{\text{single}} = \frac{1}{2\pi} \int_{\beta=-1}^{\beta=1} \frac{\mathrm{e}^{\mathrm{i}\sqrt{\Lambda}\mathcal{V}}}{\left(1-(y^2-\beta)^2\right)^{1/4}\left(1-\beta^2\right)^{1/4}}\, d\beta \tag{9.22}$$

where $\mathcal{V}$ is one of the four phases. An isolated, real, stationary point can be handled by *the* method of stationary phase. The generalisation of this technique to two real stationary points uses a similar formalism, so it will be instructive to do more than quote the well known result of the single point case. One proceeds by mapping onto a new integration variable w; let

$$\mathcal{V}(\beta) = \mathcal{V}(\beta_r) + aw^2 \tag{9.23}$$

where β_r is the stationary point, so that the phase is now manifestly quadratic. One chooses

$$a = \begin{cases} +1 & \text{if } \mathcal{V}\,''(\beta_r) > 0 \\ -1 & \text{if } \mathcal{V}\,''(\beta_r) < 0. \end{cases} \tag{9.24}$$

In terms of the new variable w, Equation (9.22) becomes

$$\Psi_{\text{single}} = \frac{\mathrm{e}^{\mathrm{i}\sqrt{\Lambda}\mathcal{V}(\beta_r)}}{2\pi} \int_{w=-\infty}^{w=\infty} \frac{\mathrm{e}^{\mathrm{i}\sqrt{\Lambda}\, aw^2}}{\left(1-(y^2-\beta(w))^2\right)^{1/4}\left(1-\beta^2(w)\right)^{1/4}} \frac{d\beta}{dw}\, dw \tag{9.25}$$

where the extension of the limits to infinity recognises that there is only one stationary point, or, if there are others, then they are well separated. An asymptotic expansion to the integral is generated by expanding the amplitude factors in powers of w about $w = 0$ (which is the stationary point, for which $\beta = \beta_r$). Only the first term,

$$\frac{1}{\left(1-(y^2-\beta)^2\right)^{1/4}\left(1-\beta^2\right)^{1/4}} \frac{d\beta}{dw} \sim \frac{1}{\left(1-(y^2-\beta_r)^2\right)^{1/4}\left(1-\beta_r^2\right)^{1/4}} \left.\frac{d\beta}{dw}\right|_{w=0} \tag{9.26}$$

will be used here; so it remains to find $d\beta(w=0)/dw$. Differentiating the mapping relation (9.23) gives

$$\mathcal{V}\,'(\beta)\frac{d\beta}{dw} = 2aw. \tag{9.27}$$

Both $\mathcal{V}\,'$ and w vanish at the stationary point, so this equation cannot be solved for $d\beta/dw$. However, differentiating a second time produces

$$\mathcal{V}\,''(\beta)\left(\frac{d\beta}{dw}\right)^2 + \mathcal{V}\,'(\beta)\frac{d^2\beta}{dw^2} = 2a. \tag{9.28}$$

Noting that the second term vanishes at β_r gives

$$\left.\frac{d\beta}{dw}\right|_{w=0} = \sqrt{\frac{2a}{\mathcal{V}\,''(\beta_r)}}. \tag{9.29}$$

And so Equation (9.25) becomes

$$\Psi^r_{\text{single}} = \frac{1}{2\pi}\frac{\mathrm{e}^{\mathrm{i}\sqrt{\Lambda}\mathcal{V}(\beta_r)}}{\left(1-(y^2-\beta_r)^2\right)^{1/4}\left(1-\beta_r^2\right)^{1/4}}\sqrt{\frac{2a}{\mathcal{V}\,''(\beta_r)}}\int_{w=-\infty}^{w=\infty}\mathrm{e}^{\mathrm{i}\sqrt{\Lambda}\,aw^2}\,dw. \tag{9.30}$$

The remaining complex Gaussian integral has the solution

$$\int_{w=-\infty}^{w=\infty}\mathrm{e}^{\mathrm{i}\sqrt{\Lambda}\,aw^2}\,dw = \sqrt{\frac{\pi}{\sqrt{\Lambda}}}\mathrm{e}^{\mathrm{i}a\pi/4} \tag{9.31}$$

giving the well known stationary phase approximation due an isolated stationary point

$$\Psi^r_{\text{single}} = \frac{1}{\sqrt{2\pi\sqrt{\Lambda}\left|\mathcal{V}\,''(\beta_r)\right|}}\,\frac{\mathrm{e}^{\mathrm{i}(\sqrt{\Lambda}\mathcal{V}(\beta_r)\pm\pi/4)}}{\left(1-(y^2-\beta_r)^2\right)^{1/4}\left(1-\beta_r^2\right)^{1/4}} \tag{9.32}$$

where $\pm$ is still given by condition (9.24)—that is replace the $\pm$ with $+a$.

9.4.2 The second derivative of the phases

The expression for the wavefunction as given by the method of stationary phase requires the 2nd differentiation of the phase w.r.t. β; $\mathcal{V}\,''$. This is explicitly calculated for $\mathcal{A}$ in Appendix G, from which one can immediately infer the others

$$\begin{aligned}\frac{d^2\mathcal{A}}{d\beta^2} &= \frac{1}{2\sqrt{2}(1+\beta)}\mathrm{F}\left(\arcsin\left[\sqrt{\frac{1+\beta-y^2}{1+\beta}}\right]\middle|\,\frac{1+\beta}{2}\right)\\ &\quad -\frac{1}{\sqrt{2}(1-\beta^2)}\mathrm{E}\left(\arcsin\left[\sqrt{\frac{1+\beta-y^2}{1+\beta}}\right]\middle|\,\frac{1+\beta}{2}\right)+\frac{y\left(2\beta-y^2\right)}{2\left(1-\beta^2\right)\sqrt{1-(y^2-\beta)^2}}\\ &\quad +\frac{1-4m}{2\sqrt{2}(1+\beta)}\left\{\mathrm{K}\left(\frac{1+\beta}{2}\right)-\frac{2}{1-\beta}\mathrm{E}\left(\frac{\pi}{2}\middle|\,\frac{1+\beta}{2}\right)\right\}\end{aligned} \tag{9.33}$$

$$\begin{aligned}\frac{d^2\mathcal{B}}{d\beta^2} &= \frac{1}{2\sqrt{2}(1+\beta)}\mathrm{F}\left(\arcsin\left[\sqrt{\frac{1+\beta-y^2}{1+\beta}}\right]\middle|\,\frac{1+\beta}{2}\right)\\ &\quad -\frac{1}{\sqrt{2}(1-\beta^2)}\mathrm{E}\left(\arcsin\left[\sqrt{\frac{1+\beta-y^2}{1+\beta}}\right]\middle|\,\frac{1+\beta}{2}\right)+\frac{y\left(2\beta-y^2\right)}{2\left(1-\beta^2\right)\sqrt{1-\left(y^2-\beta\right)^2}}\\ &\quad -\frac{1+4m}{2\sqrt{2}(1+\beta)}\left\{\mathrm{K}\left(\frac{1+\beta}{2}\right)-\frac{2}{1-\beta}\mathrm{E}\left(\frac{\pi}{2}\middle|\,\frac{1+\beta}{2}\right)\right\} \qquad (9.34)\end{aligned}$$

$$\begin{aligned}\frac{d^2\mathcal{C}}{d\beta^2} &= -\frac{1}{2\sqrt{2}(1+\beta)}\mathrm{F}\left(\arcsin\left[\sqrt{\frac{1+\beta-y^2}{1+\beta}}\right]\middle|\,\frac{1+\beta}{2}\right)\\ &\quad +\frac{1}{\sqrt{2}(1-\beta^2)}\mathrm{E}\left(\arcsin\left[\sqrt{\frac{1+\beta-y^2}{1+\beta}}\right]\middle|\,\frac{1+\beta}{2}\right)-\frac{y\left(2\beta-y^2\right)}{2\left(1-\beta^2\right)\sqrt{1-\left(y^2-\beta\right)^2}}\\ &\quad +\frac{1-4m}{2\sqrt{2}(1+\beta)}\left\{\mathrm{K}\left(\frac{1+\beta}{2}\right)-\frac{2}{1-\beta}\mathrm{E}\left(\frac{\pi}{2}\middle|\,\frac{1+\beta}{2}\right)\right\} \qquad (9.35)\end{aligned}$$

$$\begin{aligned}\frac{d^2\mathcal{D}}{d\beta^2} &= -\frac{1}{2\sqrt{2}(1+\beta)}\mathrm{F}\left(\arcsin\left[\sqrt{\frac{1+\beta-y^2}{1+\beta}}\right]\middle|\,\frac{1+\beta}{2}\right)\\ &\quad +\frac{1}{\sqrt{2}(1-\beta^2)}\mathrm{E}\left(\arcsin\left[\sqrt{\frac{1+\beta-y^2}{1+\beta}}\right]\middle|\,\frac{1+\beta}{2}\right)-\frac{y\left(2\beta-y^2\right)}{2\left(1-\beta^2\right)\sqrt{1-\left(y^2-\beta\right)^2}}\\ &\quad -\frac{1+4m}{2\sqrt{2}(1+\beta)}\left\{\mathrm{K}\left(\frac{1+\beta}{2}\right)-\frac{2}{1-\beta}\mathrm{E}\left(\frac{\pi}{2}\middle|\,\frac{1+\beta}{2}\right)\right\}. \qquad (9.36)\end{aligned}$$

9.4.3 Determining the number of stationary points

When automating the calculation of the uniform approximation it is useful to know, for given values of (y, z_c), when the phases $\mathcal{A}$ and $\mathcal{B}$ register two stationary points and when they only register one. It is important to distinguish the coalescence of two stationary points (at the caustic), from the situation when these phases genuinely have only one simple zero. This latter case, as illustrated by Figure 9.1, arises because of the abrupt disappearance of the left hand piece of the 'parabola'—the phase becomes complex at this point. It is thus desirable to locate the (y, z_c) co-ordinates at which these special events take place.

For an arbitrarily chosen angle y, the bottom of the 'parabola' belonging to the differentiated phases $d\mathcal{A}/d\beta$ and $d\mathcal{B}/d\beta$ is determined by the vanishing of the second derivative of these phases

$$\left.\frac{d^2\mathcal{A}}{d\beta^2}\right|_{\beta_{\mathrm{caustic}}} = 0 \qquad (9.37)$$

$$\left.\frac{d^2\mathcal{B}}{d\beta^2}\right|_{\beta_{\mathrm{caustic}}} = 0. \qquad (9.38)$$

As for the first derivatives, the zeros of the second derivatives can only be found numerically. Once $\beta_{\mathrm{caustic}}(y)$ has been found, it is then substituted into the first derivative expression to discover the

value of z_c (the second derivatives do not contain z_c) at which the bottom of the parabola exactly touches the zero line. In fact, such a procedure amounts to finding the co-ordinates of the caustics.

For z_c less than this value the phases register no stationary points (for this particular value of m). For z_c greater than this value, then it is the $\mathcal{A}(\mathcal{B})$ phase (depending on whose turn it is to produce the current cusp-fold assembly) which solely gives the two stationary points; a situation which persists until the left hand stationary point ceases to be real. This moment is defined by the vanishing of the incomplete elliptic integral contained in the first derivative. By examining the amplitude (that is, the upper limit of the elliptic integral), this occurs when

$$\beta = y^2 - 1. \tag{9.39}$$

The corresponding value of z_c then follows from the first derivative equations. For example, for the phase $\mathcal{A}$, one immediately finds

$$z_c = (4m-1)\mathrm{K}\left(\frac{1+\beta}{2}\right) = (4m-1)\mathrm{K}\left(\frac{y^2}{2}\right). \tag{9.40}$$

9.4.4 Rainbow scattering

The use of the term 'rainbow' refers to scattering into angles close to, or at, a direction for which the classical deflection function has a fold caustic. The usage was abstracted away from its natural setting[1] by Ford and Wheeler [32, 31]. Mathematically, rainbow scattering derives from the close approach and then coalescence of two stationary points of the phase. This is symptomatic of the phase locally being a cubic function of β, and so this time the phase is mapped onto the strict cubic

$$\mathcal{V}(\beta, y, z_c) = -\eta(y, z_c)\, w + \frac{w^3}{3} + A(y, z_c). \tag{9.41}$$

Finally the connection with catastrophe theory has become explicit, since this is none other than (up to a constant which is taken outside the integration) the cubic normal form of Equation (3.45). From the purely utilitarian point of view, catastrophe theory can be regarded as a technique for stationary phase integrals with phases of a polynomial structure; the cubic being the first of the hierarchy.

The stationary points of the r.h.s. of (9.41) occur for

$$-\eta + w^2 = 0 \tag{9.42}$$

that is, when

$$w = \pm\sqrt{\eta}. \tag{9.43}$$

[1] One of the first scientifically credible studies of the rainbow was made by René Descartes.

So there are two real stationary points when $\eta > 0$ (the oscillatory side of the Airy function), and two imaginary stationary points when $\eta < 0$ (the decaying side). For the mapping to be well defined, $\beta(w)$ must be monotonic so that the correspondence is one-to-one. Monotonicity is assured if the Jacobian

$$\frac{d\beta}{dw} = \frac{-\eta + w^2}{\mathcal{V}'(\beta)} \tag{9.44}$$

is never equal to zero or infinity. Since $\mathcal{V}'(\beta)$ is zero at the stationary points $\beta_{1,2}$, the equivalent points are fixed by associating

$$w = +\sqrt{\eta} \quad \longleftrightarrow \quad \beta = \beta_1 \tag{9.45}$$

$$w = -\sqrt{\eta} \quad \longleftrightarrow \quad \beta = \beta_2. \tag{9.46}$$

This enables the functions $\eta(y, z_c)$ and $A(y, z_c)$ to be ascertained from the mapping definition (9.41)

$$\mathcal{V}(\beta_1) \equiv \mathcal{V}_1 = -\eta^{3/2} + \tfrac{\eta^{3/2}}{3} + A = -\frac{2}{3}\eta^{3/2} + A(y, z_c) \tag{9.47}$$

$$\mathcal{V}(\beta_2) \equiv \mathcal{V}_2 = +\eta^{3/2} - \tfrac{\eta^{3/2}}{3} + A = +\frac{2}{3}\eta^{3/2} + A(y, z_c). \tag{9.48}$$

Thus, defining

$$\bar{\mathcal{V}}(y, z_c) \equiv \frac{\mathcal{V}_1 + \mathcal{V}_2}{2} \tag{9.49}$$

$$\Delta\mathcal{V}(y) \equiv \mathcal{V}_2 - \mathcal{V}_1 \tag{9.50}$$

one has

$$A(y, z_c) = \bar{\mathcal{V}}(y, z_c) \tag{9.51}$$

$$\eta(y, z_c) = \left(\frac{3\Delta\mathcal{V}(y, z_c)}{4}\right)^{2/3}. \tag{9.52}$$

So the double stationary point terms of Equation (9.6) become

$$\Psi_{\text{rainbow}} = \frac{\mathrm{e}^{\mathrm{i}\sqrt{\Lambda}\bar{\mathcal{V}}(y,z_c)}}{2\pi} \int_{w=-\infty}^{w=\infty} \frac{\mathrm{e}^{\mathrm{i}\sqrt{\Lambda}\,(w^3/3 - \eta w)}}{\left(1 - (y^2 - \beta(w))^2\right)^{1/4} \left(1 - \beta^2(w)\right)^{1/4}} \frac{d\beta}{dw}\, dw. \tag{9.53}$$

Again an asymptotic series can be obtained by expanding the amplitude factor. For the single turning point case only the first term of the asymptotic expansion was retained since in the limit of vanishing Λ only the value at the stationary point was important. Here however, the expansion must provide a reasonable approximation to the amplitude factor throughout the region between the two stationary points since it is exactly this 'interaction' between the two points which must be accounted for. Chester *et al.* [23] suggested (and proved the validity of) an expansion of the form

$$\frac{1}{\left(1 - (y^2 - \beta(w))^2\right)^{1/4} \left(1 - \beta^2(w)\right)^{1/4}} \frac{d\beta}{dw} = \sum_m p_m \left(w^2 - \eta\right)^m + \sum_m q_m w \left(w^2 - \eta\right)^m \tag{9.54}$$

which is a sum of even and odd terms that vanishes except for the constant p_0 at the two stationary points $w = \pm\sqrt{\eta}$. This expansion is therefore the closest possible analogy to the single point expansion but is valid at both stationary points. Keeping just the lowest two terms one hopes to capture the principal variation of the amplitude with just a linear function

$$\frac{1}{(1-(y^2-\beta(w))^2)^{1/4}\,(1-\beta^2(w))^{1/4}}\,\frac{d\beta}{dw} \sim p + qw \tag{9.55}$$

the indices on p and q no longer being required to this approximation. One evaluates p and q by calculating (9.55) at β_1 and β_2

$$\frac{1}{(1-(y^2-\beta_1)^2)^{1/4}\,(1-\beta_1^2)^{1/4}}\,\frac{d\beta_1}{dw} = p + q\sqrt{\eta} \tag{9.56}$$

$$\frac{1}{(1-(y^2-\beta_2)^2)^{1/4}\,(1-\beta_2^2)^{1/4}}\,\frac{d\beta_2}{dw} = p - q\sqrt{\eta} \tag{9.57}$$

from which one obtains

$$p = \frac{1}{2}\left(\frac{1}{(1-(y^2-\beta_1)^2)^{1/4}\,(1-\beta_1^2)^{1/4}}\,\frac{d\beta_1}{dw} + \frac{1}{(1-(y^2-\beta_2)^2)^{1/4}\,(1-\beta_2^2)^{1/4}}\,\frac{d\beta_2}{dw}\right) \tag{9.58}$$

$$q = \frac{1}{2\sqrt{\eta}}\left(\frac{1}{(1-(y^2-\beta_1)^2)^{1/4}\,(1-\beta_1^2)^{1/4}}\,\frac{d\beta_1}{dw} - \frac{1}{(1-(y^2-\beta_2)^2)^{1/4}\,(1-\beta_2^2)^{1/4}}\,\frac{d\beta_2}{dw}\right). \tag{9.59}$$

It remains to find $d\beta_{1,2}/dw$, but this comes from differentiating the mapping relation

$$\mathcal{V}\,'(\beta)\frac{d\beta}{dw} = -\eta + w^2. \tag{9.60}$$

As before one must differentiate a second time

$$\mathcal{V}\,''(\beta)\left(\frac{d\beta}{dw}\right)^2 + \mathcal{V}\,'(\beta)\frac{d^2\beta}{dw^2} = 2w \tag{9.61}$$

to give

$$\frac{d\beta_1}{dw} = \left.\frac{d\beta}{dw}\right|_{\beta_1} = \sqrt{\frac{2\sqrt{\eta}}{\mathcal{V}\,''(\beta_1)}} \tag{9.62}$$

$$\frac{d\beta_2}{dw} = \left.\frac{d\beta}{dw}\right|_{\beta_2} = \sqrt{\frac{-2\sqrt{\eta}}{\mathcal{V}\,''(\beta_2)}}. \tag{9.63}$$

Now p and q are known, Equation (9.53) becomes

$$\Psi_{\text{rainbow}} = \frac{\mathrm{e}^{\mathrm{i}\sqrt{\Lambda}\bar{\mathcal{V}}(y,z_c)}}{2\pi}\left[p\int_{w=-\infty}^{w=\infty}\mathrm{e}^{\mathrm{i}\sqrt{\Lambda}\,(w^3/3-\eta w)}\,dw + q\int_{w=-\infty}^{w=\infty}w\,\mathrm{e}^{\mathrm{i}\sqrt{\Lambda}\,(w^3/3-\eta w)}\,dw\right]. \tag{9.64}$$

It should be noted that the expansion (9.54) was set up so that at the point where $\mathcal{V}\,''$ goes to zero, which is at the coalescence of the two stationary points, that is $\beta_1 = \beta_2$, q and η vanish so any potential divergences are tamed. Hence, both the phase and the amplitude are truly 'uniform'.

The success of the cubic uniform method lies in the recognition of the two integrals involved as being variants of the well known Airy function and its derivative

$$\mathrm{Ai}(C) = \frac{1}{2\pi}\int_{-\infty}^{\infty} \mathrm{e}^{\mathrm{i}(t^3/3+Ct)}\,dt \tag{9.65}$$

$$\mathrm{Ai}'(C) = \frac{d\mathrm{Ai}(C)}{dC} = \frac{\mathrm{i}}{2\pi}\int_{-\infty}^{\infty} t\,\mathrm{e}^{\mathrm{i}(t^3/3+Ct)}\,dt \tag{9.66}$$

in terms of which the uniform rainbow contribution to the wavefunction finally becomes

$$\begin{aligned}\Psi_{\mathrm{rainbow}} =& \frac{\mathrm{e}^{\mathrm{i}\sqrt{\Lambda}\bar{\mathcal{V}}(y,z_c)}}{\sqrt{2}}\Bigg[\quad\Bigg(\frac{1}{(1-(y^2-\beta_1)^2)^{1/4}\,(1-\beta_1^2)^{1/4}\,\sqrt{\mathcal{V}\,''(\beta_1)}}\\ &+\frac{1}{(1-(y^2-\beta_2)^2)^{1/4}\,(1-\beta_2^2)^{1/4}\,\sqrt{-\mathcal{V}\,''(\beta_2)}}\Bigg)\left(\frac{3\Delta\mathcal{V}}{4\Lambda}\right)^{1/6}\mathrm{Ai}\left(-\left(\frac{3\sqrt{\Lambda}\Delta\mathcal{V}}{4}\right)^{2/3}\right)\\ &-\mathrm{i}\Bigg(\frac{1}{(1-(y^2-\beta_1)^2)^{1/4}\,(1-\beta_1^2)^{1/4}\,\sqrt{\mathcal{V}\,''(\beta_1)}}\\ &-\frac{1}{(1-(y^2-\beta_2)^2)^{1/4}\,(1-\beta_2^2)^{1/4}\,\sqrt{-\mathcal{V}\,''(\beta_2)}}\Bigg)\left(\frac{4}{3\Lambda^2\Delta\mathcal{V}}\right)^{1/6}\mathrm{Ai}'\left(-\left(\frac{3\sqrt{\Lambda}\Delta\mathcal{V}}{4}\right)^{2/3}\right)\Bigg].\end{aligned} \tag{9.67}$$

The traditional *transitional* approximation on the other hand does not include the Airy function derivative, and this is an important difference. Very close to the caustic ($\Delta\mathcal{V}=0$), the undifferentiated term dominates, and so the uniform approximation reduces to the transitional form.

The use of the smoothly matched Airy function and trigonometric W.K.B. expressions in this and the previous chapter penetrate to the very heart of semiclassical analysis. In particular, they explain that the reason the semiclassical limit is not elementary (as, say, the relativistic to Newtonian limit is) is because of the different $\hbar$ dependence of the solutions at the different scattering angles y. Denoting the rainbow angle (fold caustic) as y_{r}, Table 9.1 categorises this changing analytic form. Note that $\Lambda \propto 1/\hbar^2$ and $\mathrm{Ai}(\delta) \to (3^{2/3}\Gamma(2/3))^{-1}$, i.e. a constant, as $\delta \to 0$.

	$y \ll y_{\mathrm{r}}$	$y \approx y_{\mathrm{r}}$	$y \gg y_{\mathrm{r}}$
Ψ	$\mathcal{O}(\hbar^{1/2}) \times \cos(\mathcal{O}(1/\hbar))$	$\mathcal{O}(\hbar^{1/3})$	$\mathcal{O}(\hbar^{1/2})\exp(-\mathcal{O}(1/\hbar))$

Table 9.1: The analytic dependence of the wavefunction on $\hbar$ as y is varied.

9.4.5 Uniform beyond the call of duty

The expansion of the amplitude term as suggested by Chester *et al.* [23] was designed to simultaneously cope with two overlapping saddles. The use of the W.K.B. approximations to the

eigenfunctions introduces the possibility of divergences that the uniform approximation was not specifically set up to handle. Although it was mentioned earlier that the use of W.K.B. functions can be regarded as being 'step 2' in Ford and Wheeler's method, namely the replacement of quantum expressions with their asymptotic approximations valid for $\hbar \to 0$, the asymptotic expressions were envisioned to be well behaved. It therefore comes as a surprise that the amplitude expansion also 'uniformises' the W.K.B. divergences.

The problematic W.K.B. amplitude is

$$|\Psi_{\mathrm{WKB}}| = \frac{1}{\left(1-(y^2-\beta)^2\right)^{1/4}} \tag{9.68}$$

which diverges when

$$y = \pm\sqrt{1 \pm \beta}. \tag{9.69}$$

So for instance, when $\beta \to y^2 \pm 1$, one could put

$$\beta = y^2 \pm 1 + \delta \tag{9.70}$$

so that the amplitude locally goes as

$$|\Psi_{\mathrm{WKB}}| \propto \frac{1}{\delta^{1/4}}. \tag{9.71}$$

Fortunately, wherever the uniform wavefunction (9.67) has a W.K.B. amplitude factor, it is multiplied by $1/\sqrt{\mathcal{V}\,''}$. Inserting (9.70) into any of the second derivative expressions (9.33–9.36) the term which dominates is the one that itself contains the W.K.B. amplitude, so one has

$$\frac{1}{\sqrt{\mathcal{V}\,''}} \propto \delta^{1/4}. \tag{9.72}$$

Thus the W.K.B. divergences are smoothed away.

9.4.6 Comparison with numerical result

The Poisson-resummed wavefunction was calculated at $z_c = 3\pi/2$ and is shown in Figure 9.3. Only three terms were required: $\mathcal{B}$ and $\mathcal{D}$ both with $m = 0$, and $\mathcal{A}$ with $m = 1$. The $m = 0$ terms correspond to the folds born as the cusp point $z_c = 0$, so they form the outer Airy fringes, although their influence extends all the way to $y = 0$. The inner Airy fringes are generated by the single $m = 1$ term. Potentially, the $\mathcal{C}$ term, with $m = 1$, could also contribute, but for this value of z_c, $\mathcal{A}$ contains both the stationary points. The chosen value of Λ is relatively small: the comparison with the numerical result improves as the system becomes more classical. In particular, the interference immediately to the outside of the inner Airy function is not captured. The coalescing stationary point has just left the real axis, so to reproduce this 'tunneling' interference one would need to

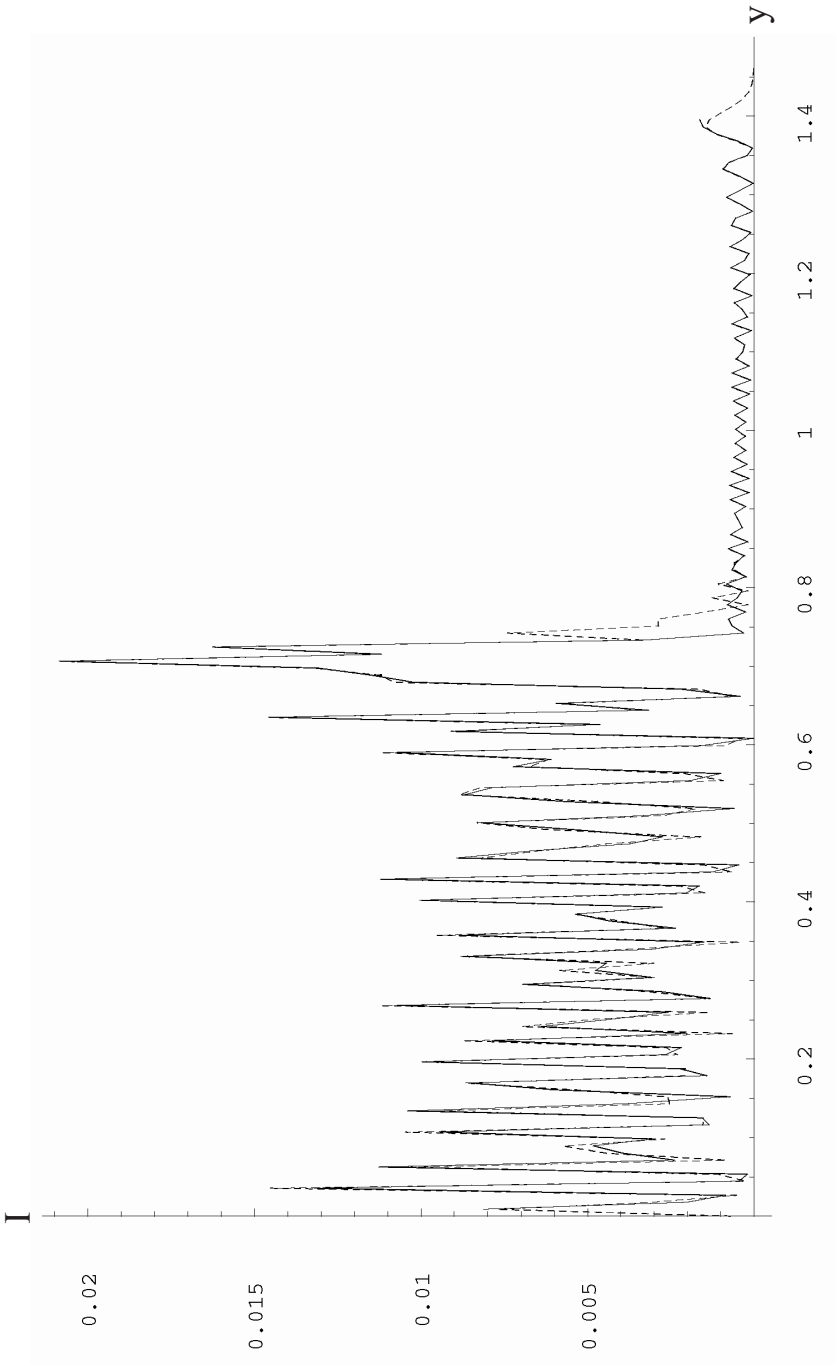

Figure 9.3: A comparison of the Poisson resummed (solid) wave function with the numerical diagonalisation calculation (dashed). $z_c = 3\pi/2$ and $\Lambda = 12500$.

evaluate the Poisson integrals in the complex plane. Similarly, with the very outer fringe of the outer Airy function: the stationary points become complex.

Conclusion

By studying the classical mechanics (geometrical optics), it becomes apparent that the farfield diffraction pattern of a beam of atoms passing through a sinusoidal light grating is dominated by caustics. These arise from the partial focussing of ray trajectories as they wind about in the anharmonic wells and proliferate with increasing thickness of the grating. From the classical solutions one can find the positions of these caustics. Using only the most general information about the system (such as the number of available parameters), catastrophe theory identifies the caustics as cusps which develop into simple folds, and even gives the form of the wavefunction local to these elementary catastrophes as being the Pearcey and Airy functions respectively.

The wave behaviour was introduced through the differential difference equations due to Raman and Nath. When the transverse kinetic energy term is retained in these equations, they describe dynamical diffraction in the long interaction time regime. For low intensity of the light grating the system is very quantum (few beams), and various perturbative solutions can be found. If the atoms traverse the grating at an oblique angle corresponding to the first Bragg angle, then the problem can be reduced to the well known 'two-beam' case. With atoms however, it is particularly easy to tailor the potential they see into a more exotic form, and, in particular, generate an imaginary potential to model dissipation due to spontaneous emission. The extra parameters associated with complex potentials mean that degeneracies, which are rare in Hermitian systems, can be located by varying the angle of incidence. The degeneracy in the non-Hermitian scattering matrix (Raman-Nath matrix) is reflected physically by anomalously high transmission at the Bragg angle. The width of the transmitted beams are also determined by the degeneracy and can become very narrow. The semiclassical limit of dissipative scattering can also be studied. It contrasts with the Hermitian case since there are no caustics: only a rather slender Gaussian survives the absorption.

The Raman-Nath equations for real potentials can be continuised in the semiclassical limit providing one employs a W.K.B. approach to find the eigenvectors. The system is quantised by a Bohr-Sommerfeld type condition. The W.K.B. eigenvectors fail at the turning-points, but accurate, uniformly valid, solutions can be found by mapping onto parabolic cylinder functions. The situation

becomes more complicated close to the separatrix where two transitional approximations must be employed. The quantisation condition is then modified (the eigenvalues are split by tunnelling) to become that which correctly matches the W.K.B. expressions issuing from the inner and outer turning points. The subtle phases contained in these W.K.B. expressions can be determined from the transitional approximations. Since the stationary Raman-Nath equations give the Fourier coefficients of the Mathieu equation, these uniform solutions represent the correct solutions to the Mathieu equation when it contains a large parameter. They are analytic save for the solution of a transcendental mapping relation.

Finally, the farfield wavefunction given by an eigensum of the W.K.B. eigenvectors can be transformed, by the Poisson summation formula, into a sum of terms with topological significance. Successive terms describe classical ray families which have oscillated a certain number of times within the potential well. This expression for the semiclassical dynamical diffraction from a thick grating has the closest connections with the classical description. The birth of each new cusp is heralded by each new term in the Poisson resummed series. By uniformly evaluating the integrals of the Poisson formula one obtains a wavefunction valid for all scattering angles (despite the use of W.K.B. eigenvectors), and, in particular, the Airy function intensity pattern is explicitly present at the caustics as predicted by catastrophe theory.

Future work

Three main areas stand out as being of merit. The first is the 'ergodic limit' of the Raman-Nath equations. This is the regime of infinitely long interaction times. The farfield pattern becomes thick with caustics, and the intensity, on average, settles down to an envelope, the analytic form of which has already been found by Michael Berry (to be published).

The second concerns moments of the farfield wavefunction: the absolute wavefunction is raised to some even power and then integrated (summed) over all space (scattering angles). If the system is classical enough, then the primary Airy peaks should survive interference and give the major contribution to the moment, leading to a universal behaviour with $\hbar$. Initial investigations show that one has to go beyond what is numerically possible and so either the uniform or Poisson methods *must* be used.

Thirdly, there seems to be no reason why the Raman-Nath equation for oblique incidence (4.37) should not be continue-and-uniformised. As the angle of incidence is changed eigenvalues can pass right through the separatrix energy leading to interesting phase effects due to tunnelling.

Appendix A

Elliptic integrals and functions

A.1 Elliptic integrals of the first kind

A.1.1 Incomplete elliptic integrals of the first kind

Elliptic integrals of the 1$^{\text{st}}$ kind are straight forward [1],

$$\mathrm{F}(\phi|m) = \int_0^{\phi} \frac{d\theta}{\sqrt{1 - m\sin^2\theta}} \tag{A.1}$$

with ϕ being known as the 'amplitude' and m the 'parameter'. Some authors, such as *Gradshteyn* and *Ryzhik* [38] use k^2 in preference to m

$$k^2 = \sin^2\alpha = m. \tag{A.2}$$

The elliptic integrals are, in a sense, generalised inverse trigonometric functions. Compare Equation (A.1)[1], with the integral definition of arcsin for instance

$$\arcsin y = \int_0^{y} \frac{dt}{\sqrt{1 - t^2}}. \tag{A.3}$$

And so, in an analogous way, the elliptic integrals can be inverted using Jacobian elliptic functions [1], which are defined so that if

$$u = \mathrm{F}(\phi|m) \tag{A.4}$$

then the two elliptic functions $\mathrm{sn}(u|m)$ and $\mathrm{cn}(u|m)$ are simply

$$\mathrm{sn}(u|m) = \sin\phi \tag{A.5}$$

$$\mathrm{cn}(u|m) = \cos\phi \tag{A.6}$$

[1] A more suitable comparison is formed by the substitution $t = \sin\theta$ into Eqn (A.1) giving $\int_0^{\sin\phi}[(1-t^2)(1-mt^2)]^{-1/2}\,dt$.

where u is known as the 'argument'. Whilst one could write

$$\phi = \arcsin[\mathrm{sn}(u|m)] \tag{A.7}$$

it is important to remember that ϕ is a multi-valued function of u, so it is usual to write the relationship between the amplitude and the argument as

$$\phi = \mathrm{am}(u|m) \tag{A.8}$$

where $\mathrm{am}(u|m)$ is called the 'Jacobi amplitude' function. Refer to Figure A.1 for plots of these two elliptic functions.

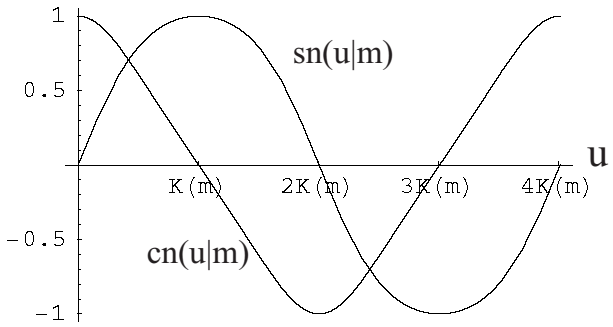

Figure A.1: Plots of a single period of $\mathrm{sn}(u|m)$ and $\mathrm{cn}(u|m)$ as functions of u for $m = 0.65$. Note that the period of both functions is 4 times the complete elliptic integral of the first kind, $\mathrm{K}(m)$. In this respect $\mathrm{K}(m)$ plays the rôle that $\pi/2$ plays for sine and cosine functions.

A.1.2 Complete elliptic integrals of the first kind

'Complete' refers to the fixed integration range $0 \to \pi/2$

$$\mathrm{K}(m) = \mathrm{F}(\pi/2|m) = \int_0^{\pi/2} \frac{d\theta}{\sqrt{1 - m\sin^2\theta}}. \tag{A.9}$$

A.2 Elliptic integrals of the second kind

A.2.1 Incomplete elliptic integrals of the second kind

More care must be taken with the notation for elliptic integrals of the 2nd kind. The notation used in this thesis will be

$$\mathrm{E}(\phi|m) = \int_0^{\phi} \sqrt{1 - m\sin^2\theta}\, d\theta \tag{A.10}$$

in line with *Gradshteyn* and *Ryzhik* [38] and the computer package *Mathematica*.

However *Abramowitz* and *Stegun* [1] take

$$\mathsf{E}(\phi\backslash\alpha) = \int_0^{\phi} \sqrt{1 - \sin^2\alpha\sin^2\theta}\, d\theta = \int_0^{\phi} \sqrt{1 - m\sin^2\theta}\, d\theta \tag{A.11}$$

and reserve $\mathsf{E}(\mathsf{u}|\mathsf{m})$ for

$$\mathsf{E}(\mathsf{u}|\mathsf{m}) = \int_0^{u} \mathrm{dn}^2(w|m)dw = \mathsf{E}(\phi\backslash\alpha) \tag{A.12}$$

where $\mathrm{dn}(u|m)$ is defined by

$$\mathrm{dn}(u|m) \equiv \sqrt{1 - m\sin^2\phi}. \tag{A.13}$$

The relationship between these two notations is defined through that between ϕ and u. Using the Jacobi amplitude (A.8)gives

$$\mathrm{E}(\phi|m) = \mathrm{E}(\mathrm{am}(u|m)|m) = \mathsf{E}(\phi\backslash\alpha) = \mathsf{E}(\mathsf{u}|\mathsf{m}). \tag{A.14}$$

A.2.2 Complete elliptic integrals of the second kind

Following the definition specified above the complete elliptic integral of the 2nd kind will be taken as

$$\mathrm{E}(m) = \mathrm{E}(\pi/2|m) = \int_0^{\pi/2} \sqrt{1 - m\sin^2\theta}\, d\theta. \tag{A.15}$$

A.3 Differentiation

When dealing with the elliptic integrals, one follows the normal procedure for differentiating an integral. With incomplete elliptic integrals one must remember that the upper limit can contain a variable. The results required for Chapters 3 and 9 concern the complete elliptic integral of the 1st kind

$$\frac{d\mathrm{K}(m)}{dm} = \frac{1}{2m(1-m)}\left(\mathrm{E}(m) - (1-m)\mathrm{K}(m)\right) \tag{A.16}$$

and the incomplete elliptic integral of the 2nd kind

$$\frac{\partial \mathrm{E}(\phi|m)}{\partial\phi} = \sqrt{1 - m\sin^2\phi} = \mathrm{dn}(\mathrm{F}(\phi|m)|m) = \mathrm{dn}(u|m) \tag{A.17}$$

$$\frac{\partial \mathrm{E}(\phi|m)}{\partial m} = \frac{1}{2m}\left(\mathrm{E}(\phi|m) - \mathrm{F}(\phi|m)\right). \tag{A.18}$$

Elliptic functions may also be differentiated w.r.t. either the argument or the parameter. The former are well known to be [1]:

$$\frac{\partial}{\partial u}\,\mathrm{sn}(u|m) = \mathrm{cn}(u|m)\mathrm{dn}(u|m) \tag{A.19}$$

$$\frac{\partial}{\partial u}\,\mathrm{cn}(u|m) = -\mathrm{sn}(u|m)\mathrm{dn}(u|m) \tag{A.20}$$

$$\frac{\partial}{\partial u}\,\mathrm{dn}(u|m) = -m\,\mathrm{sn}(u|m)\mathrm{cn}(u|m) \tag{A.21}$$

whilst the latter are more rarely quoted, but may be found in Lawden, P.82, [47]:

$$\frac{\partial}{\partial m}\mathrm{sn}(u|m) = \left(u - \frac{\mathrm{E(am(u|m)}\,|m)}{(1-m)}\right)\frac{\mathrm{cn}(u|m)\mathrm{dn}(u|m)}{2m} + \frac{\mathrm{sn}(u|m)\mathrm{cn}^2(u|m)}{2(1-m)} \tag{A.22}$$

$$\frac{\partial}{\partial m}\mathrm{cn}(u|m) = \left(\frac{\mathrm{E(am(u|m)}\,|m)}{(1-m)} - u\right)\frac{\mathrm{sn}(u|m)\mathrm{dn}(u|m)}{2m} - \frac{\mathrm{sn}^2(u|m)\mathrm{cn}(u|m)}{2(1-m)} \tag{A.23}$$

$$\frac{\partial}{\partial m}\mathrm{dn}(u|m) = \left(\frac{\mathrm{E(am(u|m)}\,|m)}{(1-m)} - u\right)\frac{\mathrm{sn}(u|m)\mathrm{cn}(u|m)}{2} - \frac{\mathrm{sn}^2(u|m)\mathrm{dn}(u|m)}{2(1-m)}. \tag{A.24}$$

Appendix B

The wavefunction from rays

This appendix aims to give a justification for the form of the semiclassical wavefunction. A more complete derivation can be found for instance in Tabor's book *Chaos and Integrability in Nonlinear Dynamics* [76], whilst the geometrical optics which will be used can be found in *The Diffraction of Light by Ultrasound* [16] by Berry, and Born and Wolf's *Principles of Optics* [19].

B.1 The short wavelength Helmholtz equation

The time-independent Schrödinger wave equation is an example of a scalar Helmoltz equation

$$\frac{\partial^2\psi}{\partial x^2}+\frac{\partial^2\psi}{\partial z^2}+\frac{2m}{\hbar^2}\left(E+V_0\cos^2 Kx\right)\psi=0 \tag{B.1}$$

where the total energy E is determined by the (constant) value of P_z and the initial entry point into the potential

$$E=\frac{P_z^2}{2m}-V_0\cos^2 Kx_0. \tag{B.2}$$

The following ansatz is made for the wavefunction,

$$\psi(x,z)=a(x,z)\mathrm{e}^{\mathrm{i}S(x,z)/\hbar} \tag{B.3}$$

which, upon substitution into the Helmholtz equation, gives

$$\begin{aligned}&\frac{\partial^2 a}{\partial x^2}+\frac{\partial^2 a}{\partial x^2}+2\frac{\mathrm{i}}{\hbar}\left(\frac{\partial a}{\partial x}\frac{\partial S}{\partial x}+\frac{\partial a}{\partial z}\frac{\partial S}{\partial z}\right)+\frac{\mathrm{i}}{\hbar}a\left(\frac{\partial^2 S}{\partial x^2}+\frac{\partial^2 S}{\partial z^2}\right)\\&-\frac{a}{\hbar^2}\left(\left(\frac{\partial S}{\partial x}\right)^2+\left(\frac{\partial S}{\partial z}\right)^2\right)+\frac{2ma}{\hbar^2}(E+V_0\cos^2 Kx)=0.\end{aligned} \tag{B.4}$$

For small $\hbar$, one can try and approximately solve Equation (B.4) by considering each order of $\hbar$ in turn. Equating the coefficients of successive powers of $\hbar$ gives the hierarchy of equations

$$\mathcal{O}(\hbar^0): \qquad -\left(\frac{\partial S}{\partial x}\right)^2 - \left(\frac{\partial S}{\partial z}\right)^2 + 2m(E + V_0 \cos^2 Kx) = 0 \tag{B.5}$$

$$\mathcal{O}(\hbar^1): \qquad 2\left(\frac{\partial a}{\partial x}\frac{\partial S}{\partial x} + \frac{\partial a}{\partial z}\frac{\partial S}{\partial z}\right) + a\left(\frac{\partial^2 S}{\partial x^2} + \frac{\partial^2 S}{\partial z^2}\right) = 0 \tag{B.6}$$

$$\mathcal{O}(\hbar^2): \qquad \frac{\partial^2 a}{\partial x^2} + \frac{\partial^2 a}{\partial z^2} = 0 \tag{B.7}$$

Only the zeroth and first order equations will be considered here.

B.2 The Hamilton-Jacobi equation

Equation (B.5) is called the *Eikonal equation* which can be shown to be a time-independent Hamilton-Jacobi equation: a first order partial differential equation for S. In the language of Goldstein [35], S can be identified with the F_2 type generating function which effects a canonical transformation from the original phase space variables (x, z, P_x, P_z) to the new ones $(\beta_1, \beta_2, \alpha_1, \alpha_2)$. The new momenta, α_1, α_2, are constants of the motion and the new co-ordinates do not appear explictly in the transformed Hamiltonian H'—they are called 'cyclic co-ordinates'. The general form of a canonical tranformation from phase space co-ordinates $(\mathbf{q}, \mathbf{p})$ to new ones $(\mathbf{Q}(\mathbf{q}, \mathbf{p}), \mathbf{P}(\mathbf{q}, \mathbf{p}))$ is established by noting that *variation* of the time integral of the Lagrangian

$$\begin{aligned} \delta I &= \delta \int_{t_0}^{t_1} L(q, \dot{q}) dt = \delta \int_{t_0}^{t_1} \left(\frac{m\dot{x}^2}{2} + \frac{m\dot{z}^2}{2} + V_0 \cos^2 Kx\right) dt \\ &= \delta \int_{t_0}^{t_1} \left(\sum_j p_j \dot{q}_j - H(\mathbf{q}, \mathbf{p})\right) dt \end{aligned} \tag{B.8}$$

is unchanged by the addition of a *total* time dervative of some function,

$$\frac{dF}{dt} = \frac{dF_1(\mathbf{q}, \mathbf{Q})}{dt} \tag{B.9}$$

say, to the integrand. Hamilton's principle of course states that the vanishing of the variation of I, subject to fixed endpoints, gives the classical trajectories, and in practice leads to the Euler-Lagrange equations—an alternative but entirely equivalent route to that pursued in Section 3.4.1.

As far as the resulting equations of motion are concerned then, the transformed version of Equation (B.8) is only defined up to the inclusion of the time-derivative of F_1 giving

$$\sum_j p_j \dot{q}_j - H(\mathbf{q}, \mathbf{p}) = \sum_j P_j \dot{Q}_j - H'(\mathbf{Q}, \mathbf{P}) + \frac{dF_1(\mathbf{q}, \mathbf{Q})}{dt} \tag{B.10}$$

and the transformation is deemed canonical if the Hamiltonian structure is retained in the new phase space co-ordinates so that

$$\dot{Q}_j = \frac{\partial H'}{\partial P_j}, \quad \dot{P}_j = -\frac{\partial H'}{\partial Q_j}. \tag{B.11}$$

These equations, together with Hamilton's equations in the original co-ordinates, can be substituted into the equality (B.10) to yield

$$p_j = \frac{\partial F_1}{\partial q_j}, \quad P_j = -\frac{\partial F_1}{\partial Q_j}. \tag{B.12}$$

F_2 generators are functions of the old co-ordinates q_j and the new momenta P_j and can be obtained from F_1 by a Legendre transform

$$F_1(\mathbf{q}, \mathbf{Q}) = F_2(\mathbf{q}, \mathbf{P}) - \sum_j Q_j P_j. \tag{B.13}$$

The equivalent equations to (B.12) for the F_2 generator are

$$p_j = \frac{\partial}{\partial q_j} F_2(x, z, \alpha_1, \alpha_2) \tag{B.14}$$

$$\beta_j = \frac{\partial}{\partial \alpha_j} F_2(x, z, \alpha_1, \alpha_2). \tag{B.15}$$

If, as stated above, an F_2 type generator can be found which produces new momenta which are constants, α_j , then the Eikonal equation (B.5) is a Hamilton-Jacobi equation and may be written

$$H(x, z, P_x, P_z) = H\left(x, z, \frac{\partial S}{\partial x}, \frac{\partial S}{\partial z}\right) = H'(\alpha_1, \alpha_2). \tag{B.16}$$

The Hamiltonian (3.4) is *separable* and so the total action $S(\equiv F_2)$ can be written as the sum of two terms—one depending only upon x and the other only upon z. For a fixed set of α_j one has, from Equation (B.14),

$$dS = \frac{\partial}{\partial x} S(x, z, \alpha_1, \alpha_2) dx + \frac{\partial}{\partial z} S(x, z, \alpha_1, \alpha_2) dz \tag{B.17}$$

or, due to the separability

$$dS = \frac{d}{dx} S_x(x, \alpha_1, \alpha_2) dx + \frac{d}{dz} S_z(z, \alpha_1, \alpha_2) dz. \tag{B.18}$$

Thus, using Equation (B.5),

$$S_x = \int_{x_0}^{x} P_x(x', \alpha_1, \alpha_2)\, dx' \tag{B.19}$$

$$S_z = \int_{z_0}^{z} P_z\, dz' \tag{B.20}$$

and

$$S = S_x + S_z \tag{B.21}$$

as asserted in Equation (3.35). The integrations have already been carried out in Section 3.4.3 giving

$$\begin{aligned} S_x =& \frac{\sqrt{2mV_0}}{K}\Bigg[\mathrm{E}\left(\arcsin\left[\frac{\sin x_c}{\sin x_{0_c}}\right] \,\middle|\, \sin^2 x_{0_c}\right) \\ &+ \cos^2 x_{0_c}\mathrm{F}\left(\arcsin\left[\frac{\sin x_c}{\sin x_{0_c}}\right] \,\middle|\, \sin^2 x_{0_c}\right) \\ &- \mathrm{E}(\sin^2 x_{0_c}) - \cos^2 x_{0_c}\mathrm{K}(\sin^2 x_{0_c})\Bigg] \end{aligned} \tag{B.22}$$

and

$$S_z = \frac{P_z^2(x_0)}{K\sqrt{2mV_0}} z_c(x_0). \tag{B.23}$$

B.3 The amplitude equation

From Equation (B.14)

$$\frac{\partial S}{\partial x} = P_x, \qquad \frac{\partial S}{\partial z} = P_z. \tag{B.24}$$

Inserting these relations into Equation B.6, one has, to first order in $\hbar$, an equation for the amplitude of the wavefunction

$$P_x\frac{\partial a}{\partial x} + P_z\frac{\partial a}{\partial z} + \frac{a}{2}\left(\frac{\partial P_x}{\partial x} + \frac{\partial P_z}{\partial z}\right) = 0. \tag{B.25}$$

This equation can be re-written in terms of distance along the ray, s, where an infinitesimal of arc-length is given by

$$ds = \sqrt{(dx)^2 + (dz)^2} = \sqrt{1 + \left(\frac{dx(x_0, z)}{dz}\right)^2}\, dz \tag{B.26}$$

and the unit vector along the ray is

$$\hat{\mathbf{s}} = \frac{P_x\hat{\mathbf{x}} + P_z\hat{\mathbf{z}}}{\sqrt{P_x^2 + P_z^2}} = \frac{\mathbf{P}}{|\mathbf{P}|}. \tag{B.27}$$

If wave fronts are determined by lines of constant phase, S, then $\hat{\mathbf{s}}$ is the normal to these wave fronts. The rate of change along a ray is therefore given by

$$\frac{d}{ds} = \hat{\mathbf{s}} \cdot \nabla \tag{B.28}$$

so, in particular,

$$\frac{dS}{ds} = \hat{\mathbf{s}} \cdot \nabla S = \sqrt{P_x^2 + P_z^2}. \tag{B.29}$$

In this terminology, Equation (B.25) becomes

$$|\mathbf{P}|\frac{da}{ds} + \frac{a}{2}\nabla \cdot \mathbf{P} = 0 \tag{B.30}$$

or

$$\frac{d\ln a^2}{ds} + \frac{1}{|\mathbf{P}|}\nabla\cdot\mathbf{P} = 0. \tag{B.31}$$

A crucial step in the determination of the amplitude of the semiclassical wavefunction is the realisation that this is a feature associated with a bundle of rays—a *ray tube*—not a single ray. The ray tube might be focussed down into a small area and the resulting amplitude would be large, or conversely, the ray tube might diverge giving a smaller amplitude. If one considers just a single ray then the solution to Equation (B.25) is $a = 1/\sqrt{P_x}$. This coincides with the W.K.B. solution—one proceeds by separating the solution into the product of a z dependent term and an x dependent term. The z dependent term is $\exp(\mathrm{i}S_z/\hbar)$ as before and the remaining one dimensional problem for x is solved with the usual W.K.B. techniques. The W.K.B. solution is, however, for a specific eigen-energy, not just a random ray. The total wavefunction is the sum over the W.K.B. eigenfunctions. The total wavefunction given by the method expounded in this appendix is given by the sum over the trajectories, which is quite different. The two solutions are related through the Poisson summation formula and this is the substance of Chapter 9. Returning now to the ray method, one can see that in evaluating the divergence of the momentum, $\nabla\cdot\mathbf{P}$, it is necessary to consider the divergence from a ray tube. The divergence of the momentum from a segment of

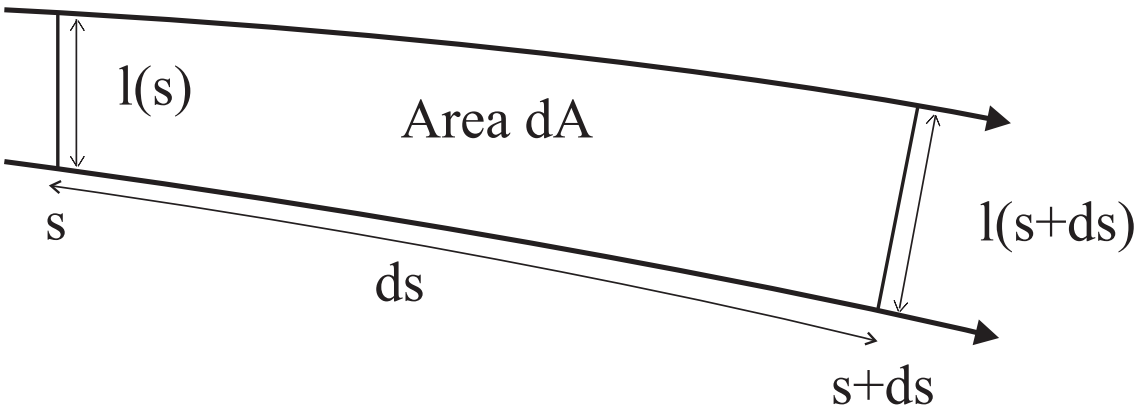

Figure B.1: A segment of a ray tube

ray tube is equal to the line integral around the perimeter of the momentum perpendicular to the perimeter

$$\nabla\cdot\mathbf{P} = \lim_{dA\to 0}\frac{1}{dA}\int \mathbf{P}\cdot\hat{\mathbf{n}}\, dl \tag{B.32}$$

where dl is a line element of, and $\hat{\mathbf{n}}$ is the normal to, the perimeter. See Figure B.1. The area of the segment is roughly given by

$$dA \approx \delta l ds. \tag{B.33}$$

In what follows it is important to realise just how small the angle is that the ray tube makes to the **z**-axis. Taking values from reference [37], one has $\Omega = 144\text{MHz}$, $\Gamma = 60\text{MHz}$, $\Delta = 1000\text{MHz}$, giving $V_0 \approx \hbar\Omega^2/4\Delta = 5.2 \times 10^{-28}\text{J}$ (See Equation (2.70)). So using Equation (3.53) one finds that the value of the deflection angle, which is the momentum ratio, can take a maximum value

$$\frac{P_x}{P_z} = \frac{dx}{dz} \leq \frac{\sqrt{2mV_0}}{P_z} \approx 1.6 \times 10^{-4}. \tag{B.34}$$

The system is definitely within the *paraxial* regime. The line integrals along the top and bottom of the tube therefore cancel, and the contributions from the two ends, which are very nearly vertical, are dominated by the $P_z dl$ term. However, P_z is a constant and may be taken outside of the integral so that Equation (B.32) becomes

$$\begin{aligned} \lim_{dA\to 0} \frac{1}{dA} \int \mathbf{P}\cdot\hat{\mathbf{n}}\, dl &= \frac{P_z}{\delta l ds}(\delta l(s+ds) - \delta l(s)) \\ &= \frac{P_z}{\delta l}\frac{d}{ds}\delta l \\ &= P_z \frac{d}{ds}\ln \delta l. \end{aligned} \tag{B.35}$$

Invoking paraxiality once more so that,

$$|\mathbf{P}| \approx P_z \tag{B.36}$$

giving

$$\frac{\nabla\cdot\mathbf{P}}{|\mathbf{P}|} = \frac{d}{ds}\ln\delta l \tag{B.37}$$

it is now possible to write Equation (B.25) entirely in terms of quantities taken along the ray tube

$$\frac{d}{ds}\ln a^2 + \frac{d}{ds}\ln\delta l = \frac{d}{ds}\ln(a^2\delta l) = 0. \tag{B.38}$$

Therefore, as one follows a particular ray tube, $a^2\delta l$ is conserved. Again, because the angles of deflection are so small, one may take $\delta l = dx$, so that the amplitude becomes

$$a = \left|\frac{dx}{dx_0}\right|^{-1/2}. \tag{B.39}$$

Now, $|\partial x/\partial x_0|$ is the Jacobian for the mapping produced under the action of the solved trajectory equation (3.28), $x(x_0, z)$, which takes initial points $(x_0, z = 0)$ to final positions (x, z), so this seems a reasonable quantity to use to describe a classical density of trajectories (intensity) and hence, via the square root, an amplitude.

B.4 The total wavefunction

The wavefunction at a point in configuration space is constructed from the sum of the contributions from each ray tube which passes through that point. On a caustic however, the individual

rays touch—the ray tube is focussed right down—and the amplitude becomes infinite. So the wavefunction cannot be evaluated too close to a caustic. Furthermore, the caustic has a dramatic effect upon the ray tubes which form it: the caustic introduces a phase retardation of $\pi/2$, see [19]. The wavefunction away from a caustic becomes

$$\Psi(x,z) = \mathcal{N}\sum_g \frac{1}{|\{\frac{dx}{dx_0}\}_g|}\mathrm{e}^{\mathrm{i}S^g/\hbar - \mathrm{i}m_g\pi/2} \tag{B.40}$$

where g labels the trajectories which pass through the point (x,z), see Chapter 3, and $\mathcal{N}$ is the normalisation. The Maslov index, m_g, records the number of caustics the ray g has been involved in during the journey from $(x = x_0, z = 0)$. A consequence of the paraxiality is that the configuration space wavefunction is very hard to determine experimentally, so one considers instead the momentum space wave function which is accessible from measurements in the farfield. Assuming that a periodic potential leads to a periodic solution, the wavefunction at the plane of emergence $z = D$ may be expanded as a Fourier series

$$\Psi(x, z = D) = \sum_{n=-\infty}^{\infty} \psi_n \mathrm{e}^{\mathrm{i}(kz + 2nKx)} \tag{B.41}$$

with the amplitudes of the diffracted beams appearing as the Fourier coefficients. Then

$$\psi_n = \frac{\mathcal{N}}{\pi}\int_{-\pi/2}^{\pi/2}\sum_g \mathrm{e}^{-\mathrm{i}m_g\pi/2}\frac{1}{\sqrt{|\{\frac{dx}{dx_0}\}_g|}}\,\mathrm{e}^{\mathrm{i}(S^g(x,D)/\hbar - 2nKx)}\,d(Kx) \tag{B.42}$$

where, during the integration over the range $Kx \to Kx + d(Kx)$, only those ray tubes along allowed classical trajectories arriving in that range, are integrated over. The allowed ray tubes are labelled by g, but the set $[g]$ is a function of x. The assumed small size of $\hbar$ relative to the classical quantities allows the integral to be evaluated by the method of stationary phase. Physically this means the phase must vary rapidly over the width of a ray tube. The phase in Equation (B.42) is stationary w.r.t. x when

$$\frac{\partial S}{\partial x} = P_x = 2n\hbar K \tag{B.43}$$

and so, as might be expected, the contributions to the n^{th} diffracted beam come from classical paths travelling at the correct angle, namely

$$\tan\theta \approx \theta = \frac{2n\hbar K}{P_z}. \tag{B.44}$$

The method of stationary phase is suitable for evaluating integrals with rapidly varying integrands of the form

$$\int_{y_1}^{y_2} A(y)\mathrm{e}^{\mathrm{i}h(y)/\hbar}\,dy \sim \sum_r \sqrt{\frac{2\pi\hbar}{|h''(y_r)|}}A(y_r)\mathrm{e}^{\mathrm{i}h(y_r)/\hbar \pm \mathrm{i}\pi/4} \tag{B.45}$$

where y_r are the stationary points of the exponent $h(y)$, and $\pm$ is chosen depending on whether $h''(y_r)$ is positive or negative. To calculate h'' one must differentiate Equation (B.43) once more. For comparison with the results of Chapter 3, it is useful to write

$$h'' = \frac{1}{K}\frac{dP_x}{dKx} = \frac{P_z}{K^2}\frac{d\theta}{dx} \tag{B.46}$$

where once again the relation $\theta \approx P_x/P_z$ has been used. The stationary phase evaluation of Equation (B.42), which gives the diffracted beam amplitudes, is thus

$$\psi_n = \mathcal{N}\sqrt{\frac{2\hbar K}{\pi P_z}}\sum_{r,g}\frac{1}{\sqrt{|\{\frac{d\theta}{dx_{0_c}}\}_{rg}|}}\,\mathrm{e}^{\mathrm{i}(S^g(x_r,\,D)/\hbar - 2nKx_r - m_g\pi/2 \pm \pi/4)}\,. \tag{B.47}$$

The n^{th} amplitude is therefore the sum over the trajectories which at the exit face $z = D$, are travelling at the angle given by Equation (B.44). These trajectories emanate from the different transverse points of the exit face labelled by x_r. Each of the allowed values of the label rg correspond to particular values of x_0. This initial transverse starting position, x_0, uniquely specifies a ray, whether it be in momentum or configuration space. This result is in correspondence with Equation (3.52) which was obtained directly in momentum space. When the phases from each contributing ray are taken to be mutually incoherent, as would be the case when $\hbar \to 0$, then the ray tube sum reduces back to the purely classical result (3.49).

Appendix C

Classical oblique incidence

The purpose of this appendix is to give an overview of the derivation of the classical equations of motion describing atoms having a non- zero initial transverse momentum.

C.1 Confined trajectories

As with perpendicular incidence, P_z is conserved. However, the initial condition, at $z = 0$, on the gradient of the trajectory is now altered to become

$$\frac{dx}{dz} = \frac{P_x}{P_z} = \theta_0. \tag{C.1}$$

When substituted into the energy equation (3.6), the equivalent to the trajectory equation (3.9) becomes

$$\frac{P_z^2}{2m}\left(\frac{dx}{dz}\right)^2 = V_0\left(\cos^2 Kx - \cos^2 Kx_0 + \frac{\theta_0^2 P_z^2}{2mV_0}\right) \tag{C.2}$$

and the solution may once again be expressed in terms of quadrature

$$\begin{aligned}\frac{\sqrt{2mV_0}}{P_z}z &= \int_{x'=x_0}^{x'=x} \frac{dx'}{\sqrt{\cos^2 Kx' - \cos^2 Kx_0 + \frac{\theta_0^2 P_z^2}{2mV_0}}} \\ &= \frac{1}{\sqrt{\sin^2 Kx_0 + \frac{\theta_0^2 P_z^2}{2mV_0}}} \int_{x'=x_0}^{x'=x} \frac{dx'}{\sqrt{1 - \frac{\sin^2 Kx'}{\left(\sin^2 Kx_0 + \frac{\theta_0^2 P_z^2}{2mV_0}\right)}}}.\end{aligned} \tag{C.3}$$

For atoms in libration, that is, those that are confined to the well in which they started,

$$\sin^2 Kx_0 + \frac{\theta_0^2 P_z^2}{2mV_0} < 1. \tag{C.4}$$

Let

$$\sin\phi = \frac{\sin Kx}{\sqrt{\sin^2 Kx_0 + \frac{\theta_0^2 P_z^2}{2mV_0}}} \tag{C.5}$$

in terms of which

$$\frac{dx}{\sqrt{\sin^2 Kx_0 + \frac{\theta_0^2 P_z^2}{2mv_0}}} = \frac{\cos\phi\, d\phi}{K\cos Kx} \tag{C.6}$$

but

$$\cos Kx = \sqrt{1 - \left(\sin^2 Kx_0 + \frac{\theta_0^2 P_z^2}{2mV_0}\right)\sin^2\phi} \tag{C.7}$$

so Equation (C.3) becomes

$$\frac{\sqrt{2mV_0}}{P_z} z = \int_{\phi_0}^{\phi} \frac{d\phi}{\sqrt{1 - \left(\sin^2 Kx_0 + \frac{\theta_0^2 P_z^2}{2mV_0}\right)\sin^2\phi}}. \tag{C.8}$$

The lower limit of the integration is determined from

$$\sin\phi_0 = \frac{\sin Kx_0}{\sqrt{\sin^2 Kx_0 + \frac{\theta_0^2 P_z^2}{2mV_0}}}. \tag{C.9}$$

As before the solution to the quadrature integral is written in terms of elliptic integrals

$$\frac{\sqrt{2mV_0}}{P_z} z = \mathrm{F}\left(\arcsin\left[\frac{\sin Kx}{\sqrt{\mu}}\right]\middle|\,\mu\right) - \mathrm{F}\left(\arcsin\left[\frac{\sin Kx_0}{\sqrt{\mu}}\right]\middle|\,\mu\right) \tag{C.10}$$

where this time

$$\mu = \sin^2 Kx_0 + \frac{\theta_0^2 P_z^2}{2mV_0}. \tag{C.11}$$

Performing the inversion into elliptic functions gives

$$\frac{\sin Kx}{\sqrt{\mu}} = \mathrm{sn}\left(\frac{\sqrt{2mV_0}}{P_z} z + \mathrm{F}\left(\arcsin\left[\frac{\sin Kx_0}{\sqrt{\mu}}\right]\middle|\,\mu\right)\middle|\,\mu\right). \tag{C.12}$$

By substituting this configuration space solution back into Equation (C.2), and making use of the identity $\mathrm{cn}^2(u|m) + \mathrm{sn}^2(u|m) = 1$, one quickly obtains the momentum space solution

$$\tan\theta = \frac{dx}{dz} = \frac{\sqrt{2mV_0}}{P_z}\sqrt{\mu}\,\mathrm{cn}\left(\frac{\sqrt{2mV_0}}{P_z} z + \mathrm{F}\left(\arcsin\left[\frac{\sin Kx_0}{\sqrt{\mu}}\right]\middle|\,\mu\right)\middle|\,\mu\right). \tag{C.13}$$

C.2 Escaping trajectories

If the initial transverse energy of an atom exceeds the barrier potential of the wells then, given a long enough interaction time, it is able to travel over the barrier tops into successive wells. The condition which must be fulfilled to allow such 'rotational' motion is

$$\sin^2 Kx_0 + \frac{\theta_0^2 P_z^2}{2mV_0} > 1. \tag{C.14}$$

There is clearly a critical value of the initial transverse kinetic energy, $\theta_0^2 P_z^2/2m$, above which all atoms, whatever their initial transverse position, are capable of rotation. This is

$$\frac{\theta_0^2 P_z^2}{2m} = V_0. \tag{C.15}$$

The equations of motion are the same as before except that the parameter μ is now greater than one. It is always preferrable to have the parameter of elliptic integrals and functions lie between zero and one, and this is made possible with the two transformations [1],

$$\mathrm{F}(\alpha|m) = \frac{1}{\sqrt{m}}\mathrm{F}(\beta|m^{-1}) \tag{C.16}$$

where

$$\sin\beta = \sqrt{m}\sin\alpha \tag{C.17}$$

and

$$\mathrm{sn}(u|m) = \frac{1}{\sqrt{m}}\,\mathrm{sn}(\sqrt{m}\,u\,|m^{-1}). \tag{C.18}$$

Together these transformations convert the configuartion space solution into

$$\sin Kx = \mathrm{sn}\left(\sqrt{\mu}\,\frac{\sqrt{2mV_0}}{P_z}z + \mathrm{F}\left(Kx_0|\,\mu^{-1}\right)\middle|\,\mu^{-1}\right). \tag{C.19}$$

The momentum space solution requires a further identity [1]

$$\mathrm{cn}(u|m) = \mathrm{dn}(\sqrt{m}\,u|m^{-1}) \tag{C.20}$$

and taken with transformation (C.16) gives

$$\frac{dx}{dz} = \frac{\sqrt{2mV_0}}{P_z}\,\sqrt{\mu}\,\mathrm{dn}\left(\sqrt{\mu}\,\frac{\sqrt{2mV_0}}{P_z}z + \mathrm{F}\left(Kx_0|\,\mu^{-1}\right)\middle|\,\mu^{-1}\right). \tag{C.21}$$

Appendix D

The action integral

The W.K.B. solution to the Raman-Nath equation requires the evalution of the integral

$$I = \int \arccos\left[y^2 - \beta\right] dy. \tag{D.1}$$

Let

$$y^2 - \beta = \cos t \tag{D.2}$$

then

$$I = \int \frac{-t \sin t}{2\sqrt{\beta + \cos t}} dt. \tag{D.3}$$

Setting

$$t = 2\tau \tag{D.4}$$

gives

$$I = \int \frac{-4\tau \sin\tau \cos\tau}{\sqrt{\beta + 1 - 2\sin^2\tau}} d\tau = -\frac{4\kappa}{\sqrt{2}} \int \frac{\tau \sin\tau \cos\tau}{\sqrt{1 - \kappa^2 \sin^2\tau}} d\tau \tag{D.5}$$

where

$$\kappa^2 = \frac{2}{1+\beta}. \tag{D.6}$$

Now let

$$\kappa \sin\tau = \sin\phi \tag{D.7}$$

so that

$$\begin{aligned} I &= -\frac{4}{\sqrt{2}}\int \frac{\tau \sin\phi\cos\phi}{\kappa\cos\phi}d\phi = -\frac{4}{\sqrt{2}\kappa}\int \arcsin\left[\frac{\sin\phi}{\kappa}\right]\sin\phi\, d\phi \\ &= -\frac{4}{\sqrt{2}\kappa}\left(-\cos\phi\arcsin\left[\frac{\sin\phi}{\kappa}\right] + \int \frac{\cos^2\phi}{\kappa\sqrt{1-(\sin^2\phi)/\kappa^2}}d\phi\right) \\ &= -\frac{4}{\sqrt{2}\kappa}\left(-\cos\phi\arcsin\left[\frac{\sin\phi}{\kappa}\right] + \int \frac{\kappa\sqrt{1-\kappa^2\sin^2\tau}\cos\tau}{\kappa\sqrt{1-\sin^2\tau}}d\tau\right) \\ &= -\frac{4}{\sqrt{2}\kappa}\left(-\tau\sqrt{1-\kappa^2\sin^2\tau} + \int \sqrt{1-\kappa^2\sin^2\tau}d\tau\right). \end{aligned} \tag{D.8}$$

Now the required range of the integration is from $y = \sqrt{1+\beta}$ to y. Since

$$\tau = \frac{1}{2}\arccos\left[y^2-\beta\right] \tag{D.9}$$

the integral reduces to

$$I = y\arccos\left[y^2-\beta\right] - 2\sqrt{1+\beta}\,\mathrm{E}\left(\frac{1}{2}\arccos\left[y^2-\beta\right]\middle|\, \frac{2}{1+\beta}\right). \tag{D.10}$$

Appendix E

A complex potential for the ground state

E.1 A non-Hermitian Hamiltonian

The spontaneous decay of the excited state can always be described phenomenologically by replacing the eigenstate

$$|b\rangle \, \mathrm{e}^{-\mathrm{i}\omega_0 t} \tag{E.1}$$

with

$$|b\rangle \, \mathrm{e}^{-\mathrm{i}(\omega_0 - \mathrm{i}\gamma/2)t} \tag{E.2}$$

for then the probability of being in the excited state decays exponentially with the time decay constant γ. This replacement leads to an imaginary factor in internal atomic Hamiltonian (2.3)

$$\begin{pmatrix} \hbar\omega_0 & 0 \\ 0 & 0 \end{pmatrix} \longrightarrow \begin{pmatrix} \hbar\left(\omega_0 - \mathrm{i}\frac{\gamma}{2}\right) & 0 \\ 0 & 0 \end{pmatrix}. \tag{E.3}$$

E.2 Evolution of the density matrix

The time evolution of the atomic density matrix is generally given by

$$\mathrm{i}\hbar\dot{\sigma} = [H, \sigma]\,. \tag{E.4}$$

If one was dealing with a simple two-level atom with spontaneous decay from the upper to the lower state, then one can preserve the Hermiticity of the evolution equation by replacing the commutator with

$$\mathrm{i}\hbar\dot{\sigma} = H\sigma - \sigma H^{\dagger}. \tag{E.5}$$

Cohen-Tannoudji *et al* [25] point out, however, that this procedure gives the correct optical Bloch equations (2.23) only up to the decay term down into the ground state population σ_{aa}, this decay term being completely absent.

Here, however, the three-level atom is considered as having non-unitary evolution, so the original commutator will be used. It should be stressed that the inclusion of an imaginary term in the Hamiltonian does not in itself necessarily have to lead to dissipation of atomic probability; with the transformation (E.5) one could ensure the evolution is in fact unitary. The dissipation originates from solely concentrating upon the ensemble of atoms which have not decayed to the third state. Using Equation (E.4) with the modified H, one finds the equations of motion for the individual atomic density matrix elements for just the *coherent* part of the ensemble (that is, atoms in the $|a\rangle$ and $|b\rangle$ states) to be (c.f. Equations (2.20–2.23))

$$\dot{\sigma}_{bb} = \mathrm{i}\Omega \cos\omega_L t\,(\sigma_{ba} - \sigma_{ab}) \tag{E.6}$$

$$\dot{\sigma}_{aa} = -\mathrm{i}\Omega \cos\omega_L t\,(\sigma_{ba} - \sigma_{ab}) \tag{E.7}$$

$$\dot{\sigma}_{ab} = \mathrm{i}\omega_0\sigma_{ab} - \mathrm{i}\Omega \cos\omega_L t\,(\sigma_{bb} - \sigma_{aa}) + \frac{\gamma}{2}\sigma_{ab} \tag{E.8}$$

$$\dot{\sigma}_{ba} = -\mathrm{i}\omega_0\sigma_{ba} + \mathrm{i}\Omega \cos\omega_L t\,(\sigma_{bb} - \sigma_{aa}) - \frac{\gamma}{2}\sigma_{ba}. \tag{E.9}$$

In the limit that the decay from $|b\rangle$ to $|a\rangle$ at rate Γ (see Figure 6.1) can be neglected in comparison to the coherent evolution at rate Ω, and the rapid decay at rate γ of $|b\rangle$ to $|c\rangle$

$$\Omega\ ,\ \gamma \gg \Gamma \tag{E.10}$$

then the Equations (E.6–E.9) turn out to correctly describe the evolution of the two working levels of the three level atom under non-unitary evolution. This time there is no need to insert any decay constants by hand.

It remains to be shown that the population of the excited state adiabatically follows that of the ground state, but under the conditions (E.10), and with a weak field, Chudesnikov and Yakovlev [24] show this to be the case. This means that the derivation of the potential in Chapter 2 is valid and can be followed through with $\Gamma = 0$ and the replacement

$$\omega_0 \longrightarrow \omega_0 - \mathrm{i}\frac{\gamma}{2} \tag{E.11}$$

which by definition (2.36) leads to

$$\Delta \longrightarrow \Delta + \mathrm{i}\frac{\gamma}{2}. \tag{E.12}$$

When $\gamma \gg \Omega$ (weak field), then Equation (2.69) can be expanded as before, this time giving the complex potential

$$V(x) = \frac{d_{ab}^2\mathcal{E}_0^2}{4\hbar\left(\Delta + \mathrm{i}\frac{\gamma}{2}\right)}\ \cos^2 Kx \tag{E.13}$$

which is the same as the expression obtained by Chudesnikov and Yakovlev [24].

Appendix F

The normalisation integral

The normalisation of the W.K.B. Bloch waves necessitates the evaluation of

$$I = \int_{-\sqrt{\beta+1}}^{\sqrt{\beta+1}} \frac{dy}{\sqrt{1-(y^2-\beta)^2}} = 2\int_0^{\sqrt{\beta+1}} \frac{dy}{\sqrt{1-(y^2-\beta)^2}}. \tag{F.1}$$

Within the specified range, $y^2-\beta$ takes on values between -1 and 1, so putting

$$y^2 - \beta = \cos t \tag{F.2}$$

means

$$dy = \frac{-\sin t\ dt}{2\sqrt{\beta+\cos t}} \tag{F.3}$$

and so

$$I = 2\int_{\arccos[-\beta]}^{0} \frac{-dt}{2\sqrt{\beta+\cos t}} = \frac{2}{\sqrt{1+\beta}} \int_0^{\arccos[-\beta]} \frac{d(t/2)}{\sqrt{1-\frac{2}{1+\beta}\sin^2(t/2)}} \tag{F.4}$$

which gives an elliptic integral of the first kind

$$I = \frac{2}{\sqrt{1+\beta}} \mathrm{F}\left(\frac{1}{2}\arccos\left[-\beta\right]\middle|\ \frac{2}{1+\beta}\right). \tag{F.5}$$

This can be further simplified by the transformation [1]

$$\mathrm{F}(\phi|m) = \frac{1}{\sqrt{m}}\mathrm{F}(\theta|m), \qquad \sin\theta = \sqrt{m}\sin\phi \tag{F.6}$$

producing

$$I = \frac{2}{\sqrt{2}} \mathrm{F}\left(\frac{\pi}{2}\middle|\ \frac{1+\beta}{2}\right) = \sqrt{2}\mathrm{K}\left(\frac{1+\beta}{2}\right). \tag{F.7}$$

Appendix G

Differentiating the phase

G.1 First differentiation

The phase term $\mathcal{A}$ as given by Equation (9.7) is

$$\begin{aligned}\mathcal{A} &= y\arccos\left[y^2-\beta\right]-2\sqrt{1+\beta}\mathrm{E}\left(\frac{1}{2}\arccos\left[y^2-\beta\right]\middle|\frac{2}{1+\beta}\right)\\ &\quad+2(4m-1)\sqrt{1+\beta}\mathrm{E}\left(\frac{1}{2}\arccos\left[-\beta\right]\middle|\frac{2}{1+\beta}\right)+\frac{\pi}{2\sqrt{\Lambda}}-\frac{\beta z_c}{\sqrt{2}}-\frac{m\pi}{\sqrt{\Lambda}}.\end{aligned}\tag{G.1}$$

When differentiating this expression, it is simplest to return to the original integrals which gave this phase in the first place, so that

$$\mathcal{A}=\int_{t=\sqrt{1+\beta}}^{y}\arccos\left[t^2-\beta\right]\;dt+(1-4m)\int_{t=\sqrt{1+\beta}}^{0}\arccos\left[t^2-\beta\right]\;dt+\frac{\pi}{2\sqrt{\Lambda}}-\frac{\beta z_c}{\sqrt{2}}-\frac{m\pi}{\sqrt{\Lambda}}.\tag{G.2}$$

And so one finds

$$\begin{aligned}\frac{d\mathcal{A}}{d\beta}&=\int_{t=\sqrt{1+\beta}}^{y}\frac{dt}{\sqrt{1-(t^2-\beta)^2}}-\arccos\left[\beta+1-\beta\right]\frac{d\sqrt{1+\beta}}{d\beta}\\&\quad+(1-4m)\left(\int_{t=\sqrt{1+\beta}}^{0}\frac{dt}{\sqrt{1-(t^2-\beta)^2}}-\arccos\left[\beta+1-\beta\right]\frac{d\sqrt{1+\beta}}{d\beta}\right)-\frac{z_c}{\sqrt{2}}.\end{aligned}\tag{G.3}$$

Since $\arccos[1]=0$, two of the terms vanish immediately. The remaining integrals are converted into elliptic integrals of the 1st kind by the change of variable

$$\cos\phi=t^2-\beta\tag{G.4}$$

giving

$$\frac{d\mathcal{A}}{d\beta}=\frac{-1}{\sqrt{1+\beta}}\mathrm{F}\left(\frac{1}{2}\arccos\left[y^2-\beta\right]\middle|\frac{2}{1+\beta}\right)-\frac{(1-4m)}{\sqrt{1+\beta}}\mathrm{F}\left(\frac{1}{2}\arccos\left[-\beta\right]\middle|\frac{2}{1+\beta}\right)-\frac{z_c}{\sqrt{2}}.\tag{G.5}$$

Using the transformation (3.16) simplifies the two elliptic integrals so that one has

$$\frac{d\mathcal{A}}{d\beta}=-\frac{1}{\sqrt{2}}\mathrm{F}\left(\arcsin\left[\sqrt{\frac{1+\beta-y^2}{1+\beta}}\right]\middle|\frac{1+\beta}{2}\right)-\frac{(1-4m)}{\sqrt{2}}\mathrm{K}\left(\frac{1+\beta}{2}\right)-\frac{z_c}{\sqrt{2}}.\tag{G.6}$$

G.2 Second differentiation

Expressing the terms of Equation (G.6) by their integral definitions and differentiating once more leads to

$$\frac{d^2\mathcal{A}}{d\beta^2} = -\frac{1}{\sqrt{2}}\left(\frac{1}{4}\int_0^{\arcsin\sqrt{\frac{1+\beta-y^2}{1+\beta}}} \frac{\sin^2 t\, dt}{\left(1-\frac{1+\beta}{2}\sin^2 t\right)^{3/2}} + \frac{y}{\sqrt{2}(1+\beta)\sqrt{1-(y^2-\beta)^2}} + \frac{1}{4}(1-4m)\int_0^{\pi/2} \frac{\sin^2 t\, dt}{\left(1-\frac{1+\beta}{2}\sin^2 t\right)^{3/2}}\right). \tag{G.7}$$

The first of these integrals can be re-written to read

$$\frac{1}{4}\int_0^{\arcsin\sqrt{\frac{1+\beta-y^2}{1+\beta}}} \frac{\sin^2 t\, dt}{\left(1-\frac{1+\beta}{2}\sin^2 t\right)^{3/2}} = -\frac{1}{2(1+\beta)}\int_0^{\arcsin\sqrt{\frac{1+\beta-y^2}{1+\beta}}} \frac{\left(-\frac{1+\beta}{2}\sin^2 t+1-1\right)\, dt}{\left(1-\frac{1+\beta}{2}\sin^2 t\right)^{3/2}} \tag{G.8}$$

which in turn is recognised as

$$\int_0^{\arcsin\sqrt{\frac{1+\beta-y^2}{1+\beta}}} \frac{\left(-\frac{1+\beta}{2}\sin^2 t+1-1\right)\, dt}{\left(1-\frac{1+\beta}{2}\sin^2 t\right)^{3/2}} = \left(\mathrm{F}\left(\arcsin\left[\sqrt{\frac{1+\beta-y^2}{1+\beta}}\right]\middle|\frac{1+\beta}{2}\right) - \Pi\left(\frac{1+\beta}{2};\arcsin\left[\sqrt{\frac{1+\beta-y^2}{1+\beta}}\right]\middle|\frac{1+\beta}{2}\right)\right) \tag{G.9}$$

where

$$\Pi(n;\phi|m) = \int_0^{\phi} \frac{dt}{\left(1-n\sin^2 t\right)\sqrt{1-m\sin^2 t}} \tag{G.10}$$

is the elliptic integral of the 3rd kind. A similar identification may then be made with the second integral in Equation (G.7) giving

$$\frac{d^2\mathcal{A}}{d\beta^2} = -\frac{1}{\sqrt{2}}\left[-\frac{1}{2(1+\beta)}\left\{\mathrm{F}\left(\arcsin\left[\sqrt{\frac{1+\beta-y^2}{1+\beta}}\right]\middle|\frac{1+\beta}{2}\right) - \Pi\left(\frac{1+\beta}{2};\arcsin\left[\sqrt{\frac{1+\beta-y^2}{1+\beta}}\right]\middle|\frac{1+\beta}{2}\right)\right\} + \frac{y}{\sqrt{2}(1+\beta)\sqrt{1-(y^2-\beta)^2}} - \frac{1-4m}{2(1+\beta)}\left\{\mathrm{K}\left(\frac{1+\beta}{2}\right) - \Pi\left(\frac{1+\beta}{2};\frac{\pi}{2}\middle|\frac{1+\beta}{2}\right)\right\}\right]. \tag{G.11}$$

However, when $n = m$, as here, the elliptic integral of the 3rd kind may itself be re-written in terms of more familiar functions (see page 600 of [1])

$$\Pi(m;\phi|m) = \frac{1}{1-m}\mathrm{E}(\phi|m) - \frac{m}{1-m}\frac{\sin 2\phi}{2\sqrt{1-m\sin^2\phi}}. \tag{G.12}$$

And so Equation (G.11) becomes

$$\begin{aligned}\frac{d^2\mathcal{A}}{d\beta^2} =& \frac{1}{2\sqrt{2}(1+\beta)}\mathrm{F}\left(\arcsin\left[\sqrt{\frac{1+\beta-y^2}{1+\beta}}\right]\middle|\,\frac{1+\beta}{2}\right) \\ &- \frac{1}{\sqrt{2}(1-\beta^2)}\mathrm{E}\left(\arcsin\left[\sqrt{\frac{1+\beta-y^2}{1+\beta}}\right]\middle|\,\frac{1+\beta}{2}\right) + \frac{y\left(2\beta-y^2\right)}{2\left(1-\beta^2\right)\sqrt{1-\left(y^2-\beta\right)^2}} \\ &+ \frac{1-4m}{2\sqrt{2}(1+\beta)}\left\{\mathrm{K}\left(\frac{1+\beta}{2}\right) - \frac{2}{1-\beta}\mathrm{E}\left(\frac{\pi}{2}\middle|\,\frac{1+\beta}{2}\right)\right\}.\end{aligned} \tag{G.13}$$

Bibliography

[1] Milton Abramowitz and Irene A. Stegun, editors. *Handbook of Mathematical Functions*. National Bureau of Standards, Washington, 1964.

[2] C. S. Adams, M. Sigel, and J. Mlynek. Atom optics. *Physics Reports*, 240:143–210, 1994.

[3] G. B. Airy. *Transactions of the Cambridge Philosophical Society*, 6:379–402, 1838.

[4] L. Allen and J. H. Eberly. *Optical Resonance and Two-Level Atoms*. Dover, New York, 1987.

[5] V. I. Arnol'd. *Russian Mathematical Surveys*, 30(5):1, 1975.

[6] V. I. Balykin and V. S. Letokhov. *Atom Optics with Laser Light*. Harwood Academic Publishers, Poststrasse 22, 7000 Chur, Switzerland, 1995.

[7] M. V. Berry. Uniform approximation for potential scattering involving a rainbow. *Proceedings of the Physical Society*, 89:479–490, 1966.

[8] M. V. Berry. Uniform approximation: a new concept in wave theory. *Scientific Progress, Oxford*, 57:43–64, 1969.

[9] M. V. Berry. Uniform approximations for glory scattering and diffraction peaks. *Journal of Physics B: Atomic and Molecular Physics*, 2:381–392, 1969.

[10] M. V. Berry. Diffraction in crystals at high energies. *Journal of Physics C: Solid State Physics*, 4:697–722, 1971.

[11] M. V. Berry. Semiclassical elastic scattering theory. Lecture notes for course given in Max-Planck Institute, Göttingen, June/July 1974.

[12] M. V. Berry. Exact Aharonov-Bohm wavefunction obtained by applying Dirac's magnetic phase factor. *European journal of Physics*, 1:240–244, 1980.

[13] M. V. Berry, B. F. Buxton, and A. M. Ozorio de Almeida. Between wave and particle—the semiclassical method for interpreting high-energy electron micrographs in crystals. *Radiation effects*, 20:1–24, 1973.

[14] M. V. Berry and K. E. Mount. Semiclassical approximations in wave mechanics. *Reports on Progress in Physics*, 35:315–397, 1972.

[15] M. V. Berry and D. H. J. O'Dell. Diffraction by volume gratings with imaginary potentials. *Journal of Physics A: Mathematical and General*, 31:2093–2101, 1998.

[16] Michael V. Berry. *The Diffraction of Light by Ultrasound*. Academic Press, London and New York, 1966.

[17] Michael V. Berry. Singularities in waves and rays. In R. Balian et al., editor, *Les Houches, Session XXXV, 1980—Physique des Dèfauts/Physics of Defects*, Course 7, pages 455–541. North-Holland Publishing Company, 1981.

[18] Felix Bloch. *Physical Review*, 70:460, 1946.

[19] Max Born and Emil Wolf. *Principles of Optics*. Pergamon Press, New York, 6^{th} edition, 1980.

[20] G. Borrmann. Über Extinkionsdiagramme von Quarz. *Physikalische Zeitschrift*, 42:157–162, 1941.

[21] Léon Brillouin. *Annal Physique*, 17:103, 1921.

[22] Léon Brillouin. *La Diffraction de la Lumière par les Ultrasons*. Hermann et Cie, Paris, 1933.

[23] C. Chester, B. Friedman, and F. Ursell. An extension of the method of steepest descents. *Proceedings of the Cambridge Philosophical Society*, 53:599–611, 1957.

[24] D. O. Chudesnikov and Y. P. Yakovlev. Bragg scattering on complex potentials and formation of supernarrow momentum distributions of atoms in light fields. *Laser Physics*, 1:111–119, 1991.

[25] Claude Cohen-Tannoudji, Jacques Dupont-Roc, and Gilbert Grynberg. *Atom-Photon Interactions*. Wiley-Interscience, New York, 1992.

[26] R. J. Cook. Atomic motion in resonant radiation: An application of Ehrenfest's theorem. *Physical Review A*, 20(1):224–228, July 1979.

[27] J. Dalibard and C. Cohen-Tannoudji. Dressed-atom approach to atomic motion in laser light: the dipole force revisited. *Journal of the Optical Society of America*, 2(11):1707–1720, Nov 1985.

[28] R. B. Dingle and G. J. Morgan. WKB methods for difference equations I. *Applied Scientific Research*, 18:221–237, Nov 1967.

[29] R. B. Dingle and G. J. Morgan. WKB methods for difference equations II. *Applied Scientific Research*, 18:238–245, Nov 1967.

[30] Albert Einstein. *Physikalische Zeitschrift*, 18:121, 1917.

[31] Kenneth W. Ford and John A. Wheeler. Application of semiclassical scattering analysis. *Annals of Physics*, 7:287–322, 1959.

[32] Kenneth W. Ford and John A. Wheeler. Semiclassical description of scattering. *Annals of Physics*, 7:259–286, 1959.

[33] David M. Giltner, Roger W. McGowan, and Siu Au Lee. Atom interferometer based on Bragg scattering from standing light waves. *Physical Review Letters*, 75(14):2638–2641, Oct 1995.

[34] David M. Giltner, Roger W. McGowan, and Siu Au Lee. Theoretical and experimental study of the Bragg scattering of atoms from a standing light wave. *Physical Review A*, 52(5):3966–3972, Nov 1995.

[35] Herbert Goldstein. *Classical Mechanics*. Addison-Wesley, Reading, Massachusetts, 2$^{\text{nd}}$ edition, 1980.

[36] Phillip L. Gould, Peter J. Martin, George A. Ruff, Richard E. Stoner, Jean-Louis Picqué, and David E. Pritchard. Momentum transfer to atoms by a standing light wave: Transition from diffraction to diffusion. *Physical Review A*, 43(1):585–588, Jan 1991.

[37] Phillip L. Gould, George A. Ruff, and David E. Pritchard. Diffraction of atoms by light: The near-resonant Kapitza- Dirac effect. *Physical Review Letters*, 56(8):827–830, Feb 1986.

[38] I. S. Gradshteyn and I. M. Ryzhik. *Table of Integrals, Series and Products*. Academic Press, New York, 4 edition, 1965.

[39] V. A. Grinchuk, E. F. Kuzin, M. L. Nagaeva, G. A. Ryabenko, A. P. Kazantsev, G. I. Surdutovich, and Y. P. Yakovlev. Scattering of atoms by coherent interaction with light. *Journal of the Optical Society of America*, 2(11):1805–1813, Nov 1985.

[40] J. H. Hannay. Private communication.

[41] J. H. Hannay. Accuracy loss of action invariance in adiabatic change of a one-freedom Hamiltonian. *Journal of Physics A: Mathematical and General*, 19:L1067–L1072, 1986.

[42] J. Heading. *An Introduction to Phase-Integral Methods*. Methuen, London, 1962.

[43] P. L. Kapitza and P. A. M. Dirac. The reflection of electrons from standing light waves. *Proceedings of the Cambridge Philosophical Society*, 29:297–300, 1932–1933.

[44] A. P. Kazantsev and G. I. Surdutovich. The Kapitza-Dirac effect for atoms in a strong resonant field. *Journal of Experimental and Theoretical Physics, Letters*, 21(6):158–159, Mar 1975.

[45] A. P. Kazantsev, G. I. Surdutovich, and V. P. Yakovlev. *Mechanical Action of Light on Atoms*. World Scientific Publishing Co., Singapore, 1991.

[46] S. Kunze, S. Dürr, and G. Rempe. Bragg scattering of slow atoms from a standing light wave. *Europhysics Letters*, 34(5):343–348, May 1996.

[47] Derek F. Lawden. *Elliptc Functions and Applications*. Number 80 in Applied Mathematical Sciences Series. Springer Verlag, New York, 1989.

[48] Rodney Loudon. *The Quantum Theory of Light*. Oxford, Oxford, U.K., 1983.

[49] René Lucas and Pierre Biquard. Propriétés optiques des milieux solides et liquides soumis aux vibrations élastiques ultra sonores. *Journal de Physique*, 3(10):464–477, 1932.

[50] M. Marte and S. Stenholm. Multiphoton resonances in atomic Bragg scattering. *Applied Physics B*, 54:443–450, 1992.

[51] Peter J. Martin, Phillip L. Gould, Bruce G. Oldaker, Andrew H. Miklich, and David E. Pritchard. Diffraction of atoms moving through a standing light wave. *Physical Review A*, 36(5):2495–2498, Sep 1987.

[52] Peter J. Martin, Phillip L. Gould, Bruce G. Oldaker, Andrew H. Miklich, and David E. Pritchard. Diffraction of atoms from a standing light wave. *Physica B*, 151:255–261, 1988.

[53] Peter J. Martin, Bruce G. Oldaker, Andrew H. Miklich, and David E. Pritchard. Bragg scattering of atoms from a standing light wave. *Physical Review Letters*, 60(6):515–518, Feb 1988.

[54] Jabez McClelland. Atoms join in the race for lithography in the next century. *Physics World*, 11(8):23, Aug 1998.

[55] N. W. McLachlan. *Theory and Application of Mathieu Functions*. Oxford, 1947.

[56] F. L. Moore, J. C. Robinson, C. Bharucha, P. E. Williams, and M. G. Raizen. Observation of dynamical localization in atomic momentum transfer: A new testing ground for quantum chaos. *Physical Review Letters*, 73(22):2974–2977, Nov 1994.

[57] Philip E. Moskowitz, Phillip L. Gould, Susan R. Atlas, and David E. Pritchard. Diffraction of an atomic beam by standing-wave radiation. *Physical Review Letters*, 51(5):370–373, Aug 1983.

[58] Philip E. Moskowitz, Phillip L. Gould, and David E. Pritchard. Deflection of atoms by standing-wave radiation. *Journal of the Optical Society of America*, 2(11):1784–1790, Nov 1985.

[59] N. S. Nagendra Nath. The diffraction of light by high frequency sound waves: Generalised theory. *Proceedings of the Indian Academy of Sciences (A)*, 4:222–242, 1936.

[60] N. S. Nagendra Nath. The diffraction of light by supersonic waves. *Proceedings of the Indian Academy of Sciences (A)*, 8:499, 1938.

[61] Otohiko Nomoto. Geometrical optical theory of the diffraction of light by ultrasonic waves. (1) approximate treatment. *Bulletin of the Kobayasi Institute of Physical Research*, 1:42–70, 1951.

[62] Markus K. Oberthaler, Roland Abfalterer, Stefan Bernet, Jörg Schmiedmayer, and Anton Zeilinger. Atom waves in crystals of light. *Physical Review Letters*, 77(25):4980–4983, 1996.

[63] T. Pearcey. *Philosophical Magazine*, 37:311, 1946.

[64] C. L. Pekeris. Ray theory vs. normal mode theory in wave propagation problems. *Proceedings of Symposia on Applied Mathematics*, 2:71–75, 1950. Electromagnetic theory.

[65] David E. Pritchard and Phillip L. Gould. Experimental possibilities for observation of unidirectional momentum transfer to atoms from standing waves of light. *Journal of the Optical Society of America*, 2(11):1799–1804, Nov 1985.

[66] Isidor I. Rabi. *Physical Review*, 51:652, 1937.

[67] C. V. Raman and N. S. Nagendra Nath. The diffraction of light by high frequency sound waves: Part I. *Proceedings of the Indian Academy of Sciences (A)*, 2:406–412, 1935.

[68] C. V. Raman and N. S. Nagendra Nath. The diffraction of light by sound waves of high frequency: Part II. *Proceedings of the Indian Academy of Sciences (A)*, 2:413–420, 1935.

[69] C. V. Raman and N. S. Nagendra Nath. The diffraction of light by high frequency sound waves: Part III. *Proceedings of the Indian Academy of Sciences (A)*, 3:74–84, 1936.

[70] C. V. Raman and N. S. Nagendra Nath. The diffraction of light by high frequency sound waves: Part IV. *Proceedings of the Indian Academy of Sciences (A)*, 3:119–125, 1936.

[71] C. V. Raman and N. S. Nagendra Nath. The diffraction of light by high frequency sound waves: Part V. *Proceedings of the Indian Academy of Sciences (A)*, 3:459, 1936.

[72] Ernst M. Rasel, Markus K. Oberthaler, Herman Batelaan, Jörg Schmiedmayer, and Anton Zeilinger. Atom wave interferometry with diffraction gratings of light. *Physical Review Letters*, 75(14):2633–2637, Oct 1995.

[73] Lord Rayleigh. *Proceedings of the Royal Society A*, 79:399, 1907.

[74] F. H. Sanders. *Canadian Journal of Research*, A14:158, 1936.

[75] E. Schumacher, M. Wilkens, P. Meystre, and S. Glasgow. Spontaneous emission in the near-resonant Kapitza-Dirac effect. *Applied Physics B*, 54:451–466, 1992.

[76] Michael Tabor. *Chaos and Integrability in Nonlinear Dynamics*. Wiley, New York, 1989.

[77] S. M. Tan and D. F. Walls. Numerical simulation of atomic diffraction in the Raman-Nath regime. *Applied Physics B*, 54:434–442, 1992.

[78] C. Tanguy, S. Reynaud, and C. Cohen-Tannoudji. Deflection of an atomic beam by a laser wave: transition between diffractive and diffusive regimes. *Journal of Physics B: Atomic and Molecular Physics*, 17:4623–4641, 1984.

[79] E. Teller. The crossing of potential surfaces. *Journal of Physical Chemistry*, 41:109–116, 1937.

[80] R. Thom. *Structural stability and Morphogenesis*. Benjamin, Reading, MA, 1975.

[81] H. C. Torrey. *Physical Review*, 76:1059, 1949.

[82] G. Venkataraman. *Journey into Light*. Indian Academy of Sciences, P.B. No. 8005, Sadashivanagar, Bangalore 560 080, India, 1988.

[83] Valery P. Yakovlev. Private communication, 1997.

[84] Anton Zeilinger. Private communication.